

**PERFORMANCE OF UN-RETROFITTED AND RETROFITTED  
WOOD I-JOISTS WITH FLANGE NOTCH OR WEB HOLE**

by

**Mohammad Shahidul Islam**

B.Sc. (Civil Engineering), Bangladesh University of Engineering and Technology, Dhaka, 2003

M. Engg. (Construction Engineering and Infrastructure Management), Asian Institute of  
Technology, Thailand, 2005

**A THESIS SUBMITTED IN PARTIAL FULFILLMENT  
OF THE REQUIREMENTS FOR THE DEGREE OF**

**DOCTOR OF PHILOSOPHY**

in

**THE COLLEGE OF GRADUATE STUDIES  
(Civil Engineering)**

**THE UNIVERSITY OF BRITISH COLUMBIA  
(Okanagan)**

**March 2017**

© Mohammad Shahidul Islam, 2017

The undersigned certify that they have read, and recommend to the College of Graduate Studies for acceptance, a thesis entitled:

**PERFORMANCE OF UNRETROFITTED AND RETROFITTED WOOD I-JOISTS WITH FLANGE NOTCH OR WEB HOLE**

---

Submitted by Mohammad Shahidul Islam in partial fulfillment of the requirements of

The degree of DOCTOR OF PHILOSOPHY.

Dr. M. Shahria Alam, Associate Professor, School of Engineering, UBC  
**Supervisor, Professor**

Dr. Kasun Hewage, Associate Professor, School of Engineering, UBC  
**Supervisory Committee Member, Professor**

Dr. Ahmad Rteil, Assistant Professor, School of Engineering, UBC  
**Supervisory Committee Member, Professor**

Dr. Thomas Johnson, Assistant Professor, School of Engineering, UBC  
**University Examiner, Professor**

Dr. Rakesh Gupta, Professor, Department of Wood Science and Engineering,  
Oregon State University, Corvallis  
**External Examiner, Professor**

21 March 2017  
**(Date submitted to Grad Studies)**

**Additional Committee Members include:**

Dr. Jonathan Holzman, Associate Professor, School of Engineering, UBCO  
**Neutral Chair**

## ABSTRACT

Composite wood I-joists have been used widely as floor and roof joists in the construction of commercial and residential buildings in Europe and North America since mid-1930s. These engineered timber I-joists are less expensive, lighter in weight, stronger, and more efficient compared to the solid sawn lumber beams. According to the Canadian Standards for Wood Design (CSA-O86) and manufacturer design guidelines, flange-cut on I-joists are strictly prohibited. However, notches in the top flange and openings in the web of I-joists are commonly made during construction to facilitate the electro-mechanical systems of a building. Due to these flange-notches and web-holes, the ultimate capacity and stiffness of the I-joist section get reduced significantly. This phenomenon will be more critical in the cases of web opening at shear span and flange notch at mid span. This may lead to the I-joist fail prematurely in shear or flexure in a brittle manner. The effect of flange-notches and web-holes on the strength properties (e.g. load carrying capacity, flexural strength, and shear strength) of timber I-joists need to be understood before reinforcing those deficient I-joists. The core objective of this thesis is to understand and predict the behavior of the I-joists having flange-notch and web-hole. Another objective of this study is to retrofit notches and web-holes with conventional and composite material, determine their performances, and provide predictive equations. For retrofitting purpose, Oriented Strand Board (OSB) collars and Glass Fibre Reinforced Polymer (GFRP) plates were used as reinforcing elements with different configurations. A total of 454 I-joists were tested with different notch and hole configurations. From the test results, it was observed that the presence of notch and hole reduced the capacity and stiffness of I-joists significantly. Findings also revealed that some retrofitting options can help improve the capacity as compared to the control I-joists. Finally, analytical models were developed to predict the behavior of flange notched and web holed I-joists and their retrofitted ones. Developed analytical models were validated with the experimental results and it was found that the analytical models can estimate the stiffness of those deficient and retrofitted I-joists with a fairly high accuracy.

## **PREFACE**

A portion of this research work has been submitted to peer-reviewed journals for publication. All analytical modeling, literature review and mathematical calculations presented in the following journal papers have been solely carried out by the author. The thesis supervisor was responsible for the research guidance and review of the work produced by the author.

### **List of Publications Related to this thesis**

- A version of Chapter 3 will be submitted to the Conference Proceedings, CSCE, May 30 - June 3, 2017, Vancouver, BC, Canada. M. Shahidul Islam, M.N. Islam, and M. Shahria Alam. Properties of Oriented Strand Board (OSB), timber and Glass Fiber Reinforced Polymer (GFRP) plate to evaluate the stiffness of retrofitted timber I-joist. I wrote the manuscript which was further edited by Dr. Alam.
- A version of chapter 4 has been published in the journal of Construction and Building Materials, 2015, M. Shahidul Islam, Md. Shahnewaz and M. Shahria Alam. Structural capacity of timber I-joist with flange notch: Experimental evaluation. I wrote the manuscript which was further edited by Dr. Alam.
- A portion of Chapter 4 has been published in Conference Proceedings, CSCE May 27-30, 2015 Regina, SK, Canada. M. Shahidul Islam, and M. Shahria Alam. Predicting Load Deflection Response of Wood I-Joists with Flange Notch. I wrote the manuscript which was further edited by Dr. Alam.
- A version of Chapter 5 will be submitted to the journal of Engineering Structures, 2016, Elsevier. M. Shahidul Islam, and M. Shahria Alam. Reinforced I-joists with Flange Notch: Experimental and Analytical Investigations. I wrote the manuscript which was further edited by Dr. Alam.



- A portion of Chapter 5 has been published in Conference Proceedings, CSCE June 01-04, 2016 London, ON, Canada. M. Shahidul Islam, Md. Shahnewaz and M. Shahria Alam. Retrofit of Wood I-Joists with Flange Notch. I wrote the manuscript which was further edited by Dr. Alam.
- A portion of chapter 6 has been published in Journal of Structural Engineering, ASCE. Md Shahnewaz, M Shahidul Islam, Moein Ahmadipour, Thomas Tannert, and M Shahria Alam 2014. Reinforced Wood I-Joists with Web Openings, Manuscript ID: STENG-4786. I conducted the partial analysis and wrote the manuscript which was further edited by Dr. Alam.
- A portion of chapter 6 has been published in World Conference on Timber Engineering (WCTE), 2016, August 22-25, Vienna, Austria. Md Shahnewaz, M Shahidul Islam, Thomas Tannert, and M Shahria Alam 2014. Reinforced Wood I-Joists with Web Openings, I conducted the partial analysis and wrote the manuscript which was further edited by Dr. Alam.
- A portion of chapter 6 has been published in Conference Proceedings, CSCE June 01-04, 2016 London, ON, Canada. Md Shahnewaz, M Shahidul Islam, Thomas Tannert, and M Shahria Alam 2016. Timber I-Joists with Web Openings: Reinforcement, Capacity Prediction and Sensitivity Analysis. I conducted the partial analysis and wrote the manuscript which was further edited by Dr. Alam.
- A portion of chapter 7 has been accepted to the Structure Congress, 2017, ASCE, Denver, Colorado, April 6-8. M. Shahidul Islam, and M. Shahria Alam. Retrofitting of wood I-Joist with Glass Fiber Reinforced Polymer (GFRP) Plates. I wrote the manuscript which was further edited by Dr. Alam.
- A portion of chapter 7 will be submitted to the Journal of Structural Engineering, ASCE, 2017. M. Shahidul Islam, and M. Shahria Alam. Retrofitting of Flange Notched or web holed

I-Joist with Glass Fiber Reinforced Polymer (GFRP) Plates. I wrote the manuscript which was further edited by Dr. Alam.

- A version of chapter 8 will be submitted to the Journal of Engineering Mechanics, ASCE, 2017. M. Shahidul Islam, and M. Shahria Alam. Performance Evaluation of Deficient and Retrofitted I-joists having a Flange Notch or Web Holes: An Analytical Approach. I conducted the analysis and wrote the manuscript which was further edited by Dr. Alam.

## TABLE OF CONTENTS

ABSTRACT .....	ii
PREFACE .....	iii
TABLE OF CONTENTS .....	vi
LIST OF TABLES .....	xiv
LIST OF FIGURES .....	xvii
LIST OF NOTATIONS .....	xxiv
ACKNOWLEDGEMENTS .....	xxv
DEDICATION .....	xxvi
CHAPTER 1: INTRODUCTION AND THESIS ORGANIZATION .....	1
1.1    General .....	1
1.2    Objectives of the Research .....	2
1.3    Scope and Significance of this Research .....	3
1.3.1    Material Property Characterization .....	4
1.3.2    Performance of Deficient I-joists with a Flange Notch or Web Hole .....	4
1.3.3    Performance of Retrofitted I-joist with OSB Collars .....	5
1.3.4    Performance of Retrofitted I-joist with GFRP Plates .....	5

1.3.5	Analytical Model Formulation for Deficient and Retrofitted I-joists .....	5
1.4	Outline of the Thesis .....	6
CHAPTER 2: Literature review .....		10
2.1	General .....	10
2.2	Wood Composite Products.....	11
2.2.1	Wood I-Joist.....	13
2.2.2	Oriented Strand Board .....	15
2.3	Opening in the Web of Wood I-joists .....	16
2.3.1	Retrofitting of Web Hole and Flange Notched I-joists .....	19
CHAPTER 3: Research Methodology and Characterization of Material Properties .....		21
3.1	General .....	21
3.2	Methodology of Experimental Program.....	22
3.3	Characterization of Material Properties .....	24
3.3.1	Properties of OSB .....	26
3.4	Properties of Timber.....	32
3.5	Properties of GFRP .....	35
3.6	Shear Properties.....	41
3.7	Constitutive Models .....	42
3.7.1	Validation of Constitutive Models.....	44

3.8	Summary .....	45
CHAPTER 4: Structural capacity of timber I-joist with flange notch: experimental evaluation		
	.....	46
4.1	General .....	46
4.2	Motivation .....	47
4.3	Literature Review .....	48
4.4	Testing of Timber I-joists with a Single Flange Cut.....	49
4.5	Results .....	52
4.5.1	Failure Mode and Load Deflection Response.....	52
4.5.2	Control I-Joists-Test Series 12-A & 20-A .....	52
4.5.3	Test Series 12-F & 20-K .....	55
4.5.4	Test Series 12-G & 20-L.....	59
4.5.5	Test Series 12-H & 20-M.....	61
4.5.6	Test Series 12-I & 20-N.....	63
4.6	Comparative Study .....	65
4.6.1	Effect of notch size and location.....	67
4.6.2	Crack Propagation Direction.....	71
4.7	Summary .....	72

CHAPTER 5: Performance of Retrofitted Flange Notched I-Joist with OSB Collars: An Experimental Investigation .....	74
5.1    General .....	74
5.2    Experimental Investigations of Timber I-joists with Flange Notches.....	75
5.2.1    Details of flange notch retrofitting.....	77
5.3    Results .....	79
5.3.1    Control I-Joists (Series 12-A/20A) .....	80
5.3.2    I-Joists with Notch (Series 12-F to 12-I and 20-K to 20-N) .....	80
5.3.3    Retrofitted Flange Notched I Joist (Series R-12-O to R-12-SF and R-20-O to R-20-SF)	87
5.3.4    Effect Analysis.....	94
5.4    Proposed Empirical Model to Estimate I-joist capacity .....	99
5.5    Summary .....	101
CHAPTER 6: Performance of Retrofitted Web Holed I-Joist with OSB Collars: Experimental Investigation .....	103
6.1    General .....	103
6.1.1    Composite I-joists .....	103
6.1.2    Web Holes in I-joists .....	104
6.1.3    Reinforcing of I-joists .....	107

6.1.4	Objective .....	108
6.2	Experimental Investigation .....	108
6.2.1	Materials .....	108
6.2.2	Specimen description .....	109
6.2.3	Reinforcement of I-joists .....	110
6.2.4	Methods.....	112
6.2.5	Results.....	112
6.2.6	Statistical Analyses .....	121
6.2.7	Proposed Analytical Model to Estimate I-joist capacity.....	123
6.3	Summary .....	126
CHAPTER 7: Performance of Retrofitted Flange NotchED and Web HoleD I-Joist with Glass		
Fiber Reinforced Polymer (GFRP) Plates: Experimental Investigation .....		128
7.1	General .....	128
7.2	Methodology .....	130
7.2.1	Fabrication of GFRP Reinforcers .....	130
7.2.2	Types of GFRP Based Flange-Notch Reinforcer (FNR) .....	134
7.2.3	Web Hole Reinforcer .....	137
7.2.4	Variations in Cross Sectional Profile: .....	139

7.2.5	Installation Procedure: .....	141
7.2.6	Experimental Procedure and Specimen Details .....	144
7.3	Results .....	148
7.3.1	Flange Notched I-Joists and its Retrofitting .....	148
7.3.2	Web Hole I-Joists Retrofitted with FRP Reinforcer .....	154
7.3.3	Comparison with Allowable Capacity and Stiffness .....	161
7.3.4	Failure Types and Location .....	162
7.4	Proposed Analytical Model to Predict Retrofitted I-joist capacity .....	165
7.5	Summary .....	168
CHAPTER 8: Performance Evaluation of Deficient and Retrofitted I-joists having a Flange Notch or Web Holes: An Analytical Approach .....		170
8.1	General .....	170
8.2	Methodology .....	173
8.2.1	Energy Method.....	173
8.1	Formulation of Models.....	175
8.1.1	Deflection for Mid-Span: .....	177
8.1.2	Maximum Deflection:.....	186
8.2	Validation of Analytical Models .....	190



8.2.1	Control I-joists .....	190
8.2.2	Flange Notched I-joists .....	191
8.2.3	Retrofitted Flange Notched I-joists.....	194
8.2.4	Web Holed I-joists .....	198
8.2.5	Retrofitted Web Holed I-joists.....	200
8.3	Summary .....	203
CHAPTER 9: CONCLUSIONS.....		205
9.1	Summary .....	205
9.2	Conclusion.....	205
9.2.1	Material Properties.....	205
9.2.2	Deficient I-joists.....	206
9.2.3	Retrofitted I-joists with OSB Collars.....	208
9.2.4	Retrofitted I-joists with GFRP Plates .....	208
9.2.5	Analytical Models .....	209
9.3	Limitations of the study.....	209
9.4	Recommendations for future research.....	210
REFERENCES .....		212
APPENDICES.....		220

Appendix A: Summary of Tested Flange notch I-joists.....	220
Appendix B: Mat lab Codes for Analytical Model Development based on <i>Castigliano's Second theorem</i> .....	221
Appendix C: Formulated Deflection Equations for Different I-joist (Control, Deficient & Retrofitted) .....	271
Appendix D: Validation of the Analytical Models .....	280

## LIST OF TABLES

Table 3.1 Summary of the Tension test of OSB in Longitudinal Direction (Sample Size, n=3)..	28
Table 3.2 Summary of the Tension test of OSB in Transverse Direction (Sample Size, n=3).....	30
Table 3.3 Summary of the Tension test of OSB in Diagonal (45°) Direction (Sample Size, n=3) .....	30
Table 3.4 Summary of the Tension test of Timber subjected to tension parallel to fiber (Sample Size, n=3) .....	35
Table 3.5 Summary of the Tension test of GFRP subjected to tension along Longitudinal Direction (Sample Size, n=3).....	38
Table 3.6 Summary of the Tension test of GFRP subjected to tension along Diagonal (D45 <sup>0</sup> ) Direction (Sample Size, n=3).....	38
Table 3.7 Summary of the Tension test of GFRP subjected to tension along Diagonal (D30 <sup>0</sup> ) Direction (Sample Size, n=3).....	40
Table 3.8 Shear Rigidity of OSB, Timber and GFRP .....	42
Table 3.9 Comparison of MOE based on Experimental Results and Developed Constitutive Models.....	45
Table 4.1: Specimen Details of I-Joist Testing .....	50
Table 4.2: Test Results of the I-Joist with flange cut at different location .....	57
Table 4.3: Comparison of ultimate load, stiffness and load at serviceability conditions of the I- joist with flange cut at different location .....	66
Table 4.4: Comparison of Calculated Moment and Measure Moment at the location of Notch at failure .....	69
Table 4.5: Propagation of Crack Growth of the I-Joist with flange cut at different location .....	72

Table 5.1: Specimen Details of I-Joist Testing .....	77
Table 5.2: Moment capacity ( $M_u$ ) and Moment at notch ( $M_{Ln}$ ) of reinforced flange notched I-Joists .....	82
Table 5.3: Load at Serviceability Conditions ( $\Delta=L/180$ & $\Delta=L/360$ ) .....	85
Table 5.4: Crack Growth Angles ( $\Theta$ ) .....	86
Table 5.5: Effect of Notch Reinforcer Length (Notch Size 100x100mm Located at 310mm from Support).....	98
Table 5.6: Comparison between experimental and predictions .....	101
Table 5.7: Performance of proposed models .....	101
Table 6.1: Summary of test series and test results .....	110
Table 6.2: ANOVA results for 12 feet I-joists .....	121
Table 6.3: ANOVA results for 20 feet I-joists .....	122
Table 6.4: Comparison between analytical models for I-joists with openings .....	124
Table 6.5: Comparison between analytical models for reinforced I-joists .....	126
Table 6.6: Performance of analytical models for I-joists with openings .....	126
Table 7.1 Mechanical properties of Timber, OSB and GFRP. ....	129
Table 7.2 Proportion of Resin Mixture for GFRP Reinforcer.....	132
Table 7.3 GFRP Reinforcer Dimensions.....	133
Table 7.4 Specimen details of Flange Notched I-Joists reinforced with FRP Reinforcer. ....	146
Table 7.5 Specimen details of Web holed I-Joists reinforced with FRP Reinforcer. ....	147
Table 7.6 Summary of Failure Location and Types occurred in Tested Flange Notched I-Joists reinforced with FRP Reinforcer. ....	163

Table 7.7 Summary of Failure Location and Types occurred in Tested Web Holed I-Joists reinforced with FRP Reinforcer. ....	165
Table 7.8 Comparison between experimental and predicted Capacity ( $P_u$ ) for Retrofitted Flange Notched I-joist with GFRP reinforcers .....	167
Table 7.9 Comparison between experimental and predicted Capacity ( $P_u$ ) for Retrofitted Web Holed I-joist with GFRP reinforcers .....	167
Table 7.10 Performance evaluation of proposed models .....	168
Table 8.1 Performance of Analytical models of Control and Flange Notched I-joists. ....	194
Table 8.2 Performance of Analytical models of Flange Notched I-joists Retrofitted with OSB Collars (Type 2). ....	196
Table 8.3 Performance of Analytical models of Flange Notched I-joists Retrofitted with GFRP Plates (Type T-1, T-2 & T-3).....	196
Table 8.4 Performance of Analytical models of Web Holed I-joists. ....	198
Table 8.5 Performance of Analytical models of Web Holed I-joists Retrofitted with OSB Collars. ....	201
Table 8.6 Performance of Analytical models of Flange Notched I-joists Retrofitted with GFRP Plates (Type T-1, T-2 & T-3).....	203
Table A.1: Measured Shear ( $V_u$ ), Ultimate Moment ( $M_u$ ), Failure Moment at Notch location ( $M_{Ln}$ ) and Maximum Deflection ( $\Delta$ ) for each type of failure occurred in all tested I-joists .....	220

## LIST OF FIGURES

Figure 1.1: I-joists with flange notch and web hole at construction site.....	3
Figure 1.2: Outline of the thesis .....	8
Figure 2.1 Classification of wood composite panels by density, particle size, and process (Youngquist 2010, Suchsland and Woodson 1986).....	13
Figure 2.2 Different type of web - flange joints: a) Tapered groove and web; b) Web nailed or bonded to double flanges; c) Routed groove with square-edged web; d) Y-groove with split web and e) Routed groove with split web (adapted from Leichti et al. 1989 and CWC 2016). .....	14
Figure 2.3 A typical stress-strain response of OSB under Tension and Compression (Zhu 2003; Zhu et al. 2005a, 2007b) .....	16
Figure 2.4 Manufacturer Guidelines for making holes in the web of I-joists (Weyerhaeuser-Trus- Joist 2014) .....	17
Figure 2.5 Tangentail Stress distribution around a web opening (Polocoser et al. 2013; Zhu 2003) .....	19
Figure 3.1: Experimental setup of a retrofitted I-Joists with flange notch and cross sectional dimensions of the tested I-joists (dimensions are in mm).....	22
Figure 3.2: Testing Frame used to perform four points bending test of I-Joists (With a 12 ft Control I-Joist). .....	24
Figure 3.3: Details of OSB coupon specimen for tension test. ....	25
Figure 3.4 Sample of a OSB Tension test specimen with a Bi-axial Strain Gauge .....	26
Figure 3.5 Stress-strain response of OSB subjected to tension along the strong axis of the OSB panel. ....	27

Figure 3.6 Stress-strain response of OSB subjected to tension along the Transverse direction of the OSB panel. ....	29
Figure 3.7 Stress-strain response of OSB subjected to tension along Diagonal (45°) direction of the OSB panel. ....	31
Figure 3.8 Details of Timber coupon specimen for tension test. ....	33
Figure 3.9 Stress-strain response of Timber subjected to tension parallel to fiber .....	34
Figure 3.10 Glass Fiber Reinforced Polymer (GFRP) Test Specimen Details .....	36
Figure 3.11 Tested specimens and Stress-strain response of GFRP subjected to tension along the longitudinal direction of the GFRP plate .....	37
Figure 3.12 Tested specimens and Stress-strain response of GFRP subjected to tension along the Diagonal direction (45°) of the GFRP plate .....	39
Figure 3.13 Tested specimens and Stress-strain response of GFRP subjected to tension along the Diagonal direction (30°/60°) of the GFRP plate. ....	40
Figure 3.14 Constitutive Models for OSB and Timber (SPF).....	42
Figure 3.15 Constitutive Models for GFRP a) Longitudinal Direction b) Diagonal 45° Direction c) Diagonal 30° Direction .....	44
Figure 4.1: Flange notched I-joists at construction site .....	47
Figure 4.2: Schematic diagram of the test setup and flange notched I joist.....	50
Figure 4.3: Typical failures: a, b) Failure due to presence of knot; c) Web-flange de-bonding; d, e) flexural failure; f) shear failure; g, h) Combined shear and flexural failure .....	54
Figure 4.4: Load-deflection curves for series 12-A and 20-A .....	55
Figure 4.5: Failure mechanisms exhibited in tested I-joists with flange notch (Series: 12-F, 12-G, 12-H, 12-I, 20-K, 20-L, 20-M, and 20-N).....	58

Figure 4.6: Failure mechanisms exhibited in 20-K-09 I-joist due to presence of knots .....	58
Figure 4.7: Load-deflection curves for series 12-F & 20-K.....	59
Figure 4.8: Failure mechanisms exhibited in I-joist 20-L-07.....	61
Figure 4.9: Box Plot of Load Capacity of 12ft (3.65m) and 20ft (6.1m) I-joists (A-Controls and 12-F, 12-G, 12-H, 12-I, 20-K, 20-L, 20-M, 20-N with Flange Cut).....	67
Figure 4.10: Effect of Notch Distance from Support (Notch Size: 100×100 mm) .....	68
Figure 4.11: Effect of Notch Size (Notch Distance 455mm from Support) .....	71
Figure 5.1: Schematic of Retrofitted I-Joists with flange notch and lateral supports along the length (dimensions are in mm).....	76
Figure 5.2: Details of Flange Notch Reinforcer (Note: Red dots represent nails) .....	79
Figure 5.3: Comparison of Capacity of Retrofitted Flange Notched I Joists (12 ft & 20ft) .....	81
Figure 5.4: Moment at notch location of flange notched I-joists. ....	84
Figure 5.5 Crack growth direction in I-joist with a flange notch. ....	87
Figure 5.6: Load –Deflection Curves for different reinforced I-Joist series having a Flange Notch. ....	89
Figure 5.7: Different types of failure occurred in reinforced flange notched I-Joists.....	93
Figure 5.8: Effect of Notch Location for 100 mm x 100 mm Notch a) Ultimate Moment ( $M_u$ ), b) Moment at Notch Location ( $M_{Ln}$ ) .....	95
Figure 5.9: Effect of Notch Size (Notch Distance 455mm from Support) a) Ultimate Moment ( $M_u$ ), b) Moment at Notch Location ( $M_{Ln}$ ) .....	97
Figure 5.10: Predicted vs experimental capacity of unreinforced and reinforced I-joists with flange notches .....	100



Figure 6.1: Schematic of I-Joists with web opening and retrofitting (left), cross section (right), and lateral support along the length (dimensions are in mm). .....	109
Figure 6.2: Retrofit of I-joists with two OSB ply in collar system .....	111
Figure 6.3: Average load-deflection for I-joists test series with opening (a) 12ft span (b) 20ft span and for retrofitted I-joists test series (c) 12ft span (d) 20ft span .....	113
Figure 6.4: Typical failures for I-joists test series A to E .....	115
Figure 6.5: Typical failures for retrofitted I-joists test series F to J .....	116
Figure 6.6: Comparison of capacity: (a)12 feet I-joists (top) and (b) 20 feet I-joists (bottom) ..	117
Figure 6.7: Comparison of Stiffness: (a)12 feet I-joists (top) and (b) 20 feet I-joists (bottom) .	118
Figure 6.8: Experimental vs predicted capacity of different models for (a) I-Joists with opening and (b) Retrofitted web hole I-Joists.....	125
Figure 7.1: Type T-1- Flange Notch Reinforcer Reinforcers a) Option-1 and b) Option-2.....	134
Figure 7.2: Type T-2- Flange Notch Reinforcer a) Part-1 and b) part- 2.....	135
Figure 7.3: Type T-1- Web Hole Reinforcers a) Option-1 and b) Option-2. ....	137
Figure 7.4: Type T-2 Web Hole Reinforcer a) Part-1 and b) Part-2 .....	138
Figure 7.5: Different Cross Sectional Profiles for Flange Notch Reinforcer .....	139
Figure 7.6: Different Cross Sectional Profiles for Web Hole Reinforcer .....	140
Figure 7.7: Installation Steps of Flange Notch Reinforcer (Type 2).....	142
Figure 7.8: Different types of GFRP based Reinforcers a) Flange Notch Type T-1; b) Web Hole Type T-1; c) Flange Notch Type T-2; d) Web Hole Type T-2; e) Flange Notch Type T-3; and f) Web Hole Type T-3 .....	143
Figure 7.9: Experimental setup of GFRP retrofitted I-Joists with flange notch and cross sectional dimensions of the tested I-joists (dimensions are in mm).....	144

Figure 7.10: Comparison of Structural Capacity ( $P_u$ ) of 12 ft flange notched I-Joists .....	149
Figure 7.11: Average Load-Deflection response of 12 ft flange notched I-Joists a) 100x100 mm Notch at 610 mm and b) 100x150 mm Notch at 455 mm.....	150
Figure 7.12: Comparison of Stiffness (K) of 12 ft flange notched I-Joists.....	151
Figure 7.13: Comparison of Capacity ( $P_u$ ) of 20 ft flange notched I-Joists .....	152
Figure 7.14: Average Load-Deflection response of 20 ft flange notched I-Joists a) 100x100 mm Notch at 610 mm and b) 100x150 mm Notch at 455 mm.....	153
Figure 7.15: Comparison of Stiffness (K) of 20 ft flange notched I-Joists.....	154
Figure 7.16: Comparison of Capacity ( $P_u$ ) of 12 ft web holed I-Joists .....	156
Figure 7.17: Average Load-Deflection response of 12 ft web holed I-Joists a) 200 mm Dia Hole at 305 mm and b) 150 mm Dia Hole at 305 mm.....	157
Figure 7.18: Comparison of Stiffness (K) of 12 ft web holed I-Joists.....	158
Figure 7.19: Comparison of Capacity ( $P_u$ ) of 20 ft web holed I-Joists .....	159
Figure 7.20: Average Load-Deflection response of 20 ft web holed I-Joists a) 200 mm Dia Hole at 305 mm and b) 150 mm Dia Hole at 305 mm.....	160
Figure 7.21: Comparison of Stiffness (K) of 20 ft web holed I-Joists .....	161
Figure 7.22: Types of Failure occurred in I-joists Retrofitted with GFRP reinforcers a) Flange Notch Failure: Type T-1; b) Web Hole Failure: Type T-1; c) Flange Notch Failure: Type T-2; d) Web Hole Failure: Type T-2; e) Flange Notch Failure: Type T-3; and f) Web Hole Failure: Type T-3.....	164
Figure 7.23: Predicted vs experimental capacity of I-joists retrofitted with GFRP reinforcers with a) flange notch and b) web hole. ....	168
Figure 8.1 Flexural and Shear Stress Distribution of I-Joist sections a) Control, b) Web Hole & c) Flange Notch. ....	171

Figure 8.2 Flow chart for calculating the maximum deflection of a flange notched or web holed I-joists.....	176
Figure 8.3 Application of Castigliano’s theorem to develop the analytical models for control I-joists. ....	178
Figure 8.4 Application of Castigliano’s theorem to develop the analytical models for flange notched I-joists. ....	179
Figure 8.5 Application of Castigliano’s theorem to develop the analytical models for retrofitted flange notched I-joists.....	182
Figure 8.6 Comparison between Analytical Models and Experimental Results of Control I-joists. ....	192
Figure 8.7 Comparison between Analytical Models and Experimental Results of Flange Notched I-joists.....	193
Figure 8.8 Comparison between Analytical Models and Experimental Results of Flange Notched I-joists Retrofitted with OSB Collars (Type 2). ....	195
Figure 8.9 Comparison between Analytical Models and Experimental Results of Flange Notched I-joists Retrofitted with GFRP Plates (Type 1 & Type 2). ....	197
Figure 8.10 Comparison between Analytical Models and Experimental Results of Web Holed I-joists. ....	199
Figure 8.11 Comparison between Analytical Models and Experimental Results of Web Holed I-joists Retrofitted with OSB Collars. ....	202
Figure 8.12 Comparison between Analytical Models and Experimental Results of Flange Notched I-joists Retrofitted with GFRP Plates (Type 1 & Type 2). ....	203
Figure C.1 Loading and Support Condition of Control I-Joists.....	271
Figure C.2 Loading and Support Condition of Flange Notch I-Joists .....	272

Figure C.3 Loading and Support Condition of Retrofitted Flange Notch I-Joists .....274

## LIST OF NOTATIONS

$P_c$	<i>Virtual load <math>P_c</math> for calculation of deflection</i>
$P_u$	<i>Load Capacity/ Ultimate Load</i>
$M_u$	<i>Moment Capacity/ Ultimate Moment</i>
$A_c, x_c$	<i>Location of virtual load <math>P_c</math></i>
$L_e, L_n$	<i>Location of Notch or Hole from the support</i>
$L$	<i>Span Length</i>
$B_n, b_n$	<i>Notch Width</i>
$D_n, d_n$	<i>Notch Depth</i>
$\emptyset$	<i>Diameter of Web Hole</i>
$D$	<i>Depth of I-Joist</i>
$b_f$	<i>Breadth of Flange</i>
$h_f$	<i>Height of Flange</i>
$t_w$	<i>Thickness of Web</i>
$h_w$	<i>Height of Web</i>
$L_r$	<i>Length of Reinforcers</i>
$L_d$	<i>Length of Reinforcers (Extended either side of the notch or hole)</i>
$E, E_n, E_r, E_{rn},$	<i>Modulus of Elasticity</i>
$G, G_n, G_r, G_{rn},$	<i>Modulus of Rigidity</i>
$f_s, f_{s_n}, f_{s_r}, f_{s_{rn}},$	<i>Form Factors</i>
$U_i$	<i>Internal Strain Energy Stored in the Body</i>
$U_w$	<i>External Work Done by the External Forces on The Body</i>
$P.F.$	<i>Performance Factor</i>
$K$	<i>Flexural/ Bending Stiffness of I-Joist</i>
$\Delta, y$	<i>Deflection</i>

## ACKNOWLEDGEMENTS

First, I would like to convey my profound respect and gratitude to the almighty Allah for blessing me with this achievement in life. I also express my sincere gratitude to my advisor, Dr. M. Shahria Alam for providing me with an opportunity to work with him at The University of British Columbia. I couldn't have asked for a better mentor and guide for my Doctoral program and I really appreciate all the support, guidance, and motivation that he has provided me through my academic career. He has been instrumental with knowledge, support, and mentoring that made my graduate experience at UBC so immaculately productive and rewarding, and made a great contribution to the success of this research.

I would like to thank my doctoral dissertation committee members, Dr. Ahmad Rteil and Dr. Kasun Hewage for always supporting my research work and providing me with great feedback from time to time, helping me improve the quality of my work immensely. Graduate school and experimental research facility at UBC's Okanagan campus has provided an excellent educational experience, and I would like to acknowledge the support I have received for pursuing a graduate degree at this Institution from Natural Sciences and Engineering Research Council of Canada (NSERC), Mitacs Accelerates Program and my industry sponsor AcuTruss Industries Ltd.

I feel privileged to get the opportunity to work with such an excellent group of graduate students in the research group especially Shahnewaz, Moein, Kader, Ashish, Mosharef, Rashed, Anant, Upol, Rafiqul, Zarah and Farshad who helped me during my experimental works, offered technical knowledge, and friendship. I would also like to acknowledge Dr. Nouroz Islam for his generous help in setting up the data acquisition system. I offer my enduring gratitude to the assistance of UBC Structures Laboratory Technicians especially Ryan Mandu, Alec Smith and Kim, for assistance with the test setup and specimen preparations.

I am truly grateful for the unconditional support of my family, without which I would likely not be here today. My parents have offered endless support, confidence in me, wise advice, and love. I am especially indebted to my wife, Jakia and my son Raiyan, for being with me and supporting me through the past years. Their support, sacrifice, and enduring love have meant the world to me throughout this process and always.

*Dedicated to my parents*  
*Mr. Mohammad Nurul Islam*  
*&*  
*Mrs. Rahima Begum*

# CHAPTER 1: INTRODUCTION AND THESIS ORGANIZATION

## 1.1 General

Timber is one of the most primitive, easiest and readily available materials to the mankind to build their shelters, and indeed it is still popular as a contemporary building material in different forms such as, solid sawn lumber, Structural Composite Lumber (SCL), Engineered Composite Timber (I-Joists), Cross Laminated Timber (CLT), Glued Laminated Timber (Glulam) etc. (*Zhu 2003*). I-joist is an engineered wood product that is cheaper, lighter in weight, stronger, and more efficient compared to the solid sawn lumber beams having similar capacity. Composite timber I-joists are widely used as floor and roof joists in the construction of commercial and residential buildings in Europe and North America. Commonly, these I-joists are made with timber or laminated veneer lumber (LVL) as flange material in combination with Oriented Strand Board (OSB) or Plywood as web materials. These structural engineered timber I-joists are less expensive, lighter in weight, stronger, and more efficient compared to the solid sawn lumber beams.

During wood frame construction, web holes and flange notches are made for passage of service ducts, plumbing and wiring. This makes the use of I-joists more popular in wood building construction because they allow builders to hide the utility services and thus reduce the floor thickness. But the presence of the opening can lead to the misuse of the I-joist in two ways: a) to facilitate the utility efficiently carpenters may unintentionally drill web opening and b) sometimes carpenters may neglect to install proper bracing, web stiffeners or end connections. Eventually, the ultimate capacity and stiffness of the I-joist section get reduced significantly. This phenomenon



will be more critical in the cases of web opening at shear span and flange notch at mid span. This may lead to the I-joist fails in premature shear or flexure which is sudden and brittle.

According to the Canadian Standard for Wood Design (CSA-O86) (*Canadian-Standard-Association 2014a*) and manufacturer design guidelines (*American-Wood-Council 1999*), (Wood I-Joist Manufacturers Association (WIJMA) 2008) flange cut on OSB webbed I-joists are strictly prohibited in the I-joist based flooring systems. Cuts and notches in the flange of I-joist are commonly made during construction to facilitate the electro-mechanical systems of the buildings. Some photographs of flange notches and web holes in a construction site have been shown in *Figure 1.1*. Those buildings were not fully loaded while those were being constructed, this might be the reason that those buildings had not experienced any failure after making those holes and flange notches. The effect of flange notches on the strength properties (e.g. load carrying capacity, flexural strength, and shear strength) of timber I-joists is not fully understood. Current design specifications (*CSA-O86*) for building construction also do not provide any design guideline for I-joists with flange cut and notches (Canadian-Standard-Association 2014a). Very few research studies on OSB webbed timber I-joists with flange cut and notch have been conducted (*Hindman and Loferski 2008*).

## **1.2 Objectives of the Research**

The primary objective of this study is to evaluate the performance of retrofitted I-joist having a flange notch or a web hole with different retrofitting technique. To this end, the following sub-objectives will be studied:

- i. Experimental investigation of the performance of deficient I-joists having a flange notch or web hole.

- ii. Experimental investigation of the performance improvement of retrofitted I-joists having a flange notch or web hole with different retrofitting techniques.
- iii. Development of an analytical model to evaluate the performance of deficient I-joists with a flange notch or web hole.
- iv. Development of an analytical model to evaluate the performance of retrofitted I-joists having a flange notch or a web hole with different retrofitting techniques.



Flange Notched I-Joists



Web Holed I-joists

***Figure 1.1: I-joists with flange notch and web hole at construction site***

### **1.3 Scope and Significance of this Research**

This research addresses an important issue that affects the performance of I-joist-based floor and roof systems. This study determines the performance of flange notched or web holed I-joists and provides different retrofitting techniques to improve their performance. As per the current

design guideline CSA O-86 (section 15.2.3.3), any kind of flange notch in prefabricated I-joist is not permitted (Canadian-Standard-Association 2014a). However, flange notches are frequently made in construction sites, which require a definite retrofitting guideline. The research will assist in developing guidelines for retrofitting of flange notched or web holed I-joists in floor design and its associated performance.

This study is original in terms of the problems addressed (i.e. performance of flange notched I joists, analytical expression for deflection of flange notched I joist, crack growth propagation direction) and methodology used. This research presents a novel approach for repairing I-joists commonly used in wood building construction, which will be a fast, efficient and economic method. To achieve the stated goal in the objectives the followings were carried out:

### **1.3.1 Material Property Characterization**

Characteristic stress-strain relationships of Timber, OSB and GFRP are an indispensable requirement for the analytical and numerical analysis of structures containing OSB panels, timber and Glass Fibre Reinforced Polymer (GFRP). However, most of the available literature focused only on the ultimate strength of these materials and did not considered the non-linearity or plasticity of the relationships. The objective of Chapter 3 is, therefore, to obtain material properties of OSB, Timber and GFRP in a way which could help develop constitutive models for analytical and numerical analysis.

### **1.3.2 Performance of Deficient I-joists with a Flange Notch or Web Hole**

Before retrofitting it is important to understand the behavior of deficient I-joists due to the presence of flange notch and web opening. To understand the effects of notch or hole location and size, four series of I-joists were tested for both types of deficient (Flange Notch & Web Hole) I-

joists. Total 180 four point bending tests were performed on 12ft and 20ft I-joists where the number of control, flange notch and web hole I-joists specimens were 20, 80 and 80, respectively. Flange Notched I-joists had two different sizes of notch (100x100mm & 100x150mm) and at three different locations (300, 455 & 600mm from support). Web Hole I-joists had three different sizes of opening ( $\varnothing=100\text{mm}$ , 150mm & 200mm) and at three different locations (305, 610 & 915mm from support).

### **1.3.3 Performance of Retrofitted I-joist with OSB Collars**

To improve the performance of deficient I-joists due to the presence of flange notch and web hole, different retrofitting techniques with OSB collars were employed and tested. Total 220 bending tests were performed on 12ft and 20ft retrofitted I-joists where the number of retrofitted flange notch and web hole I-joists specimens were 120 and 100, respectively.

### **1.3.4 Performance of Retrofitted I-joist with GFRP Plates**

To improve structural capacity further to make the deficient I-joists comparable to the control I-joists, Glass Fiber Reinforced Polymer (GFRP) plates were used to retrofit timber I-joists containing a notch at the top flange and a hole or opening in the web. Three types (T-1, T-2 & T3) of GFRP reinforcing plates were employed to retrofit 27 flange notched and 27 web holed I-joists for two span lengths (12ft & 20 ft).

### **1.3.5 Analytical Model Formulation for Deficient and Retrofitted I-joists**

As the last objective of this thesis an analytical approach was used to evaluate the performance of the deficient and retrofitted flange notched and web holed I-joists. Proposed analytical model were validated by comparing with the experimental results conducted to achieve earlier goals.

## 1.4 Outline of the Thesis

This thesis is organized in nine chapters. The outline of the thesis is depicted in *Figure 1.2*. In the present chapter (**Chapter 1**) a short preface, research objectives and scope are presented. The content of this thesis is organized into the following chapters:

In **Chapter 2**, as only a handful study exists on flange notch I-joists, the author has carried out a comprehensive literature review on timber I-joists with a web hole and its retrofitted one. Several important experimental studies on the behavior of timber I-joists are reviewed.

In **Chapter 3**, overall methodology of the experimental program to evaluate the performance of I-joist with different flange notch and web hole has been discussed. In addition to that, engineering material properties of OSB, Timber and GFRP has been evaluated by conducting a set of tension tests in different directions. Finally, constitutive models were proposed and validated with experimental results for each material.

In **Chapter 4**, performance of flange notched I-joists has been evaluated in terms of the load carrying capacity, stiffness, crack growth angle and compared with the control I-joist's performance based on the experiment conducted on 80 flange notched I-joist specimens with a 12ft and 20ft span lengths. In addition to that, twenty control I-joists has also been tested for the comparison purpose. Effects of size and locations of flange notch have also been discussed.

**Chapter 5** demonstrates a comparative study of performance of retrofitted flange notched I-joists with two different types of retrofitting technique with OSB collars and flange notched I-joists. To do this end, a total of 120 retrofitted I-joists have been tested on 12ft and 20ft span lengths. Best fitted load-deflection ( $P-\Delta$ ) responses of retrofitted I-joists and flange notched I-joists

have been plotted and compared with the control I-joist's load-deflection ( $P-\Delta$ ) responses. Finally, a prediction model was proposed based on the experimental results and validated with the experimental results.

In **Chapter 6**, based on the four point bending test of 80 web holed and 100 retrofitted web holed I-joists, a comparative study of performance of retrofitted web hole I-joists with OSB collars and web holed I-joists has been presented. Best fitted load-deflection ( $P-\Delta$ ) responses of retrofitted web holed I-joists and deficient web holed I-joists have been plotted and compared with the control I-joist's load-deflection ( $P-\Delta$ ) responses. Finally, a prediction model was proposed based on the experimental results and compared with the experimental results and other proposed models available in the literature.

**Chapter 7** demonstrates the fabrication process of Glass Fiber Reinforced Polymer (GFRP) based reinforcers for retrofitting of flange notch and web hole. It also provides the detail application process of attaching these reinforcers to the deficient I-joists with Sikadur 30 adhesives. A comparative study of performance of retrofitted flange notch & web hole I-joists with GFRP plates and OSB collars has been presented. Best fitted load-deflection ( $P-\Delta$ ) responses of retrofitted flange notch & web hole I-joists with GFRP plates and OSB collars I-joists have been plotted and compared with the control I-joist's load-deflection ( $P-\Delta$ ) responses. Finally, a prediction model was proposed based on the experimental results and validated with the experimental results.

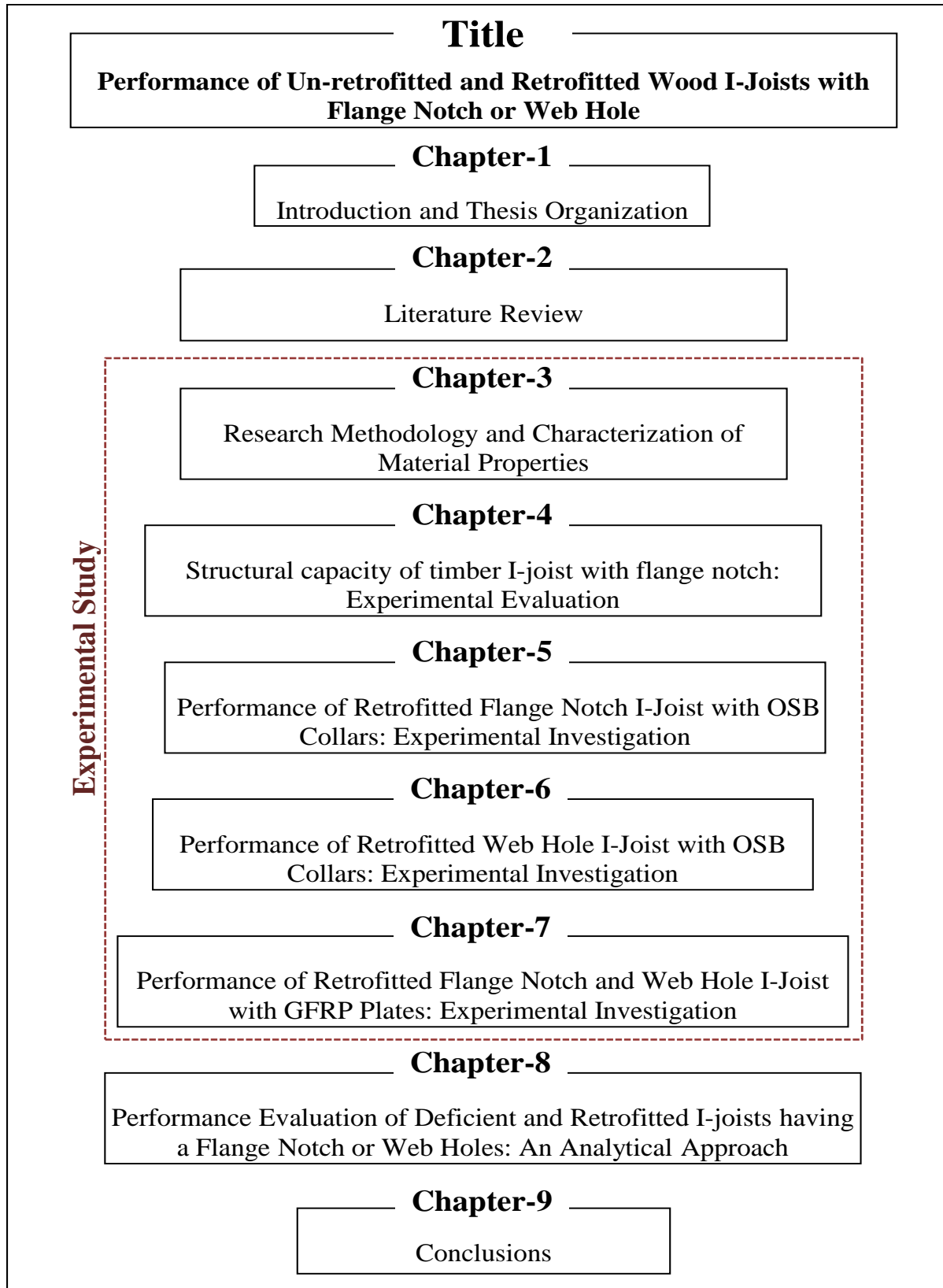


*Figure 1.2: Outline of the thesis*

**Chapter 8** demonstrates an analytical procedure to develop models for evaluating the performance of flange notched, web holed and their retrofitted one. Based on the conservation of energy, i.e.  $U_i=U_e$  (also known as **Castigliano's Second theorem**) of the I-joists, models were developed and validated with the experimental results for deficient and retrofitted I-joists.

Finally, **Chapter 9** presents the conclusion of this research. Some recommendations for future research on this topic have also been suggested in this chapter.



## CHAPTER 2: LITERATURE REVIEW

### 2.1 General

The aim of this chapter is to collect up-to-date information on the behavior of timber I-joist and their retrofitting or strengthening techniques for a structurally deficient I-joist due to the presence of a web hole and flange notches. A good number of studies on the composite timber I-joists are available (Afzal et al. 2006; Aschheim et al. 2010; Chen et al. 2015; Chui et al. 2005; Clinch 1993; Damery 2006; Davids et al. 2011; Grandmont et al. 2010a; Harte and Baylor 2011; Hindman and Loferski 2008; Islam et al. 2015; Koz and Hulimka 2014; Morrissey et al. 2009; Pirzada et al. 2008; Polocoser et al. 2012; Wisniewski and Manbeck 2003; Wu and Asce 2014; Zhang et al. 2010; Zhu et al. 2006, 2007a) which mostly highlighted the effects of web hole and their retrofitting with OSB collar on the overall performance of I-joists. Leichti et al. (1989, 1990) conducted an extensive review on the existing literature available till late 1980s. However, this study only focused on summarizing the existing retrofitting techniques to improve the performance of deficient I-joists due to web hole and flange notch without providing any insight into the potential of different types of retrofitting techniques. However, a significant amount of research work was conducted over the last 2 decades and different types of reinforcers were introduced or proposed to retrofit deficient I-joists.

During construction, openings are often introduced to the webs of wood I-joists for passage of service ducts, plumbing and wiring. It allows builders to hide the utility services and reduce the floor height. But the presence of the web openings leads to the reduction in stiffness and capacity of I-joists. This phenomenon is the most critical in the cases of web openings that are close to supports and may cause I-joists to fail in premature sudden and brittle shear. The current edition

of the Canadian Standard for Engineering Design in Wood (*CSA086 2014*) provides no guidance for such openings in I-joists. The National Design Specification for Wood Construction in the US (*NDS 2015*) recommends manufacturer specifications for I-joists with openings.

*Zhu et al. (2005)* investigated the failure load of wood I-joists with and without web openings using finite element analyses (FEA) and observed that the joist capacity decreases linearly with opening size, whilst location of opening has little effect on the reduction of capacity; however, their model significantly under-estimated the capacity of a joist with openings. *Zhu et al. (2007)* developed additional models to predict I-joist failure considering material nonlinearity and crack propagation and achieved a better fit with experimental results. *Pirzada et al. (2008)* developed another mechanics-based method to predict the capacity of wood I-joists with circular web holes and achieved conservative predictions. *Guan and Zhu (2004)* performed non-linear FEA to predict the behavior of wood I-joists with openings where the opening sizes varied from one-quarter to three-quarter of the height of the I-joists. A good correlation was found between tests and FE results. They observed that the predicted capacity for I-joist with circular openings was 20% higher than the I-joists with rectangular openings. In their recent study, *Guan and Zhu (2009)* developed anisotropic elasto-plastic constitutive models that are able to identify the location of initial crack, the growth of crack, the stress states, the capacity of wooden I-joist.

## **2.2 Wood Composite Products**

High quality and larger size of timbers are becoming ever more expensive due to its unavailability and required time to grow trees. Hence, wood industry emerging to an alternative solution to make Engineered Wood Products (EWP) or Wood Composite Products, which helps provide a viable solution in terms of sustainability issues. Wood based composites are referred to

as a biologically degradable composites (*Bledzki et al. 2002*). It is reported that the wastage of material to produce solid timber is about 60% whereas the wastage of material to produce a useful engineered/composite timber product is about 10-20% depending on the type of EWP being produced. This lower wastage is possible for EWP as these products are made with a smaller dimensions of wood (e.g. Strand, Fiber, Flakes, Veneer etc.) and adhesives as a raw material to produce a larger sized composite elements (e.g. beams, panels, sheets etc.) (*Rainforest Information Centre 2016*). To meet the engineering and architectural desires to utilize the sustainable features of timber in homogeneous and planar elements, timber can be broken down into sequentially smaller fractions which can then be reassembled into glued composite members, labelled engineered wood products (EWPs) (*Vallée et al. 2016*). Depending on the wood fraction used as raw material, EWPs can be classified into lumber-based such as Glued-Laminated-Timber, veneer-based such as plywood or Laminated Veneer Lumber (LVL), strand-based such as Oriented Strand Board (OSB) or Laminated-Strand-Lumber (LSL), and particle-based products such as Fiber-board. Different types of composite panels produced around the world based on the different processes (dry or wet), and raw materials has been presented in *Figure 2.1*.

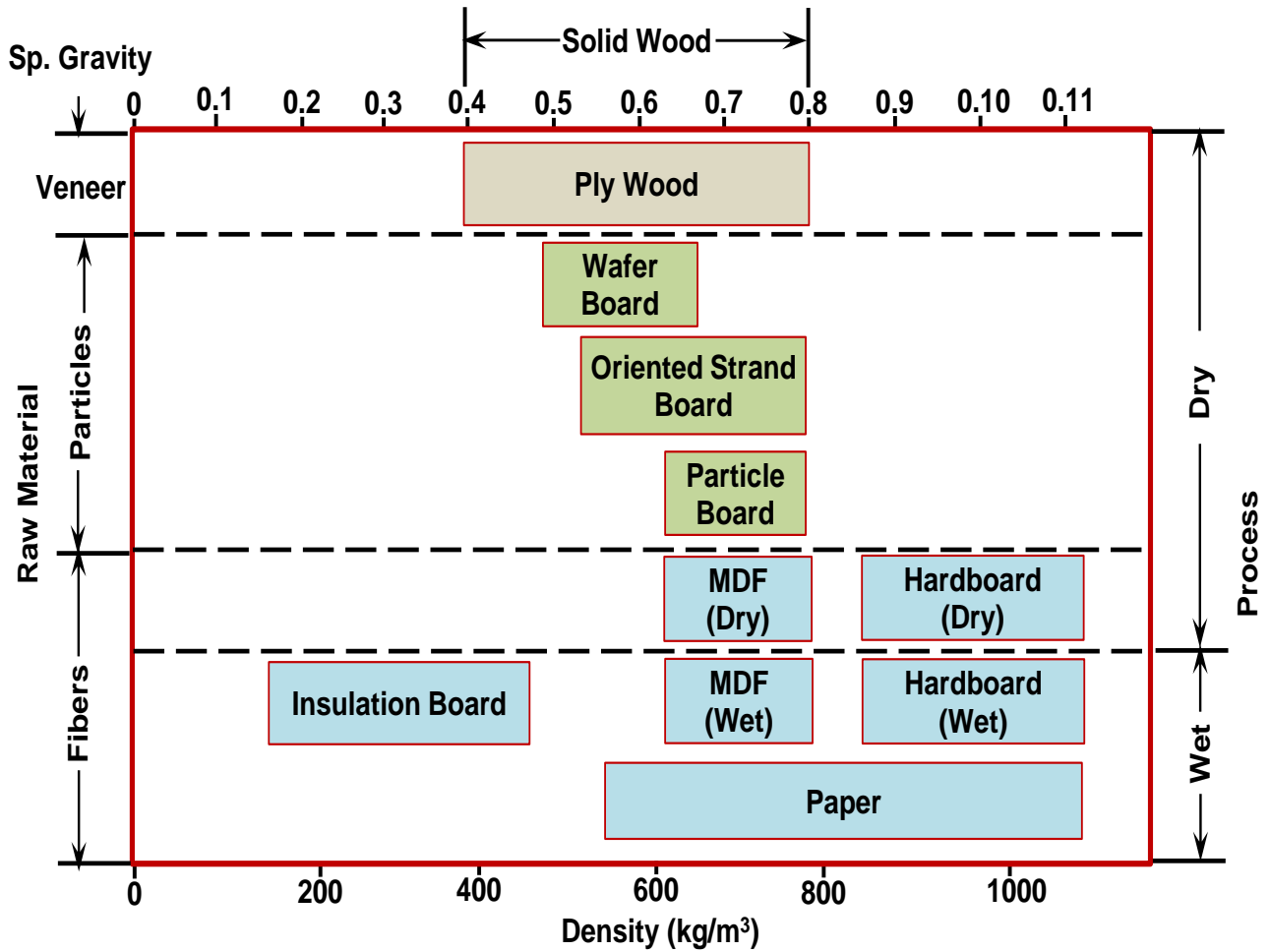


*Figure 2.1 Classification of wood composite panels by density, particle size, and process (Youngquist 2010, Suchsland and Woodson 1986)*

### 2.2.1 Wood I-Joist

Wood I-joist is a prefabricated proprietary structural wood products made with two flanges connected with a thin web. Generally, flanges are made with structurally graded solid sawn lumber or laminated veneer lumber (LVL) and webs are made with thin composite materials (e.g. plywood or Oriented Strand Board panel). Webs of prefabricated wood I-joists must meet the requirements of the CSA O121, CSA O151, CSA O153 (Exterior Bond), or CSA O325 (Canadian-Standard-Association 2013a; b, 2014b, 2016). Exterior rated phenol-formaldehyde and phenol-resorcinol are the most commonly used adhesives to attach the web to the flanges and web to web joints

(CWC 2016). The web-flange bond is one of the most critical factors to achieve the specified strength and capacity of the wood I-joist. Different types of web to flange joints are presented in **Figure 2.2**. (Zhang et al. 2010) investigated the bonding behavior of joints between flange and web (OSB and Plywood) of I-joists. They discovered that the tanks depth and length of the joint are the most significant factors for the web-flange joints of I joist.

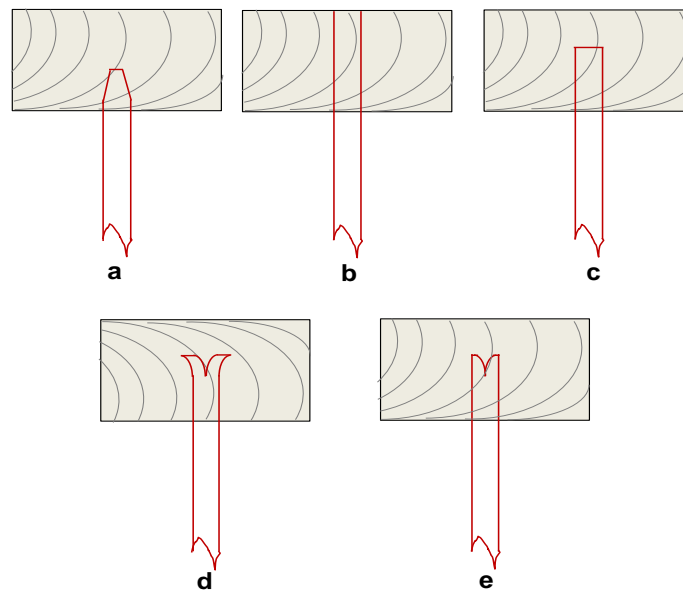


**Figure 2.2** Different type of web - flange joints: a) Tapered groove and web; b) Web nailed or bonded to double flanges; c) Routed groove with square-edged web; d) Y-groove with split web and e) Routed groove with split web (adapted from Leichti et al. 1989 and CWC 2016).

Another research study was conducted by (Koz and Hulimka 2014) on hybrid timber-glass I-beams. Based on their experimental study, it is found that the capacity of timber glass hybrid I-beams are much higher than the load at which the glass web initiates to crack. They have also conducted an analytical and numerical analysis for the timber glass hybrid I-beams and they have found that the numerical models with the used parameters suitably simulate the linear elastic behavior. Aschheim et al. (2010) conducted a research study by changing the flange and web materials. They used 2.5inx1.5in flanges each consists of two ply bamboo and two types of web materials, which are 3 ply bamboo and bamboo OSB. Based on the experimental results on 3.5 ft

bamboo I-joists, they found that the elastic moduli are similar to those of available soft wood. Their study also showed that bamboo based OSB can be used as web material of the I-joists to provide superior shear stiffness and reduce the shear deflection of the joist. Earlier, *Skaggs and Bender (1995)* proposed a shear deflection equation based on analytical procedures for layered composite wood beams and performed the sensitivity analysis to understand the effect of E/G ratio and L/d ratio of the beam.

### **2.2.2 Oriented Strand Board**

Oriented Strand Board (OSB) are wood engineered composite panel products. Usually made of Aspen or Poplar strands (*Zhou 1990*) which are cemented together under a specified range of heat and pressure with a water proof phenolic resin adhesives or other equivalent binder meeting the requirements of CSA-O112 (Canadian-Standard-Association 2014a; c). OSB panels have two directions, which are long or strong axis and transverse axis. Along the long axis, OSB is stronger than the other direction as the strands are oriented along the long axis in the outer faces of the panel. OSB panels are manufactured as per the requirements stated in the Canadian Standards Association (CSA) standard CSA O325 (*Canadian-Standard-Association 2016*). The strands used to manufacture OSB are commonly up to 6 inch (150 mm) long in the grain direction and 1 inch (25 mm) wide and less than 1/32 inch (1 mm) in thickness. OSB panels have many applications in construction such as roof, wall and floor sheathing, diaphragm and shear-wall applications. OSB is also used as the web material for some types of prefabricated wood I-joists (*CWC 2016*). The strength and stiffness of OSB under tension is lower as than the strength and stiffness under compression loading as shown in *Figure 2.3*.

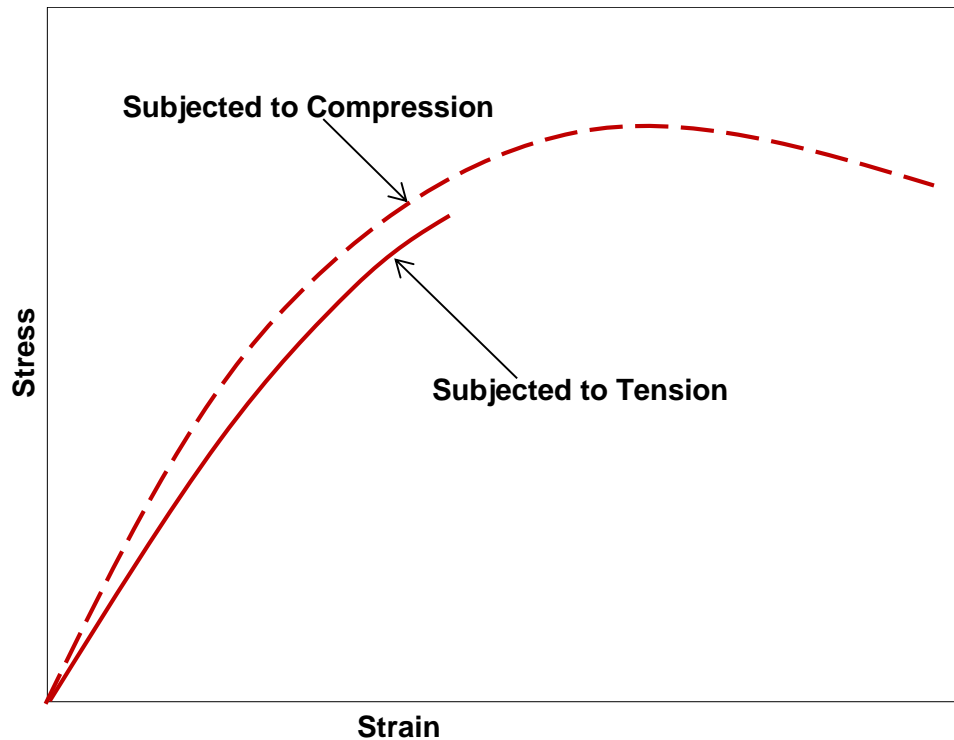


**Figure 2.3** A typical stress-strain response of OSB under Tension and Compression (Zhu 2003; Zhu et al. 2005a, 2007b)

(Davids et al. 2011) examined the bending and creep performance of timber joists panel. They reported that the strength and stiffness of panels is 59 to 124% and 79 to 115% higher than those of the single I-joists, respectively. It is also reported that the creep performance was better for the shorter span panels in comparison to the longer span panels. Recently, Wu and Asce (2014) conducted an experimental investigation on bending resistance of bamboo composite I-beam, in which flanges and web were connected with a series of steel angle & bamboo diaphragm. These I-beams were tested after pre-stressing with a bar/tube to improve their stiffness and load bearing capacity.

### 2.3 Opening in the Web of Wood I-joists

Creating a hole in the web of composite I-joists is allowed to provide access for plumbing and mechanical ductworks, but must be followed the guideline provided by the manufacturers as

shown in **Figure 2.4**. Some manufacturers also provide factory-pre-punched knock-out holes in the webs to facilitate the installation of electro-mechanical services (**CWC 2016**).

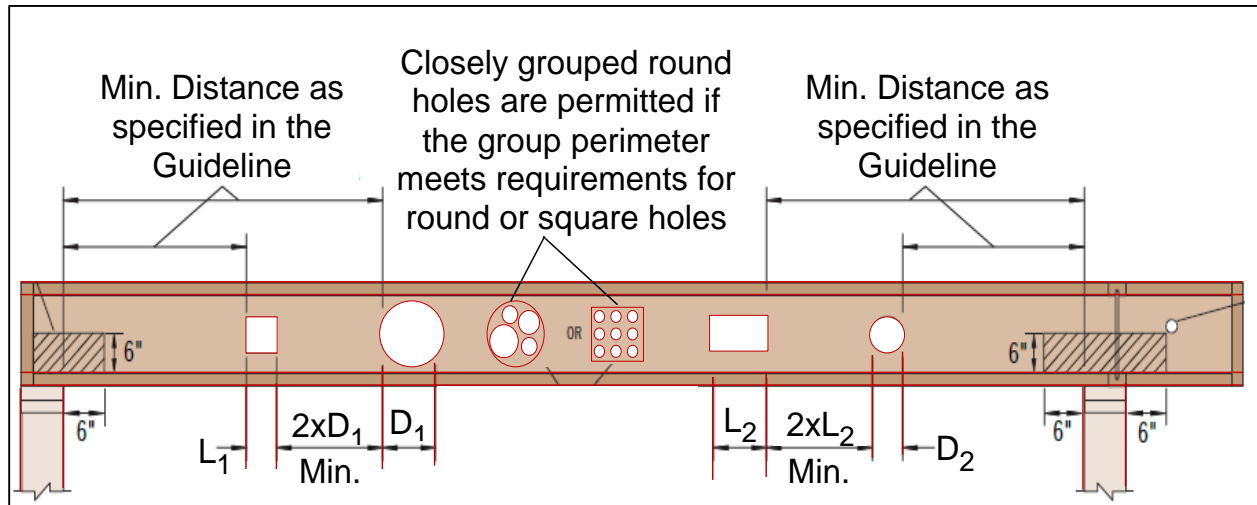


**Figure 2.4 Manufacturer Guidelines for making holes in the web of I-joists (Weyerhaeuser-Trus-Joist 2014)**

Previous research evaluated the failure mode and capacity reduction of wood I-joists with web openings. **Morris et al. (1995)** summarized three failure modes as web fracture, web buckling, and de-bonding of web-flange adhesive joint. **Fergus (1979)** studied the effect of circular openings on moment-governed 7.3m long I-joists and shear-governed 2.4m long I-joists and found no significant change in stiffness with a web removal of up to 70% of total height. This finding, however, was limited for the specific location of the web opening in the moment critical I-joists close to support and close to mid-span in the shear critical I-joists. On the contrary, **Maley (1987)** and **Wang and Cheng (1995)** reported that openings do reduce stiffness and shear capacity. Wang and **Cheng (1995)** investigated 2.8m to 3.6m long I-joists with rectangular web openings of 33% to 100% web height placed at a distance of 0.5m to 1.0m from the support and observed that the shear strength was reduced up to 79% when the opening height was equal to the height of web. No significant changes occurred for opening heights of 33% of web height. Several research studies



(Polocoser 2012; Polocoser et al. 2012; Zhu 2003; Zhu et al. 2005b) were conducted to understand the stress concentration occurred around the web hole. The stress concentration usually occurred at the four corners of the hole as shown in *Figure 2.5*.

*Hilson and Rodd (1984)* determined the critical location of holes in the web to minimize the shear capacity reduction and proposed an equation to predict the reduction in relation to size and position of holes. *Leichti et al. (1990a and b)* reviewed studies on I-beams with openings and reported that the restriction on the web opening position depends on types and sizes of openings. They concluded that rectangular openings are more restrictive than circular openings (due to the stress concentration at corners), that a 38mm opening can be placed anywhere in the web, but larger openings require specified minimum distances from supports and flange edges.

*(Harte and Baylor 2011)* evaluated the structural performance of castellated timber I joists and proposed two models to determine shear capacity for circular and rectangular holes of castellated timber I joists. It is found that the bending response of the castellated timber I joists is fairly linear elastic until failure.

Recently *(Chen et al. 2015)* have conducted an experimental study on the performance of OSB webbed bamboo I-joists with square and round hole in the web. They found that the cracking load with circular web hole is 10% higher than that of the cracking load with a hole having sharp corner, i.e. square hole, which is due to the stress concentration occurrence at the sharp corners. Earlier *(Morrissey et al. 2009)* conducted a similar study for OSB webbed timber I-joists and the findings were similar.

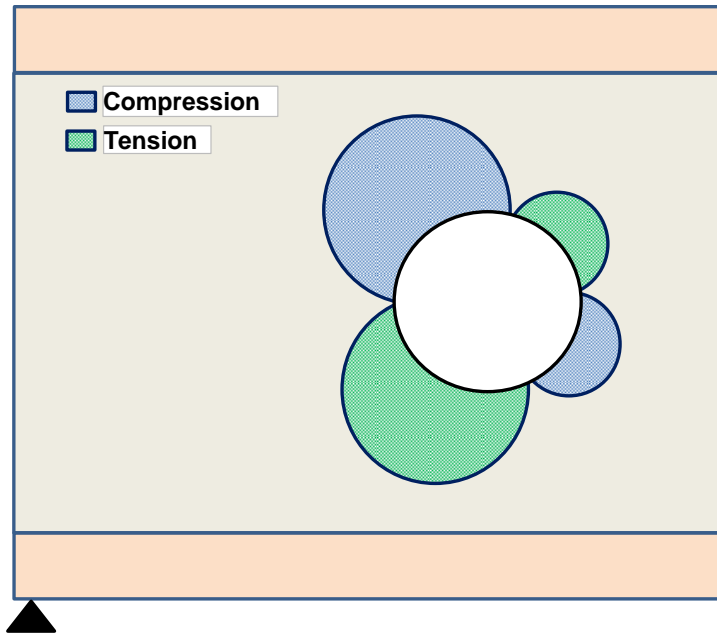


*Figure 2.5 Tangential Stress distribution around a web opening (Polocoser et al. 2013; Zhu 2003)*

### 2.3.1 Retrofitting of Web Hole and Flange Notched I-joists

(Polocoser et al. 2013) conducted a research study on the remediation technique of timber I joist having holes in the web by using OSB collar. The OSB collar remediation technique was more effective for the longer span joists with higher moment-shear ratio than the shorter span beams. Earlier, Jalla (1999) proposed a design method for deficient lumber joist having a hole or notch.

Until today only few research studies were found related to deficient I-joists with flange notches or cuts at the top flange, which is subjected to flexural compression force. Although, Hindman and Loferski (2008) did carry out a pertinent study to investigate the improved load capacity and stiffness of flange cut I-joists retrofitted with cold formed steel reinforcers in relation to uncut control I-joists, they did not perform any test to determine the capacity and stiffness of un-retrofitted flange cut I-joists. Their study shows that the strength and stiffness of reinforced/ repaired flange cut I-joists are lower than those of the uncut or control I-joists by 39.8% and 33%,

respectively. *Foliente and McLain (1993)* proposed an alternative design method based on critical fillet hoop stress (CFHS) theory and compared with the existing design method based on either notch-factor or linear-elastic fracture mechanics (LEFM) based approaches for a notched wood beam. Another research study was conducted by *Yusof and Saleh (2010)*, on flexural strengthening of timber beams using Glass Fiber Reinforced Polymer (GFRP). They used GFRP rods with different combination and diameters at the bottom of the beams to resist tensile forces due to bending of the beam.

## **CHAPTER 3: RESEARCH METHODOLOGY AND CHARACTERIZATION OF MATERIAL PROPERTIES**

### **3.1 General**

Oriented Strand Board (OSB) is a wood based engineering panel product. OSB has various applications in manufacturing other engineering products and construction related products, such as I-joists, floor & roof sheathing, shear wall panels etc. Hence, OSB exhibits mechanical properties similar to those of wood. For example, OSB behaves elastically and elasto-plastically when it is subjected to the tension and compression, respectively (*Zhu et al. 2005a*).

Characteristic stress-strain relationships of timber, OSB, and GFRP are essential for the analytical and numerical analysis of structures containing OSB panels, timber and Glass Fiber Reinforced Polymer (GFRP). However, most of the available literature focused only on the ultimate strength of these materials and did not consider the non-linearity or plasticity in the relationships. The objective of this Chapter is, therefore, to obtain material properties of OSB, Timber and GFRP, which could help develop constitutive models for analytical and numerical analysis.

The objectives of this chapter are summarised below:

- To discuss the overall methodology of the experimental program performed in different phases of this research study.
- To evaluate the material properties of OSB, Timber and Glass Fiber Reinforced Polymer (GFRP).

- To develop the constitutive models of OSB, Timber and Glass Fiber Reinforced Polymer (GFRP) and validate them with the experimental results obtained from the 4<sup>th</sup> series of the specimens.

### 3.2 Methodology of Experimental Program

All the wood I-joist specimens were prepared at AcuTruss Industries Ltd. facility, Canada. The specification of the I-joists was chosen from the NASCOR I-joist series named as NJH12 (*Nascor 2010*). The flange of the NJH12 was made of solid timber and the web was made of oriented standard board (OSB). Total height of the specimen was 302 mm (11 $\frac{7}{8}$  inches) and the flange width and height was 63.5 mm (2 $\frac{1}{2}$  inches) and 38 mm (1 $\frac{1}{2}$  inches), respectively, as shown in *Figure 3.1 (a)*. The thickness of the web was 9.5 mm (3/8 inch).

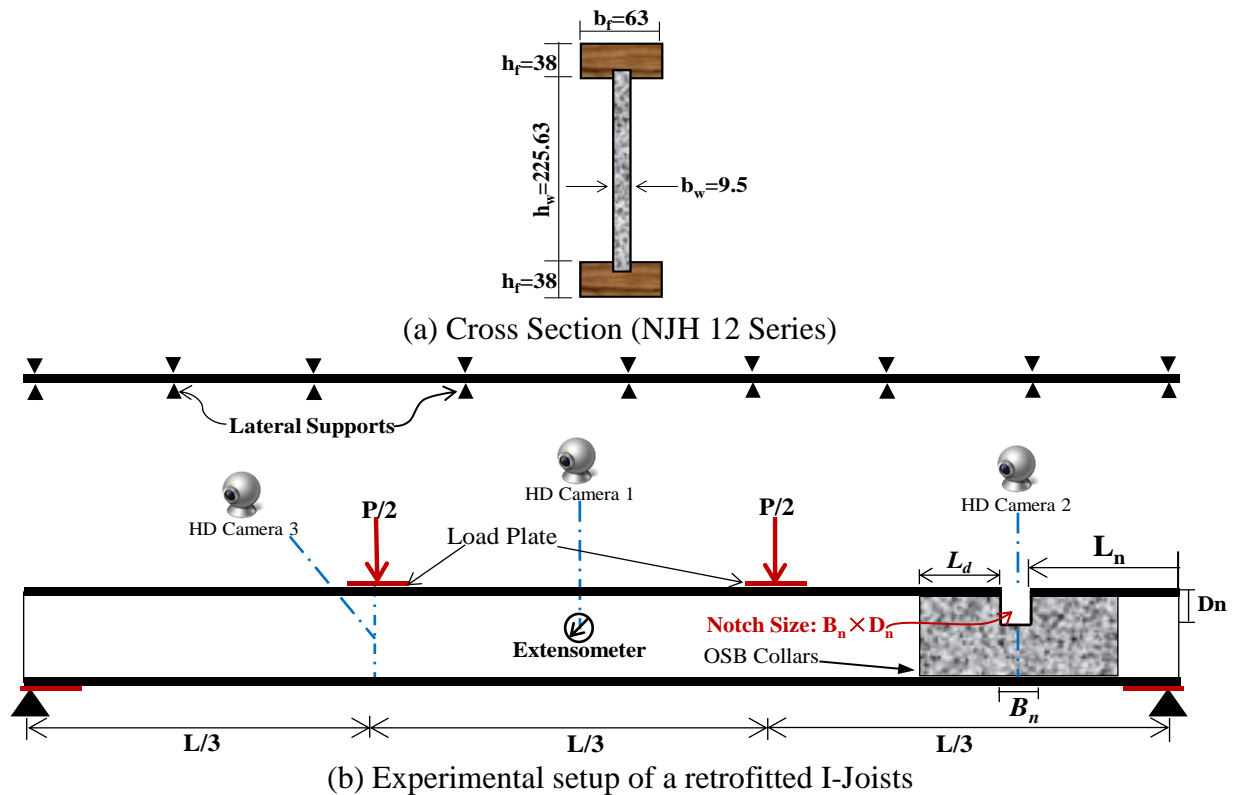


*Figure 3.1: Experimental setup of a retrofitted I-Joists with flange notch and cross sectional dimensions of the tested I-joists (dimensions are in mm).*

The average peak load and stiffness were determined to evaluate the degradation and improvement of the I-joist performance with flange cut or web hole, and with reinforcer, respectively. Stiffness was also measured as described by Hindman and Loferski (*Hindman and Loferski 2008*), which is defined as the slope of the load deflection curve in the linear elastic region of the curve. Due to the extensive deflection of the I-joists, their performances have also been evaluated based on the load at a specific deflection as per the serviceability design provision of CSA-O86 (Canadian-Standard-Association 2014a) and NBCC-Part 9 (*NBCC 2015*), which are  $L (mm)/180$  and  $L (mm)/360$ . Here, deflections,  $\Delta=L/180$  and  $\Delta=L/360$  represent the limiting deflections (serviceability condition) for roof and flooring systems subjected to total load (dead load + live load + snow load) (*Canadian-Standard-Association 2014a*) and only live load (*NBCC 2015*), respectively.

The specimens were tested under four-point bending test setup with a simply supported loading condition following ASTM D5055 (*ASTM-D5055 2013*). The loads were applied from the top using a hydraulic pressure with the loading rate as specified in the standard. Three HD cameras were installed along with the test setup to monitor the deflection, crack pattern, and failure of the specimens. The cameras were focused at the mid-span, at the location of opening and at the loading point as shown in *Figure 3.1 (b)*. In addition, an extensometer was used to measure the mid-point deflection of the I-joists and validate the deflection measured based on image processing technique. However, the extensometer was removed after certain time (either reaching at 1500 N or the maximum allowable limit of the extensometer, which is 50mm) to avoid any damage to the extensometer. MATLAB image processing toolbox (The MathWorks Inc. 2012) was used to calculate the deflection of the I-joists. To prevent lateral buckling of the I-joists, a series of lateral support was used with an average spacing of 450 mm. The failure of each specimen was also

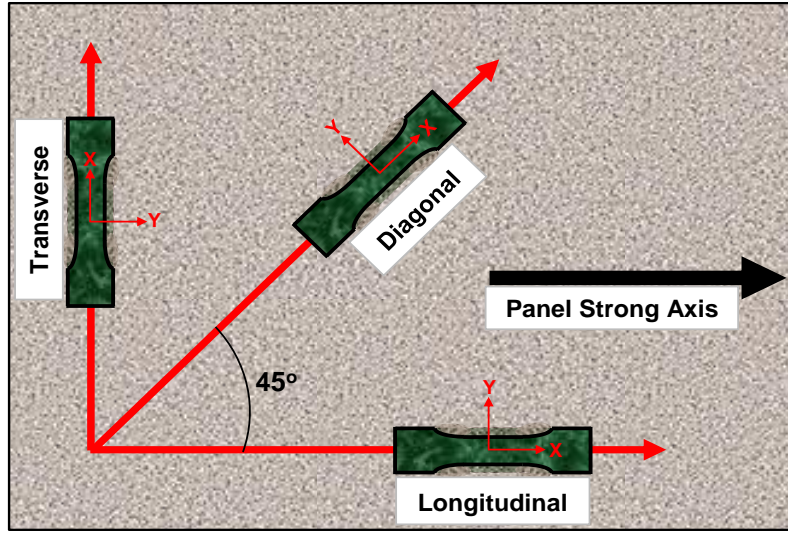
photographed and documented. The steel loading plates were 100 mm long and 10 mm thick. The testing frame for performing the four-point bending test is presented in **Figure 3.2**.



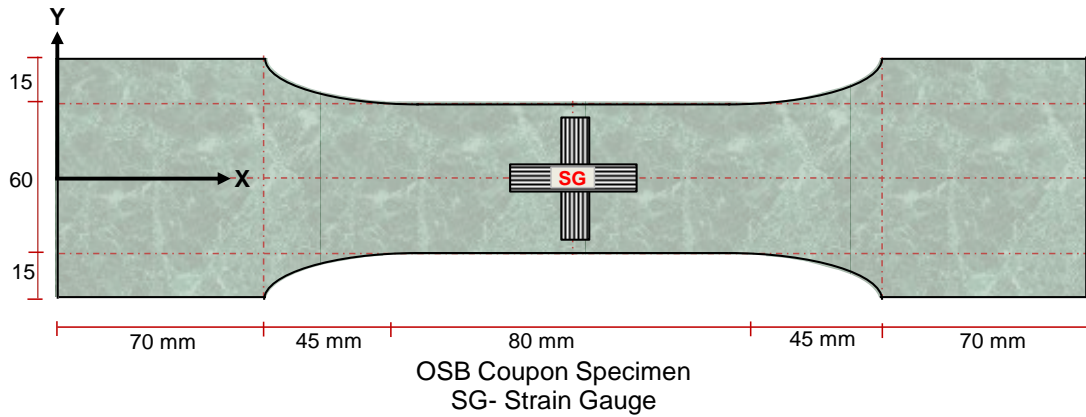
**Figure 3.2: Testing Frame used to perform four points bending test of I-Joists (With a 12 ft Control I-Joist).**

### 3.3 Characterization of Material Properties

To investigate the strength, elastic modulus and Poisson's ratio of OSB, tension test of OSB was conducted in three in-plane directions of the OSB panel, which are longitudinal (along strong axis of the panel), transverse (perpendicular to the strong axis) and Diagonal ( $45^0$  with the strong axis) direction as demonstrated in **Figure 3.3**. Four specimens from each direction were prepared from a standard 1220x2400mm OSB panel. Three specimens were used for data analysis and the test results from 4<sup>th</sup> specimen was used for the validation of the constitutive model. All tested specimens were prepared from the materials which were sampled directly from the I-joist manufacturing product line at AcuTruss Industries Ltd., in Kelowna, BC, Canada.



(a) Direction of OSB Test Specimens



(b) Dimensions of OSB Coupon

**Figure 3.3: Details of OSB coupon specimen for tension test.**

A bi-axial strain gauge was used to capture the strain along the loading direction (X-axis) and the transverse direction (Y-axis) of the coupon specimens (OSB, Timber, GFRP) subjected to the tension load as shown in **Figure 3.4**. Gauge length and resistance of the used strain gauges was 50 mm and 120 $\Omega$ , respectively. Tension test was performed by using Instron universal testing machine with a capacity of 250 kN, where the load was applied hydraulically during the test at a constant rate of 4mm/min, as specified in the *ASTM-D1037 (2014)*. All specimens were prepared



from the samples picked from the I-joist manufacturer product line at different time and different lot of the materials, to ensure the randomness of the samples.



**Figure 3.4** Sample of a OSB Tension test specimen with a Bi-axial Strain Gauge

### 3.3.1 Properties of OSB

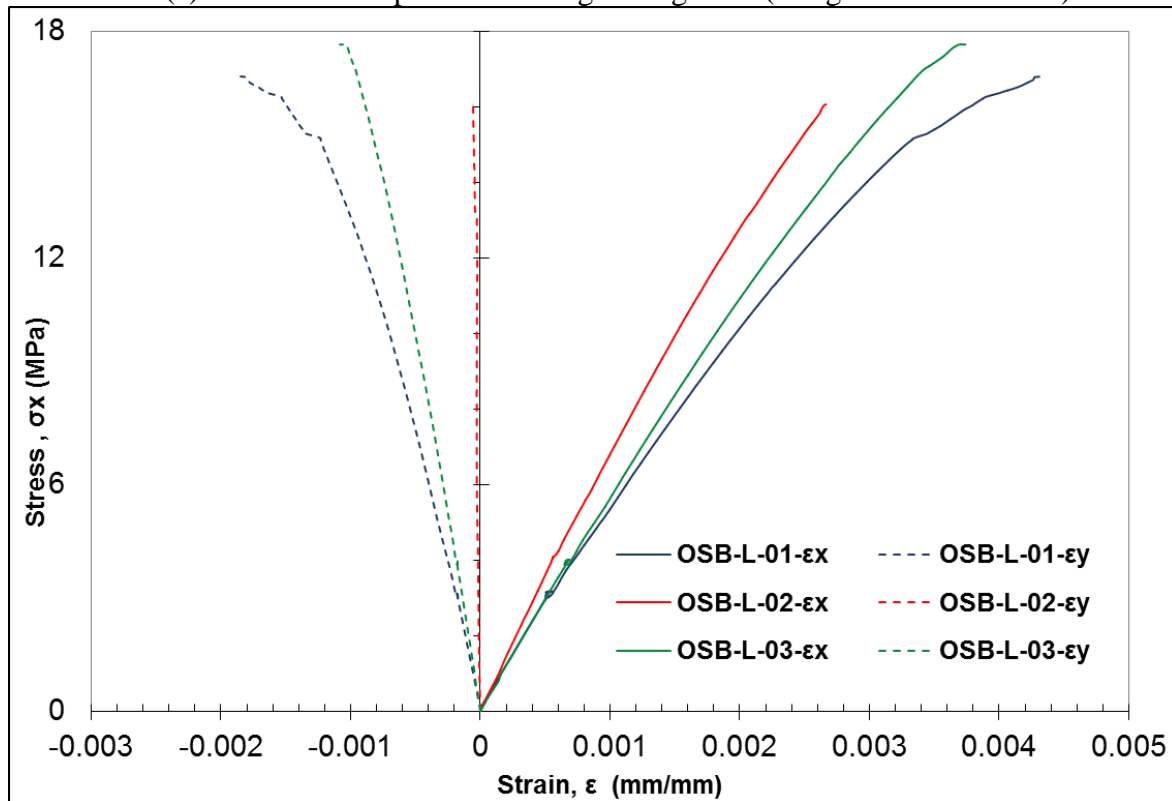
Strengths, elastic modulus and Poisson's ratios of OSB in three in-plane directions of the OSB panel (Longitudinal, Transverse and Diagonal) were determined by conducting tension test in three different directions.

#### 3.3.1.1 Longitudinal Direction

**Figure 3.5** shows stress-strain curves for OSB subjected to tension along the longitudinal direction of the OSB panel. All stress-strain curves exhibit linear behavior at the initial stage followed by plastic behavior. Summary of tension test results of OSB in longitudinal direction are summarized in **Table 3.1**. Average strength and modulus of elasticity in longitudinal direction was found to be 16.84 MPa and 5738 MPa, respectively. Average Poisson's ratio ( $\nu_{LT}$ ) was found to be 0.309. The Poisson's ratio obtained from the specimen OSB-L-02 was discarded as the strain gauge perpendicular to the loading direction was de-bonded just after starting the test.



(a) Tested OSB Specimens along Strong Axis (Longitudinal direction)



(b) Stress-Strain Response of OSB subjected to tension along strong axis (Longitudinal direction)

**Figure 3.5 Stress-strain response of OSB subjected to tension along the strong axis of the OSB panel.**

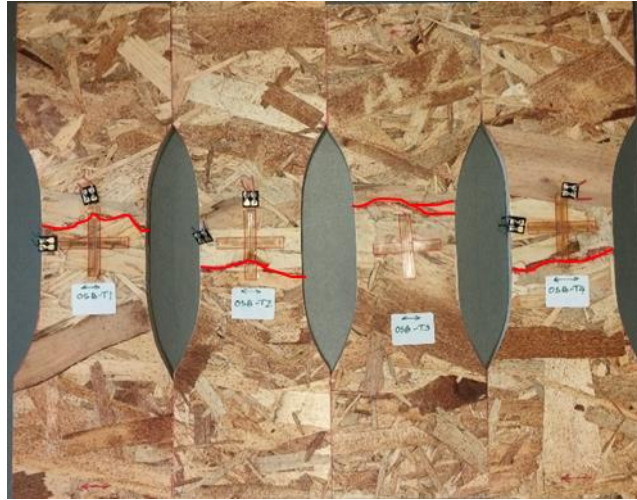
**Table 3.1 Summary of the Tension test of OSB in Longitudinal Direction (Sample Size, n=3)**

<b>Specimen ID.</b>	<b>Max. <math>\sigma_x</math> (MPa)</b>	<b>Max. <math>\epsilon_x</math> (mm/mm)</b>	<b>Max. <math>\epsilon_y</math> (mm/mm)</b>	<b>MOE (MPa)</b>	<b><math>\nu_{XY}</math> or <math>\nu_{LT}</math></b>
<b>OSB-L-01</b>	16.80	4.36E-03	-7.83E-09	5057.7	0.3479
<b>OSB-L-02</b>	16.06	2.69E-03	-3.88E-09	5417.01	-
<b>OSB-L-03</b>	17.65	3.77E-03	-4.37E-08	5493.09	0.27007
<b>Average</b>	<b>16.84</b>	<b>3.61E-03</b>	<b>-1.85E-08</b>	<b>5322.60</b>	<b>0.3090</b>
<b>SD</b>	<b>0.80</b>	<b>8.45E-04</b>	<b>2.20E-08</b>	<b>232.54</b>	<b>0.0550</b>
<b>COV</b>	<b>5%</b>	<b>23%</b>	<b>-119%</b>	<b>4%</b>	<b>18%</b>

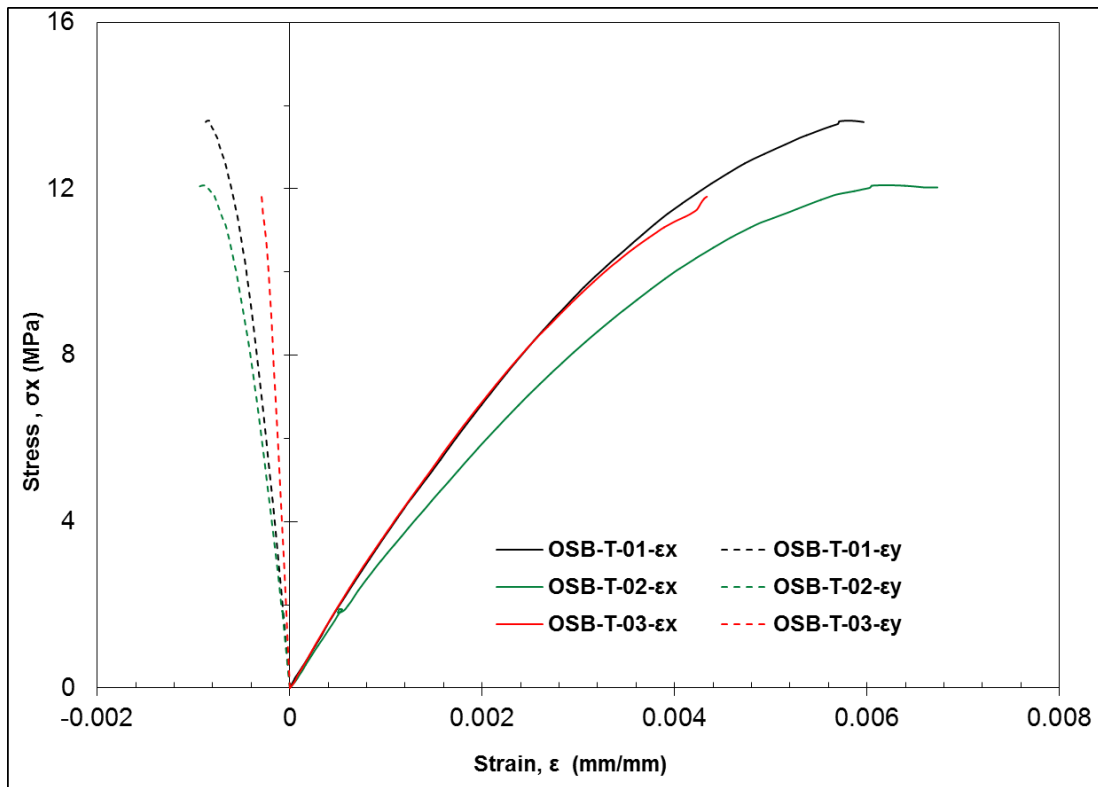
### **3.3.1.2 Transverse Direction**

Strength, Modulus of Elasticity and Poisson's ratio of OSB in transverse direction (perpendicular to strong axis) is also required to understand the behavior of OSB. Average strength and modulus of elasticity of OSB along panel transverse direction was obtained to be 12.51MPa and 3231 MPa, respectively. The average Poisson's ratio ( $\nu_{TL}$ ) was found to be 0.14628 with a 1% COV. Acquired data obtained from the strain gauge attached perpendicular to the loading direction had an error reading due to early de-bonding of the gauge, hence the Poisson's ratio obtained from the OSB-T-03 has been considered as an outlier. The summary of the tension test along the panel transverse direction has been presented in **Figure 3.6** and **Table 3.2**.

From **Figure 3.6** it can be observed that the stress-strain relationships behave elasto-plastically for OSB subjected to the tension in transverse direction of the OSB panel. However, **Zhu et al. (2005)** found that OSB behaves liner-elastically under tension in panel transverse direction.



(a) Tested OSB Specimens (Transverse direction)



(b) Stress-Strain Response of OSB subjected to tension along Transverse direction

**Figure 3.6 Stress-strain response of OSB subjected to tension along the Transverse direction of the OSB panel.**

**Table 3.2 Summary of the Tension test of OSB in Transverse Direction (Sample Size, n=3)**

<b>Specimen ID.</b>	<b>Max. <math>\sigma_x</math> (MPa)</b>	<b>Max. <math>\epsilon_x</math> (mm/mm)</b>	<b>Max. <math>\epsilon_y</math> (mm/mm)</b>	<b>MOE (MPa)</b>	<b><math>v_{XY}</math> or <math>v_{TL}</math></b>
<b>OSB-T-01</b>	13.64	5.96E-03	-2.22E-08	3341.33	0.14525
<b>OSB-T-02</b>	12.09	6.73E-03	-5.23E-08	2850.75	0.14731
<b>OSB-T-03</b>	11.81	4.54E-03	-2.34E-08	3499.95	
<b>Average</b>	<b>12.51</b>	<b>5.75E-03</b>	<b>-3.26E-08</b>	<b>3230.68</b>	<b>0.1463</b>
<b>SD</b>	<b>0.98</b>	<b>1.11E-03</b>	<b>1.71E-08</b>	<b>338.45</b>	<b>0.0015</b>
<b>COV</b>	<b>8%</b>	<b>19%</b>	<b>-52%</b>	<b>10%</b>	<b>1%</b>

### **3.3.1.3 Diagonal Direction**

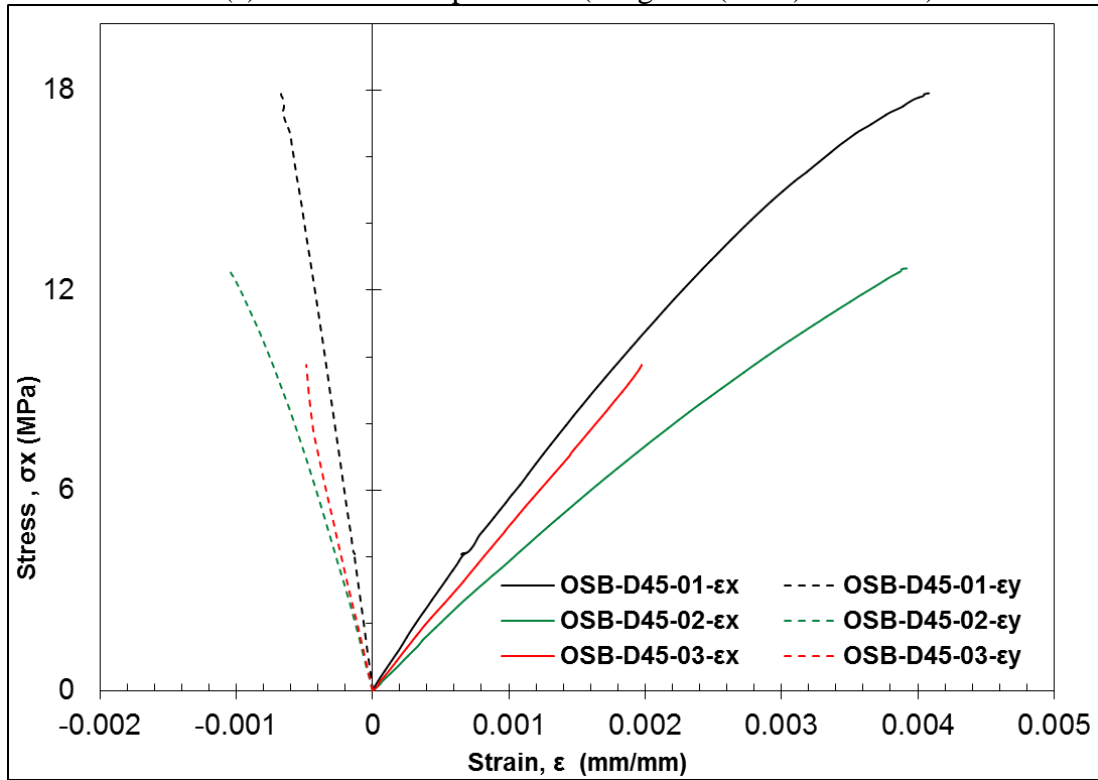
To understand the shear properties of OSB panel, tension test in diagonal direction (45° with the strong axis) has been performed. The summary of the tension test along the panel transverse direction has been presented in *Figure 3.7* and *Table 3.3*.

**Table 3.3 Summary of the Tension test of OSB in Diagonal (45°) Direction (Sample Size, n=3)**

<b>Specimen ID.</b>	<b>Max. <math>\sigma_x</math> (MPa)</b>	<b>Max. <math>\epsilon_x</math> (mm/mm)</b>	<b>Max. <math>\epsilon_y</math> (mm/mm)</b>	<b>MOE (MPa)</b>	<b><math>v_{XY}</math> or <math>v_{D45}</math></b>
<b>OSB-D45-01</b>	17.92	4.25E-03	-2.62E-08	3385.1	0.20098
<b>OSB-D45-02</b>	12.65	3.92E-03	-6.89E-08	3656.6	0.25888
<b>OSB-D45-03</b>	9.98	1.97E-03	-6.69E-08	4068.2	0.28457
<b>Average</b>	<b>13.52</b>	<b>3.38E-03</b>	<b>-5.40E-08</b>	<b>3703.3</b>	<b>0.2481</b>
<b>SD</b>	<b>4.04</b>	<b>1.23E-03</b>	<b>2.41E-08</b>	<b>343.9</b>	<b>0.0428</b>
<b>COV</b>	<b>30%</b>	<b>36%</b>	<b>-45%</b>	<b>9%</b>	<b>17%</b>



(a) Tested OSB Specimens (Diagonal (D45<sup>0</sup>) direction)



(b) Stress-Strain Response of GFRP subjected to tension along Diagonal (D45<sup>0</sup>) direction

**Figure 3.7 Stress-strain response of OSB subjected to tension along Diagonal (45°) direction of the OSB panel.**

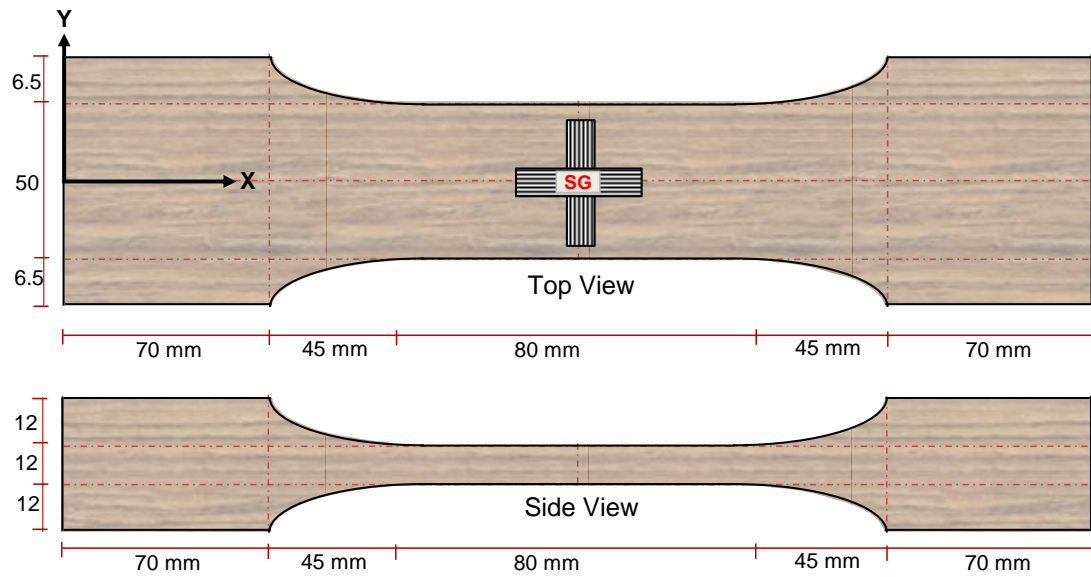
These results presented above show that the tested Oriented Strand Board (OSB) has engineering properties comparable with those found by *Chui et al. (2005)* for similar materials, and by *(Zhu 2003)* for OSB web of British I-joists. However, the obtained MOE at longitudinal

direction is higher whereas, it is lower at transverse direction compared to those reported by *Karacabeyli et al. (1996)* for structural grade Canadian OSB. These dissimilarities were unexpected, considering the same evaluated products. In contrast, the MOE obtained by *Grandmont et al. (2010a)* was lower than the obtained results for both directions.

### 3.4 Properties of Timber

To evaluate the engineering properties of timber, tension test was performed according to *ASTM-D143 (2014)*. The details of the timber tension test specimen are presented in *Figure 3.8*. *Figure 3.9* shows stress-strain curves for timber (SPF) subjected to tension load parallel to the fiber direction of the flange material. All stress-strain curves exhibit linear behavior at the initial stage followed by plastic behavior. Summary of tension test results of timber along fiber direction are summarized in *Table 3.4*. Average strength and modulus of elasticity along fiber direction was found to be 57.02 MPa and 17699.42 MPa, respectively. Average Poisson's ratio ( $\nu$ ) was found to be 0.325 with a co-efficient of variation (COV) of 21%. From the stress-strain (Transverse,  $\epsilon_y$ ) response of the tension test (*Figure 3.9*), the crack initiation stage was identified and found to be at a stress of 30.37 MPa with a COV of 6%.



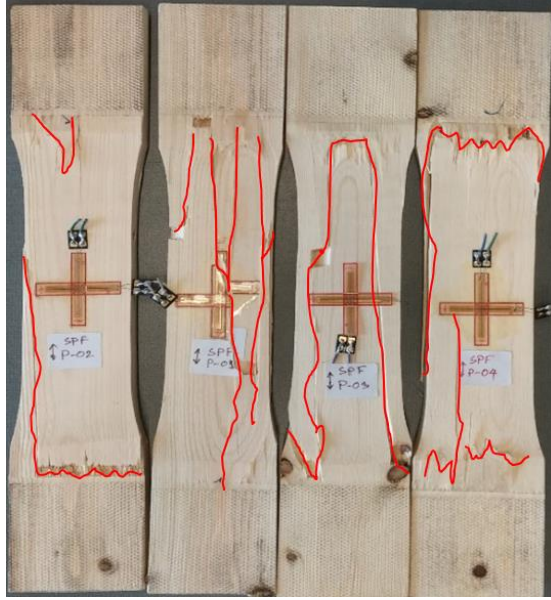


Timber Coupon Specimen  
SG- Strain Gauge

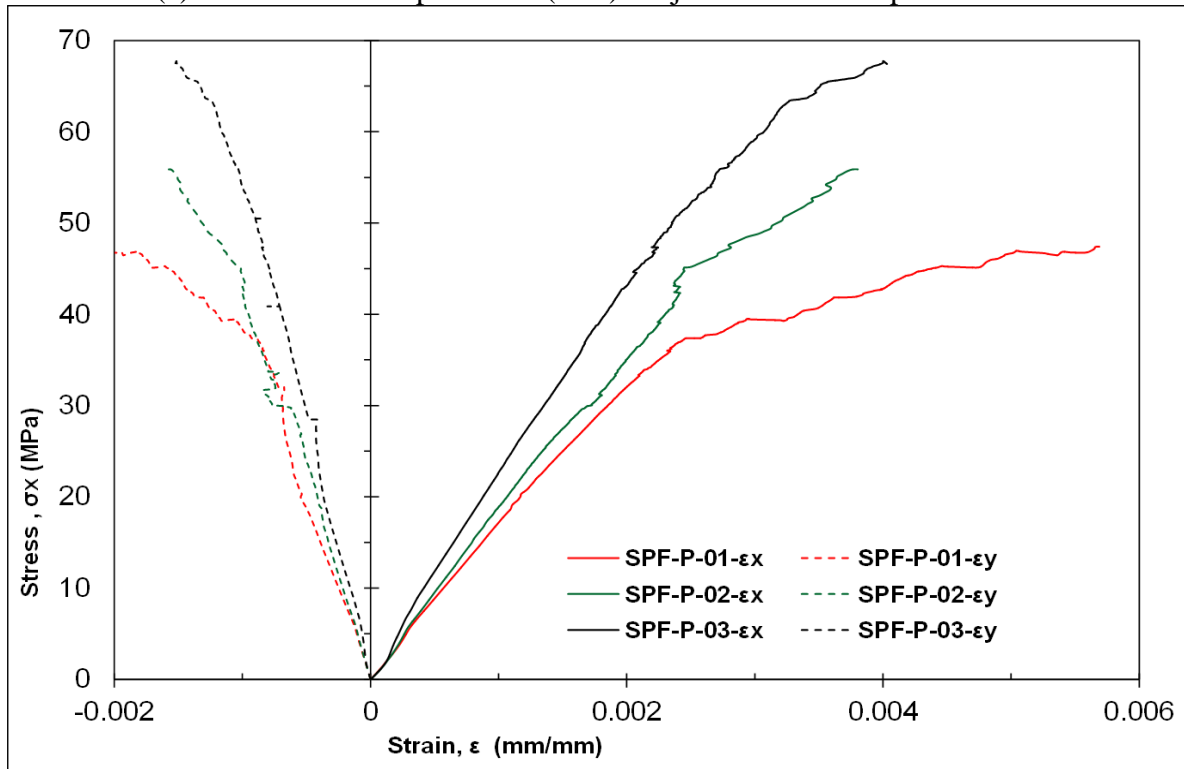
**Figure 3.8 Details of Timber coupon specimen for tension test.**







(a) Tested Timber Specimens (SPF) subjected to tension parallel to fiber



(b) Stress-Strain Response of Timber subjected to tension parallel to fiber

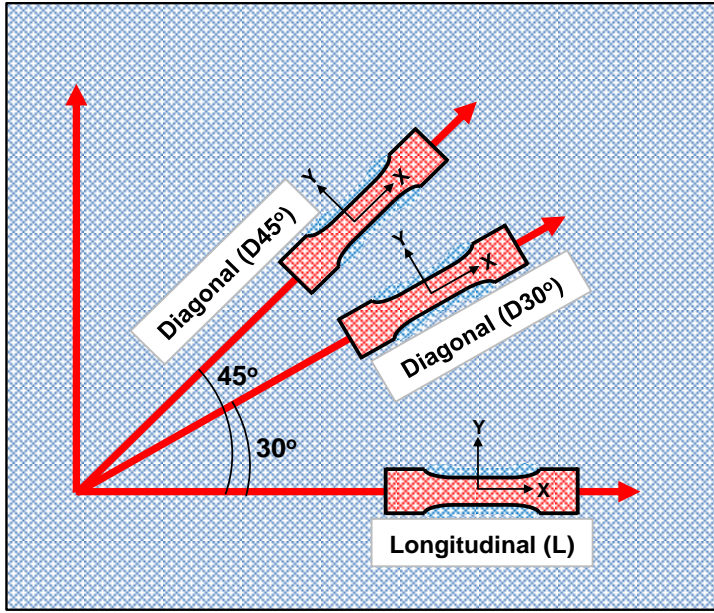
**Figure 3.9 Stress-strain response of Timber subjected to tension parallel to fiber**

**Table 3.4 Summary of the Tension test of Timber subjected to tension parallel to fiber (Sample Size, n=3)**

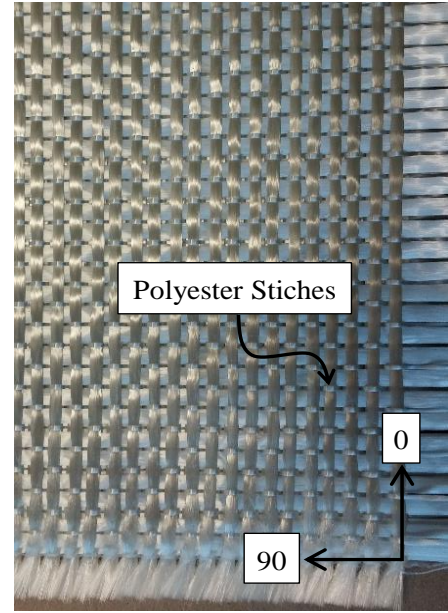
Specimen ID.	Max. $\sigma_x$ (MPa)	Crack Initiation Stress (MPa)	Max. $\epsilon_x$ (mm/mm)	Max. $\epsilon_y$ (mm/mm)	MOE (MPa)	$\nu_{XY}$ or $\nu_P$
SPF-P-01	47.42	32.1	5.69E-03	-1.01E-07	14993.87	0.32333
SPF-P-02	55.89	30.3	3.80E-03	-1.05E-07	16766.29	0.39316
SPF-P-03	67.75	28.7	4.03E-03	-1.90E-07	16427.41	0.2585
<b>Average</b>	<b>57.02</b>	<b>30.37</b>	<b>4.51E-03</b>	<b>-1.32E-07</b>	<b>16062.52</b>	<b>0.3250</b>
<b>SD</b>	<b>10.21</b>	<b>1.70</b>	<b>1.03E-03</b>	<b>5.02E-08</b>	<b>940.86</b>	<b>0.0673</b>
<b>COV</b>	<b>18%</b>	<b>6%</b>	<b>23%</b>	<b>-38%</b>	<b>6%</b>	<b>21%</b>

### 3.5 Properties of GFRP

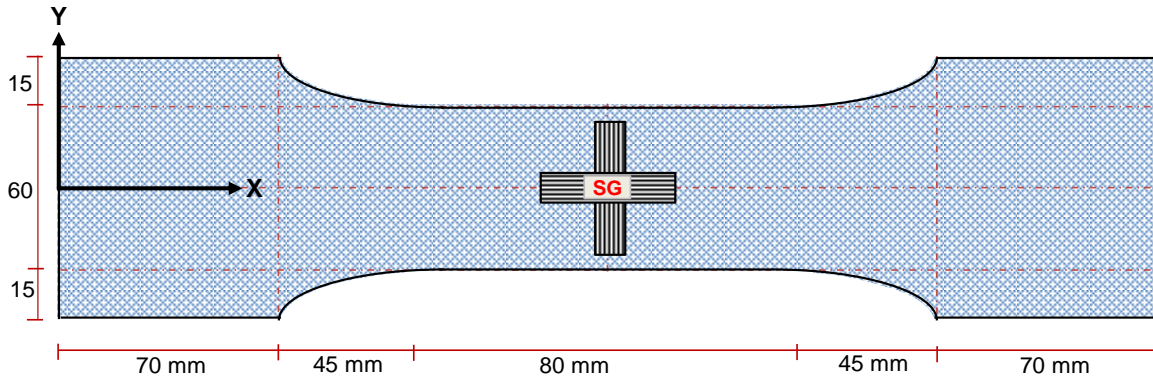
Glass Fiber Reinforced Polymer (GFRP) plates with a dimension of 500x500mm were prepared and then cut for tension test specimens in three directions (Longitudinal and two Diagonal Directions, i.e.  $30^\circ$  and  $45^\circ$  with respect to the longitudinal direction (L) as shown in **Figure 3.10**. GFRP plates were fabricated in the laboratory using the hand layup process. GFRP plate fabrication was done in three steps: pre-fabrication, fabrication, post fabrication as described in **Chapter 6 (Section 6.2.1)**. Bi-axial woven Glass Fiber mat (E-Glass TG-54-N manufactured by Texonic JB Martin) with a 1.0 Resin-fiber volume fraction ( $V_f$ ) was used for fabrication of GFRP test specimens. The test procedure was followed as specified in ASTM Standards (**ASTM-D4762 2014; ASTM-D7205 2014; ASTM-D638 2014**).



(a) Direction of GFRP Test Specimens



(b) E-Glass TG-54-N (*Sultana-Mir 2015*)

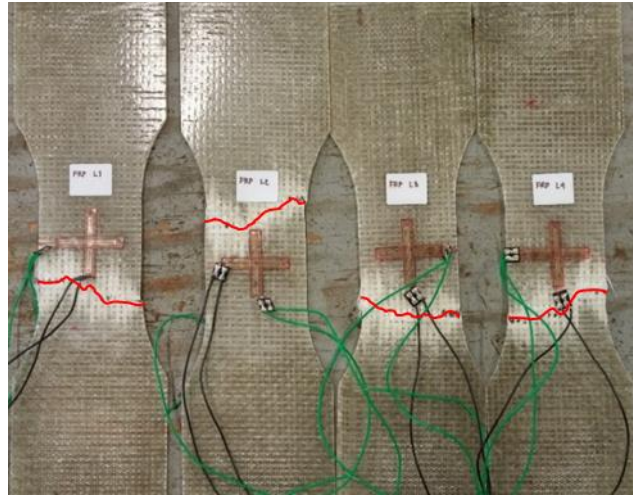


(a) Dimensions of GFRP Coupon

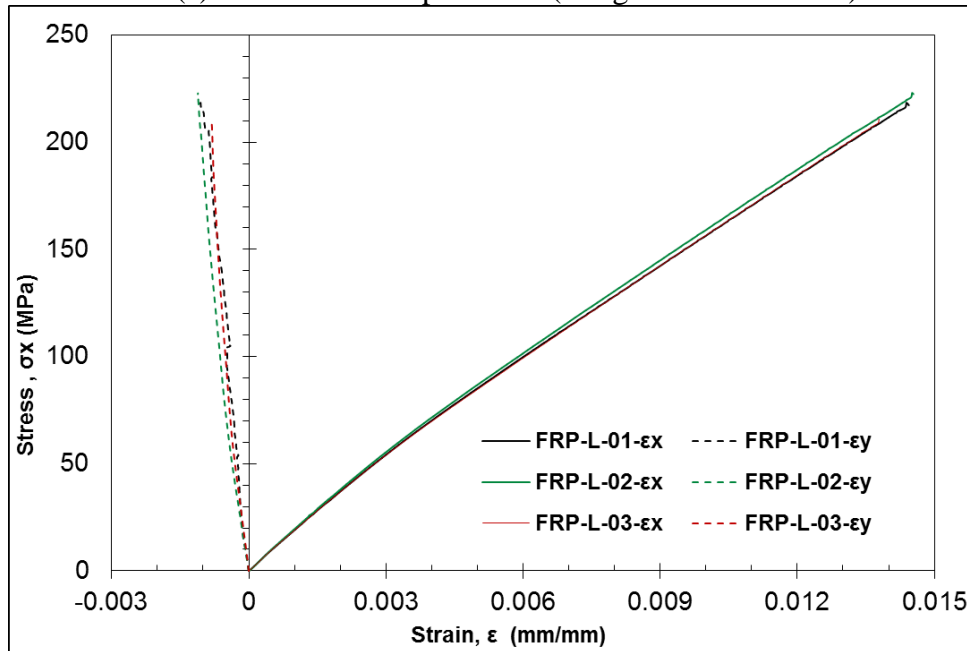
**Figure 3.10 Glass Fiber Reinforced Polymer (GFRP) Test Specimen Details**

Stress-strain response of GFRP plates subjected to tension loads along the longitudinal, Diagonal D45<sup>0</sup>, and Diagonal D30<sup>0</sup> directions have been presented in **Figure 3.11**, **Figure 3.12** & **Figure 3.13**, respectively. Stress-strain curves in the longitudinal direction exhibit elastic behavior until failure, whereas the stress-strain curves along diagonal directions (D45<sup>0</sup> & D30<sup>0</sup>) exhibit linear behavior at the initial stage followed by plastic behavior. This excessive deformation along the diagonal directions (D45<sup>0</sup> & D30<sup>0</sup>) was due to the trellising effects (relative rotation of the weft and warp of the fibers around their crossings) of crossed glass fibers (*Ballhause et al. 2008*;

*Komeili, and Milani 2013*). Summary of tension test results of GFRP plates are summarised in *Table 3.5, Table 3.6 & Table 3.7*. Average strength and modulus of elasticity in longitudinal direction was found to be 217.41 MPa (COV 3%) and 16855 MPa (COV 2%), respectively. Average Poisson's ratio ( $\nu_{xy}$ ) was found to be 0.1147 (COV 14%).



(a) Tested GFRP Specimens (Longitudinal direction)



(b) Stress-Strain Response of GFRP subjected to tension along longitudinal direction

**Figure 3.11 Tested specimens and Stress-strain response of GFRP subjected to tension along the longitudinal direction of the GFRP plate**

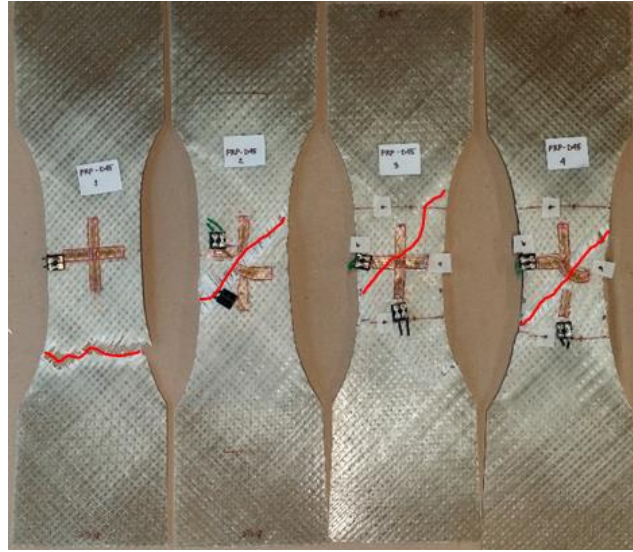
As shown in *Figure 3.12 & Figure 3.13*, the initial portion of the data was acquired by the strain gauge. The strain gauges were de-bonded at a strain close to 0.04 to 0.05 (mm/mm) due to excessive deflection/distortion of the specimens. Hence, to capture the strain data beyond the debonding point, an open source video analysis and modeling tool/software (Tracker 4.94) was used (*Open Source Physics 2016*). During the test, it was observed that the entire applied tension forces were carried by the Glass Fiber after failure of the resin matrix.

***Table 3.5 Summary of the Tension test of GFRP subjected to tension along Longitudinal Direction (Sample Size, n=3)***

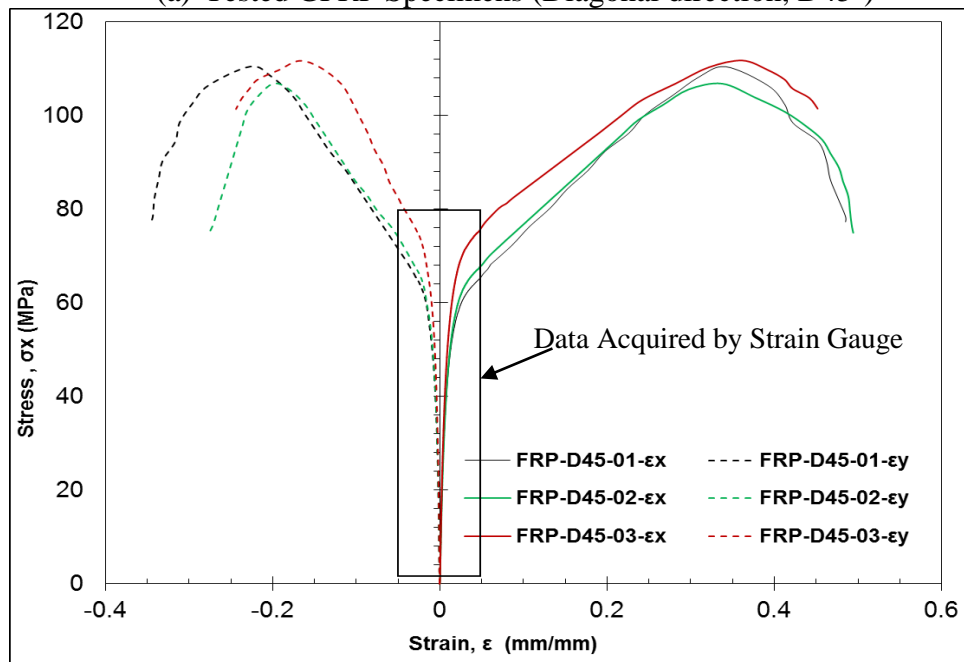
<b>Specimen ID.</b>	<b>Max. <math>\sigma_x</math> (MPa)</b>	<b>Max. <math>\epsilon_x</math> (mm/mm)</b>	<b>Max. <math>\epsilon_y</math> (mm/mm)</b>	<b>MOE (MPa)</b>	<b><math>v_{xy}</math></b>
<b>FRP-L-01</b>	218.40	1.38E-02	-8.21E-04	16692.35	0.10474
<b>FRP-L-02</b>	223.06	1.45E-02	-1.11E-03	17250.9	0.13305
<b>FRP-L-03</b>	210.77	1.38E-02	-8.21E-04	16621.88	0.10629
<b>Average</b>	<b>217.41</b>	<b>1.40E-02</b>	<b>-9.17E-04</b>	<b>16855.04</b>	<b>0.1147</b>
<b>SD</b>	<b>6.21</b>	<b>4.29E-04</b>	<b>1.66E-04</b>	<b>344.63</b>	<b>0.0159</b>
<b>COV</b>	<b>3%</b>	<b>3%</b>	<b>-18%</b>	<b>2%</b>	<b>14%</b>

***Table 3.6 Summary of the Tension test of GFRP subjected to tension along Diagonal (D45°) Direction (Sample Size, n=3)***

<b>Specimen ID.</b>	<b>Max. <math>\sigma_x</math> (MPa)</b>	<b>Max. <math>\epsilon_x</math> (mm/mm)</b>	<b>Max. <math>\epsilon_y</math> (mm/mm)</b>	<b>MOE (MPa)</b>	<b><math>v_{xy}</math> or <math>v_{D45}</math></b>
<b>FRP-D45-01</b>	110.44	4.72E-02	-3.76E-02	6270	0.56609
<b>FRP-D45-02</b>	106.84	4.72E-02	-4.64E-02	3687	0.62316
<b>FRP-D45-03</b>	111.78	4.82E-02	-4.91E-02	4478	0.58876
<b>Average</b>	<b>109.69</b>	<b>4.75E-02</b>	<b>-4.44E-02</b>	<b>4811.67</b>	<b>0.5927</b>
<b>SD</b>	<b>2.55</b>	<b>5.94E-04</b>	<b>6.03E-03</b>	<b>1323.43</b>	<b>0.0287</b>
<b>COV</b>	<b>2%</b>	<b>1%</b>	<b>-14%</b>	<b>28%</b>	<b>5%</b>



(a) Tested GFRP Specimens (Diagonal direction,  $D45^0$ )

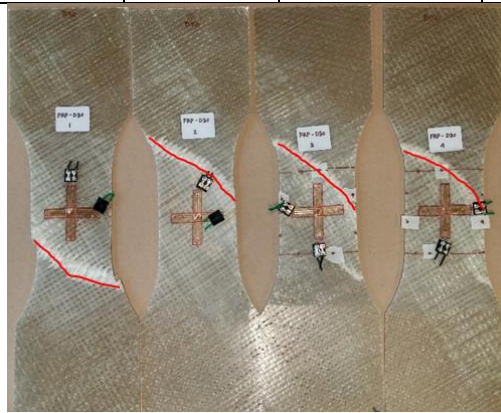


(b) Stress-Strain Response of GFRP subjected to tension along Diagonal direction ( $D45^0$ )

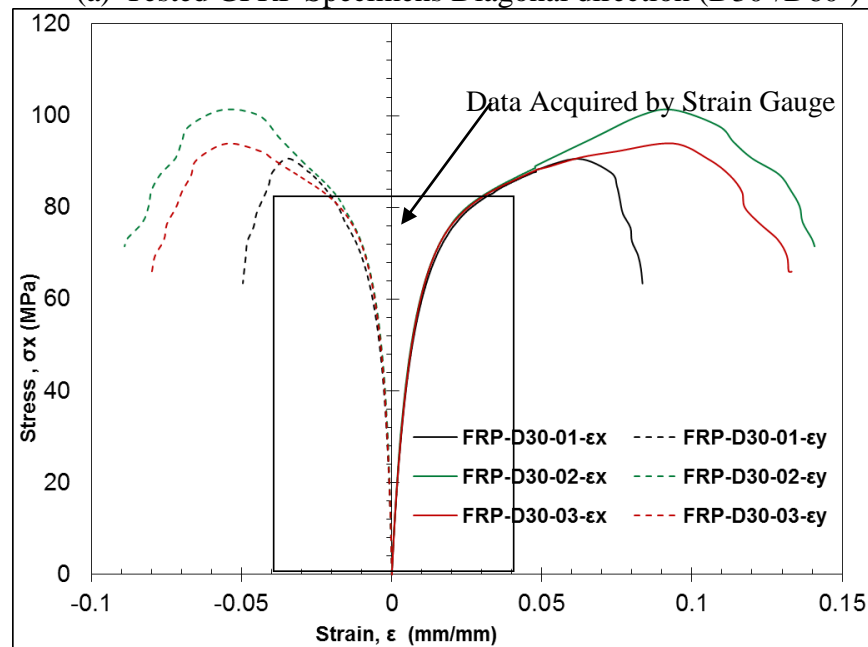
**Figure 3.12 Tested specimens and Stress-strain response of GFRP subjected to tension along the Diagonal direction ( $45^0$ ) of the GFRP plate**

**Table 3.7 Summary of the Tension test of GFRP subjected to tension along Diagonal ( $D30^\circ$ ) Direction (Sample Size,  $n=3$ )**

Specimen ID.	Max. $\sigma_x$ (MPa)	Max. $\epsilon_x$ (mm/mm)	Max. $\epsilon_y$ (mm/mm)	MOE (MPa)	$\nu_{xy}$ or $\nu_{D30}$
FRP-D30-01	90.60	8.35E-02	-4.95E-02	10212.8	0.50227
FRP-D30-02	101.26	1.41E-01	-8.91E-02	9578.3	0.49006
FRP-D30-03	93.96	1.00E-01	-5.29E-02	10116.4	0.48919
Average	95.27	1.08E-01	-6.38E-02	9969.17	0.4938
SD	5.45	2.95E-02	2.19E-02	341.91	0.0073
COV	6%	27%	-34%	3%	1%



(a) Tested GFRP Specimens Diagonal direction ( $D30^\circ/D60^\circ$ )



(b) Stress-Strain Response of GFRP under tension along Diagonal direction ( $D30^\circ/60^\circ$ )

**Figure 3.13 Tested specimens and Stress-strain response of GFRP subjected to tension along the Diagonal direction ( $30^\circ/60^\circ$ ) of the GFRP plate.**



### 3.6 Shear Properties

The shear properties of OSB include those of inter-laminar shear or planar shear (also referred to as shear in plane), shear through the thickness or panel shear (also referred to as edge shear) and rolling shear (*Shrestha 1999, Zhu 2003*). The planar shear of OSB is the most important property to resist the shear forces acting in the beam. Planar shear occurs due to bending moments and in-plane forces as specified in CSA Standard (*CSA-O86 2014*). Planar shear property due to bending is the particular interest of this chapter since there is no in-plane forces acting on the beams (needed to be considered for glued web-flange joint of the I-joist), and the shear through thickness (panel shear) is needed to be considered for web-web joints (*CSA-O86 2014*). Planar shear properties (Shear Rigidity,  $G_{xy}$ ) can be derived from the tension / compression tests along three in-plane directions (*Zhu 2003, Morris et al. 1996, Kaw 2006, Grandmont et al. 2010b*). By using *Eq. 3-1*, shear properties of OSB have been determined by using three measured MOE values tension test of OSB along three directions of the OSB panel as shown in *Figure 3.3 (a)*. As reported by (Zhu 2003), OSB is weaker in tension than in compression, and a single value from tension or compression can be used for the analysis of the I-joist. Hence, in this chapter, only tension tests are conducted to evaluate the shear properties of OSB. Similarly, shear properties of Timber and GFRP were also determined as presented in *Table 3.8*.

$$G_{xy} = \left( \frac{4}{E_{D45}} - \frac{1 - \nu_{xy}}{E_x} - \frac{1}{E_y} \right)^{-1} \quad \text{Eq. 3-1}$$

Where,

$G_{xy}$  = Shear Rigidity (MPa)

$\nu_{xy}$  = Poisson's Ratio

$E_{D45}$  = MOE along Diagonal ( $45^\circ$ ) direction (MPa)

$E_x$  = MOE along Longitudinal direction (MPa)

$E_y$  = MOE along Transverse direction (MPa)



**Table 3.8 Shear Rigidity of OSB, Timber and GFRP**

	OSB	Timber	FRP
Avg. G (MPa)	1574	416*	1405

\* Derived with a value of  $E_T$  and  $E_{45}$  from (Guan and Zhu 2009)

### 3.7 Constitutive Models

As discussed earlier, the main objective of this chapter is to develop the constitutive models for OSB, Timber and GFRP plates. To this end, a regression analysis was performed for OSB, Timber and GFRP test results. Proposed constitutive models are expressions of Strain ( $\epsilon_x$ ) and Ultimate Stress ( $\sigma_u$ ). The general form of the proposed constitutive models is presented in *Eq. 3-2*.

$$\sigma_x = A * \left( \epsilon_x / \sigma_u \right)^B \quad \text{Eq. 3-2}$$

Where,

$\sigma_x$  = Stress (MPa) ;  $\epsilon_x$  = Strain (mm/mm) ;  $\sigma_u$  = Ultimate Stress (MPa)

A, B = Model Coefficients/Constants

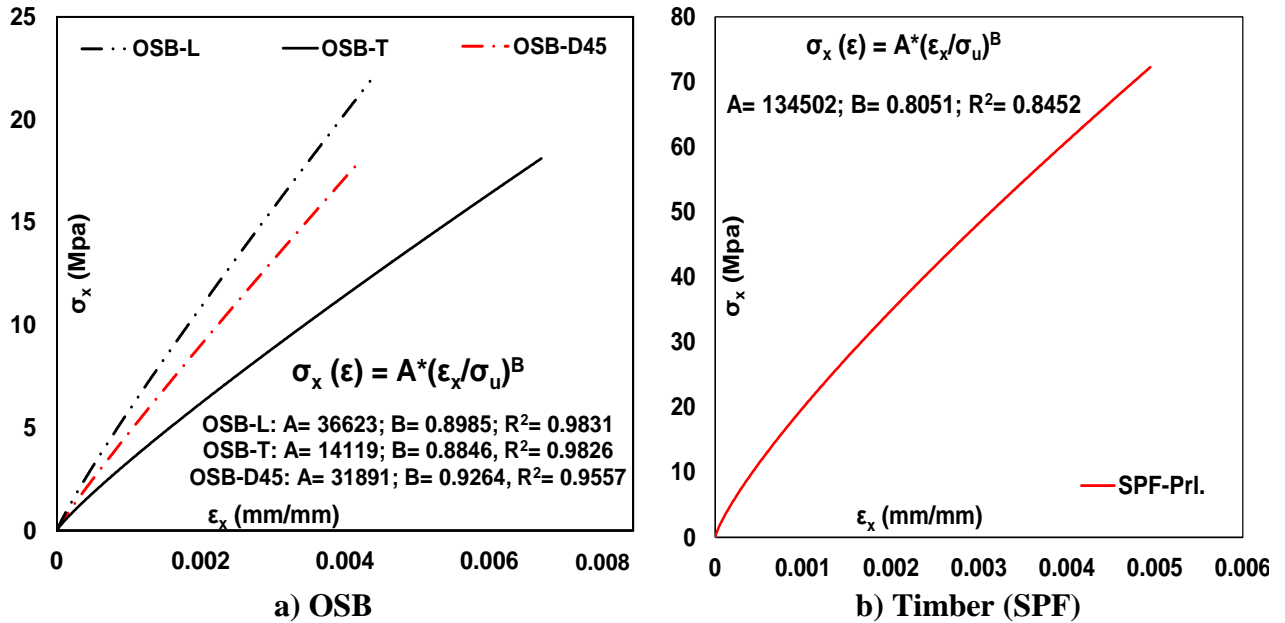
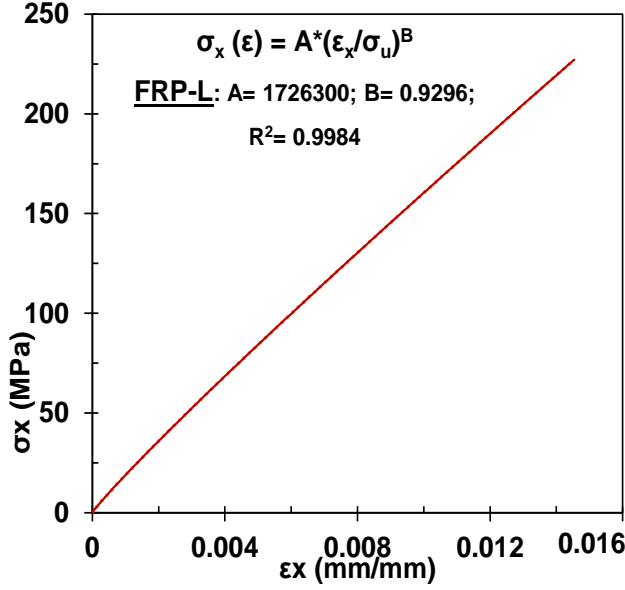


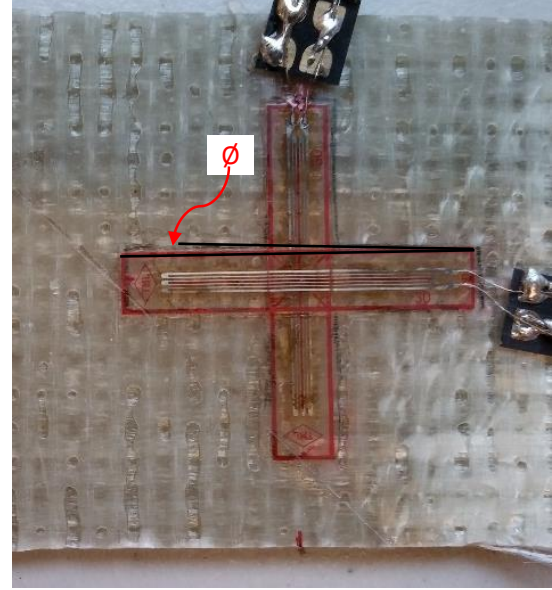
**Figure 3.14 Constitutive Models for OSB and Timber (SPF)**

Based on the tension test results, constitutive models are developed for OSB (L, T & D45<sup>0</sup>), Timber and GFRP (L, D45<sup>0</sup> & D30<sup>0</sup>) as shown in **Figure 3.14** and **Figure 3.15**. Constitutive models of GFRP along both diagonal (D45<sup>0</sup> & D30<sup>0</sup>) directions consist of two expressions (Part1 & Part 2). Expression of Part 1 can be used up-to a strain level of 0.018 and 0.015 for the constitutive model of Diagonal D45<sup>0</sup> & D30<sup>0</sup> direction, respectively. Beyond this point expression of Part 2 must be used.

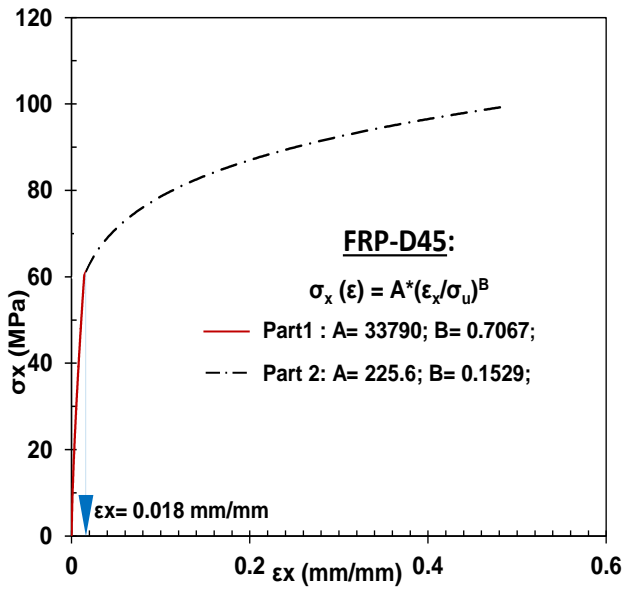
Interestingly, the power coefficient (B) for the best fitted constitutive model of GFRP specimen along longitudinal direction is not equal to 1, i.e. not perfectly elastic. The main reason of this is the orientation of glass fibre in the matrix with respect to the strain gauges as shown in **Figure 3.15 (b)**. Another reason could be the internal orientation i.e. twisting of Glass fibres in the matrix during the application of resin with the brush.



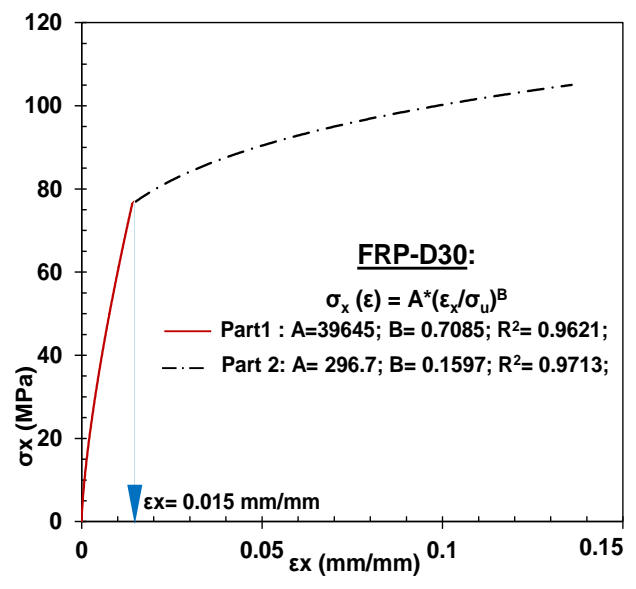
(a) Longitudinal Direction



(b) Obliquity ( $\emptyset$ ) between Fibre and Strain Gauge



(c) Diagonal 45° Direction



(d) Diagonal 30° Direction

**Figure 3.15 Constitutive Models for GFRP a) Longitudinal Direction b) Diagonal 45° Direction c) Diagonal 30° Direction**

### 3.7.1 Validation of Constitutive Models

Developed constitutive models have been validated by comparing them with the experimental results from the 4<sup>th</sup> set of tested specimens. A summary of the comparison has been presented in **Table 3.9**. It is found that the performance of the developed constitutive models are satisfactory

with a Performance Factor (P.F.) being very close to 1.0, except for the GFRP along D45<sup>0</sup>, which overestimate the modulus of Elasticity (MOE) with an error of 14%. On the other hand, the constitutive model of GFRP along D30<sup>0</sup> underestimates the MOE with an error of 1%.

**Table 3.9 Comparison of MOE based on Experimental Results and Developed Constitutive Models**

<b>Materials</b>	<b>Direction</b>	<b>4<sup>th</sup> Specimen MOE<sub>Exp</sub> (MPa)</b>	<b>MOE<sub>Model</sub> (MPa)</b>	<b>P.F.</b>
<b>OSB</b>	L	5891.5	6111.4	1.04
	T	3162.3	3413.0	1.08
	D45 <sup>0</sup>	3722.0	4912.2	1.32
<b>Timber</b>	Parallel to Fiber	16999.3	17736.0	1.04
<b>GFRP</b>	L	16555.7	17063.1	1.03
	D45 <sup>0</sup>	5023.2	5704.9	1.14
	D30 <sup>0</sup>	9578.3	9494.1	0.99

### 3.8 Summary

- From the tension tests conducted in this chapter, it was observed that under tension both OSB and GFRP exhibit the weakest and the strongest mechanical behaviour in the transverse and longitudinal directions, respectively, while properties along the diagonal directions are in between the longitudinal and transverse directions.
- Constitutive models developed in this chapter can be utilized in analysing the performance and predicting the load carrying capacity of I-joist.

## CHAPTER 4: STRUCTURAL CAPACITY OF TIMBER I-JOIST WITH FLANGE NOTCH: EXPERIMENTAL EVALUATION

### 4.1 General

Composite timber I-joists are widely used as floor and roof joists in the construction of commercial and residential buildings in Europe and North America. Commonly, these I-joists are made with timber or laminated veneer lumber (LVL) as flange material in combination with Oriented Strand Board (OSB) or Plywood as web materials. These structural engineered timber I-joists are less expensive, lighter in weight, stronger, and more efficient compared to the solid sawn lumber beams.

According to the manufacturer design guidelines (*American-Wood-Council 1999*), (Wood I-Joist Manufacturers Association (WIJMA) 2008), flange cut on OSB webbed I-joists are strictly prohibited to use during construction sites. Cuts and notches in the flange of I-joist are commonly made during construction to facilitate the electro-mechanical systems of the buildings. Some photographs of flange notches in a construction site have been shown in *Figure 4.1*. The effect of flange notches on the strength properties (e.g. load carrying capacity, flexural strength, and shear strength) of timber I-joists is not fully understood and current design specifications (*CSA-086*) for building construction do not provide any design guideline for I-joists with flange cut and notches (Canadian-Standard-Association 2014a). Very few research studies on OSB webbed timber I-joists with flange cut and notch have been conducted (*Hindman and Loferski 2008*).

The primary objective of this chapter is to compare the load capacity and stiffness of single flange cut I-joists with those of an uncut I-joist (control specimen). In the current research study, an experimental work was carried out on OSB webbed timber I-joists with flange notches or cuts

at different locations along the length as well as two different sizes of flange cuts. A total of 80 I-joist specimens with flange notched and 20 uncut (control) I-joists were tested in this experimental study to investigate the strength reduction and failure pattern of I-joists with flange notches.



*Figure 4.1: Flange notched I-joists at construction site*

## **4.2 Motivation**

Very often builders cut the flange of I-joists during the construction phase of a project without considering the structural integrity to accommodate the service conduits and ducts. Eventually these flange notched I-joists are required to be replaced or retrofitted to meet the design requirements, which may affect the project cost, time schedule and safety of the project. Flange notches of I-joists may affect performance in terms of deflections, load carrying capacity and vibration of the structure. The primary impact of flange notches on I-joists is on the flexural strength as well as the shear strength. The Wood I-joist Manufacturer Association (WIJMA) has a published reference to determine the shear strength of I-joist with web holes, which is well accepted by building code evaluation services as the procedure to evaluate the strength of I-joist with web holes (Wood I-Joist Manufacturers Association (WIJMA) 2008). However, there is no guideline for evaluation of the strength of timber I-joists with flange notches.

### 4.3 Literature Review

Until today no research work was found related to the deficit of load capacity and stiffness of I-joists with flange notches or cuts at the top flange, which is subjected to flexural compression force. Although, Hindman and Loferski (*Hindman and Loferski 2008*) did carry out a pertinent study to investigate the improved load capacity and stiffness of flange cut I-joists retrofitted with cold formed steel reinforcers in relation to uncut control I-joists, they did not perform any test to determine the capacity and stiffness of un-retrofitted flange cut I-joists. Their study shows that the strength and stiffness of reinforced/ repaired flange cut I-joists are lower than those of the uncut or control I-joists by 39.8% and 33%, respectively. Before studying the retrofitting technique it is important to understand the behavior of flange notched I-joists.

Most of the previous research studies were carried out on the timber I-joists with web holes rather than with flange notch or cut. An experimental study and finite element modeling was conducted by Zhu et al. (*Zhu et al. 2005b*), Guan and Zhu (*Guan and Zhu 2009*) & Zhu et al. (*Zhu et al. 2007a*) and they found that stress concentrations occur around the web opening. They also observed that fractures were formed in tension zones around the opening of the OSB web and the cracks developed towards the beam flanges in a direction roughly at  $45^0$  to the beam axis. Later on, Zhu et al. (*Zhu et al. 2006*) conducted both experimental investigation and finite element analysis to investigate the buckling behavior of OSB webbed I-joists and found that good correlation exist between analytical and experimental results.

Pirzada et al. (*Pirzada et al. 2008*) predicted the strength of timber I-joists with web holes by applying fracture mechanics based on the Finite Area Method (FAM). Afzal et al. also conducted an experimental study to evaluate the I-joist strength with web holes (*Afzal et al. 2006*). Later on

Morrissey et al. (*Morrissey et al. 2009*) conducted an experimental and analytical investigation with excess web openings. Finite-element analyses of all test configurations were conducted to understand the effects of web openings (circular and square) on the stiffness, stress distributions around openings, and ultimate failure mechanisms. They observed that square web openings are more critical than the circular web openings for load carrying capacity due to the occurrence of stress concentration at the corner of the square opening. The load carrying capacity of I-joists with circular web openings was 45% lower than that of the control I-joists, whereas for I-joists with square openings, it was 53% lower than that of the control I-joists.

#### **4.4 Testing of Timber I-joists with a Single Flange Cut**

Two different span lengths of I-joists were tested; 12ft and 20ft. These joists were produced by an I-joist manufacturer (AcuTruss Industries Limited) in Kelowna, Canada. I-joists were produced with a 9.5mm thick OSB web and 38mm by 63mm lumber flanges as shown in *Figure 3.1 a*. Test set-up and specimen dimensions were selected by strictly following the provisions of ASTM-D5055 (*ASTM-D5055 2013*) and WIJMA guideline (Wood I-Joist Manufacturers Association (WIJMA) 2008). According to the manufacturer (NASCOR) Specifier Guideline (*NASCOR 2010*), the maximum allowable span (simple) is 20 feet for the I-joists with the selected cross sectional geometry. The test setup and loading diagram are shown in *Figure 4.2*. To prevent lateral buckling of tested I-joists a sufficient number of lateral supports was provided as shown in *Figure 4.2*. A total of 4 series of I-joists for each span length i.e. a total of 80 specimens were tested with flange notches at different locations with 100mm×100mm and 100mm×150mm notch sizes. Two series of control I-joists (i.e. 20 specimens) were also tested for each span length (12ft



and 20ft). Thus a total of 100 I-joist specimens were tested where each series consists of 10 samples.

**Table 4.1: Specimen Details of I-Joist Testing**

Specimen Code	Span Length, L (mm)	Size of Cut ( $B_n \times D_n$ ) (mm)	Distance from Support, ( $L_n$ ) (mm)	Number of Samples
12-A--	3650 (12ft)	-	-	10
12-F--	3650 (12ft)	100x100	305	10
12-G--	3650 (12ft)	100x100	455	10
12-H--	3650 (12ft)	100x100	610	10
12-I--	3650 (12ft)	100x150	455	10
20-A--	6100 (20ft)	-	-	10
20-K--	6100 (20ft)	100x100	305	10
20-L--	6100 (20ft)	100x100	455	10
20-M--	6100 (20ft)	100x100	610	10
20-N--	6100 (20ft)	100x150	455	10

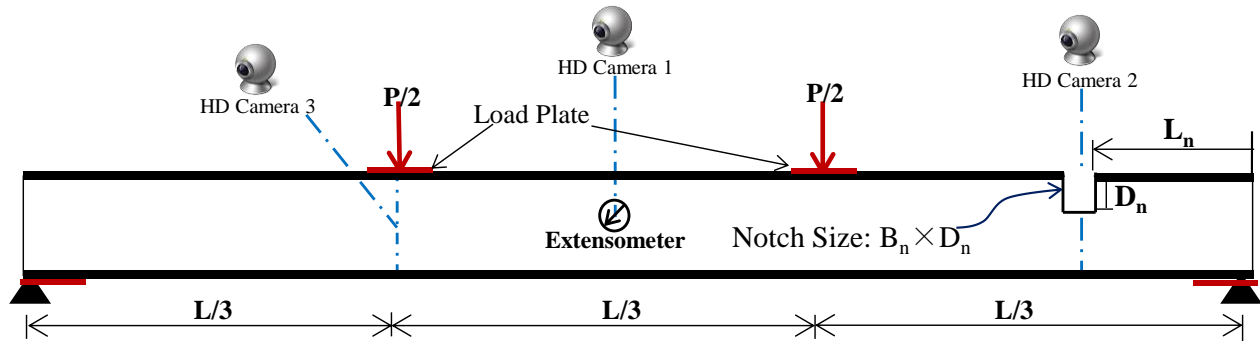


**Figure 4.2: Schematic diagram of the test setup and flange notched I joist.**

**Table 4.1** shows the different configurations of flange cut I-joists tested including the distance of the cut from the support of the beam ( $L_n$ ), span length ( $L$ ), dimensions of the flange cut ( $B_n \times D_n$ ), and number of samples. The locations of the flange notch were selected as per the most common scenarios experienced by the I-joist installation and manufacturing industry. I-joist manufacturing

industry usually faces the notch related problems within 600 mm (2 ft) from the end support due to the presence of floor drains of sewer and sanitary pipes and conduits. Here, the specimens are designated as 12-A-01, 20-M-10, etc. The first two digits of the specimen name denote the span length (in ft.). The letters of the specimen name denote the series number (A, F-I, K-N). The last two digits (--) denote the specimen number (01 to 10). Load and deflection response was measured continuously during the entire test. The deflection was measured in two different methods; an extensometer was used to measure the deflection of I-joists at the mid span up to a certain limit (usually the maximum measurement limit of the extensometer, which was 2.5 inch or 50 mm) and image processing analysis was used beyond that certain limit until the failure occurred. Considering the large length of the specimen, three High Definition (HD) cameras were used to record the entire test of each specimen in three different locations (mid span, one loading point and flange cut) for continuous monitoring of deflection and crack development.

The average peak load and stiffness were determined to evaluate the degradation of the I-joist performance with flange cut. Stiffness was measured as described by Hindman et al. (*Hindman and Loferski 2008*), which is defined as the slope of the load deflection curve in the linear elastic region of the curve. Due to the extensive deflection of the I-joists their performances have also been evaluated based on the load at a specific deflection as per the serviceability design provision of CSA-O86 (Canadian-Standard-Association 2014a) and NBCC-Part 9 (*NBCC 2015*), which are  $L (mm)/180$  and  $L (mm)/360$ . Here, deflections,  $\Delta=L/180$  and  $\Delta=L/360$  represent the limiting deflections for roof and flooring systems subjected to total load (dead load + live load + snow load) (Canadian-Standard-Association 2014a) and only live load (*NBCC 2015*), respectively.

## 4.5 Results

In the following section a detailed discussion and comparison have been made on the experimental results of the tested I-joists. Among the test specimens, series A is the control I-joist without any notch, series 12-F to 12-I and series 20-K to 20-N are the I-joists with two different notch sizes in the flange at two different locations, respectively.

### 4.5.1 Failure Mode and Load Deflection Response

The behavior of I-joists can be attributed to the load-deflection response as demonstrated in a four point bending test. Load deflection responses until failure of 12ft and 20ft span length I-joists are presented in the following section. It was perceptible from the load deflection response of individual tested I-joists that most of the I-joists exhibited linear behavior during the entire test duration until failure. However, some I-joists also showed a linear relationship at the beginning of the test, which can be attributed to the elastic region of the load deflection response, followed by a nonlinear portion which can be attributed to the inelastic state of the load deflection response of the I-joists. In the following sub-sections failure mode and load deflection responses (load carrying capacity, deflection, stiffness, and load at serviceability condition) of the tested I-joists have been discussed in details.

### 4.5.2 Control I-Joists-Test Series 12-A & 20-A

I-joist test series A represents the control beam which has no flange notch. Two types of failure were observed in the 12 feet control I-joists: 1) shear at support and 2) flexure at mid-span. The failure was initiated mostly by the presence of knots in the flanges as shown in **Figure 4.3 (a) & Figure 4.3 (b)** or due to the de-bonding of the OSB web from the flange as shown in **Figure 4.3 (c)**. Six specimens (12-A1, 12-A2, 12-A7, 12-A8, 12-A9 & 12-A10) failed in flexure at mid-span

(*Figure 4.3 (d) & (e)*) and three specimens (12-A3, 12-A4, and 12-A6) failed in end shear (*Figure 4.3 (f)*). Only specimen 12-A5 failed in both shear failure at support and flexural failure at mid-span (*Figure 4.3 (g) & (h)*). A de-bonding was also observed in the web and flange connection at the top flange of this specimen. For 20 feet control I-joists, all the specimens failed in flexure at mid-span (*Figure 4.3 (e)*) which was due to de-bonding of Flange-OSB joint. But some of the I-joists also failed due to the presence of knot at flange, such as 20-A-5. No shear failure was observed in any of the 20 feet control specimens. The load-deflection curves are plotted in *Figure 4.4*. The average load capacities of the 12 feet and 20 feet beams were 31.88 kN and 22.07 kN, respectively. The average stiffness of the 12 feet and 20 feet I-joists was 1082 (N/mm) and 275 (N/mm), respectively. The average deflection at failure of the beams was 29 mm and 81 mm, respectively for the 12 feet and 20 feet control I-joists. The results showed that the 12 feet I-joists had on an average 43% higher load carrying capacity compared to those of 20 feet I-joists. From the load deflection curves of the control specimens (*Figure 4.4*), it is observed that only three specimens (12-A1, 12-A8 & 20-A10) failed at very low loads compared to the other specimens of the series. The loads carrying capacities for these three joists were 15.6 kN, 15.73 kN and 12.10 kN; which are around 50% of the average load carrying capacity of the respective series. This low load carrying capacity was due to the presence of a large size knot in the flange (*Figure 4.3 (b)*).



(a)



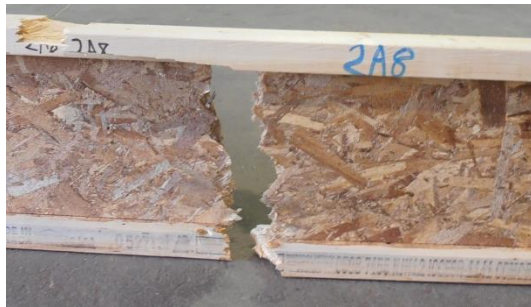
(b)



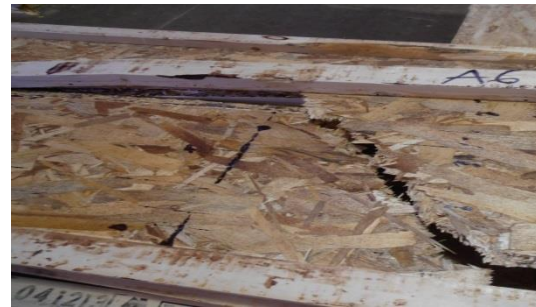
(c)



(d)



(e)



(f)



(g)



(h)

**Figure 4.3: Typical failures: a, b) Failure due to presence of knot; c) Web-flange de-bonding; d, e) flexural failure; f) shear failure; g, h) Combined shear and flexural failure**

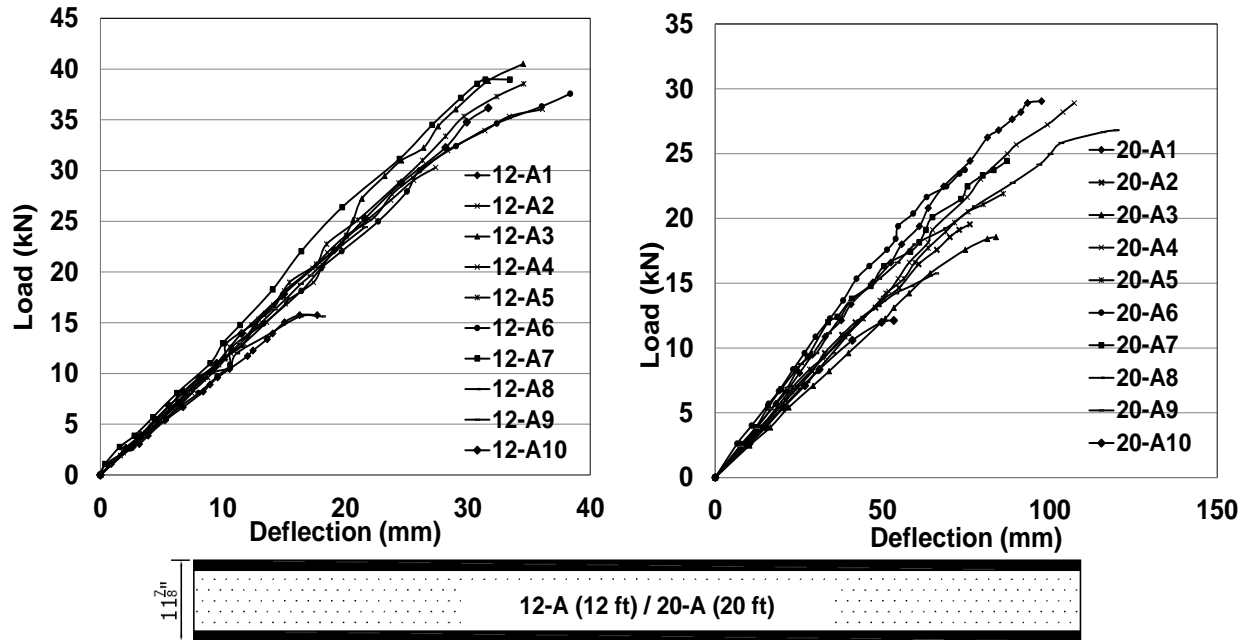


*Figure 4.4: Load-deflection curves for series 12-A and 20-A*

#### 4.5.3 Test Series 12-F & 20-K

Series 12-F and 20-K has a notch with the dimension of 100mm×100 mm at a distance of 305 mm from the right support. Due to the presence of notch, the bending and shear strength was significantly reduced and therefore, all the 12 feet I-joists of series 12-F failed in flexure and shear at the location of notch. The webs failed in shear with an angle ranging from  $58^{\circ}$  to  $69^{\circ}$  (Average value  $63^{\circ}$ ) with the longitudinal axis of the joist, whereas the flanges failed in flexural tension as shown in *Figure 4.5 (a), (b) & (c)*. De-bonding of web-flange joint was not observed in any specimen of this series. Except for one (20-K9), all the specimens of 20 feet I-joists (20-K) also failed in a similar mode to 12 feet I-joists (12-F). Specimen 20-K9 experienced flexural failure at the mid-span. For this specimen, the failure was initiated due to the presence of knot in the flange, which was subjected to flexural tension (*Figure 4.6 (a) & (b)*). Combined flexural and shear failure was observed in 12-F8 and 20-K10 I-joists. However, from the video of these two I-joist tests, it was found that flexural failure was occurring before the shear failure. Occurrence of different types

of failure observed in the tested I-joists and the average applied shear ( $V_u$ ), moment at notch location ( $M_{Ln}$ ), flexural strength ( $M_u$ ) have been presented in details in **Table A.1 (In Appendix A)**. The load-deflection curves are plotted in **Figure 4.7**. The average capacities of the 12 feet and 20 feet beams were 15.67 kN and 12.35 kN, respectively as shown in **Table 4.2**. Experimental results indicated that the average strength reduction of 12 feet and 20 feet I-joists were 51% and 44%, respectively compared to that of the corresponding control I-joists. The average deflection at failure was 17 mm and 48 mm, respectively for the 12 feet and 20 feet I-joists, which was reduced by 42% and 40% from the control beams' maximum deflection. The average stiffness and average load at serviceability condition ( $\Delta = L/180=20.3$  mm) of the 12 feet I-joists were 916 N/mm and 22.36 kN, respectively. On the other hand, the average stiffness and average load at serviceability condition ( $\Delta = L/180=33.9$  mm) of the 20 feet I-joists were 214 N/mm and 7.98 kN, respectively. It was found that the average stiffness reduction of 12 feet and 20 feet I-joists were 15% and 22%, respectively compared to that of their control I-joists, which signifies that the presence of an opening makes the longer span joists less stiff. It was also found that the average load reduction of 12 feet and 20 feet I-joists were 13% & 17% for roof & flooring system subjected to total load (at  $\Delta = L/180$ ) and 12% & 14% for roof & flooring system subjected to live load (at  $\Delta = L/360$ ), respectively compared to that of their control I-joists.

**Table 4.2: Test Results of the I-Joist with flange cut at different location**

Spec. Code	Avg. Max. Load (kN)	COV	Avg. Stiffness (N/mm)	COV	Avg. Load at $\Delta = L/180$ (kN)	COV	Avg. Load at $\Delta = L/360$ (kN)	COV
<b>12-A</b>	31.9 (37.2)	32.5% (9.0%)	1082	7.6%	22.35 (23.91)	14.4% (7.2%)	10.69	12.2%
<b>12-F</b>	15.7	9.5%	916	10.6%	19.42	10.1%	9.42	8.4%
<b>12-G</b>	9.1	10.9%	727	16.4%	15.09	11.0%	7.83	9.5%
<b>12-H</b>	6.4	7.6%	666	12.2%	11.48	15.7%	6.20	9.0%
<b>12-I</b>	5.7	21.9%	587	10.3%	11.10	15.5%	5.32	14.1%
<b>20-A</b>	22.1 (24.1)	25.4% (16.5%)	275	15.1%	9.62	13.9%	4.24	20.9%
<b>20-K</b>	12.4 (12.7)	14.4% (11.6%)	214	8.0%	7.97	7.8%	3.64	8.5%
<b>20-L</b>	9.7	8.4%	201	7.2%	7.61	7.5%	3.40	7.2%
<b>20-M</b>	6.7	14.2%	201	16.7%	8.07	7.4%	3.76	15.0%
<b>20-N</b>	5.5 (5.7)	15.3% (9.6%)	186	11.4%	7.05	19.5%	3.35	10.1%

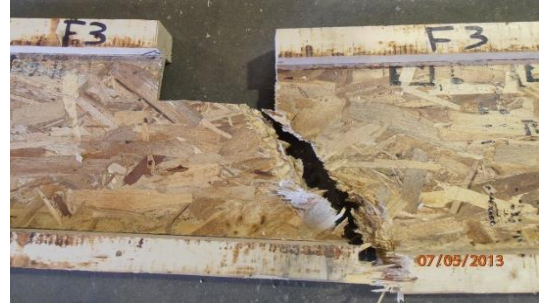
**Note:**

1. Values specified in parenthesis are obtained by discarding the test results from the faulty I-joists with the presence of knot at flanges.
2. Avg. Load at  $\Delta = L/180$  is the serviceability condition for flooring & roofing system (CSA-O86, 2010)
3. Avg. Load at  $\Delta = L/360$  is the serviceability condition for flooring & roofing system based on Live Load (NBCC, Part 9)





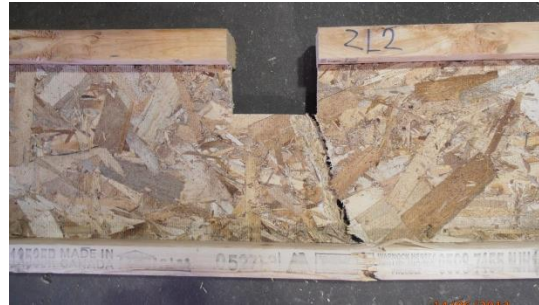
(a) Pure flexural failure: 12 feet I-joists



(b) Combined flexural and shear failure: 12 feet I-joists



(c) Pure flexural failure: 20 feet I-joists



(d) Combined flexural and shear failure: 20 feet I-joists

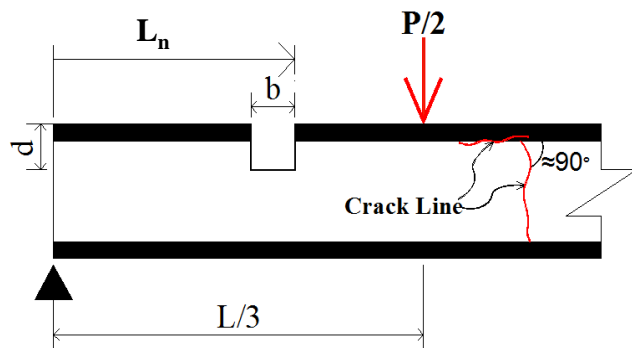
**Figure 4.5: Failure mechanisms exhibited in tested I-joists with flange notch (Series: 12-F, 12-G, 12-H, 12-I, 20-K, 20-L, 20-M, and 20-N)**



○ - Knot

Crack Line

(a) Crack/Failure occurred at mid span due to knot



(b) Schematic diagram of failure occurred at 20-K-09 I-joist due to presence of knots

**Figure 4.6: Failure mechanisms exhibited in 20-K-09 I-joist due to presence of knots**

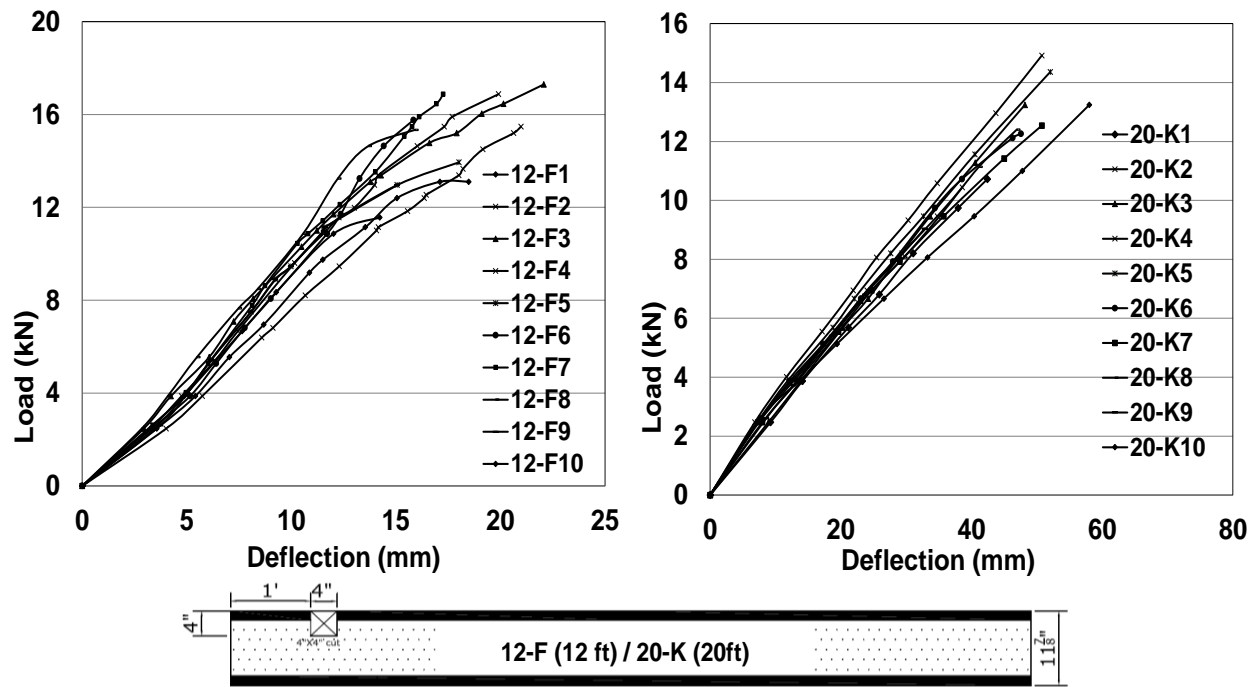


Figure 4.7: Load-deflection curves for series 12-F & 20-K

#### 4.5.4 Test Series 12-G & 20-L

Test Series 12-G and 20-L consist of 12 ft and 20 ft I-joist specimens respectively, with a 100×100 mm flange notch located at 455 mm away from the right end support. During the static load test it was observed that failure type for specimens from G series is equally dominated by flexure and combined flexure & shear type of failure. Five specimens from G Series (12-G2, 12-G3, 12-G4, 12-G7, and 12-G10) experienced flexural failure as shown in *Figure 4.5 (a) & (c)* while failure type for the rest of the specimens (12-G1, 12-G5, 12-G6, 12-G8, and 12-G9) were dominated by combined flexure and shear (*Figure 4.5 (b) & (d)*) type failure at the location of the notch. Most of the cases failure was triggered due to the crack initiation at the lower right corner of the flange notch, which experienced higher moment demand. However, the crack propagation in these specimens were not similar to what was being exhibited in the test samples from 12-F and

20-K series. Due to having a large failure angle (Average value  $71^0$ ) with the longitudinal axis, the longitudinal components reduced to large extent compared to others. This is due to the increment of flexural demand at the notch location as the notch has been moved towards the higher flexural zone in the joist. For 12-G series, de-bonding of web-flange joint was not observed for any specimen.

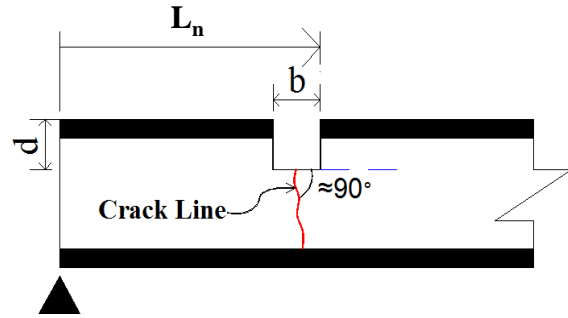
The only difference that exist between specimens from 12-G and 20-L series is the length of the I-joists, which supposedly does not shift the failure type to large extent. Six specimens from 20-L series (20-L1, 20-L5, 20-L7, 20-L8, 20-L9, and 20-L10) experienced flexure type failure while rest of the specimens (20-L2, 20-L3, 20-L4, and 20-L6) failed in combined flexure and shear initiated at notch location. Similar nature of crack pattern was also observed for these specimens as discussed in previous section for G series. Similar to **Figure 4.7**, load-deflection curves for specimens of series 12-G and 20-L are plotted as well. In the 20 feet series, specimen 20-L7 failed in bending, however, the crack initiated at the middle of the notch as shown in **Figure 4.8**, while for all other specimens, crack initiated at the inner corner of the notch. From the static load test the average capacity of the 12 feet and 20 feet I-joists was 9.14 kN and 9.68 kN, respectively. Experimental results indicate that the average strength reduction of the 12 feet and 20 feet I-joists was 71% and 56%, respectively compared to that of the corresponding control I-joists. The average maximum deflection at failure was 14 mm and 38 mm, respectively for the 12 feet and 20 feet I-joists, which is 54% and 53% less than the ultimate deflection of control joists.

The average stiffness and average load at serviceability condition ( $\Delta = L/180=20.3$  mm) of the 12 feet I-joists (12-G) were 727 (N/mm) and 15.09 kN, respectively. On the other hand, the average stiffness and average load at serviceability condition ( $\Delta = L/180=33.9$  mm) of the 20 feet I-joists

(20-L) were 201 N/mm and 7.59 kN, respectively. Consequently, the average stiffness reduction of 12 feet and 20 feet I-joists was 33% and 27%, respectively compared to that of their control I-joists. The average load reduction of 12 feet and 20 feet I-joists was 32% & 21% for roof & flooring system subjected to total load (at  $\Delta = L/180$ ) and 27% & 20% for roof & flooring system subjected to live load (at  $\Delta = L/360$ ), respectively compared to that of their control I-joists.



(a) Crack occurred at the middle of the notch width instead of the corner.



(b) Schematic diagram of failure occurred at 20-L-07 I-joist due to presence of knot.

**Figure 4.8: Failure mechanisms exhibited in I-joist 20-L-07**

#### 4.5.5 Test Series 12-H & 20-M

With an intention to observe the effect of notch location on the failure type and capacity Series 12-H and 20-M have been created with a 100×100 mm flange notch located at 610 mm from the end support. With increasing distance between support and the flange notch, an upward tendency in percentage of flexural failure can be observed for specimens from 12-H series. Seven test samples from this series (12-H1, 12-H3, 12-H4, 12-H5, 12-H7, 12-H8, and 12-H10) has suffered flexure type failure as shown in **Figure 4.5 (a) & (c)**, while the rest of the specimens (12-H2, 12-H6, and 12-H9) failed in combined bending and shear (**Figure 4.5 (b) & (d)**) at the location of notch. Combined flexural and shear failure occurred with the similar fashion of series 12-F and 20-K as discussed earlier. However, propagation of crack growth (longitudinal components) was even smaller with a higher failure angle (Average value  $77^\circ$ ) with the longitudinal axis of the joist

compared with the crack growths exhibited in the specimens of series (12-F, 20-K) and (12-G, 20-L). This is due to the further increment of flexural demand at the notch location as the notch has been moved towards the higher flexural zone in the joist.

Shifting the notch location from 455 mm to 610 mm inwards does not show any noticeable changes for 20ft long I-joists. Five specimens (20-M1, 20-M3, 20-M4, 20-M8, and 20-M9) of the 20 feet I-joists of series 20-M failed in flexural (**Figure 4.5 (a) & (c)**) and rest of the specimens (20-M2, 20-M5, 20-M6, 20-M7, and 20-M10) failed in combined bending and shear (**Figure 4.5 (b) & (d)**) at the location of notch. The crack propagation was also in similar fashion to 12 feet I-joists (12-G). Similar to the **Figure 4.7**, load-deflection curves for specimens of series 12-H and 20-M are plotted. The average load carrying capacity of the 12 feet and 20 feet I-joists was 6.40 kN and 6.72 kN, respectively. Experimental results indicated that the average strength reduction of 12 feet and 20 feet I-joists was 80% and 70%, respectively compared to that of the corresponding control I-joists. The average deflection at failure was 9.9 mm and 25.85 mm, respectively for 12 feet and 20 feet I-joists which was reduced by 67% and 68%, respectively from the ultimate deflection of control joists.

The average stiffness and average load at serviceability condition ( $\Delta = L/180=20.3$  mm) of the 12 feet I-joists (12-H) were 666 (N/mm) and 11.49 kN, respectively. On the other hand, the average stiffness and average load at serviceability condition ( $\Delta = L/180=33.9$  mm) of the 20 feet I-joists (20-M) were 201 (N/mm) and 8.08 kN, respectively. The average stiffness reduction of 12 feet and 20 feet I-joists was 38% and 27%, respectively compared to that of their control I-joists. The average load reduction of 12 feet and 20 feet I-joists was 49% & 16% for roof & flooring systems

subjected to total load (at  $\Delta = L/180$ ) and 42% & 11% for roof & flooring systems subjected to live load (at  $\Delta = L/360$ ), respectively compared to that of their control I-joists.

#### 4.5.6 Test Series 12-I & 20-N

Series 12-I and 20-N has a notch at a distance of 305 mm from the support which is similar to the series 12-F and 20-K, but this series has a deeper notch with a depth of 150 mm instead of 100 mm. Only four specimens (12-I1, 12-I3, 12-I4, and 12-I9) of the 12 feet I-joists of series 12-I failed in bending as shown in **Figure 4.5 (a) & (c)** and rest of the specimens (12-I2, 12-I5, 12-I6, 12-I7, 12-I8, and 12-I10) failed in combined bending and shear (**Figure 4.5 (b) & (d)**) at the location of notch. Combined flexural and shear failure was occurred with the similar fashion of series 12-F and 20-K. However, it is noticed that propagation of crack growths (longitudinal components) was lower, i.e. higher failure angle (average value  $72^0$ ) with the longitudinal axis of the joist in comparison with the crack growths exhibited in the specimens of series (12-F, 20-K). This is due to the further reduction of shear strength of the I-joists at notch location by a deeper cut of the web. Six specimens (20-N2, 20-N3, 20-N5, 20-N6, 20-N8, and 20-N9) of the 20 feet I-joists of series 20-N failed in flexure (**Figure 4.5 (a) & (c)**) and rest of the specimens (20-N1, 20-N4, 20-N7, and 20-N10) failed in combined bending and shear (**Figure 4.5 (b) & (d)**) at the location of notch. The crack propagation was also in similar fashion to 12 feet I-joists (12-I). It is observed that one specimen (20-N6) of the 20-N series has a knot in the bottom flange at notch location of the joist. Similar to **Figure 4.7**, load-deflection curves for specimens of series 12-I and 20-N are plotted in **Figure 4.6**. From the load deflection curves, it is observed that the 12-I4 specimen has the lowest (4.15 kN) load carrying capacity, whereas the 12-I5 specimen failed at the maximum load (7.79 kN). For 20 feet I-joists series, specimen 20-N1 and 20-N10 failed at the lowest and maximum load, respectively. The average load carrying capacities of the 12 feet and 20 feet I-joists with a

150 mm deep flange notch were 5.69 kN and 5.47 kN, respectively. Experimental results indicated that the average strength reduction of 12 feet and 20 feet I-joists were 82% and 75%, respectively compared to that of the corresponding control I-joists. However, the average strength reduction of 12-I and 20-N series of I-joists was 38% and 44%, respectively compared to that of the 12-F and 20-K series of I-joist. This strength reduction was completely due to the reduction of shear strength of the I-joist at notch location. The average deflection at failure load was 10.7 mm and 25.85 mm, respectively for 12 feet and 20 feet I-joists which was reduced by 64% and 68% respectively from the ultimate deflection of control joists.

The average load at serviceability condition ( $\Delta = L/180=20.3$  mm) were 11.1 kN and 7.05 kN for the 12 feet (12-I) and 20 feet (20-N) I-joists, respectively. The average stiffness was 587 (N/mm) and 186 (N/mm) for the 12 feet (12-I) and 20 feet (20-N) I-joists, respectively. It is found that the average stiffness reduction of 12 feet and 20 feet I-joists were 46% and 33%, respectively compared to that of their control I-joists. However, the average stiffness reduction of 12-I and 20-N series of I-joists was 19% and 8%, respectively compared to that of the 12-F and 20-K series of I-joist. It is also found that the average load reduction of 12 feet and 20 feet I-joists was 26% & 7% for roof & flooring system subjected to total load (at  $\Delta = L/180$ ) and 32% & 2% for roof & flooring system subjected to live load (at  $\Delta = L/360$ ), respectively compared to that of the load at serviceability conditions of I-joists series of 12-F and 20-K. These reductions of stiffness and load at serviceability condition were due to the reduction of shear stiffness of the I-joist at notch location.

## 4.6 Comparative Study

The I-Joist manufacturer guideline (Wood I-Joist Manufacturers Association (WIJMA) 2008) does not allow any cut or notch at any flange and it is quite unsafe to cut the bottom flange which is under tension stresses. Any kind of notch in the flange has a significant effect on the stiffness and strength of the I-joists; however the presence of notches changes the failure mode. Reduced bending and shear strength were observed by the removal of flange and web material at the location of notches.

The average and coefficient of variation (COV) of the peak load, stiffness, and load at serviceability conditions (load at deflection of  $L/180$  and  $L/360$ ) are presented in **Table 4.2**. From test results it is found that the stiffness and strength (peak load) of I-joists with flange notches were lowered within the range of 15% - 46% and 44% - 82%, respectively compared to control I-joist series as shown in **Table 4.3**. For the peak load values, the COV varied from 7.6% to 32.5% and 8.4% to 25.4% for 12ft span and 20ft span, respectively. For the stiffness values, the COV varied from 7.6% to 16.43% and 7.2% to 15.1% for 12ft span and 20ft span, respectively. The COV of the load at  $L/180$  ranged from 10.1% to 15.70% for 12ft span I-joists and 7.4% to 19.5% for 20ft span I-joists. The COV values for the load at the deflection of  $L/180$ ,  $L/360$  and stiffness varied within a narrow range which is expected for timber composite I-joists. However, the peak load values varied over a higher range in the presence of large size knots in the flanges. For instance, knots were present in few samples for the 12-A, 20-A, 20-K and 20-N series I-joists. **Table 4.2** shows higher COV for these series, where neglecting those samples could significantly reduce the variations as shown in parenthesis (e.g. COV of peak load for 12ft span I-joists significantly reduced from 32.5% to 9%).



**Table 4.3: Comparison of ultimate load, stiffness and load at serviceability conditions of the I-joist with flange cut at different location**

Spec. Code	Avg. Capacity (kN)	% reduction		Avg. Stiffness (N/mm)	% reduction		Avg. Load at $\Delta = L/180$ (kN)	% reduction		Avg. Load at $\Delta = L/360$ (kN)	% reduction	
12-A	31.9	0% *	-	1082	0% *	-	22.35	0% *	-	10.69	0% *	-
12-F	15.7	51%		916	15%		19.42	13%		9.42	12%	
12-G	9.1	71%	0% *	727	33%	0%	15.09	32%	0% *	7.83	27%	0% *
12-H	6.4	80%	-	666	38%	-	11.48	49%	-	6.20	42%	-
12-I	5.7	82%	38%	587	46%	19%	11.10	50%	26%	5.32	50%	32%
20-A	22.1	0% *	-	275	0% *	-	9.62	0% *	-	4.24	0% *	-
20-K	12.4	44%		214	22%		7.97	17%		3.64	14%	
20-L	9.7	56%	0% *	201	27%	0% *	7.61	21%	0% *	3.40	20%	0% *
20-M	6.7	70%	-	201	27%	-	8.07	16%	-	3.76	11%	-
20-N	5.5	75%	44%	186	33%	8%	7.05	27%	7%	3.35	21%	2%
Note: * 0% indicates comparison was made with that I-joist series.												

It was found that the maximum load carrying capacity was reduced by 80% and 70% for series H and series M with a flange notch at 605mm from the support with a dimension of 100mm×100mm for 12ft and 20ft span I-joists, respectively (**Table 4.3**). Moreover, the strength was further reduced with the increasing depth of the notches (150mm), which is expected due to the reduction of shear stiffness of the web as the web materials are removed.

Box plot is a simple but powerful graphical tool to illustrate the spread and variances of samples. The box plot of the load carrying capacity of the tested I joists, illustrates whether the test results obtained from the four point bending tests are normal or slightly skewed up/down (right/left). In **Figure 4.9** each test series has a box diagram where the height signifies the numerical range of data (minimum and maximum values) for load carrying capacity. The “boxes”

signify the inter quartile range 25th percentile (Q1) through the 75th percentile (Q3) of the data set. The boundary line of the shaded portions of the box is the median value (i.e.50th percentile). The box and whisker plots as shown in **Figure 4.9**, clearly indicate that most of the load carrying capacities of tested I-joist closely follow the normal distribution pattern, except the 12-A and 12-I series. The median and the mean values of the tested I-joist series are very close, which clearly signifies that the data points follow the central tendency of the normal distribution curve. For 12-A I-joist series most of the test results fall in the lower range of the median, which is negatively skewed. On the other hand, the load carrying capacities of tested I-joists of series 12-I are positively skewed, which reflects that test results fall in the upper range of the median. For analyzing the whisker plots, outlier data points were checked and discarded.

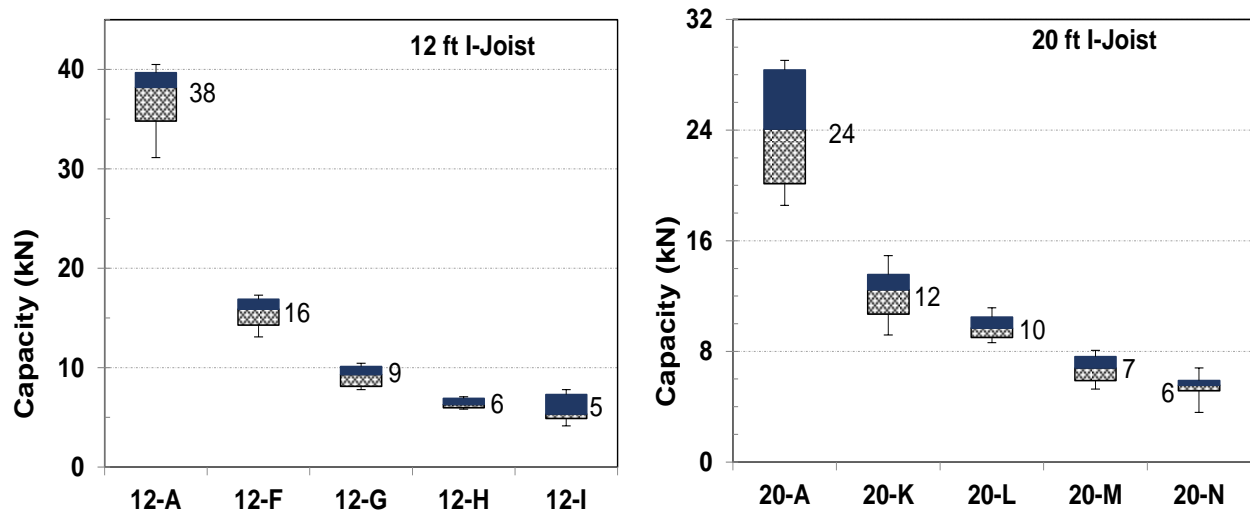


**Figure 4.9: Box Plot of Load Capacity of 12ft (3.65m) and 20ft (6.1m) I-joists (A-Controls and 12-F, 12-G, 12-H, 12-I, 20-K, 20-L, 20-M, 20-N with Flange Cut).**

#### 4.6.1 Effect of notch size and location

To investigate the effect of size and location of the flange notch, two different sizes ( $B_n \times D_n$ : 100 mm $\times$ 100 mm, 100 mm $\times$ 150 mm) of the notch and three locations ( $L_n$ : 305mm, 455mm, 610mm from one support) were selected (as shown in **Table 4.1**). The failure pattern and crack

locations are almost the same for all flange cut specimens irrespective of the size and location of the notches. In most of the cases, failure occurs at either corner of the notches at web due to deficiencies of resistance against combined compression bending and shear in these zones. However, the cracking pattern changes in the presence of a flange knot of a significant size, as shown in *Figure 4.6*.

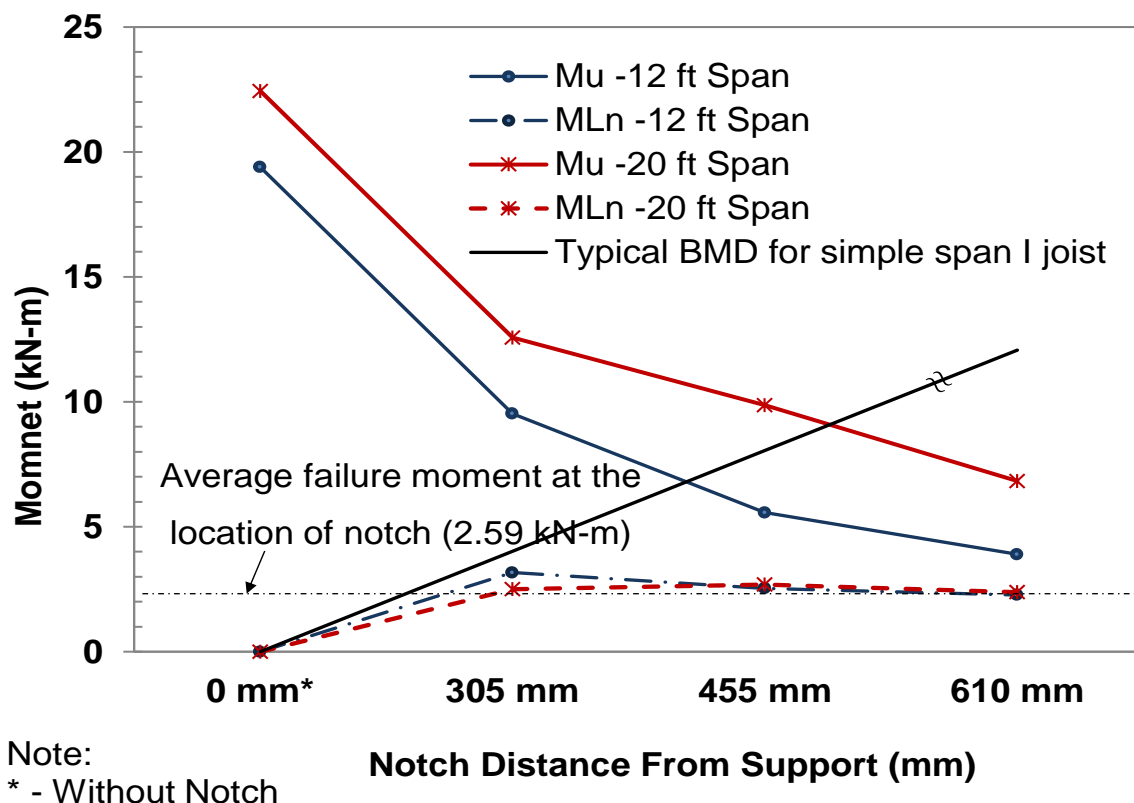


*Figure 4.10: Effect of Notch Distance from Support (Notch Size: 100×100 mm)*

**Table 4.4: Comparison of Calculated Moment and Measure Moment at the location of Notch at failure**

Specimen Code	Size of Notch	Moment at Notch Location ( $M_{Ln}$ )	
		Calculated	Measured (Avg.)
	(mm)	kN-m	kN-m
12-F--	100x100	16.60	2.67
12-G--	100x100		
12-H--	100x100		
12-I--	100x150	7.21	1.61
20-K--	100x100	16.60	2.54
20-L--	100x100		
20-M--	100x100		
20-N--	100x150	7.21	1.51

Location of flange notch has a significant effect on the strength of the I-joist. It is obvious that the presence of a flange notch significantly reduces the ultimate flexural strength ( $M_u$ ) of the I-joist as shown in **Figure 4.10**. The presented flexural strengths ( $M_u$ ) and moment at the location of notches ( $M_{Ln}$ ) of the tested I-joists are determined based on the analytical procedure as stated in equations **Eq. 4-1 & Eq. 4-2**, respectively. From **Figure 4.10**, it can be observed that the failure moments at notch locations are very close to each other, with an average failure moment of  $(2.67 \pm 0.45)$  kN-m and  $(2.54 \pm 0.16)$  kN-m for 12ft and 20ft span I-joist, respectively. This signifies that the failure of the I-joists with flange notch completely depends on the reduced stiffness ( $EI$ ) of the I-joists due to the flange cut or notch. The moment capacities of flange notched I-joists were calculated based on the modulus of elasticity and strength of the flange lumber and OSB as specified in the Canadian Wood Design Manual (CSA O86) (Canadian-Standard-Association 2014a). The calculated values were compared with the failure moment at the location of notch ( $M_{Ln}$ ) as shown in **Table 4.4**. The calculated moment of flange notched I-joist sections were 16.60 kN-m and 7.21 kN-m for 100×100mm and 100×150mm notch, respectively. Calculated moment

capacities of notched I-joists are comparatively higher than that of the failure moments ( $M_{Ln}$ ), which is due to several influencing factors, such as, web-flange slippage, stress concentration at the corner of the notch, type of the notch (square/rectangular), lateral torsional buckling and the uncertainties in the mechanical properties used in the calculation.

$$M_u = \frac{P_{max}}{2} * L/3 \quad \text{Eq. 4-1}$$

$$M_{Ln} = \frac{P_{max}}{2} * L_n \quad \text{Eq. 4-2}$$

where,  $M_u$  = Flexural Strength (kN-m)

$M_{Ln}$  = Moment at the location of Notch at failure (kN-m)

$L_n$  = Notch Distance from Support (mm)

$P_{max}$  = Average Load Carrying Capacity (kN)

The flexural strength ( $M_u$ ) of the I-joist reduces with the increasing distance of the flange notch from the support due to increasing demand for moment. However, the shear force acting on the two end span ( $L/3$ ) remains the same for any I-joist irrespective of the location of the notches as notch locations are varied within this end span strip of  $L/3$  length, which signifies that the flexural strength ( $M_u$ ) is critical, compared to the shear strength of the I-joists with flange cuts. Moreover, size of the notch also has great impact on the strength of the I-joist, as shown in **Figure 4.11**. Strength of I-joists reduced by 71% and 56% in comparison with the control I-joists due to the presence of a 100mm depth notch at the location of 455mm from the support for 12ft and 20ft span I-joists, respectively. Another strength reductions of 37% and 44% were observed for I-joists with a 150 mm notch depth, in comparison with the I-joists with a 100 mm notch depth at the same location (455mm) from the support for 12ft and 20ft span I-joists, respectively. This additional

strength reduction occurred due to the reduced shear stiffness of I-joists and the presence of 50mm deeper notch into the web.

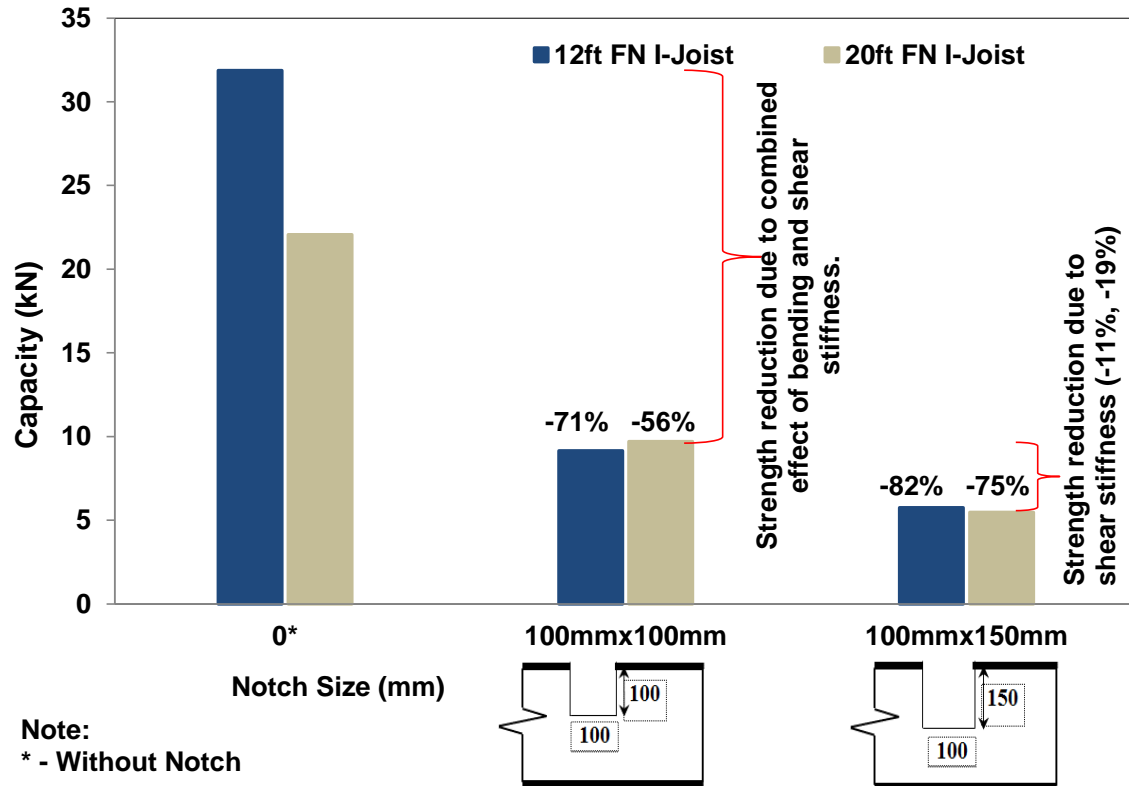


Figure 4.11: Effect of Notch Size (Notch Distance 455mm from Support)

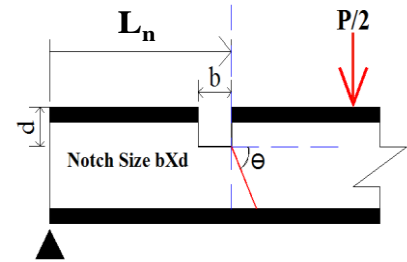
#### 4.6.2 Crack Propagation Direction

In this current study, crack growth or propagation of notched I-joists has also been investigated. The crack growth propagation was measured as the angle ( $\theta$ ) between the failure line and the longitudinal axis of the I-joists as shown in **Table 4.5**. The summary of crack propagation angles observed in the tested I-joists with a flange notch has been presented in **Table 4.5**. It is found that the average crack propagation angle for series 12-F ( $63^\circ$ ) and 20-K ( $69^\circ$ ) were lowest as the notches for these two series of I-joists were closest to the left support. The average crack propagation angles were increased with the increase of the distance of notch from the support as exhibited in I-joist series of 12-G ( $\theta=71^\circ$ ), 12-H ( $\theta=77^\circ$ ), 20-L ( $\theta=73^\circ$ ), & 20-M ( $\theta=76^\circ$ ). However, the

increment of crack propagation angle for longer span I-joists; 20-L (+7%), & 20-M (+10%), were lower compared to the shorter span I-joists, 12-G (+13%), 12-H (+22%). This signifies that the notch distance-span ratio ( $L_n/L$ ) has a significant effect on the crack growth direction.

**Table 4.5: Propagation of Crack Growth of the I-Joist with flange cut at different location**

Angle of Crack Growth ( $\Theta$ ), Degree					
$L_n$ (mm)	0	305	455	610	305
Series	12-A	12-F	12-G	12-H	12-I
Average	$\approx 90^\circ$	$63^\circ$	$71^\circ$	$77^\circ$	$72^\circ$
$\sigma$	-	$3.2^\circ$	$7.7^\circ$	$5.3^\circ$	$4.5^\circ$
COV ( $\sigma/\mu$ )	-	5.1%	10.8%	6.9%	6.2%
Series	20-A	20-K	20-L	20-M	20-N
Average	$\approx 90^\circ$	$69^\circ$	$73^\circ$	$76^\circ$	$74^\circ$
$\sigma$	-	$10.1^\circ$	$3.4^\circ$	$5.1^\circ$	$10.7^\circ$
COV ( $\sigma/\mu$ )	-	14.7%	4.6%	6.8%	14.5%



## 4.7 Summary

The recommendations based on this limited number of experiments are not intended to validate the justification of allowing flange notches at OSB webbed timber I-joists beyond the I-joists manufacturer guideline. However, these experiments do provide tentative course of direction on how it behaves with unintentional flange cuts or notches that are beyond these limits. It is also significant to accentuate that no notches or cuts are allowed into the flange of timber I-joists, which can lead to a hazardous condition. Based on the experiments performed in this study the following conclusions can be drawn:

- In terms of failure mode of I-joists with notches, the most common failure mode was the combined flexural and shear failure, where crack initiates at the right bottom corner of the notch and propagates to the bottom flange in an angle ranging from  $63^\circ$  to  $77^\circ$  with respect

to the I-joist longitudinal axis. However, for combined type failure most of the cases, shear failure was occurred by following flexural failure.

- Due to the presence of flange notches in the I-joists, the load carrying capacity decreased up to 80% in comparison with the uncut I-joist with the increasing distance of the notch from the support, which is due to the increasing flexural stresses.
- With a 100 mm flange notch at a location ( $L_n = 455\text{mm}$ ) in the I-joists (series: 12-G and 20-L), the strength of 12ft and 20ft span I-joists reduced to 71% and 56%, respectively compared to that of the uncut/control I-joists (**Figure 4.11**). Moreover, further 11% and 19% reductions of strength were observed for 12ft and 20ft span I-joists, respectively for a deeper notch (150 mm) in the I-joists (series: 12-I and 20-N) at the same location ( $L_n = 455\text{mm}$ ) (**Figure 4.11**). It is obvious that this reduction occurred due to the decrease in web materials, which provides the stiffness against shear stress.
- The stiffness of the I-joists with flange notches is reduced up to 46% and 33% from the stiffness of the control I-joists for 12ft and 20ft span length I-joists, respectively.
- Average load for serviceability condition is also reduced up to 50% and 37% from the average load at serviceability condition of the control I-joists for 12ft and 20ft span length I-joists, respectively.
- Notch distance-span ratio has a significant effect on the crack growth direction.



## CHAPTER 5: PERFORMANCE OF RETROFITTED FLANGE NOTCHED I-JOIST WITH OSB COLLARS: AN EXPERIMENTAL INVESTIGATION

### 5.1 General

Timber I-joists are very common as a structural element especially as beam for construction of residential and small scale commercial buildings around the world. Timber I-joists are commonly known as engineered I-joist due to the utilization of engineered wood products. For instance, such as Oriented Strand Board (OSB) or Plywood as web materials and timber or laminated veneer lumber (LVL) is used as flange materials for manufacturing of I-joist. These engineered I-joists have several advantages over the solid sawn lumber joists, i.e. robustness, easy handling, light weight, sustainability. Moreover, these engineered I-joists are very good to facilitate different services including plumbing and HVAC systems in buildings without increasing the height of the structure. To facilitate these services, notching of flanges are very common as described by (Islam et al. 2015). However, it is strictly prohibited to make any notch at top/bottom flange of OSB webbed I-joists (American-Wood-Council 1999), (Wood I-Joist Manufacturers Association (WIJMA) 2008). Some photographs of flange notches collected from different construction sites have been shown in **Figure 1.1 and Figure 4.1**. Until today, only few research studies on OSB webbed timber I-joists with flange cut and notch have been conducted (e.g., Islam et al. 2015 and Hindman and Loferski 2008). Current design specifications (CSA-O86) for timber building construction do not provide any design guideline for retrofitting/strengthening of I-joists with flange cut and notches to maintain/improve the structural integrity of the flooring or roofing system (Canadian-Standard-Association 2014a). As there is no specific guideline to strengthen or retrofit flange-notched I-joists, I-joist manufacturers or building designers frequently face problems in

retrofitting such deficient I-joists. Different engineers or manufacturers retrofit or strengthen the notched I joists with different techniques as per their experiences and availability of materials. However, a specific guideline is required to retrofit/strengthen the flange notched I-joists to reduce the uncertainty of their performance.

The primary objective of this chapter is to evaluate the performance (e.g. capacity and stiffness) of un-retrofitted and retrofitted OSB webbed timber I-joists with a notch at the top flange. Here, OSB and sawn lumber are used as web and flange material, respectively for the I-joists. OSB - a low cost reinforcing material has been used in the form of a collar around the I-joist flange notch for retrofitting. To investigate the performance of such retrofitting technique, an extensive experimental work was carried out on the engineered I-joists having a flange notch of two different sizes (100 mm x 100 mm & 100 mm x 150 mm) at three different locations (300, 450, and 600 mm) from the support. A total of 220 I-joist specimens (20 uncut, 80 notched, 120 retrofitted) were tested in this experimental study to investigate the strength reduction after making notch, and strength improvement after retrofitting of those notched I-joists.

## **5.2 Experimental Investigations of Timber I-joists with Flange Notches**

In this experimental study, improvements in the structural capacity of retrofitted flange notched I-joists were tested with two different span lengths: 12 ft and 20 ft. These joists were produced by an I-joist manufacturer (AcuTruss Industries Limited) in Kelowna, Canada. These I-joist specimens were produced with a 9.5 mm thick OSB web and 38 mm by 63 mm lumber flanges as shown in **Figure 3.1 (a)**. Test set up and specimen dimensions were selected and determined with strict adherence to the provisions of ASTM-D5055 (*ASTM-D5055 2013*) and WIJMA guideline (Wood I-Joist Manufacturers Association (WIJMA) 2008). According to the manufacturer

(NASCOR) Specifier Guideline (*NASCOR 2010*), the maximum allowable span (simple) is 20 ft for the I-joists with the selected cross sectional geometry. The test setup and loading diagram are shown in **Figure 5.1**. This figure shows the use of a sufficient number of lateral supports to prevent lateral buckling in tested I-joists. There are 4 series of I-joists for each span length, 12F-12I and 20K-20N as listed in the Flange Notched I-joist details section of Error! Reference source not found. **Table 5.1**. With 10 samples for each series, a total of 80 specimens were tested with flange notches of either 100 mm  $\times$  100 mm or 100 mm  $\times$  150 mm notch sizes at different locations (e.g. 300, 450, and 600 mm from the support). These flange notched I-joist series were retrofitted with two different techniques (Type T-1 and T-2, details of these two techniques have been provided in the following section) and tested (series 12O -12SF and 20O-20SF) as shown in **Table 5.1** and **Figure 5.2**. Two series of control I-joists, 12-A and 20-A (20 specimens) were also tested for each span length (12 ft and 20 ft). Thus, a total of 220 I-joist specimens were tested where, each series consists of 10 samples.

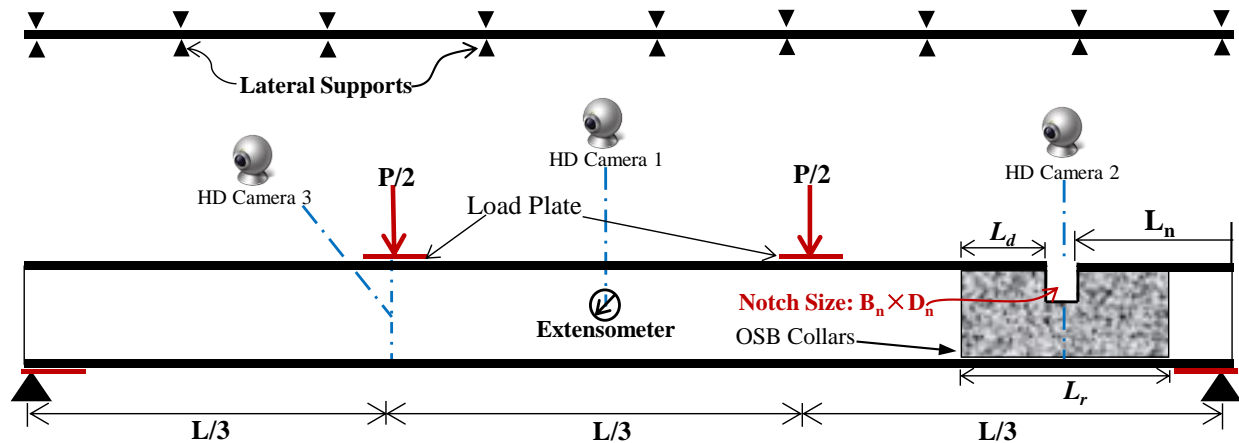


**Figure 5.1: Schematic of Retrofitted I-Joists with flange notch and lateral supports along the length (dimensions are in mm).**

**Table 5.1: Specimen Details of I-Joist Testing**

Flange Notched I-joist details					Retrofitted I-joist details			
Sample Code	Span, L <sub>o</sub> (mm)	Hole size, (B <sub>n</sub> xD <sub>n</sub> ) (mm)	Location, (L <sub>n</sub> ) (mm)	No. of Specimen	Retrofitted Sample Code	OSB Collar  L <sub>d</sub> (mm)      Type		No. of Specimen
12-A--		-	-	10	-	-		-
12-F--	3650 (12ft)	100x100	305	10	R-12-O--	305	T-1	10
				R-12-OF--	305	T-2	10	
12-G--			455	10	R-12-P--	305	T-1	10
12-H--			610	10	R-12-Q--	305	T-1	10
				R-12-R--	610	T-1a	10	
				R-12-S--	455	T-1	10	
12-I--			100x150	455	10	R-12-SF--	455	T-2
20-A--		-	-	10	-			-
20-K--	6100 (20ft)	100x100	305	10	R-20-OF--	305	T-2	10
20-L--			455	10	R-20-PF--	305	T-2	10
				R-20-QF--	305	T-2	10	
20-M--			610	10	R-20-RF--	610	T-2a	10
20-N--			100x150	455	10	R-20-SF--	455	T-2
Total				100				120

### 5.2.1 Details of flange notch retrofitting

I-joists with the same dimensions and openings of series 12-F to 12-I and 20-K to 20-N sizes were retrofitted to investigate and analyze the improvement in capacity. A total of seven and five more series (series 12-O to 12-S, 12-OF and 12-SF for 12 ft I-joists and series 20-OF to 20-SF for 20 ft I-joists) of I-joist specimens with the same span length of 12 ft (3.66 m) and 20 ft (6.10 m), respectively, were tested after being retrofitted around the flange notch with the two types of retrofitting techniques using OSB collar, as shown in **Figure 5.2**. Two types of retrofitting techniques, Type T-1 and Type T-2, can be seen from the retrofitting details in **Table 5.1**. Type T-2 corresponds to the series with the addition of the letter F, which means filled. **Figure 5.2 (b and c)** illustrates the cross section of the I-joist after retrofitting with Type T-1 and Type T-2

techniques, respectively. However, to investigate the effect of OSB collar length ( $l_d$ ), an additional type of reinforcement was employed in the test series as designated by Type T-1a or Type T-2a. For both of these retrofitting techniques, the OSB collar length ( $l_d$ ) was doubled for Type T-1 and Type T-2 retrofitting, respectively. Series R-12-R and R-20-RF were retrofitted with OSB collar(s) having a length ( $l_d$ ) of 610 mm, which is doubled compared to those of R-12-Q and R-20-QF. **Figure 5.2 (a)** shows the retrofitted flange notched I joist and the placement of the OSB collar, with a notch size of  $B_n \times D_n$  located at a distance of  $L_n$  from the right support of the I-joist to the edge of the notch as shown in **Figure 5.2 (a)**. The length of the OSB collar on each side of the flange notch was kept constant ( $l_d = 305$  mm, 455 mm or 610 mm) for all series, with a total length of reinforcer ( $L_r = 2 * L_d + B_n$ ). OSB collars were attached to the flange and web with a series of nails with a spacing of 75 mm as shown in **Figure 5.2 (a)**. I-joists retrofitted with type T-1 and type T-2 techniques have been presented in **Figure 5.2 (a and e)**, respectively. Type T-1 retrofitting technique was not used for 20 ft I-joists as it was observed that the performance improvement was not significant for the 12 ft notched I-joists retrofitted with this method.

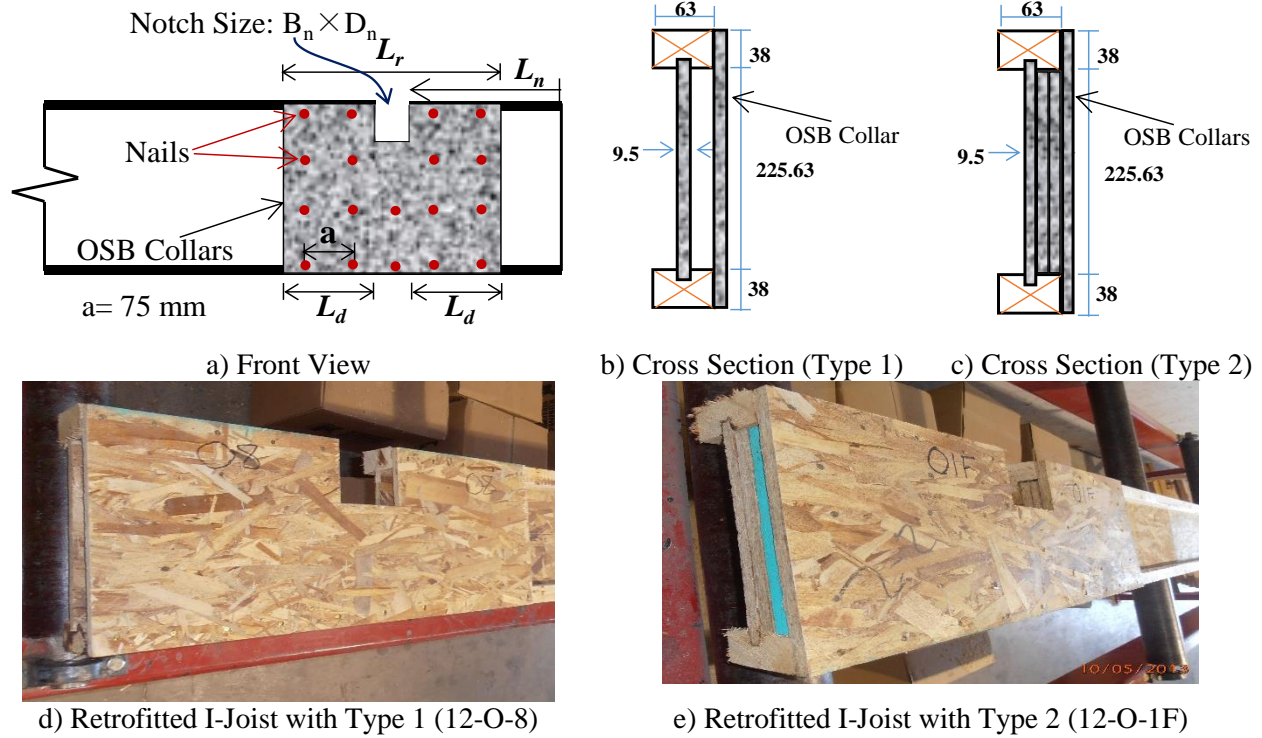


**Figure 5.2: Details of Flange Notch Reinforcer (Note: Red dots represent nails)**

### 5.3 Results

In the following section a detailed discussion and comparison have been made on the experimental results of the tested I-joists. Among the test specimens, series A is the control I-joist without any notch, series 12-F to 12-I and series 20-K to 20-N are the I-joists with two different notch sizes in the flange at two different locations, respectively. Series R-12-O to R-12-S and R-20-OF to R-20-SF are the retrofitted I-joists with different techniques as discussed earlier. Based on the experimental results obtained from the 12 ft reinforced flange notched I-joists, it was found that the performance improvement of Type T-1 reinforcing technique was not enough to be compared with the control I-joist. Hence, Type T-1 technique was discontinued for the 20 ft reinforced flange notched I-joists to save time and cost of the experimental program.

The behavior of I-joists can be evaluated by the load deflection response of the I-joists as prescribed by ASTM-D5055 (*ASTM-D5055 2013*). For all tested I-joists, load deflection responses exhibit a linear elastic behavior until failure as presented in **Figure 4.4**, hence only the best fitted load deflection response is presented and discussed in this study.

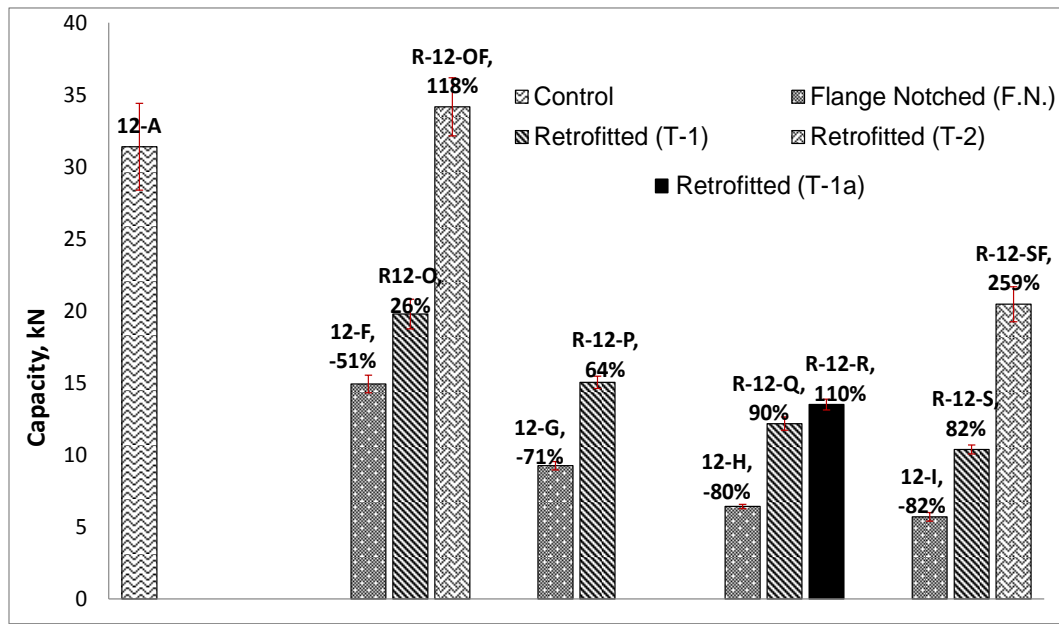
### **5.3.1 Control I-Joists (Series 12-A/20A)**

The initial test on the 12-A and 20-A control specimens yielded two failure types: shear failure at the support and flexural failure in the mid-span. The cause of these failure was due to the presence of knots in the flange or de-bonding of the OSB web from the flange. Typical failure modes observed in the control I-joist have been presented in **Figure 4.3**. The average load capacities of the 12 ft and 20 ft beams were 31.39 kN (Coefficient of Variation, COV = 30%) and 22.08 kN (COV = 25%), respectively. The average stiffness of the 12 ft and 20 ft I-joists was 1071 and 275 N/mm, respectively, which was 112% and 151% higher than those of specified by the I-joist manufacturer (design stiffness of 511 N/mm and 110 N/mm for the 12 ft and 20 ft I-joists, respectively). The average maximum deflections of the 12-A and 20-A were 29.96 mm and 81.00 mm, respectively. In comparison to the two control series, it became evident that the average load carrying capacity of the 12 ft I-joist was 43% higher than that of the 20 ft I-joist due to its higher stiffness and lower span-depth ratio.

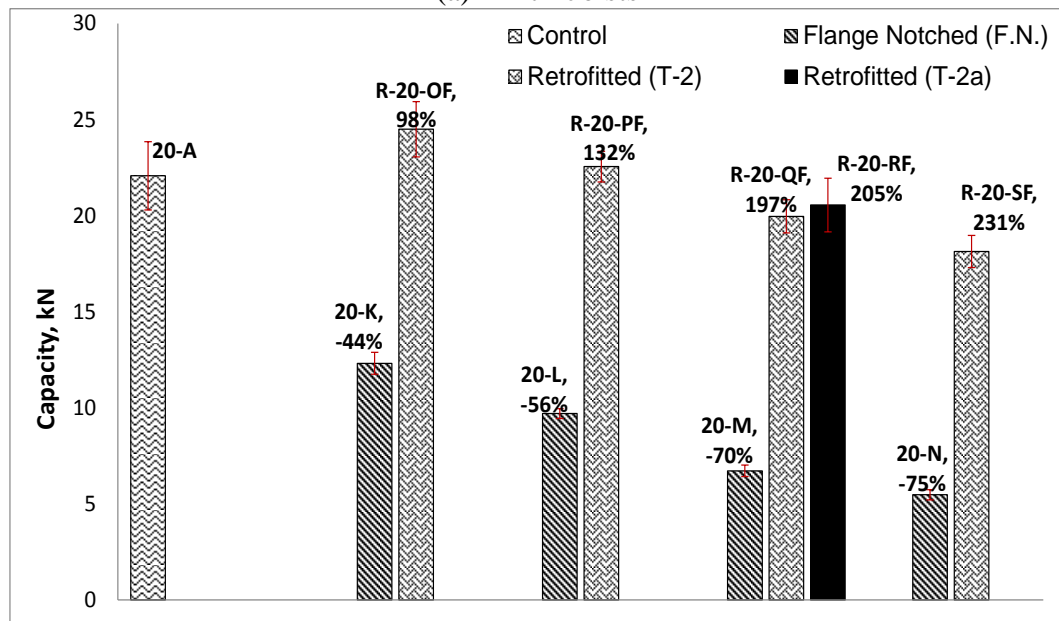
### **5.3.2 I-Joists with Notch (Series 12-F to 12-I and 20-K to 20-N)**

Ten specimens from the I-Joist series 12-F to 12-I (12 ft span length ) and 20-K to 20-N (20 ft span length), each having a flange notch of two different dimensions ( $B_n \times D_n$ ) at three different locations ( $L_n$ ), were tested and compared to the un-notched control I-joist 12-A and 20-A. The primary criterion in comparing the behavior of different I-joist series and specimens was the load-

deflection response measured by four-point bending test. Detailed analysis and comparison of the failure mode and load-deflection response, comprising of load carrying capacity, deflection, stiffness and load at serviceability condition, will be further discussed in the following section.



(a) 12 ft I-Joists



(b) 20 ft I-joists

**Figure 5.3: Comparison of Capacity of Retrofitted Flange Notched I Joists (12 ft & 20ft)**



The average of the peak load, stiffness, and load at serviceability condition (load at deflections of L/180 and L/360) and their percent reductions in comparison to the control I-joist are presented in *Figure 5.3 and Table 5.2*. From the test results the following observations are made:

**Table 5.2: Moment capacity ( $M_u$ ) and Moment at notch ( $M_{Ln}$ ) of reinforced flange notched I-Joists.**

Series	$M_u$	$M_{Ln}$	% Reduction/Improvement of $M_{Ln}$			Reinforcement Type
	N-m	N-m				
<b>12-A</b>	19391	0				
<b>12-F</b>	9522	3170	<b>00*</b>	<b>00*</b>		
<b>R-12-O</b>	12027	4003		26%	<b>00*</b>	T-1
<b>R-12-OF</b>	20781	6917		118%	73%	T-2
<b>12-G</b>	5566	2539	-20%	<b>00*</b>		
<b>R-12-P</b>	9143	4171		64%		T-1
<b>12-H</b>	3896	2274	-28%	<b>00*</b>		
<b>R-12-Q</b>	7399	4318		90%	<b>00*</b>	T-1
<b>R-12-R</b>	8207	4789		111%	11%	<b>T-1a</b>
<b>12-I</b>	3503	1598	-37%	<b>00*</b>		
<b>R-12-S</b>	6310	2878		80%	<b>00*</b>	T-1
<b>R-12-SF</b>	12444	5676		255%	97%	T-2
<b>20-A</b>	22432	0				
<b>20-K</b>	12565	2503	<b>00*</b>	<b>00*</b>		
<b>R-20-OF</b>	24905	4961		98%		T-2
<b>20-L</b>	9863	2692	8%	<b>00*</b>		
<b>R-20-PF</b>	22929	6259		132%		T-2
<b>20-M</b>	6835	2387	-5%	<b>00*</b>		
<b>R-20-QF</b>	20299	7088		197%	<b>00*</b>	T-2
<b>R-20-RF</b>	20896	7296		206%	3%	<b>T-2a</b>
<b>20-N</b>	5570	1520	-44%	<b>00*</b>		
<b>R-20-SF</b>	18436	5032		231%		T-2
<b>Note: * 00 - represents the Comparisons were made with this Series of I-Joist.</b>						

- **Load Carrying Capacity:** The strength (peak load) of the flange notched I-joists was reduced by 51% ( $D_n = 100\text{mm}$ )-82% ( $D_n = 150\text{mm}$ ) and 44% ( $D_n = 100\text{mm}$ ) -75% ( $D_n = 150\text{mm}$ ) compared to those of the control I-joists for the 12ft and 20ft span I-joists,

respectively. Additional reductions, i.e. 38% and 44% were observed for the deeper ( $D_n=150$  mm) notch series 12-I and 20-N compared to those of the I-joist series 12-G and 20-L having a relatively shallower notch ( $D_n=100$  mm).

- Stiffness:** The average stiffness of the I-joists having a  $100\text{ mm} \times 100\text{ mm}$  notch at top flange was reduced by 15% ( $D_n=100\text{mm}$ ) -38% ( $D_n=150\text{mm}$ ) and 22% ( $D_n=100\text{mm}$ )-70% ( $D_n=100\text{mm}$ ) for the 12ft and 20ft span I-joist, respectively compared to that of the control I-joists. A further reductions of 19% and 8% were observed for the deeper notch ( $D_n=150\text{mm}$ ) (series 12-I & 20-N) compared to that of the I-joists (series 12-G & 20-L) having a shallower notch ( $D_n=100\text{mm}$ ).
- Moment Capacity:** The moment at notch location ( $M_{Ln}$ ) is the most critical factor for performance of a notched I-joist. From the experimental results, it shows that the average failure moments at notch location ( $M_{Ln}$ ) were not varying significantly while varying the notch locations in the I-joists as observed in *Figure 5.4*. The average failure moment at notch location ( $M_{Ln}$ ) was 2594 N-m, with a coefficient of variation (COV) of 12.2%, whereas the average moment capacity ( $M_u$ ) of those I-joists series was 8041 N-m with a COV of 39.6% as presented in *Table 5.2*.
- Serviceability Limit Condition:** An average service load capacity reduction at a deflection of  $\Delta = L/180$  was 14% ( $D_n=100\text{mm}$ ) to 51% ( $D_n=150\text{mm}$ ), and 16% ( $D_n=100\text{mm}$ ) to 27% ( $D_n=150\text{mm}$ ), respectively for the flange-notched 12 ft and 20 ft I-joists in comparison to the uncut (control) I-joists for roof and flooring systems as presented in *Table 5.3*. However, these service live load capacity reductions at a deflection of  $\Delta = L/360$  varied from 11 to 50% and 11 to 21% respectively, for the 12 ft and 20 ft I-joists in comparison to the control I-joists for roof and flooring systems.

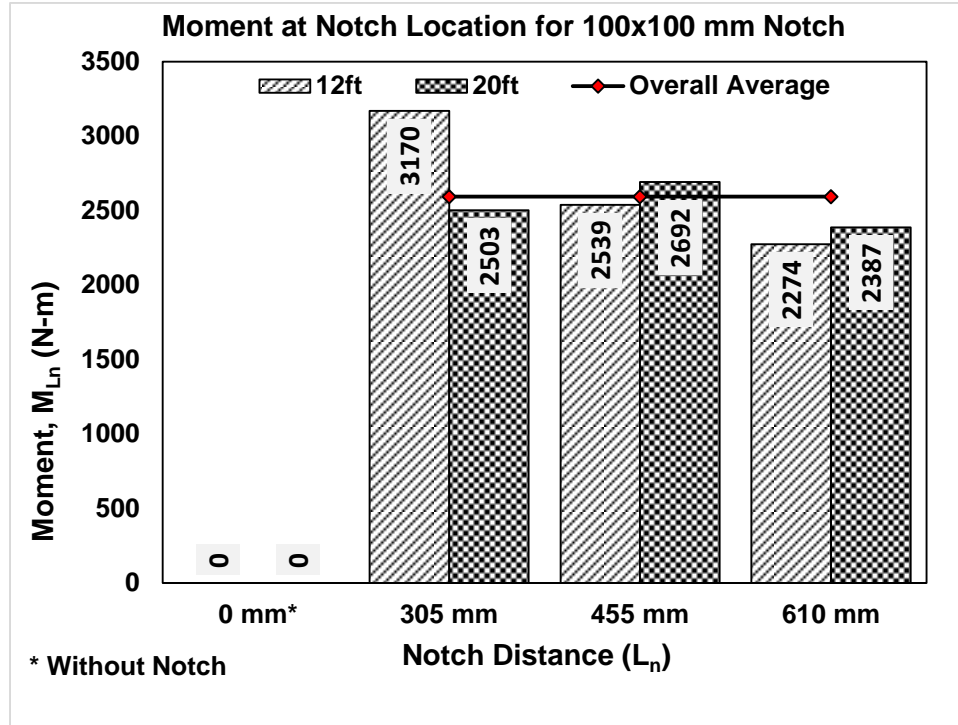


*Figure 5.4: Moment at notch location of flange notched I-joists.*

- Failure Mode:** Most of the I-joists having a notch at top flange exhibited flexural failure as the flexural stiffness was reduced significantly due to the presence of notch. However, web material (that provides shear strength) removal had also negative effect on the strength and stiffness of the notched I-joist, which can be attributed to the further reduction of strength, stiffness, and load at serviceability conditions for a deeper notch ( $D_n = 150$  mm) (i.e. removal of additional web material). The presence of flange notch changes the mode and location of failures. Different types of failures have been shown in *Figure 5.5 (a-d)*.

**Table 5.3: Load at Serviceability Conditions ( $\Delta=L/180$  &  $\Delta=L/360$ )**

		P (N) , ( $\Delta=L/360$ )				P (N), ( $\Delta=L/180$ )					
Series		Avg.	% Reduction		% Improvement		Avg.	% Reduction		% Improvement	
12 ft	12-A	10600	00*		00*		22530	00*		00*	
	12-F	9429	-11%		00*		19435	-14%		00*	
	R-12-O	8820			-6%	-17%	18271			-6%	-19%
	R-12-OF	10333			10%	-3%	21357			10%	-5%
	12-G	7835	-26%		00*	00*	15101	-33%		00*	00*
	R-12-P	10138			29%	-4%	19303			28%	-14%
	12-H	6205	-41%		-	00*	11489	-49%		-	00*
	R-12-Q	8227			33%	-22%	15938			39%	-29%
	R-12-R	8772			41%	-17%	16492			44%	-27%
	12-I	5321	-50%		-32%	00*	11106	-51%		-26%	00*
	R-12-S	8174			54%	-23%	15134			36%	-33%
	R-12-SF	8670			63%	-18%	18594			67%	-17%
20 ft	20-A	4246	00*		00*		9621	00*		00*	
	20-K	3647	-14%		00*		7977	-17%		00*	
	R-20-OF	4611			26%	9%	9517			19%	-1%
	20-L	3406	-20%		00*	00*	7613	-21%		00*	00*
	R-20-PF	4371			28%	3%	9338			23%	-3%
	20-M	3762	-11%		00*		8073	-16%		00*	
	R-20-QF	4221			12%	-1%	9072			12%	-6%
	R-20-RF	4244			13%	0%	9096			13%	-5%
	20-N	3355	-21%		-2%	00*	7058	-27%		-7%	00*
R-20-SF	4150			24%	-2%	8883			26%	-8%	
Note: * 00 - represents the Comparisons were made with this Series of I-Joist.											

- Crack growth angle:** The average crack growth propagations (angle between the failure line and the longitudinal axis of the I-joists as depicted in **Figure 5.5 (e)**) varied from 63° to 77° and 69° to 76° respectively for the 12 ft and 20 ft I-joists having a notch of 100 mm x 100 mm. An increasing trend of this angle was observed with the increase of notch

distance ( $L_n$ ) from the support while the notch size was kept constant. However, the direction of crack growth slightly changed (only 1.1% for 12 ft and 1.3% for 20 ft I-joist) with the increase of depth of notch from 100 mm (series 12-G & 20-L) to 150 mm (series 12-I & 20-N) for a constant notch distance ( $L_n=455\text{mm}$ ), as presented in **Table 5.4** and **Figure 5.5 (e)**.

**Table 5.4: Crack Growth Angles ( $\theta$ )**

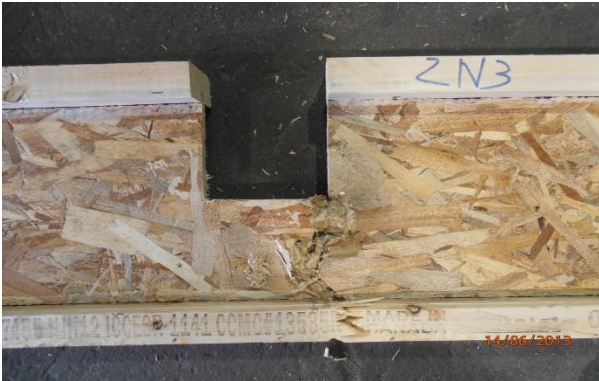
Series	$L_n$ mm	Avg. $\theta$ (Deg.)	COV	Series	$L_n$ mm	Avg. $\theta$ (Deg.)	COV
12-A	0	90°	-	20-A	0	90°	-
12-F	305	63°	5.1%	20-K	305	69°	14.7%
R-12-O	305	73°	8.4%	R-20-OF	305	72°	13.8%
R-12-OF	305	83°	14.5%	20-L	455	73°	4.6%
12-G	455	71°	10.8%	R-20-PF	455	68°	20.7%
R-12-P	455	73°	5.0%	20-M	610	76°	6.8%
12-H	610	77°	6.9%	R-20-QF	610	68°	14.7%
R-12-Q	610	78°	8.2%	R-20-RF	610	73°	15.6%
R-12-R	610	79°	7.2%	20-N	455	74°	14.5%
12-I	455	72°	6.2%	R-20-SF	455	81°	13.0%
R-12-S	455	80°	6.2%				
R-12-SF	455	82°	8.0%				



(a) Pure flexural failure: 12 feet I-joists



(b) Combined flexural and shear failure: 12 feet I-joists



(c) Pure flexural failure: 20 feet I-joists



(d) Combined flexural and shear failure: 20 feet I-joists

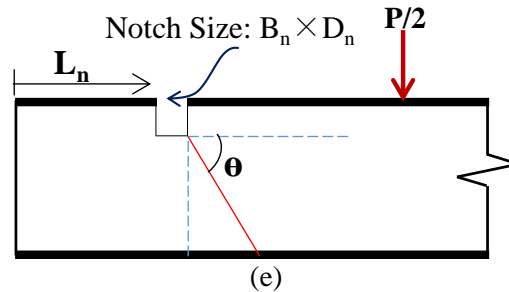


*Figure 5.5 Crack growth direction in I-joist with a flange notch.*

### 5.3.3 Retrofitted Flange Notched I Joist (Series R-12-O to R-12-SF and R-20-O to R-20-SF)

Performance improvement of the retrofitted I-joists was measured in terms of capacity ( $P_u$ ) and stiffness ( $k$ ) with respect to un-retrofitted I-joists having same notch details (size and location). After retrofitting, the load carrying capacity ( $P_u$ ) of flange notched I-joists increased from 26% to 259% and 98% to 231% compared to their un-retrofitted one for the 12 ft and 20 ft I-joists, respectively. However, once the flange notched I-joists were retrofitted with Type T-1 technique,

as described earlier, the load carrying capacity increased 26-90% for the 12 ft span I-joists. Further retrofitting by using Type T-2 technique, which includes three layers of OSB collars, the load carrying capacity increased by 73% (i.e. 118% improvement compared to the notched joist) and 97% (i.e. 259% improvement compared to the notched joist) for the 12 ft I-joist.

#### ***5.3.3.1 Performance of I-joists with varying Notch Size and Location***

##### **a) Notch (100mm x 100 mm) at 305 mm from Support**

###### *Capacity ( $P_u$ ):*

This section deals with only one size 100mm x 100mm notch size located at 305 mm from support. It was observed from the results that the load carrying capacity decreases due to the presence of flange notch. However, once the flange notched I-joists were retrofitted with Type T-1 technique as described earlier, the load carrying capacity of R-12-O series increased by 27% compared to that of 12-F I joists. Retrofitted flange notched I-joists with Type T-2 technique (which includes a fill), increased by 79% compared to that of Type T-1.

###### *Stiffness ( $K$ ):*

The load deflection curves in **Figure 5.6 (a)** represent the stiffness of the control, the flange notched, and retrofitted I-joists. For the 12 ft I-joist, the general trend indicates that the stiffness of flange-notched I joist, 12-F decreases with respect to the control I joist 12-A. After retrofitting, it can be observed that not all of the techniques are effective in improving the stiffness of the I-joists compared to the control ones. For instance, flange-notched I-joist series retrofitted with Type T-1 (e.g. R-12-O) had lower stiffness (14%) compared to the control I joist, 12-A. 12 ft I-joist series were also retrofitted with T-2 option (e.g. R-12-OF) where the results show improvement (7%) in stiffness compared to that of 12-F. Although T-2 retrofitting improved the stiffness compared

to that of T-1, the stiffness was still 9% lower compared to that of control I-joist. For the 20-ft I-joist, a similar pattern was observed; the flanged notched I-joist (20-K) had a reduced stiffness (22%) in comparison to the control specimen (20-A) and an improved stiffness (26%) after Type T-2 retrofitting (e.g. R-20-OF) compared to that of the flange-notched I-joist (20-K) as shown in *Figure 5.6 (a)*.

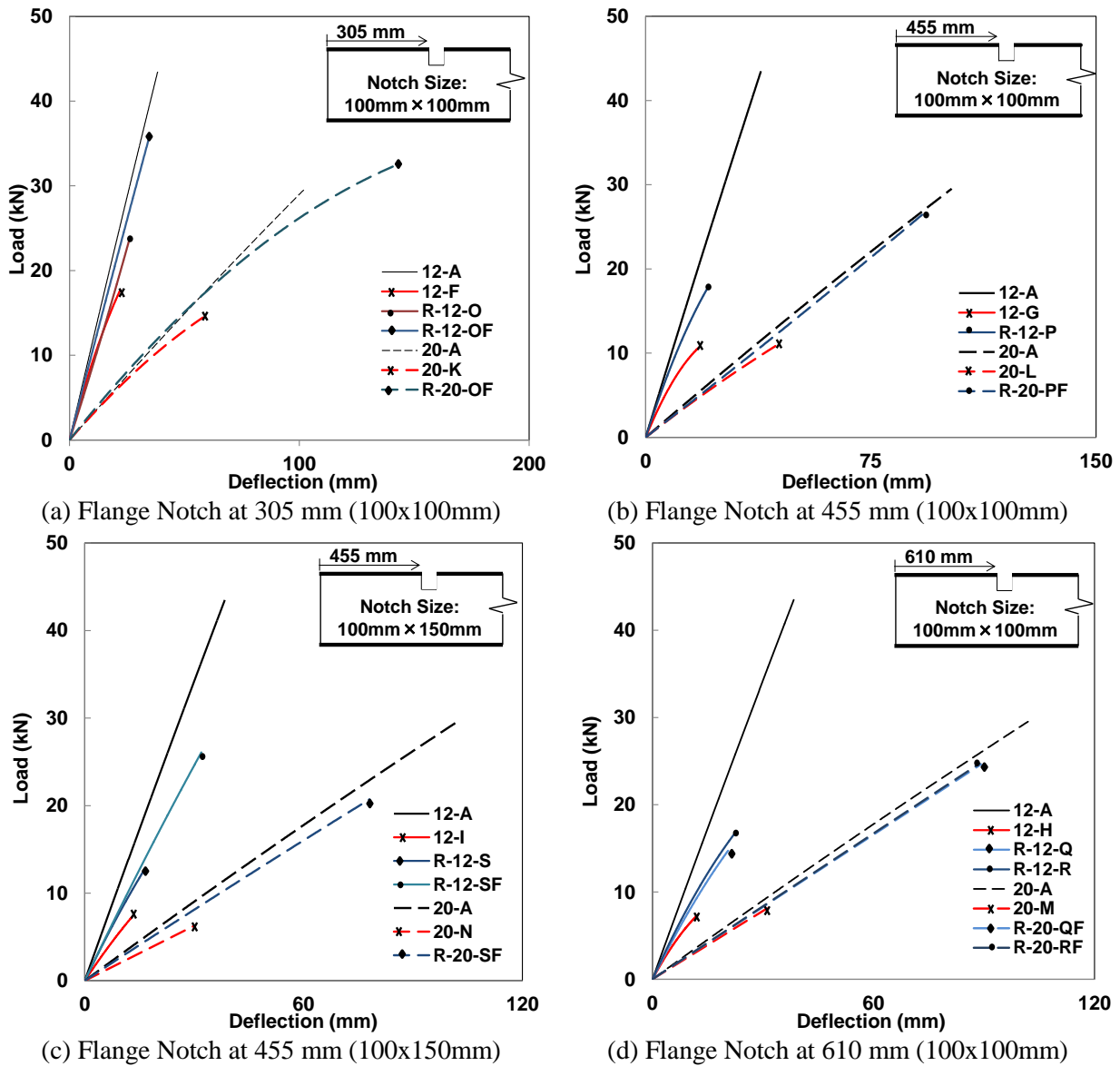


**Figure 5.6: Load –Deflection Curves for different reinforced I-Joist series having a Flange Notch.**



#### **b) Notch (100 mm x 100 mm) at 455 mm from Support**

##### *Capacity ( $P_u$ ):*

Similar to the previous section, this section deals with I-joists with a flange notch located at 455 mm from support. The 12 ft and 20 ft I-joists were retrofitted using Type T-1 and Type T-2 methods, respectively. The load capacity of both 12 ft (12-G) and 20 ft (20-L) I-joists reduced by 71% and 56%, respectively, compared to those of the control 12-A and 20-A I-joists after introducing the flange cut. After Type T-1 retrofitting, the load capacity of R-12-P increased 64% compared to that of 12-G. After retrofitting 20-L, the load capacity of R-20-PF surpassed the 20-L by a significant margin (132%). It should be noted that R-20-PF even had 2% higher capacity compared to that of the control I-joist, 20-A, alluding Type T-2 retrofitting to be more effective.

##### *Stiffness ( $K$ ):*

Both the 12ft and 20ft control I-Joists (12-A and 20-A) exhibit the highest stiffness among various series. The stiffness decreases with the introduction of the flange notch by 32% (12-G) and 27% (20-L), respectively. Due to the retrofitting of the flange notched I-joists stiffness of the retrofitted I-joists increased by 35% (R-12-P) and 37% (R-20-PF) compared to that of the flange notched I-Joists (12-G and 20-L) for 12 ft and 20 ft I-joists, respectively. Despite the increase in stiffness, as shown in **Figure 5.6 (b)**, the original stiffness of the control I-joist was not achieved.

#### **c) Notch (100 mm x 150 mm) at 455 mm from Support**

##### *Capacity ( $P_u$ ):*

This series of I-joists has a different notch depth (150 mm) compared to other series. The load carrying capacity of this reinforcer, however, still follows the general trend. The addition of the flange notch to both the 12 ft and 20 ft series initiates a significant reduction of 82% (12-I) and 75

% (20-N), respectively. Type T-1 retrofitting of the 12 ft I-joist allows an improvement of 82%, whereas Type T-2 retrofitting of the 12 ft and 20 ft led to a 259% (R-12-SF) and 231% (R-20SF) increase in load capacity, respectively.

*Stiffness (K):*

Considering the stiffness of the controls to be at a 100%, addition of the flange notch decreases that percentage by 45% (12-I) and 33% (20-N) for the 12 ft and 20 ft I-joist, respectively. Similar to previous series, retrofitting leads to an improvement in the stiffness. For the 12 ft I joist, Type T-2 retrofitting results in a higher stiffness than type T-1. Type T-2 retrofitting for both span lengths leads to an increase from the flanged notch I-joist by 45% and 40% for 12 ft and 20 ft respectively and a further 21% and 6% improvements are required, respectively, to be equivalent to the stiffness of the control I-joist as shown in **Figure 5.6 (c)**.

**d) Notch (100 mm x 100 mm) at 600 mm from Support**

*Capacity ( $P_u$ ):*

The flange cut at 610 mm from the support, similar to the reinforcer with a higher notch depth, has a significant impact on the load capacity. The introduction of the flange notch significantly reduces the load capacity in comparison to the control. The 20 ft and 12 ft flange notched I-joists have reduced capacities by 80% (12-H) and 70% (20-M), respectively. However, the retrofitting methods contributed to a high level of improvement as can be seen from **Figure 5.3** and **Figure 5.6**. Two different lengths ( $l_d = 305$  mm and 610 mm) of OSB collars were used to retrofit these two series (12-H and 20-M) of flange notched I-joists as shown in **Table 5.1**. Type T-1 and T-1a retrofitting of the 12 ft I-joist led to a 90% (R-12-Q) and 110% (R-12-R) improvement compared to that of the flange notched I-joists (12-H). Type T-2 and T-2a retrofitting of the 20 ft I joist led

to a 197% (R-20-QF) and 203% (R-20-RF) improvement compared to that of the flange notched I-joist (20-M). By increasing the length of the OSB collars (Type T-1a & Type T-2a) can improve the capacity by 20% and 8% respectively for the 12 ft and 20 ft I-joists compared to the flange notched I-joist retrofitted with a shorter OSB collars (Type T-1 & Type T-2).

*Stiffness (K):*

The stiffness (K) of the I-joist decreases with the flange cut and then increases after retrofitting, similar to the other series. Compared to the control I-joist, series 12-H and 20-M had a decrease in the stiffness by 38% and 27%, respectively. Initial retrofitting (Type T-1) of the 12 ft series led to 18% (R-12-Q) increase and then, Type T-1a retrofitting led to a 27% (R-12-R) increase in stiffness compared to that of the flange notched I-joists (12-H). For the 20 ft series, the stiffness was improved by 29% (R-20-QF) and 28% (R-20-RF) respectively for Type T-2 and Type T-2a retrofitting methods compared to that of the flange notched I-joists (20-M) as determined from *Figure 5.6 (d)*.

**Serviceability Limit Condition:** The Average load at serviceability limit conditions (i.e. Deflection,  $\Delta = L/180$  and  $\Delta = L/360$ ) were measured and the averaged loads were increased by 10-67% and 10-63%, respectively for the 12ft retrofitted flange notched I-joists in comparison to the un-retrofitted (notched) I-joists, whereas the average load at serviceability conditions ( $\Delta = L/180$  &  $\Delta = L/360$ ) of the 20ft I-joists were increased by 12-26% as presented in *Table 5.3*.

**Crack growth angle and Failure Mode:** The average crack growth propagations were varied from 73° to 83° and 68° to 73° for 12ft and 20ft retrofitted I-joists having a notch of 100mmx100mm. The crack growth angles were increased by 13% (R-12-OF) and 2% (R-12-SF) due to increase the thickness of the reinforcer (Type T-1 to Type T-2) for the 100mmx100mm (R-

12-OF) and 100mmx150mm (R-12-SF) notch, respectively. The summary of the crack growth propagations of each series of tested I-Joists have been presented in **Table 5.4**. Different types of failure and crack growth directions have been shown in **Figure 5.7**. It is observed that the most of the 20 ft reinforced I-Joists were failed in flexure at zero shear zone (middle span), whereas 12ft reinforced I-Joists exhibited both types of failure (flexure & shear). Shear failure was eliminated for longer span (20 ft) I-Joists by using reinforcer, which basically reduced the shear stress in the web by increasing the thickness of the web.



(a) Pure flexural failure: Retrofitted 12 feet I-joists



(b) Combined flexural and shear failure: Retrofitted 12 feet I-joists



(c) Pure flexural failure: Retrofitted 20 feet I-joists



(d) Combined flexural and shear failure: Retrofitted 20 feet I-joists

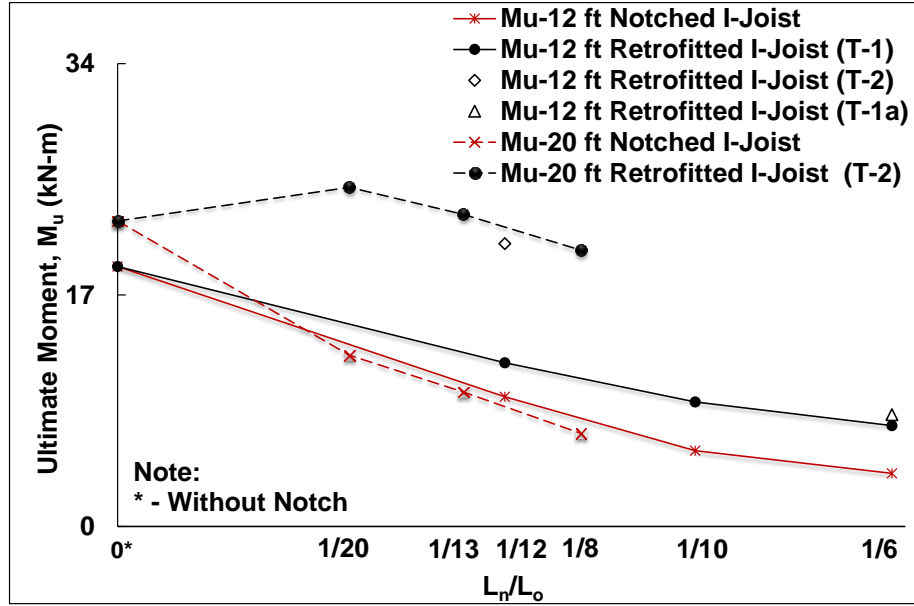
**Figure 5.7: Different types of failure occurred in reinforced flange notched I-Joists.**

### 5.3.4 Effect Analysis

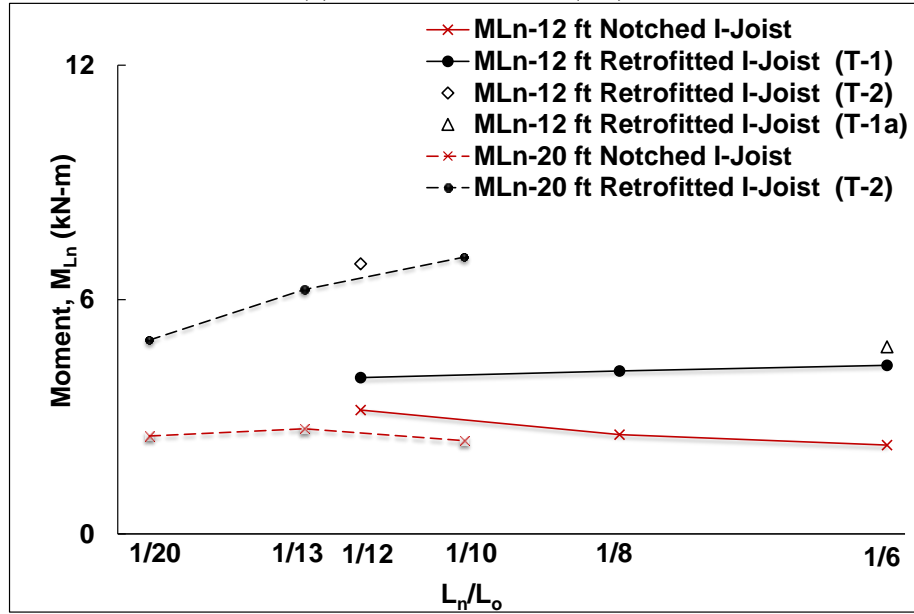
#### 5.3.4.1 Effect of Notch Location

When the notch locations of the I-joists are compared, it was evident that the location of notch plays a significant role in the moment and load capacities of the I-joists. **Figure 5.8** represents the ultimate moment and the moment at notch location of the 12 ft and 20 ft flange notched I-joists with different types of retrofitting. The moments are illustrated in regards to the ratio of the notch location ( $L_n$ ) and span length ( $L_o$ ).

From **Figure 5.8 (a)** it can be observed that the ultimate moment ( $M_u$ ) decreases as the  $L_n/L_o$  ratio increases (i.e. the location of the notch moves away from the support) for all series of I-joists (deficient and retrofitted). As the distance of the notch location increased, the moment demand at notched section increased and thus the moment capacity decreased. The notched I- joist experienced the least moment, but with retrofitting (Type T-1, Type T-1a, and Type T-2) the moment capacity increased. The ultimate moment ( $M_u$ ) had an identical trend for both of the notched and the retrofitted I-joist. However, these trends are different for 12 ft (retrofitted with Type T-1) and 20 ft (retrofitted with Type T-2) span length I-joists. For the retrofitted flange notched I-joist, the ultimate moment decreased with an increase in the  $L_n/L_o$  ratio, but for the type T-2 retrofitted I-Joist, the ultimate moment initially increased and then decreased as the ratio increased. The ultimate moment capacity of the retrofitted I-joists (20 ft) with Type T-2 method having a flange notch of 100mm x100 mm at 305 mm from the support was exceeded that of the control I-joists.



(a) Ultimate Moment ( $M_u$ )



(b) Moment at Notch Location ( $M_{Ln}$ )

**Figure 5.8: Effect of Notch Location for 100 mm x 100 mm Notch** a) Ultimate Moment ( $M_u$ ),  
b) Moment at Notch Location ( $M_{Ln}$ )

The moment at notch location ( $M_{Ln}$ ) of the 12 ft and 20 ft I-Joist for different ratios of the notch location to the span length of I-joist are shown in **Figure 5.8 (b)**. It can be observed that the moment at the notch location ( $M_{Ln}$ ) slightly decreases as the  $L_n/L_o$  ratio increases for both of the short and long span I-joists. On the contrary, for retrofitted (with Type T-1 for 12 ft span and Type

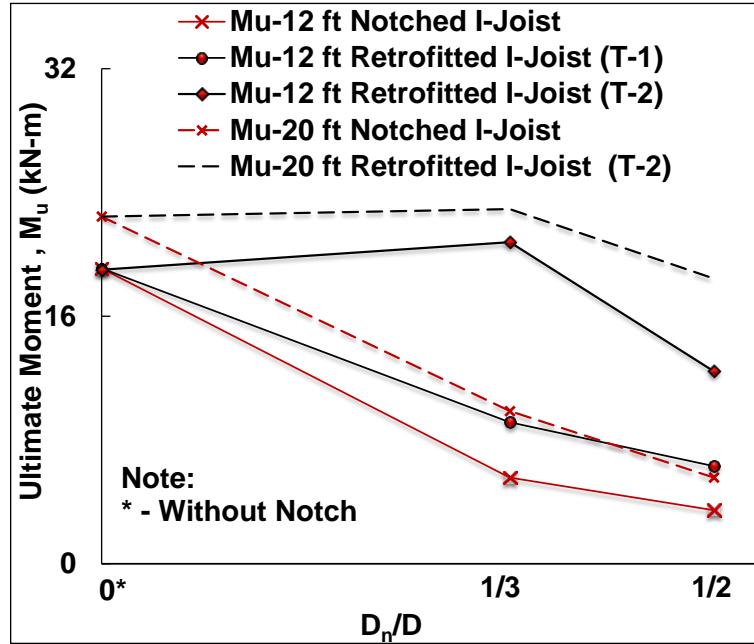
T-2 for 20 ft span) flange notched I-joist, surprisingly the moment at notch location ( $M_{Ln}$ ) increases as the notch  $L_n/L_o$  ratio increases. However, the average moment at notch location ( $M_{Ln}$ ) of flange notched and retrofitted flange-notched I-joists are very close as expected for a specific size of the notch (100 mmx100mm) as the flexural stiffness ( $EI$ ) of notched sections are same. Which signifies that the moment at notch location ( $M_{Ln}$ ) is the critical factor for determining the capacity of the flange notched I-joists. Retrofitting of flange notched I-joists using Type-T-1a and Type T-2 increases the moment at notch location ( $M_{Ln}$ ) compared to the un-retrofitted flange notched I-joist and Type T-2 retrofitting technique is the most effective among the retrofitting techniques used in this study.

#### **5.3.4.2 Effect of Notch Size**

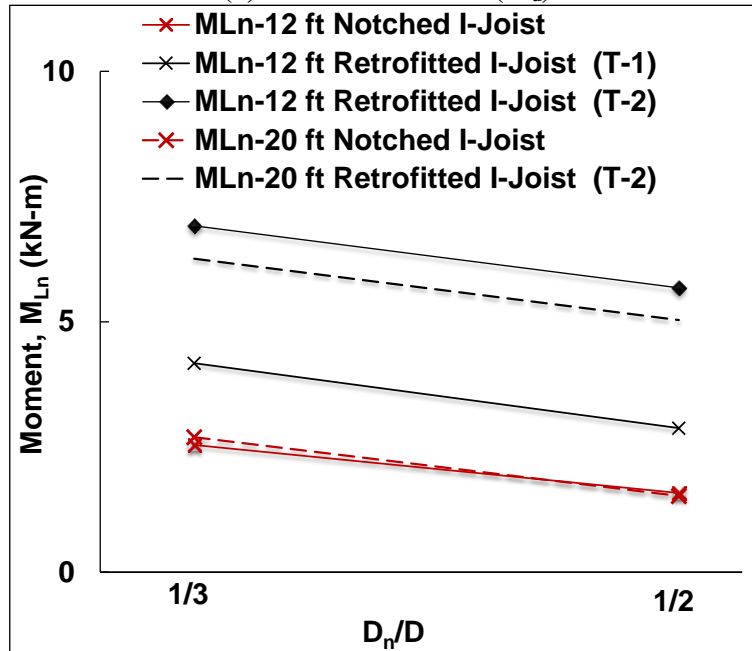
To understand the effects of notch size on the moment capacity of flange notched and their retrofitted I-joists series has been compared in **Figure 5.9** for two different notch sizes (100mmx100mm and 100mmx150mm). It can be observed that the size of the notch depth affects the moment at the notch and the ultimate moment.

A decreasing pattern is observed in the ultimate moment ( $M_u$ ) for both of the short and long span I-joists as shown in **Figure 5.9 (a)**.  $M_u$  drops from 18 kN-m to about 4 kN-m and for the 20 ft I-joist, 23 kN-m to about 5 kN-m for 12 ft and 20 ft I-joist, respectively Type T-1 retrofitting leads to an increase in  $M_u$ , but still followed the decreasing trend. Type T-2 retrofitting exhibited a constant (identical pattern) decreasing trend with the increase of  $D_n/D$  due to the reduction of the flexural stiffness ( $EI$ ) and shear rigidity ( $GA$ ) as expected at the high shear zone of the I-joists. Type T-2 retrofitting of 20 ft flange notched I-joist, improves the  $M_u$  equivalent to the  $M_u$  of Control I-joist, and then a reduction (to a value of about 21 kN-m) of  $M_u$  is observed due to the

deeper notch size. Which signifies that Type T-2 retrofitting technique can fully recover the moment capacity of the long span I-joist having a shallower flange notch.



(a) Ultimate Moment ( $M_u$ )



(b) Moment at Notch Location ( $M_{Ln}$ ) ( $L_n=455$  mm)

Figure 5.9: Effect of Notch Size (Notch Distance 455mm from Support) a) Ultimate Moment ( $M_u$ ), b) Moment at Notch Location ( $M_{Ln}$ )



For the I-joist with a notch distance of 455 mm from the support, the moment at the notch location,  $M_{Ln}$ , decreases as the depth of notch or the ratio of notch depth to the I-Joist depth increases as shown in **Figure 5.9 (a)**. As the ratio ( $D_n/D$ ) increases to 1/2 (for a deeper notch  $D_n=150$  mm), the moment at notch location,  $M_{Ln}$ , slightly decreases for all series (deficient and retrofitted I-joists) which is mainly because of the reduction of the shear stiffness. On the contrary, for short span retrofitted (with Type T-2) flange notched I-joist, surprisingly the moment at notch location ( $M_{Ln}$ ) increases as the notch depth  $D_n$  increases from 100 mm to 150 mm.

#### 5.3.4.3 Effect of Notch Reinforcer Length

**Table 5.5: Effect of Notch Reinforcer Length (Notch Size 100x100mm Located at 310mm from Support)**

Span	Control / Flange Notched I-Joists			Retrofitted Flange Notched I-Joists				
	Series	$M_u$ (kN-m)	$M_{Ln}$ (kN-m)	Series	$M_u$ (kN-m)	$M_{Ln}$ (kN-m)	$L_r = B_n + 2 * L_d$ (mm)	Type
12 ft	12-A	19.1	0.0				0+0+0	-
	12-H	3.9	2.3	R-12-Q	7.4	4.3	100+2×305	T-1
				R-12-R	8.2	4.8	100+2×610	T-1a
20 ft	20-A	22.4	0.0				0+0+0	-
	20-M	6.8	2.4	R-20-QF	20.3	7.1	100+2×305	T-2
				R-20-RF	20.9	7.3	100+2×610	T-2a

The average values of the ultimate moment,  $M_u$  and the moment at notch location,  $M_{Ln}$  of the Control, Flanged Notch I-Joists, and the Retrofitted Flange Notched I-joist series have been summarized in **Table 5.5** with the change of the length of the reinforcers ( $L_r$  or  $L_d$ ). From the table, it can be inferred that the 20 ft span length of the I-joist yielded the largest  $M_u$  for each series, with the control 20A having a  $M_u$  of 22.4 kN-m; the 12ft I-Joist had a  $M_u$  of 19.1 kN-m. The presence of a notch decreases the ultimate moment to 3.9 and 6.8 kN-m for the 12 and 20 ft I-Joist, respectively. The moment at the notch location,  $M_{Ln}$  for the un-retrofitted flange notched I-joists

is 2.3 and 2.4 kN-m respectively for the 12 and 20 ft I-joist. This low moment value increases with the aid of retrofitting.  $M_u$  and  $M_{Ln}$  increase with addition of Type T-1, Type T-2, Type T-1a or Type T-2a retrofitting techniques. R-12-Q, R-12-R, R-20-QF, and R-20-RF have a  $M_u$  of 7.4, 8.2, 20.3, and 20.9 kN-m, respectively. Their corresponding  $M_{Ln}$  was 4.3, 4.8, 7.1, and 7.3 kN-m, respectively. With the help of retrofitting ( $L_d = 305$  mm), series R-12-Q and R-20-QF experienced a significant improvement of  $M_u$  and  $M_{Ln}$  from the flanged notched I-joist. Further increasing the length of reinforcers ( $L_d = 610$  mm), reinforced series R-12-R and R-20-RF observed additional 11% and 3% improvement, respectively, for both of  $M_u$  and  $M_{Ln}$ .

#### 5.4 Proposed Empirical Model to Estimate I-joist capacity

A polynomial regression analysis was performed by using the test results to develop models for predicting the capacity of unreinforced and reinforced I-joists with flange notches. I-joist span length ( $L$ ), height ( $D$ ), notch depth ( $D_n$ ), and location ( $L_n$ ), which affect the capacity of I-joist, were considered in the regression model. However, it should be noted that only Type T-2 reinforced series were considered while developing the model for reinforced I-joists as the performance improvement of Type T-1 reinforced I-joists are not sufficient to satisfy the requirements. The proposed equations for unreinforced and reinforced I-joists with flange notches are:

$$P_{Notched} = 38.7 - 0.023 \left( \frac{L}{D} \right)^2 - 26.6 \left( \frac{D_n}{D} \right) - 170.9 \left( \frac{L_n}{L} \right) + 298.4 \left( \frac{L_n}{L} \right)^2 \quad \text{Eq. 5-1}$$

$$P_{Retrofitted} = 66.5 - 0.094 \left( \frac{L}{D} \right)^2 + 17.5 \left( \frac{D_n}{D} \right) - 464.5 \left( \frac{L_n}{L} \right) + 19.2 \left( \frac{L}{D} \right) \left( \frac{L_n}{L} \right) - 52.4 \left( \frac{D_n}{D} \right)^2 \quad \text{Eq. 5-2}$$

The expected capacities of I-joists with flange notches and reinforced I-joists for the tests, as presented herein, were calculated using analytical proposed models as shown in *Eq. 5-1 and Eq. 5-2*. The predicted capacities were presented in *Table 5.6* and *Figure 5.10*. The maximum error

compared to the experimental results observed from unreinforced and reinforced series I-joists were 10% and 5%, respectively. The accuracies of the proposed models were compared using six descriptive statistical parameters: a) average performance factor (PF): the average ratio of experimental capacity to calculated capacity ( $P_{exp}/P_{cal}$ ), b)  $\chi$  factor defined as the inverse of the slope of a linear least square regression of the calculated capacity ( $P_{cal}$ ) versus the experimental capacity ( $P_{exp}$ ), c) standard deviation ( $SD$ ), d) sample variance ( $VAR$ ), e) co-efficient of variation ( $COV$ ), and f) average absolute error (AAE). The analysis results showed that the proposed models are highly accurate to predict the experimental capacity, with all statistical measures are found very low, as shown in **Table 5.7**. The proposed models (**Eq. 5-1 and Eq. 5-2**) show good accuracy with average PF and  $\chi$  values being close to 1.0. Moreover, COV values of the proposed equations (unreinforced and reinforced I-joists) were only 5% and 2%, respectively.

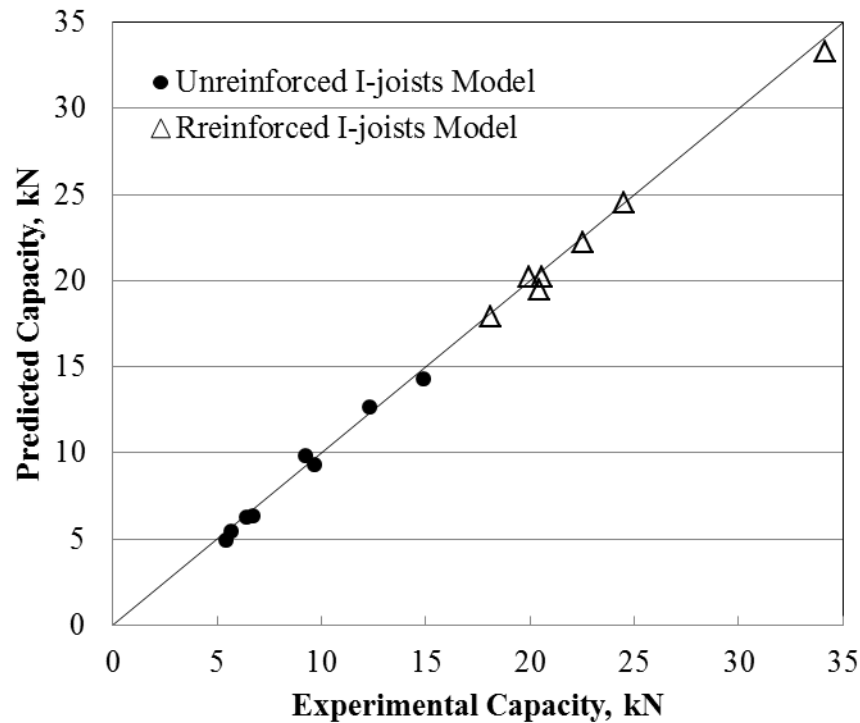


**Figure 5.10: Predicted vs experimental capacity of unreinforced and reinforced I-joists with flange notches**

**Table 5.6: Comparison between experimental and predictions**

I-Joist	Series ID	$L/D$	$D_n/D$	$L_n/L$	$P_{exp}$	$P_{cal}$	
					kN	kN	Error %
Unreinforced Series	12-F	12.1	0.33	0.084	14.92	14.3	4
	12-G	12.1	0.33	0.12	9.24	9.8	6
	12-H	12.1	0.33	0.17	6.42	6.3	2
	12-I	12.1	0.50	0.12	5.69	5.4	5
	20-K	20.2	0.33	0.05	12.32	12.6	2
	20-L	20.2	0.33	0.07	9.70	9.3	4
	20-M	20.2	0.33	0.10	6.72	6.3	6
	20-N	20.2	0.50	0.07	5.48	4.9	10
Reinforced Series	R-12-OF	12.1	0.33	0.084	34.16	33.3	2
	R-12-SF	12.1	0.50	0.12	20.46	19.5	5
	R-20-OF	20.2	0.03	0.05	24.49	24.5	0
	R-20-PF	20.2	0.33	0.07	22.55	22.2	2
	R-20-QF	20.2	0.33	0.10	19.97	20.2	1
	R-20-RF	20.2	0.33	0.10	20.55	20.2	1
	R-20-SF	20.2	0.50	0.07	18.13	17.9	1

**Table 5.7: Performance of proposed models**

Parameters	Unreinforced I-joists	Reinforced I-joists
Average PF	1.03	1.01
$\chi$	1.02	1.02
SD	0.05	0.02
VAR	0.00	0.00
COV (%)	5.17	1.98
AAE (%)	5.06	1.88

## 5.5 Summary

Based on the experimental results and effect analysis presented in this chapter following conclusion can be made:

- Type T-2 retrofitting technique containing 3 layers of OSB collar improves the load carrying capacity significantly.

- Shear failure was controlled by using reinforcer, which basically reduced the shear stress in the web by increasing the thickness of the web. A different reinforcing technique have to be introduced to increase the flexural stiffness and strength of the notched I-Joists.
- Length of the reinforcer ( $L_r$ ) also has a significant effect to improve the capacity of the retrofitted flange notched I-joists.
- Proposed empirical models are highly accurate to predict the experimental capacity with average PF and  $\chi$  value being close to one.
- Based on the effect analysis it was found that  $D_n/D$  and  $L_n/L$  had the maximum contribution on unreinforced and reinforced I-joists, respectively.
- Moment at notch location ( $M_{Ln}$ ) is the critical factor for determining the capacity of the flange notched and retrofitted flange notched I-joists with the OSB collars.

## CHAPTER 6: PERFORMANCE OF RETROFITTED WEB HOLED I-JOIST WITH OSB COLLARS: EXPERIMENTAL INVESTIGATION

### 6.1 General

Timber is a widely used renewable material that exhibits several favorable characteristics, such as high strength to weight ratio, low carbon footprint, and good insulation properties. Solid timber as a natural material, however, exhibits very large variability in its properties and quality and can only be used to produce linear members. Historical timber structures were often characterized by elements which were limited both in their cross-sectional dimensions and length by the dimensions of the existing trees in the surrounding area (*Dietsch and Tannert 2015*). To meet the engineering and architectural desires to utilize the sustainable features of timber in homogeneous and planar elements, timber can be broken down into sequentially smaller fractions which can then be reassembled into glued composite members, labelled engineered wood products (EWPs) (*Vallée et al. 2016*). Depending on the wood fraction used as raw material, EWPs can be classified into lumber-based such as Glued-Laminated-Timber, veneer-based such as plywood or Laminated Veneer Lumber (LVL), strand-based such as Oriented Strand Board (OSB) or Laminated-Strand-Lumber (LSL), and particle-based products such as Fiber-board.

#### 6.1.1 Composite I-joists

EWPs are combined to produce prefabricated composite structural members such as wooden I-joists which are popular in light frame construction as floor and roof joists because of their high strength and stiffness, low weight, dimensional stability and low cost in comparison to solid timber (*Anon 2001*). The flanges and the web are glued together to form an I-shaped cross-section that can save 50% of wood fiber compared to solid lumber beams (*Leichti and Tang 1983; Islam et*

*al. 2011*). Composite I-joists often consist of a flange made of LVL or LSL with the web made of OSB or plywood where the flanges and webs are designed to carry moment and shear forces, respectively, and the stresses between flanges and web are transmitted through the flange-web glue line. Early studies on wood I-joists (*Fergus 1979; Hilson and Rodd 1979; Samson 1983; Leichti and Tang 1983, Leichti and Tang 1986; Leichti et al. 1989*) focused on determining the influence of the flange and web materials on the capacity, stiffness and stability and provided the groundwork for the widespread structural application of I-joists.

Modern wood I-joists are proprietary products with producers providing their specific design values after conducting tests according to *ASTM D5055 (2010) and WIJMA (1999)*. The design criteria for prefabricated composite I-joists include: i) bending resistance, governed by the flanges; ii) shear resistance, governed by the web; iii) deflection limits for live and dead loads; iv) bearing deformation at supports; v) span to height ratio to prevent web instability, especially when web holes are present; and; vi) bracing for lateral stability. The manufacturers furthermore list their limitations with respect to concentrated loads and web openings.

### **6.1.2 Web Holes in I-joists**

During construction, openings are often introduced to the webs of I-joists for passage of service ducts, plumbing and wiring (*Islam et al. 2015*). Openings allow builders to hide the utility services and reduce the floor height, but the presence of the web openings leads to reductions in stiffness and capacity. Such reductions are most critical in the cases of web openings located close to supports and may cause I-joists to fail in premature sudden and brittle shear failure. The current edition of the Canadian Standard for Engineering Design in Wood (*CSA086 2014*) provides no guidance for such openings in I-joists and the National Design Specification for Wood

Construction in the US (*NDS 2015*) recommends manufacturer specifications for I-joists with openings.

Previous research evaluated the failure mode and capacity reduction of wood I-joists with web openings. *Morris et al. (1995)* summarized three failure modes as web fracture, web buckling, and de-bonding of web-flange adhesive joint. *Fergus (1979)* studied the effect of circular openings on moment-governed 7.3m long I-joists and shear-governed 2.4m long I-joists and found no significant change in stiffness with a web removal of up to 70% of total height. This finding, however, was limited for the specific location of the web opening in the moment critical I-joists close to support and close to mid-span in the shear critical I-joists. On the contrary, *Maley (1987)* and *Wang and Cheng (1995)* reported that openings do reduce stiffness and shear capacity. *Wang and Cheng (1995)* investigated 2.8m to 3.6m long I-joists with rectangular web openings of 33% to 100% web height placed at a distance of 0.5m to 1.0m from the support and observed that the shear strength was reduced up to 79% when the opening height was equal to the height of web. No significant change occurred for opening heights of 33% of web height.

*Leichti et al. (1990a and b)* reviewed previous studies on I-beams with openings and reported that the restriction on the web opening position depends on types and sizes of openings. They concluded that rectangular openings are more restrictive than circular openings (due to the stress concentration at corners), that a 38mm opening can be placed anywhere in the web, but larger openings require specified minimum distances from supports and flange edges.

*Afzal et al. (2006)* performed tests on wood I-joists with circular and square openings. The I-joists were 302mm and 406mm deep and the opening size was varied up to 100% of web height. While the opening size-to-web depth and the span-to-depth ratio both affected the capacity, the



type of opening (circular/square) was found insignificant. **Zhu et al. (2005)** investigated the failure load of wood I-joists with and without web openings, observed that capacity decreases linearly with opening size, whilst location of opening has little effect on the reduction of capacity and proposed an empirical formula to calculate the capacity of I-Joists with openings:

$$P_u = 36.4 - 25.9 \left( \frac{d}{h_w} \right) \quad \text{Eq. 6-1}$$

where  $P_u$  is the capacity of I-Joists with opening in kN,  $d$  is the diameter of circular opening,  $h_w$  is the web height. **Zhu et al. (2007)** developed additional models to predict I-joist failure considering material nonlinearity and crack propagation and achieved a better fit with experimental. **Pirzada et al. (2008)** developed another mechanics-based method to predict the capacity of wood I-joists with circular web holes:

$$P_{failure} = 2 \sqrt{\frac{x_0 E^* G_c}{2\pi}} \left[ \sigma_t \left( 2\sqrt{(pk)\pi x_0} - (pk)\pi \right) \right]^{-1} P_{applied} \quad \text{Eq. 6-2}$$

where  $P_{failure}$  is the load causing fracture in web,  $P_{applied}$  is the applied load,  $p$  is the web hole ratio,  $k$  is the factor related to I-joist depth with circular hole,  $x_0$  is the length parameter related to characteristic material properties,  $E^*$  is the equivalent modulus of elasticity of web, and  $G_c$  is the critical fracture energy of web.

**Guan and Zhu (2004)** performed finite-element-analyses (FEA) to predict the behavior of wood I-joists with openings where the opening sizes were varied from one-quarter to three-quarter to the height of the I-joists. They observed that the predicted capacity for I-joist with circular openings was 20% higher than the I-joists with rectangular openings. In their more recent study, **Guan and Zhu (2009)** developed anisotropic elasto-plastic constitutive models that are able to

identify the location of initial crack, the growth of crack, the stress states, the capacity of wooden I-joist. While previous attempts to FEA provided some valuable insight, further experiments are deemed necessary before predictive FEA models can reliably be used for the investigation of I-joists with openings.

*Islam et al. (2015)* tested nearly 100 I-joist specimens with flange notches at different locations under four point bending test. The results show reduction of load carrying capacity even up to 80% compared to an uncut I-joist. As the notch location moves away from the support towards mid-span, the flexural capacity decreases significantly. In most cases, the specimens experienced combined flexural-shear failure.

### **6.1.3 Reinforcing of I-joists**

To increase the flexural and shear capacity of timber beams, several techniques can be used: attaching metal, solid timber or EWP plates, or Fiber-Reinforced-Polymer (FRP) sheets either by mechanical means or adhesive bonding (*Franke et al. 2015*). Previous studies performed on wood I-joists with openings mostly focused on the change in capacity caused by the openings and only very few studies investigated reinforcing techniques. *Morrissey et al. (2009)* investigated reinforced I-joists with steel angles attached to both sides of the web and the flange above and below the openings and obtained an increase in capacity up to 39%. *Polocoser et al. (2013)* reinforced wood I-joists around the openings with U-shaped LSL and OSB patches and OSB collars. They performed tests on 356mm and 406mm deep I-joists with spans of 2.4m and 4.9m and openings of up to 63% of the joist depth which reduced the capacity up to 58%. After retrofitting, some of the specimens regained the capacity of the original joists. Among the three different techniques, the OSB collar was found to be most effective.

Other studies focused on reinforcing solid timber and glulam beams using carbon-FRP (*Nowak et al. 2013, Borri et al. 2005, and Li et al. 2009*) or glass-FRP (*Raftery and Harte 2011*), but very few studies, e.g. *Hallström 1996*, investigated glass- GFRP reinforcement of glulam beams with both circular and rectangular openings (finding that shear capacity improved up to 100% compared to unreinforced beams). No study on using FRP to reinforce wooden I-joists has been reported in the literature so far.

#### **6.1.4 Objective**

Placing web openings in I-joists is common practice that can lead to significant reduction in stiffness and capacity which – if not appropriately considered in design – may cause excessive deflections and premature failure of the element and possibly the structure. Practitioners, however, are not provided with sufficient design guidance that captures the reduction in capacity and stiffness of I-joists with web openings. The objectives of this research are to investigate the impacts of: i) size and location of web openings on failure modes, capacity and stiffness; and ii) reinforcing I-joists with web openings with OSB collars on the failure modes, capacity and stiffness on I-joists with web openings.

### **6.2 Experimental Investigation**

#### **6.2.1 Materials**

All wood I-joists' specimens for experiment were prepared at the facility of AcuTruss Industries Ltd., Canada. The specifications were chosen from the NASCOR NJH12 I-joist series (*Nascor 2010*). Flanges were made of LVL from SPF No2, webs were made from OSB manufactured to meet the requirements of the Performance Standard for Wood-Based Structural-Use Panels (*PS2 2010*) and *CSA-O325 (2012)*. The OSB was 'APA Rated Sheathing' grade with



**Table 6.1: Summary of test series and test results**

I-Joist	Series ID	L	D	L <sub>n</sub>	L <sub>r</sub> = (L <sub>d</sub> +D+ L <sub>d</sub> )	k		F <sub>exp</sub>	
		mm	mm	mm	mm	N/m m	COV	kN	COV
Control	12-A	3650	-	-	-	1220	17	40.5	30.4
	20-A	6100	-	-	-	310	10	28.9	14.3
I-Joists with Opening		3650	213	305	-	1000	10	18.3	11.7
	12-C	3650	213	610	-	1035	10	17.1	9.72
	12-D	3650	150	305	-	1080	14	27.5	9.5
	12-E	3650	100	305	-	1165	16	36.5	18.9
	20-B	6100	213	305	-	364	12	20.7	13.1
	20-C	6100	213	914	-	315	14	20.1	13.1
	20-D	6100	150	305	-	345	11	27.9	15.2
	20-E	6100	100	305	-	305	9	26.3	24.8
Reinforced I-Joist	12-F	3650	213	305	D+D+D	1045	13	21.9	13.4
	12-G	3650	213	610	D+D+D	1085	8	20.5	9.7
	12-H	3650	150	305	D+D+D	1115	9	35.2	13.9
	12-I	3650	100	305	D+D+D	1180	14	40.7	24.1
	12-J	3650	100	305	2D+D+2D	1240	15	45.9	24.7
	20-F	6100	213	305	D+D+D	310	12	21.1	13
	20-G	6100	213	914	D+D+D	310	8	22.2	10.6
	20-H	6100	150	305	D+D+D	305	9	30.5	16.8
	20-I	6100	100	305	D+D+D	320	15	29.2	9.9
	20-J	6100	100	305	2D+D+2D	315	11	26.7	15.1

### 6.2.3 Reinforcement of I-joists

I-joists with the same dimensions and openings as series B to E were reinforced with OSB collars to investigate the impact of the retrofit on capacity and stiffness. Five more series (series F to J) of specimens with the same span length of 3.66m (12ft) and 6.10m (20ft) were tested after being reinforced around the opening with an OSB collar. Collars were located on only one side of

the web and consisted of two layers, each layer composed of 9.5mm (3/8inch) OSB. The first layer was arranged around the opening and glued directly onto the web. The second layer was glued on top of the first collar. The adhesive was a two-component epoxy containing a resin (*Cascophen 4001-5*) and a catalyst (*Cascoset 5830S.5*). The reinforcement length ( $L_r$ ) of the OSB collar on each side of the opening was kept equal to the diameter of the opening (series F to I). Only for series J, the collar (reinforcement) length was doubled to evaluate the capacity improvement due to OSB collar length. The details of the reinforced I-joists are given in **Figure 6.2 and Table 6.1**. A total of 100 reinforced specimens were tested with ten replicates in each test series.

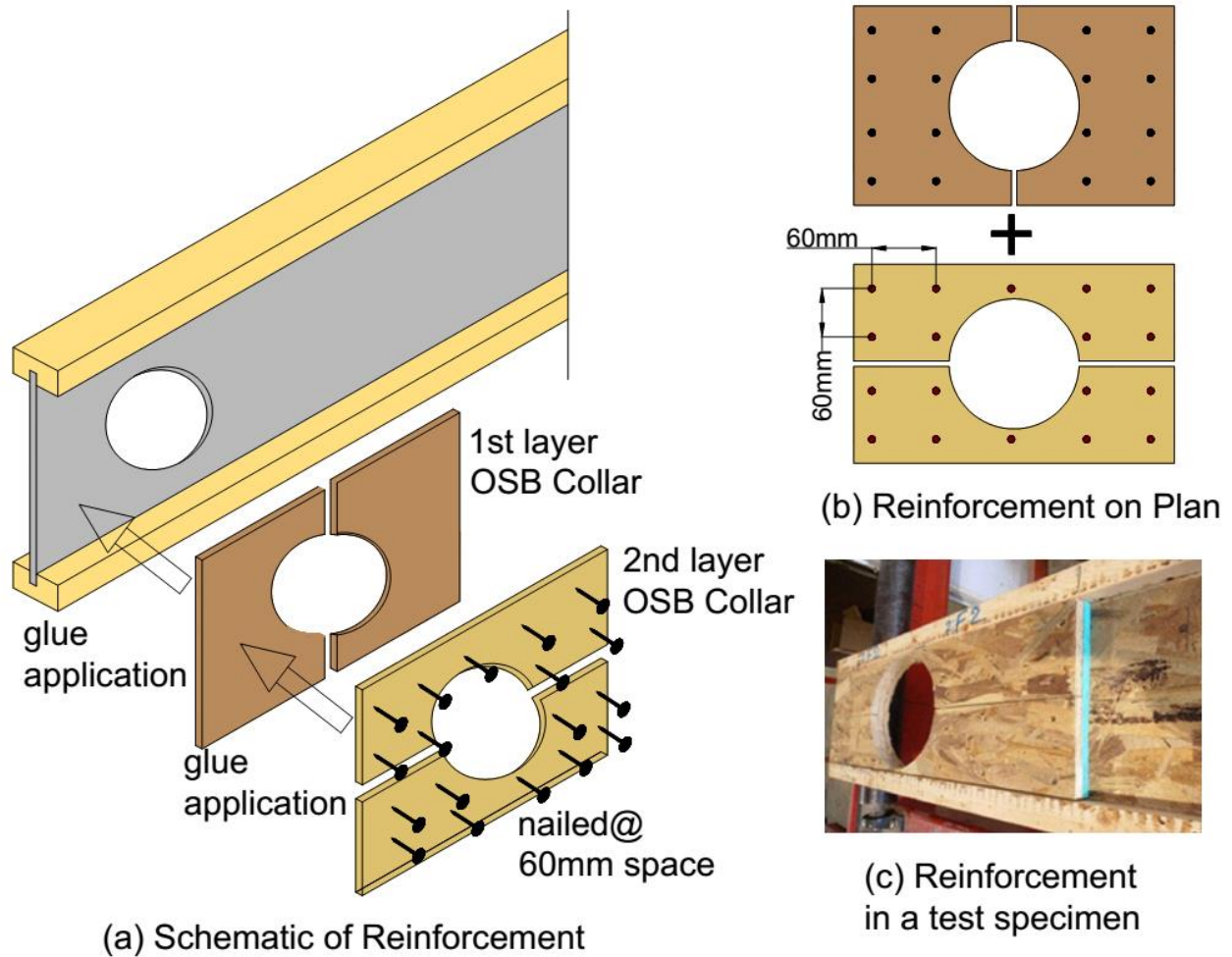


**Figure 6.2: Retrofit of I-joists with two OSB ply in collar system**

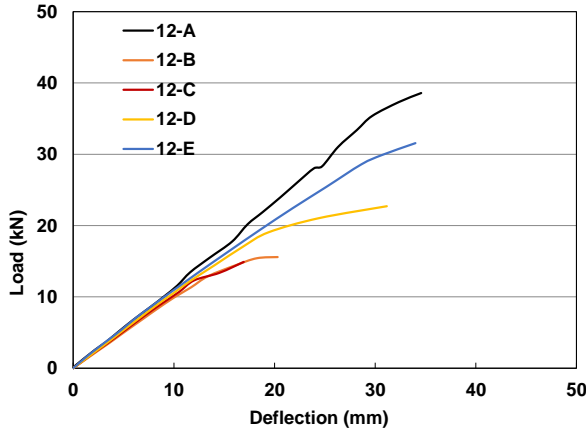
#### 6.2.4 Methods

The specimens were tested as simply supported beams in four-point bending according to *ASTM D5055 (2013)*. The loads were applied by a hydraulic actuator with a loading rate of 4mm/min. Hollow structural section (HSS) rectangular tubes were placed vertically on both sides of the flanges along the length of I-Joists at a spacing of 610mm to ensure concentric loading and to prevent lateral buckling (see *Figure 6.1*). The joist deflections were measured by placing an extensometer at mid-span. The stiffness was calculated for the range of 10% to 40% of capacity according to EN 26891 (*CEN 1991*). Three cameras, focused at the mid-span, at the location of opening and at the loading point, were installed to monitor the crack pattern and failure of the specimens.

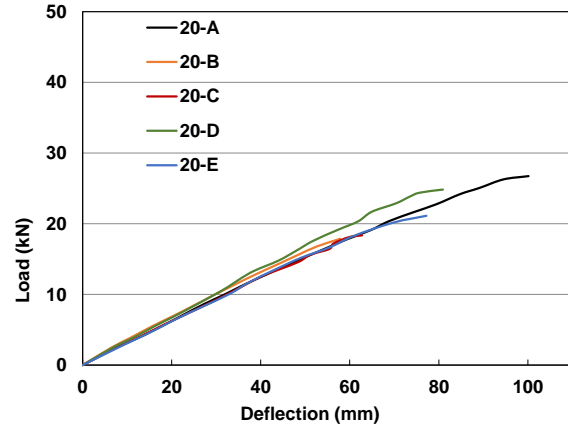
Analysis of variance (ANOVA) was performed to identify the statistical significance of differences between test series (*Montgomery 2008*). A probability of ‘Type I’ error,  $\alpha = 0.05$ , was considered; the response variables were capacity and stiffness of I-joists. To evaluate which individual test series are different from each other, Fisher’s least significant difference (LSD) test was used to identify the groups that are different (*Williams and Abdi 2010*).

#### 6.2.5 Results

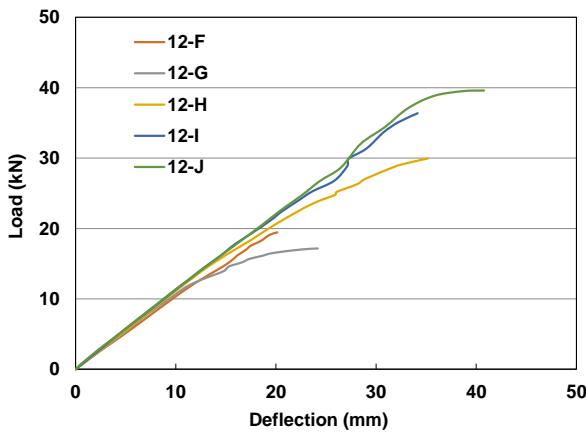
The load-deflection curves of all specimens were linear up to failure. Since all individual specimens exhibited similar load-deformation behavior, only the average load-deflection curves are plotted in *Figure 6.3*. The average capacities and stiffness for all test series as well as the corresponding coefficient of variations (COV) are summarized in *Table 6.1*.



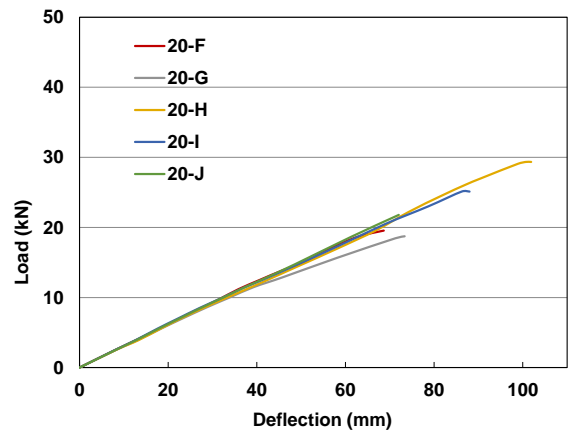
(a) 12 ft web hole I-joist



(b) 20 ft web hole I-joist



(c) 12 ft retrofitted web hole I-joist



(d) 20 ft retrofitted web hole I-joist

**Figure 6.3: Average load-deflection for I-joists test series with opening (a) 12ft span (b) 20ft span and for retrofitted I-joists test series (c) 12ft span (d) 20ft span**

#### 6.2.5.1 Series A (Control I-Joist)

Series A represents the control beams without any opening. The 12ft I-joists failed in either shear at support or flexure at mid-span. The failure was initiated mostly by the presence of knots in the flanges or due to de-bonding of the OSB webs. Three specimens (12-A3, 12-A4 and 12-A6) failed in shear (*Figure 6.4 (a) left*) and the rest of the specimens failed in flexure at mid-span (*Figure 6.4 (a) middle*). In the case of 20ft I-joists, all the specimens failed in flexure at mid-span and there was no shear failure in any of the 20ft specimens. The average capacity of the 12ft and 20ft control test series was 32kN and 24kN, respectively with a COVs of 30% and 25%. The



experimental capacity for the 12ft and 20ft I-joists was found to be 3.4 and 4.0 times higher, respectively, than the specified design capacity from the manufacturer. Similarly, the average stiffness of 12ft and 20ft control I-joists was 1,220N/mm and 310N/mm, respectively, which was 2.4 and 2.8 times higher than the specified design stiffness from manufacturer (design stiffness of 511N/mm and 110N/mm for 12ft and 20ft I-joists, respectively). According to *ASTM D5055 (2004)*, wood I-joists require the allowable capacity to be “the lower 5% tolerance limit with 75% confidence divided by 2.1.” The factor of safety from the present test results was found to comply with this requirement.

#### **6.2.5.1 I-Joist Series with Opening (Series B to E)**

The presence of an opening changed the failure mode and capacity of the I-joists. Series B specimens featured an opening equal to the height of the web and located 305mm from the leading edge. All 12ft and most 20ft series B I-joists failed in shear at the opening (*Figure 6.3 b*), the exceptions being specimen 20-B9 which failed in shear right next to the opening and specimen 20-B10 which experienced flexural failure at mid-span. In both specimens failure was initiated at a knot. Compared to the control series, the average capacity of 12ft series B I-joists was reduced by 53% and for the 20ft I-joists was reduced by 21%, see *Figure 6.6*. While the average stiffness of the 12ft I-joists in series B was reduced by 18%, stiffness of the 20ft I-joists was not affected by the presence of openings (see *Table 6.1 and Figure 6.7*).

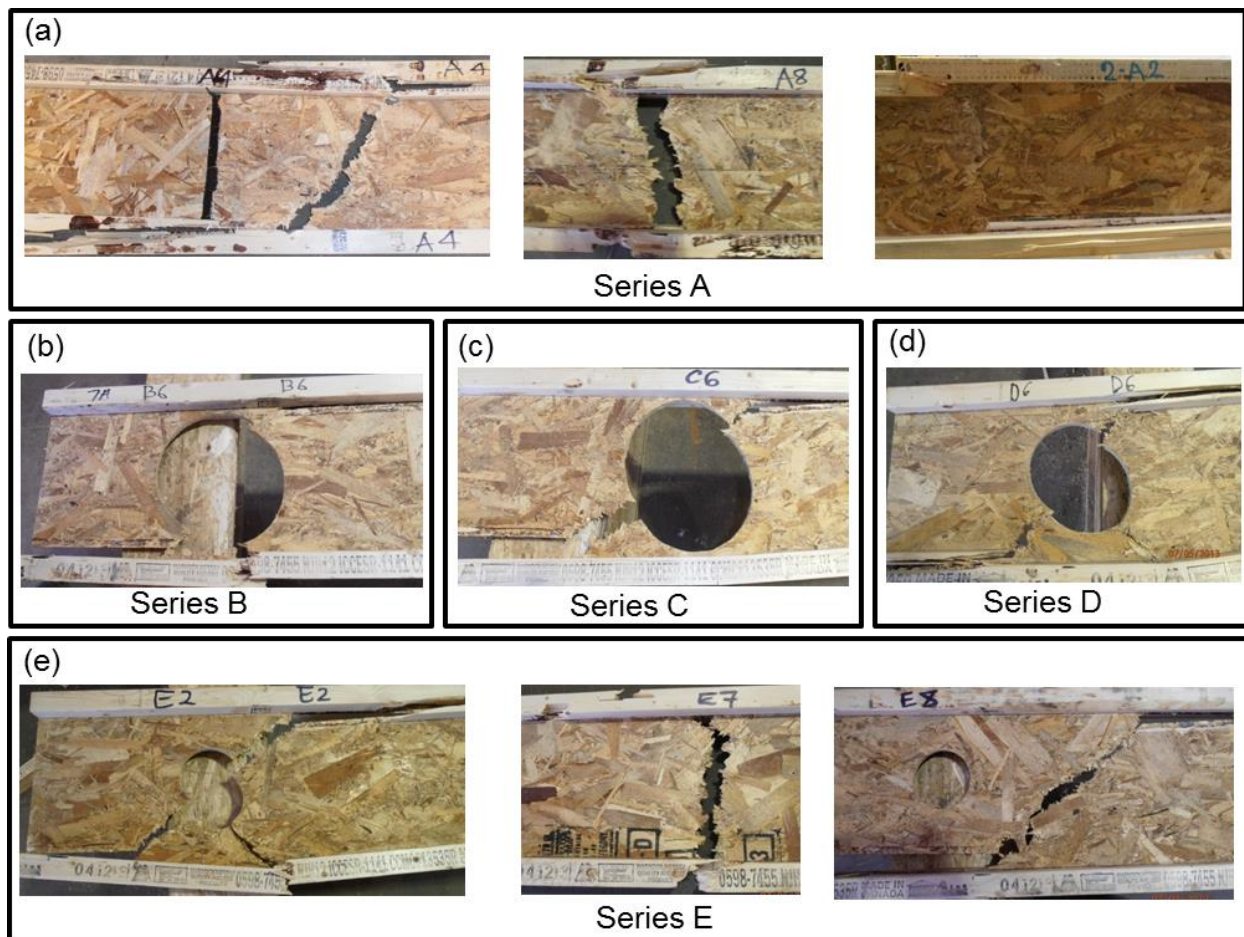


**Figure 6.4: Typical failures for I-joists test series A to E**

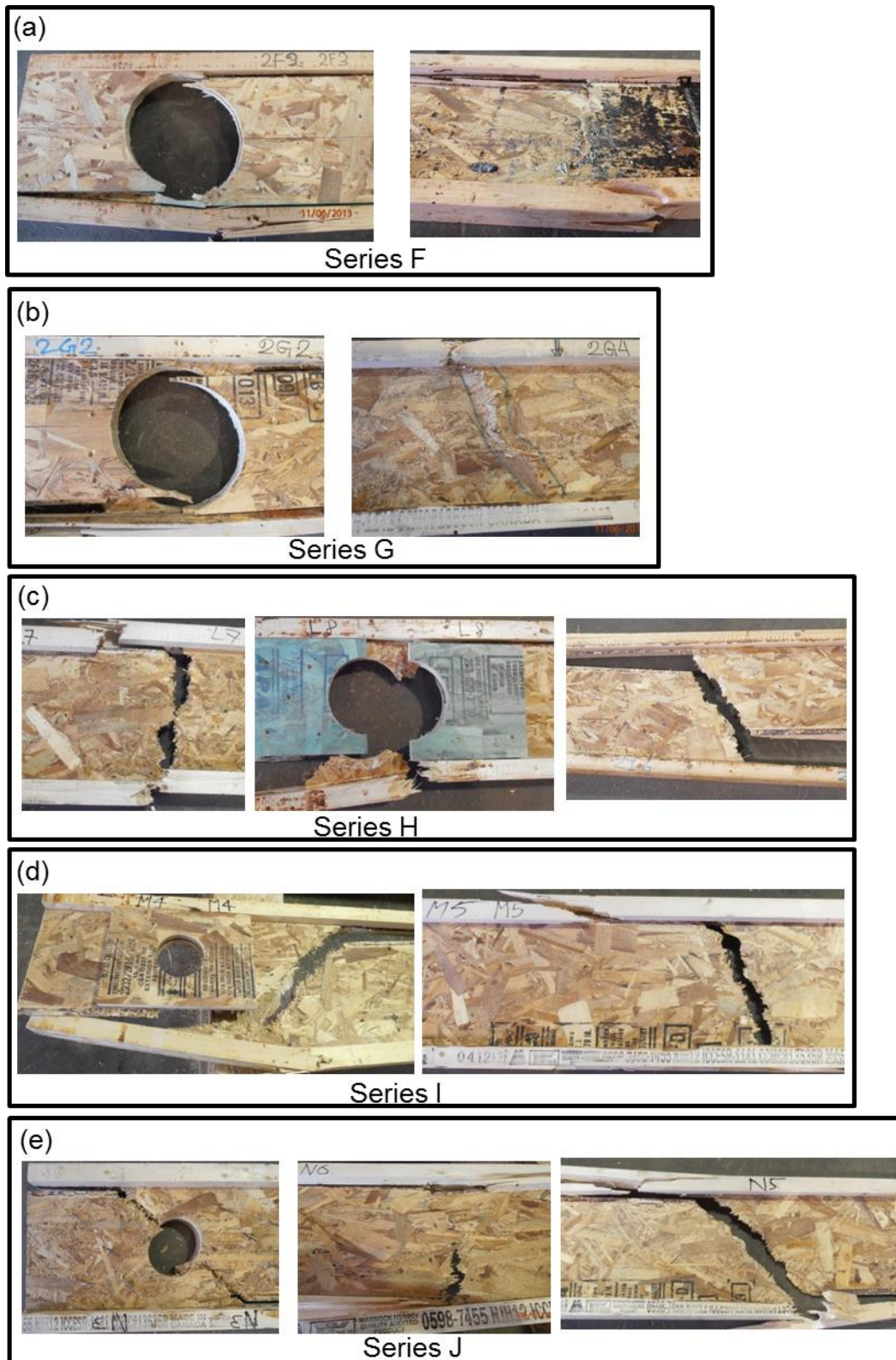


**Figure 6.5: Typical failures for retrofitted I-joists test series F to J**

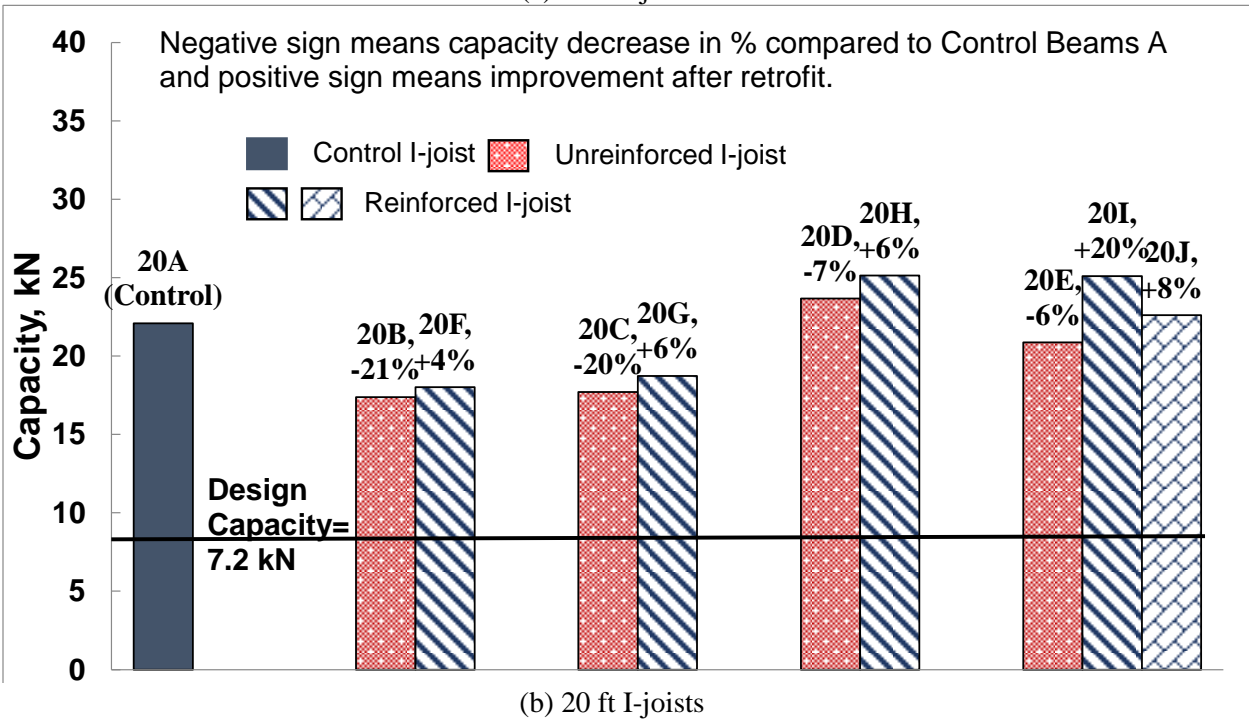
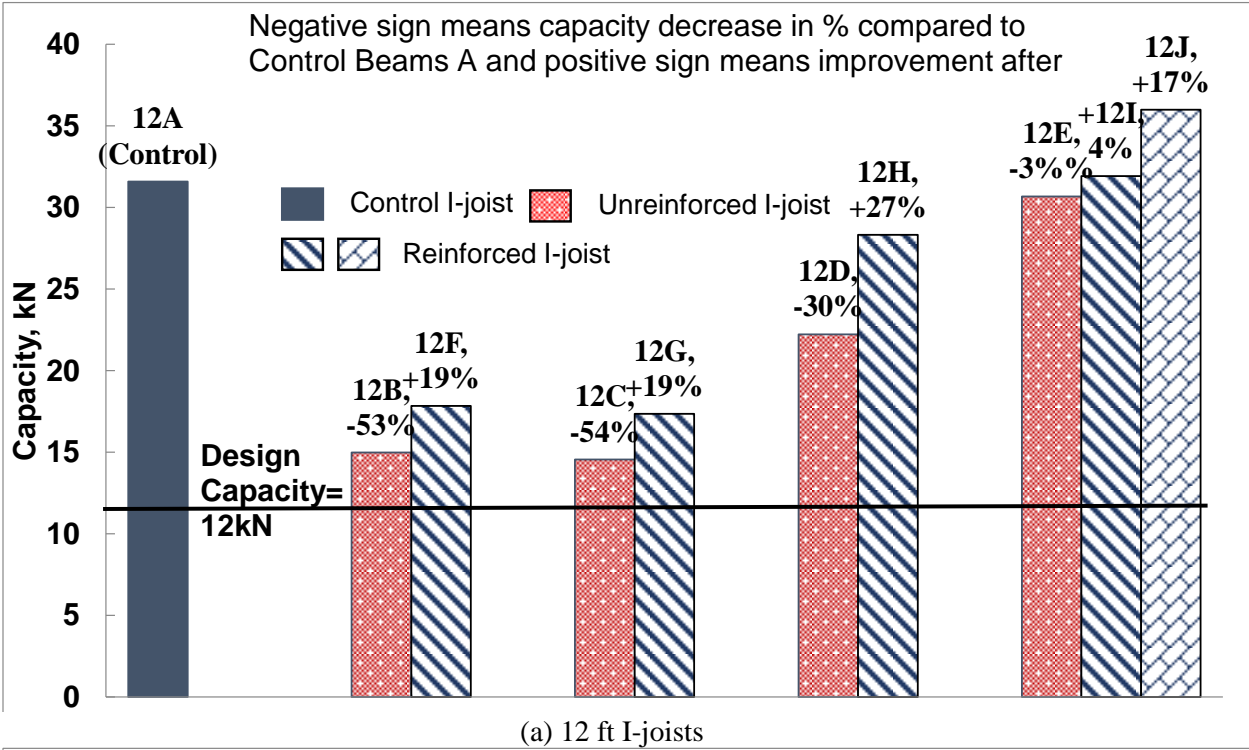
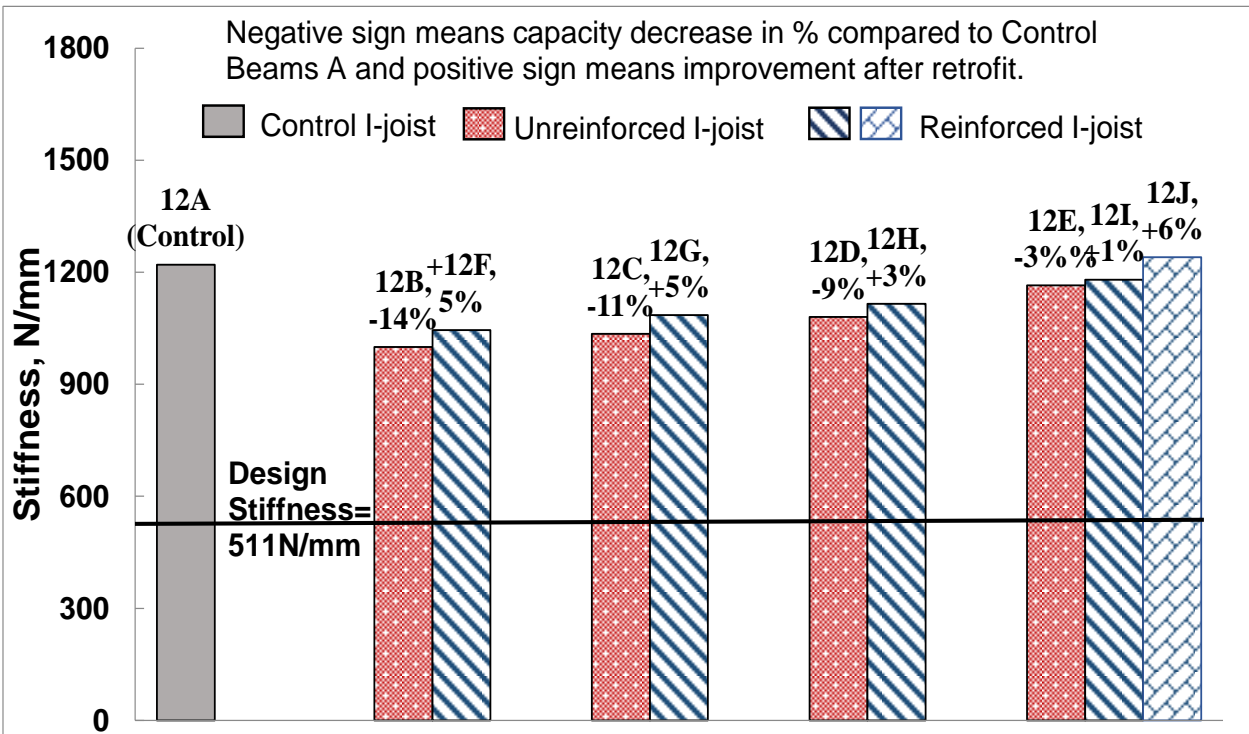
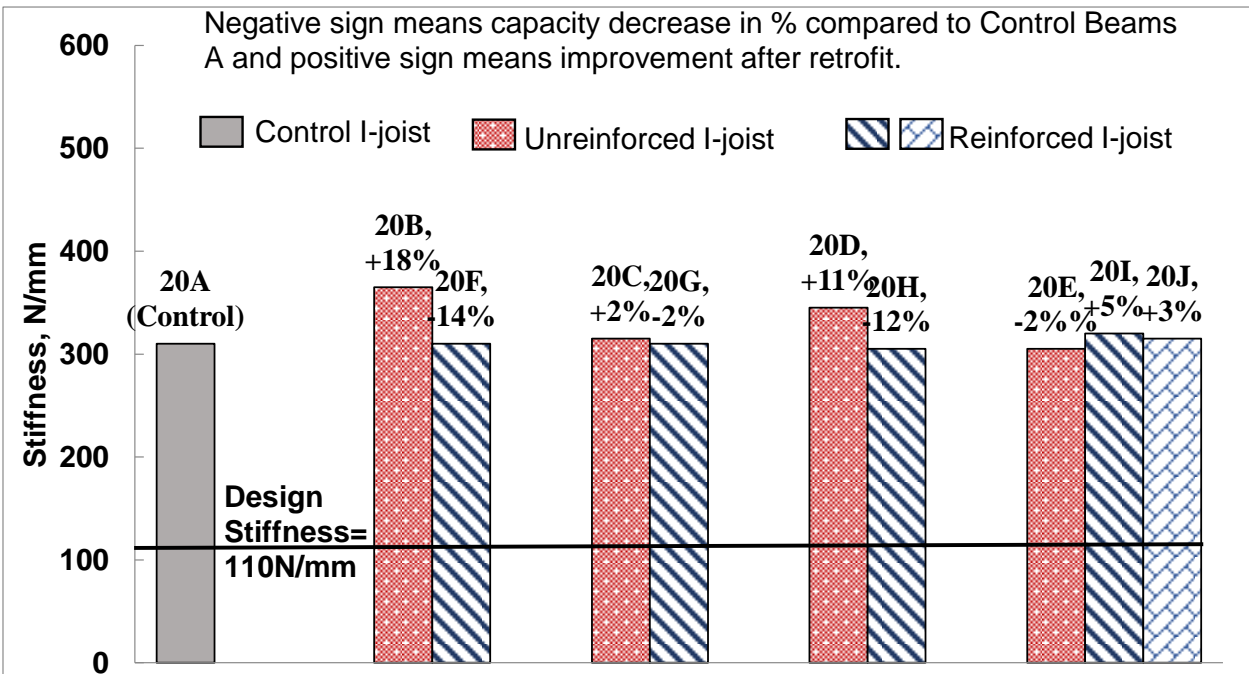


Figure 6.6: Comparison of capacity: (a) 12 feet I-joists (top) and (b) 20 feet I-joists (bottom)





(a) 12 ft I-joists



(b) 20 ft I-joists

Figure 6.7: Comparison of Stiffness: (a) 12 feet I-joists (top) and (b) 20 feet I-joists (bottom)

Series C featured the same opening size as series B but located at 610 mm and 915 mm from the support for 12ft and 20ft I-joists, respectively. All specimens of series C failed in shear at the location of the opening (**Figure 6.4 (c)**). The average capacity of series C for the 12ft I-joists was reduced by 54%, and by 20% for the 20ft I-joists when compared to series A, see **Figure 6.6**. Though the average stiffness of the 12ft I-joists in series C was reduced by 15%, stiffness of the 20ft I-joists was not affected by the presence of openings (see **Table 6.1 and Figure 6.7**).

All specimens of series D (openings 66% the height of the web and located 305mm from the support) failed in shear, with failure starting diagonally at the opening by cracking of OSB followed by web-flange joint de-bonding and finally diagonal splitting of the flange (**Figure 6.4 (d)**). While the average capacity of the 12ft I-joists was 30% lower than series A, the average capacity of 20ft I-joists was found same. Half of the 12ft specimens of Series E (openings about 50% of the web height, also located at 305mm from the support) failed in shear diagonally along the opening similar to series D (**Figure 6.4 (e)**). The rest of the 12ft span I-joists specimens failed in flexure at mid-span, the average capacity of 12ft31kN being very close to series A. The average stiffness of the 12ft I-joists was reduced by 5%, whereas the average stiffness of 20ft I-joists was close to the control series. The failure patterns of the 20ft I-joists were similar to the control series A with all specimens failing in flexure close to mid span and capacity was similar to the control beams, see **Figure 6.6**.

#### **6.2.5.2 Reinforced I-Joist Series (Series F to J)**

The opening in each I-joist of series F through I were reinforced by attaching an  $L_r = D$  OSB collar around the opening. This collar prevented abrupt failure at the location of the opening. The majority of specimens still failed in shear diagonally which was followed by de-bonding of web-

flange joint (**Figure 6.5(a)**). The OSB collar de-bonded at the end of the failure process. In two series F specimens (20-F2 and 20-F10), the OSB collar prevented the shear failure and instead induced a flexural failure. In series G, all 12ft I-joists and all but two 20ft specimens failed in shear diagonally at opening (**Figure 6.5(b)**). The exceptions failed in flexure at mid-span. Compared to unreinforced series B the capacity of both 12ft F and G series specimens was found to be 19% higher, see **Figure 6.6**.

Most 12ft and all 20ft specimens from series H failed in flexure, similar to control I-joists series A (**Figure 6.5(c)**), and compared to unreinforced series D, their capacity increased 27% and 13% 12ft 20ft, respectively. Likewise, in series I the reinforcement collar efficiently prevented failure at the opening and the failure of the both 12ft and 20ft I-joists was in flexure. Compared to unreinforced series E, average capacity improved by 4% and 13%, respectively, for 12ft and 20ft reinforced I-joists, see **Figure 6.6**.

In series J, the length of the OSB collar on each side of the opening was doubled compared to series I to  $L_r = 2D$ . Most of the 12ft and all of the 20ft reinforced I-joists failed similar to the control specimens either in flexure at mid-span or in shear at the loading point (**Figure 6.5(e)**). The capacity of the 12ft and 20ft I-joists increased 17% and 8%, respectively, compared to unreinforced series E and even 14% and 5% compared to the control series, see **Figure 6.6**.

The average stiffness of the reinforced 12ft I-joists was lower than that of the control series, except in series J, where it remained approximately the same. Compared to the unreinforced test series with openings, however, the average stiffness was increased up to 6%. In the 20ft I-joists series, the reinforcement did not alter stiffness.

## 6.2.6 Statistical Analyses

*Table 6.2* and *Table 6.3* summarize the ANOVA. The  $P$ -value for the response variables (capacity and stiffness) were found less than  $\alpha = 0.05$  for both the 12ft and the 20ft test series. Therefore, the null hypothesis of the averages being equal was rejected and it was statistically confirmed that web openings and reinforcements create significant changes in I-joists' capacity and stiffness.

**Table 6.2: ANOVA results for 12 feet I-joists**

Parameter	P-value	Test Series	Mean difference	LSD	Comment
Capacity	$0.00 < \alpha$	12A-12B	16.2	4.8	Significant
		12A-12C	16.9		Significant
		12A-12D	9.2		Significant
		12A-12E	0.8		Not Significant
		12B-12F	2.6		Not Significant
		12C-12G	2.8		Not Significant
		12D-12H	6.0		Significant
		12E-12I	1.0		Not Significant
		12E-12J	5.3		Significant
Stiffness	$0.00 < \alpha$	12A-12B	217.2	129.7	Significant
		12A-12C	182.4		Significant
		12A-12D	136.8		Significant
		12A-12E	49.7		Not Significant
		12B-12F	47.6		Not Significant
		12C-12G	53.6		Not Significant
		12D-12H	36.8		Not Significant
		12E-12I	15.2		Not Significant
		12E-12J	72.9		Not Significant



**Table 6.3: ANOVA results for 20 feet I-joists**

Parameter	P-value	Test Series	Mean difference	LSD	Comment
Strength	$0.00 < \alpha$	20A-20B	4.7	3.2	Significant
		20A-30C	5.2		Significant
		20A-20D	1.6		Not Significant
		20A-20E	1.0		Not Significant
		20B-20F	0.6		Not Significant
		20C-20G	1.8		Not Significant
		20D-20H	1.5		Not Significant
		20E-20I	4.0		Significant
		20E-20J	1.5		Not Significant
Stiffness	$0.00 < \alpha$	20A-20B	71.7	32.9	Significant
		20A-30C	25.6		Not Significant
		20A-20D	52.3		Significant
		20A-20E	12.4		Not Significant
		20B-20F	54.3		Significant
		20C-20G	8.7		Not Significant
		20D-20H	37.6		Significant
		20E-20I	14.5		Not Significant
		20E-20J	7.9		Not Significant

LSD was calculated to identify the statistical significance of the observed differences. Openings in joist series B, C and D had significant mean difference in capacity and stiffness compared to control series A. The LSD value for series E indicated that an opening with a diameter of half of the web height does not affect the I-joist capacity. For 20 feet joists, it was found that the mean strength of series B and C and the mean stiffness for series B and D are different than that of the control series. The other opening layouts had no statistically significant effect on capacity and stiffness.

Capacity of 12ft joists of series H and J had significant improvement compared to their unreinforced series of D and E, respectively. For the 20ft series, however, only I-Joists series I exhibited an improvement in capacity. While stiffness of the 12ft specimens was not affected by

reinforcements (**Table 6.2**), some 20ft reinforced series (F, H, J) showed significant improvement in stiffness (**Table 6.3**).

### 6.2.7 Proposed Analytical Model to Estimate I-joist capacity

A regression analysis was performed using the test results to develop models to predict the capacity of unreinforced and reinforced I-joists with web openings. I-joist span length-to-height ratio ( $L/h$ ) and opening size to web height ratio ( $D/h_w$ ) affect the capacity of I-joist (*Afzal et al. 2006*) and were considered in the regression model. The proposed equations for unreinforced and reinforced I-joists with web opening are:

$$P_u = 64.8 - 1.5(L/h) - 54.3\left(\frac{D}{h_w}\right) + 1.9(L/h)\left(\frac{D}{h_w}\right) \quad \text{Eq. 6-3}$$

$$P_u = 105.6 - 3.5(L/h) - 90.8\left(\frac{D}{h_w}\right) + 3.8(L/h)\left(\frac{D}{h_w}\right) \quad \text{Eq. 6-4}$$

where,  $L$  is the I-joist span length (m),  $h$  is the height of I-joists,  $D$  is the size of opening size and  $h_w$  is the height of web.

The expected capacities of I-joists with openings and reinforced I-joists for the tests as presented herein, as well as previous tests performed by *Afzal et al. (2006)* and *Polocoser et al. (2013)*, were calculated using analytical models proposed by *Zhu et al. (2005)*, see **Eq. 6-1**, *Pirzada et al. (2008)*, see **Eq. 6-2** and the new models proposed in this research, see **Eq. 6-3** and **Eq. 6-4**. The predictions using these three models compared against the test results are illustrated in **Figure 6.8** and summarized in **Table 6.4** and **Table 6.5**. The percentage errors of the models as compared to test results are also reported in **Table 6.4** and **Table 6.5**. While Zhu's model significantly under-predicts capacity by up to 73%, Pirzada's model seems appropriate for small web opening sizes up to web depth ratio ( $D/h_w < 0.5$ ) but also significantly under-predicts for

larger openings  $D/h_w > 0.5$ . In case of reinforced I-joists, it was observed that both Zhu's and Pirzada's model significantly under-predicts capacity by up to 67% and 73%, respectively. One of the reasons is that both models ignore the effect of span to height ratio of I-joists, which is one key parameter. In addition, the previous models were derived from few test specimens and were not verified against other test results.

**Table 6.4: Comparison between analytical models for I-joists with openings**

Series ID	L/h	D/h <sub>w</sub>	F <sub>exp</sub>	<sup>1</sup> F <sub>zhu</sub>		<sup>2</sup> F <sub>pirzada</sub>		<sup>3</sup> F <sub>proposed</sub>	
			kN	kN	Δ %	kN	Δ %	kN	Δ %
12-B	12.1	0.94	18.3	12.0	34	6.7	63	17.7	3
12-C	12.1	0.94	17.1	12.0	30	6.7	61	17.7	4
12-D	12.1	0.66	27.5	18.9	31	19.5	29	26.4	4
12-E	12.1	0.44	36.5	24.7	32	29.7	19	33.3	9
20-B	20.2	0.94	20.7	12.0	42	6.7	68	20.4	1
20-C	20.2	0.94	20.1	12.0	40	6.7	67	20.4	2
20-D	20.2	0.66	27.9	18.9	32	19.5	30	24.8	11
20-E	20.2	0.44	26.3	24.7	6	29.7	13	28.4	8
She-16-66*	4.3	0.2	53.8	31.2	42	40.9	24	49.3	8
She-16-132*	4.3	0.4	42.8	26.0	39	31.7	26	40.1	6
She-16-198*	4.3	0.6	31.0	20.9	33	22.5	27	30.9	0
She-16-264*	4.3	0.8	22.0	15.7	29	13.3	39	21.7	2
She-16-330*	4.3	1	15.5	10.5	32	4.2	73	12.5	20
She-16-264-18*	8.8	0.8	20.5	15.7	23	13.3	35	22.0	7
She-12-56*	5.2	0.25	42.6	29.9	30	38.6	9	46.2	8
She-12-113*	5.2	0.5	30.2	23.5	22	27.1	10	35.1	16
She-12-170*	5.2	0.75	21.3	17.0	20	15.6	27	23.9	12
She-12-226*	5.2	1	14.4	10.5	27	4.2	71	12.8	11
She-12-170-12*	9.2	0.75	21.3	17.0	20	15.6	27	23.8	12
She-12-170-24*	13.2	0.75	21.3	17.0	20	15.6	27	23.7	11

Notes: \*tests as reported by Afzal et al. (2006), <sup>1</sup>Zhu et al. (2005), <sup>2</sup>Pirzada et al. (2008), <sup>3</sup>Proposed Model.

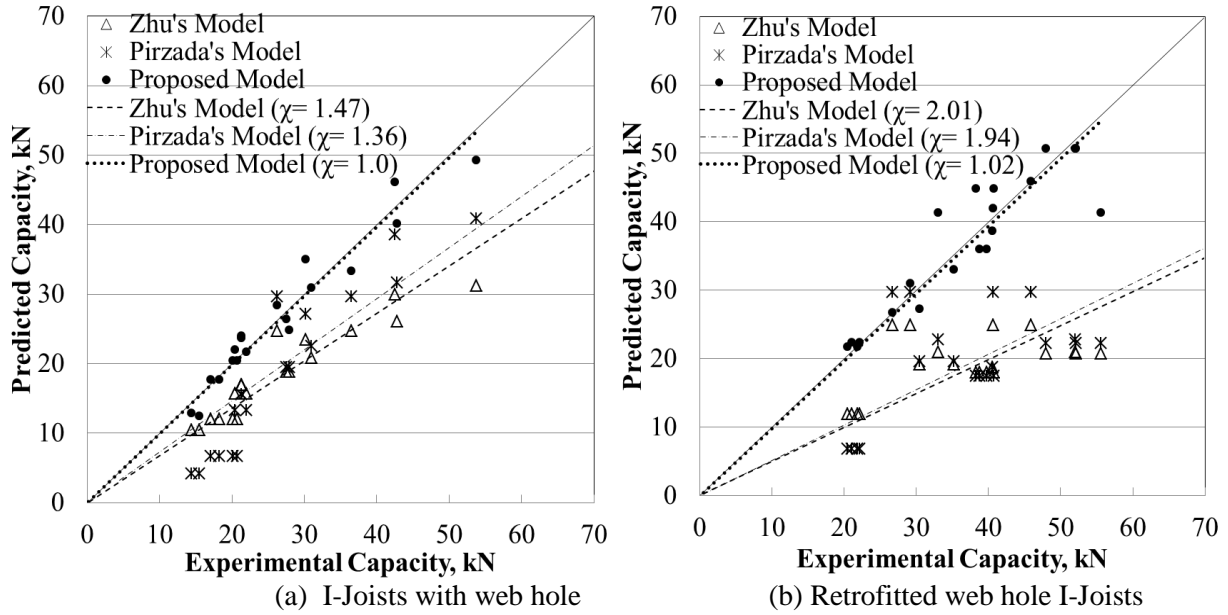


**Figure 6.8: Experimental vs predicted capacity of different models for (a) I-Joists with opening and (b) Retrofitted web hole I-Joists**

The accuracies of the proposed model and the previous models were compared using four descriptive statistical parameters: a) average performance factor (PF): the average ratio of experimental capacity to calculated capacity ( $F_{exp}/F_{cal}$ ), b)  $\chi$  factor: inverse of the slope of a linear least square regression of the calculated capacity ( $F_{cal}$ ) versus the experimental capacity ( $F_{exp}$ ), c) standard deviation (SD), and d) sample variance (VAR). The analysis results showed that the previous models proposed by *Zhu et al. (2006)* and *Pirzada et al. (2008)* are under-predicting the experimental capacity, with all statistical measures being rather high compared to the new model, see *Table 6.6*. The proposed models (*Eq. 6-3* and *Eq. 6-4*) show good accuracy with average PF and  $\chi$  value being close to 1.0. Moreover, SD values of the proposed equations (unreinforced and reinforced I-joists) were only one-tenth and one-sixteenth, respectively, compared to Pirzada's equation.

**Table 6.5: Comparison between analytical models for reinforced I-joists**

Series ID	L/h	D/h <sub>w</sub>	F <sub>exp</sub>		<sup>1</sup> F <sub>Zhu</sub>		<sup>2</sup> F <sub>Pirzada</sub>		<sup>3</sup> F <sub>proposed</sub>	
			kN	kN	Δ %		kN	Δ %	kN	Δ %
12-F	12.1	0.94	21.9	12.0	45		6.8	69	21.7	1
12-G	12.1	0.94	20.5	12.0	42		6.8	67	21.7	6
12-H	12.1	0.66	35.2	19.2	45		19.6	44	33.0	6
12-I	12.1	0.44	40.7	24.9	39		29.7	27	42.0	3
12-J	12.1	0.44	45.9	24.9	46		29.7	35	45.9	0
20-F	20.2	0.94	21.1	12.0	43		6.8	68	22.4	6
20-G	20.2	0.94	22.2	12.0	46		6.8	69	22.4	1
20-H	20.2	0.66	30.5	19.2	37		19.6	36	27.2	11
20-I	20.2	0.44	29.2	24.9	15		29.7	2	31.0	6
20-J	20.2	0.44	26.7	24.9	7		29.7	11	26.7	0
B*	13.7	0.71	38.8	18.0	54		17.5	55	36.0	7
C*	13.7	0.71	39.8	18.0	55		17.5	56	36.0	10
D*	12.0	0.59	33.1	21.0	36		22.8	31	41.3	25
E*	12.0	0.68	40.6	18.7	54		18.8	54	38.6	5
F*	12.0	0.60	55.6	20.8	63		22.3	60	41.3	26
H*	6.9	0.71	40.8	18.0	56		17.5	57	44.9	10
I*	6.9	0.71	38.3	18.0	53		17.5	54	44.9	17
J*	6.0	0.59	52.0	21.0	60		22.8	56	50.7	2
K*	6.0	0.60	52.1	20.8	60		22.3	57	50.7	3
L*	6.0	0.60	48	20.8	57		22.3	54	50.7	6

Notes: \*tests as reported by Polocoser et al. (2013), <sup>1</sup>Zhu et al. (2005), <sup>2</sup>Pirzada et al. (2008), <sup>3</sup>Proposed Model.

**Table 6.6: Performance of analytical models for I-joists with openings**

I-Joist	Models	Average PF	χ	SD	VAR
Opening	Zhu et al. (2006)	1.44	1.47	0.17	0.03
	Pirzada et al. (2008)	1.85	1.36	0.88	0.77
	Proposed	1.01	1.00	0.09	0.01
Reinforced	Zhu et al. (2006)	1.94	2.01	0.43	0.18
	Pirzada et al. (2008)	2.13	1.94	0.69	0.48
	Proposed	1.01	1.02	0.11	0.01

### 6.3 Summary

The experimental investigation on the performance of 12ft and 20ft composite wood I-joists with web openings (unreinforced and reinforced) allows the following conclusions to be drawn:

- The experimental capacity and stiffness of the regular I-Joists without openings were at least three times higher than the specified design values which satisfies the requirements according to *ASCE 7-10.1 (2010)* and *ASTM D5055 (2004)*.
- A stiffness reduction of up to 12% in 12ft series and up to 11% in 20ft series, respectively, was observed compared to the control series. The change in the position of the opening in shear span, however, did not affect the joist stiffness.
- An opening had more impact on smaller span beams. Most of the 12ft test specimens with openings showed premature shear failures at the location of the opening. The capacity of 12ft I-joists was reduced up to 54%, while for 20ft I-joists, the capacity was reduced only up to 21%.
- In the case of 20ft I-joists, presence of openings about half of the web height did not have any effect on longer span beams. The statistical analyses confirmed these findings.
- The reinforcement of I-Joists using OSB collars was effective to prevent shear failure close to a web opening and increased the stiffness of the I-joists up to 6% and 8% for 12ft and 20ft I-joists, respectively
- The reinforcement of I-Joists with OSB collars significantly increased the capacity (27% and 20% respectively for 12ft and 20ft I-joists). Furthermore, the capacities of the reinforced I-Joists (series I and J) were found almost equal to the control series capacity.
- The newly proposed model to predict I-joist capacity with openings was superior compared to existing models from the literature, while the new model to predict the capacity of an I-joist with reinforced openings was also sufficiently accurate in predicting capacities from previous tests.

## CHAPTER 7: PERFORMANCE OF RETROFITTED FLANGE NOTCHED AND WEB HOLED I-JOIST WITH GLASS FIBER REINFORCED POLYMER (GFRP) PLATES: EXPERIMENTAL INVESTIGATION

### 7.1 General

Engineered timber I-joists are commonly used as a building material for the construction of residential and commercial buildings in North America, Australia, and Europe. It is also very common to make notch at the top flange of the I-Joist or hole in its web in order to allow the passageway of electro-mechanical systems. As reported by several researchers, these structural discontinuities (i.e. notch and hole) make the installed I-joist structurally deficient (*Islam et al. 2015; Morrissey et al. 2009; Pirzada et al. 2008; Wang and Cheng 1995; Zhu et al. 2007; Afzal et al. 2006 & Chen et al. 2015*). Researchers have also investigated the performance of such I-joists after retrofitting with different techniques, such as Oriented Strand Board (OSB) collar (*Islam et al. 2016; Polocoser et al. 2013; Shahnewaz et al. 2016*) and cold form steel reinforcers (*Hindman and Loferski 2008*). These retrofitting techniques can improve the structural capacity of flange notched- and web holed- I-joists up to a certain level. However, this strength improvement is not sufficient to that of the control I-joist having no notch or hole. Hence, different retrofitting techniques have been introduced to strengthen those flange notched and web holed I-joists. The new retrofitting technique is employed by using Glass Fiber Reinforced Polymer (GFRP) plates, which is known as GFRP reinforcer. These GFRP reinforcers help structural engineers and builders avoid the replacement of critically notched or holed I joists. These reinforcers reduce significant amount of cost and time to finish the construction projects. GFRPs possess superior mechanical properties compared to the OSB or timber. The mechanical properties of GFRP, timber and OSB are presented in *Table 7.1*.

***Table 7.1 Mechanical properties of Timber, OSB and GFRP.***

<b>Material</b>	<b><math>\sigma_x</math> (SD) (Mpa)</b>	<b><math>E_x</math> (SD) (Mpa)</b>	<b><math>G_{xy}</math> (SD) (Mpa)</b>
Timber	57.0 (10.2)	16063 (941)	416 (1)
OSB	16.84 (0.8)	5333 (233)	1574 (226)
GFRP	217.4 (6.2)	16855 (345)	1390 (454)

In this chapter, light weight GFRP-based reinforcers have been used for retrofitting I-joists having web holes (openings) or flange notch (cut). These new joist reinforcers are novel in terms of application and cross sectional profiles. The flange notch reinforcers have a top wing which will be attached to the bottom of the floor/sheathing in order to improve the bending stiffness of the notched I-joists. The web hole reinforcers are unique based on the cross sectional profiles. All cross sectional profiles are designed to optimize the cost and performance. Type T-2 reinforcers are introduced to facilitate the application of reinforcer after installing the service pipes, conduits, and ducts. Unlike the steel-based bracket/reinforcers, these GFRP based reinforcing plates are more durable as the GFRP is not susceptible to rust.

The Joist reinforcing systems are designed for strengthening/retrofitting I-Joists having a flange notch and/or web hole. Both Flange Notch Reinforcer (FNR) and Web Hole Reinforcer (WHR), have mainly two types: Type T-1 and Type T-2, which are designed based on their installation technique. Type T-1 has a notch or hole in the center of the reinforcer, whereas Type T-2 has a notch or hole cut on the sides and consists of 2 parts. Two different types of reinforcers were used to facilitate the different installation processes depending on the presence of the utility ducts and conduits. Type T-1 is generally preferred over Type T-2 as it provides better integrity, and is more cost effective, requiring only one part. However, for example, if a conduit is pre-installed through an I-joist and requires retrofitting, the optimal choice would be a Type T-2



reinforcer that will fit the conduits from both sides. Similar to Type T-1, another type of reinforcer, Type T-3 is also introduced that has additional two cross strips. The advantage of Type T-3 reinforcer (on site hand layup) is that it can fit into any cross-sectional profile without the requirement of a mold. Furthermore, the reinforcers can consist of 3 profiles depending on the size and location of the hole or notch on the I-joist to be retrofitted.

The objectives of this chapter are summarized as follows:

- Evaluating the performance of I-joists with a flange notch and web hole retrofitted with different types of GFRP based reinforcers.
- Comparing the performance of flange notched and web holed I-joists retrofitted with GFRP based reinforcers with that of OSB collar retrofitted I-joists.
- Developing mathematical models to predict the structural capacity of the retrofitted flange notched and web holed I-joists with GFRP reinforcers.

## **7.2 Methodology**

### **7.2.1 Fabrication of GFRP Reinforcers**

Several GFRP reinforcers were fabricated in the laboratory by hand layup process. GFRP-based reinforcer fabrication was done in three steps, which are pre-fabrication, fabrication, and post-fabrication. Three steps are described in the following sections:

**Pre-Fabrication:** The fabrication process started with the making of inverse molds for Notch and Hole reinforcers (made of steel plates). The woven glass fiber was first cut into rectangular pieces with a specific dimension (500m x 585mm). The cut fibers were then placed on the molds made out of steel having different profiles for different types of reinforcers (e.g. web holed

reinforcer, flange notched reinforcer). Mold was first sanded using sandpaper in order to remove the attached hardened resin from the mold surface. Then, a thin coat of Mold Release was used to de-mold the fabricated FRP reinforcer.

**Fabrication:** For a Bi-axial woven Glass fiber mat (E-Glass TG-54-N manufactured by Texonic JB Martin) weighing 500g, a 1.0 Resin-fiber volume fraction ( $V_f$ ) was used for the fabrication of GFRP reinforcers. The resin mixture consists of 0.14% cobalt solution (Conc. 12%) by volume of resin, and 1.5% initiator CADOX L50 by mass of resin. Amount of raw materials used for different types of reinforcers are presented in *Table 7.2*. The mixture was applied as a layer, and then downward strokes were quickly applied to the whole sample to make sure that the mixture sufficiently penetrates into the fibers. The sample was cured for 24 hours in a chamber (to avoid spreading of odor of resin mixture) at room temperature (20-25° C) and then, the reinforcers were post-cured in an oven at 45°C for 2 hours.

**Table 7.2 Proportion of Resin Mixture for GFRP Reinforcer.**

Materials	Ratio	Amount
<b>Flange Notch GFRP Reinforcer (Type T-1): Area=1836 cm<sup>2</sup></b>		
Glass Fiber (1824 gm/m <sup>2</sup> , Compressed Thickness= 1.52 mm)		550 gm
Polyester Resin	100% by mass of Resin	550 gm
12% Cobalt Solution	0.14% by volume of Resin	480 µml
Catalyst/Initiator (Cadox L50)	1.5% by mass of Resin	3.4 gm
<b>Flange Notch GFRP Reinforcer (Type T-2): Area=1632x2 cm<sup>2</sup></b>		
Glass Fiber (1824 gm/m <sup>2</sup> , Compressed Thickness= 1.52 mm)		550 gm
Polyester Resin	100% by mass of Resin	550 gm
12% Cobalt Solution	0.14% by volume of Resin	480 µml
Catalyst/Initiator (Cadox L50)	1.5% by mass of Resin	3.4 gm
<b>Web Hole GFRP Reinforcer (Type T-1): Area= 1566 cm<sup>2</sup></b>		
Glass Fiber (1824 gm/m <sup>2</sup> , Compressed Thickness= 1.52 mm)		550 gm
Polyester Resin	100% by mass of Resin	550 gm
12% Cobalt Solution	0.14% by volume of Resin	480 µml
Catalyst/Initiator (Cadox L50)	1.5% by mass of Resin	3.4 gm
<b>Web Hole GFRP Reinforcer (Type T-2): Area= 1632x2 cm<sup>2</sup></b>		
Glass Fiber (1824 gm/m <sup>2</sup> , Compressed Thickness= 1.52 mm)		550 gm
Polyester Resin	100% by mass of Resin	550 gm
12% Cobalt Solution	0.14% by volume of Resin	480 µml
Catalyst/Initiator (Cadox L50)	1.5% by mass of Resin	3.4 gm

**Post Fabrication:** After post curing all GFRP reinforcers were cut as per the dimensions presented in *Table 7.3* by using the water jet machine. Then, the back surface of the reinforcers

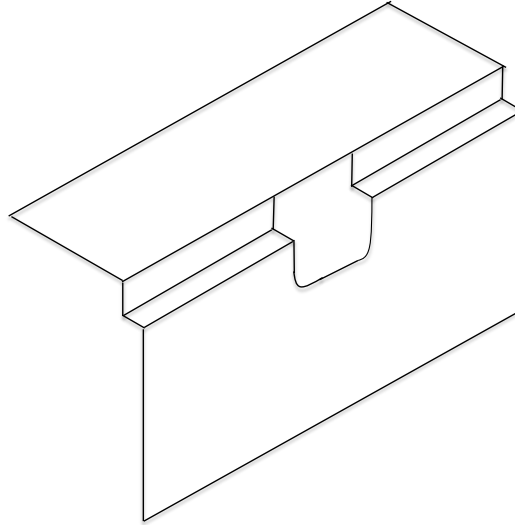
was sanded to make it rough and remove the residue of the resin attached to the back surface to ensure a proper bonding between the GFRP plate and OSB/Timber.

**Table 7.3 GFRP Reinforcer Dimensions.**

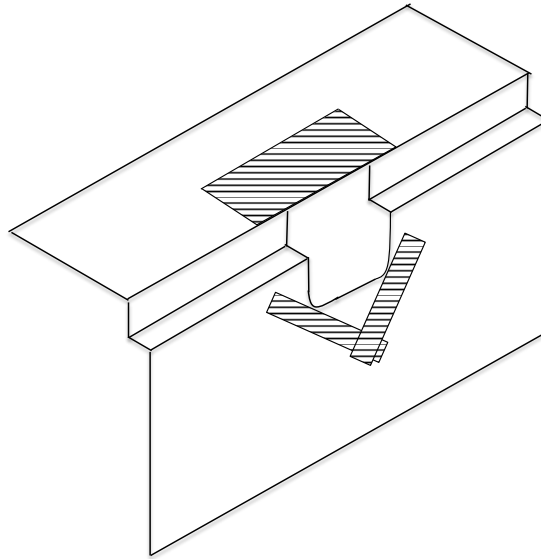
GFRP Reinforcer	Reinforcer Length (L <sub>r</sub> ) (mm)	Notch Size (B <sub>n</sub> xD <sub>n</sub> ) (mm x mm)	Hole Size (Φ <sub>n</sub> ) (mm)	Top Wing Width (W <sub>t</sub> ) (mm)	Total Depth (D <sub>t</sub> ) (mm)
Flange Notch Reinforcer					
Type T-1	450	100x100 and 100x150	-	150	38+220
Type T-2	400	100x100 and 100x150	-	150	38+220
Type T-3	450	100x100	-	150	38+220
Option 2 for all Types (T-1 to T-3) (as shown in <b>Figure 7.1-b</b> )	<ul style="list-style-type: none"> <li>• Two numbers of 50 mm x 150 mm cross GFRP Strips</li> <li>• One 150 mm x 200 mm GFRP strip at Top Wing</li> </ul>				
Web Hole Reinforcer					
Type T-1	450	-	150 and 200	-	38+220+38
Type T-2	400 or 450*	-	150 and 200	-	38+220+38
Type T-3	450	-	200	-	38+220+38
Option 2 for all Types (T-1 to T-3) (as shown in <b>Figure 7.3-b</b> )	<ul style="list-style-type: none"> <li>• Four numbers of 50 mm x 200 mm cross GFRP Strips</li> <li>• Two numbers of 50 mm x 225 mm vertical GFRP strips for full depth hole (when Φ<sub>n</sub>= h<sub>w</sub>).</li> </ul>				
<b>Note:</b> B <sub>n</sub> - Notch Width; D <sub>n</sub> - Notch Depth; Φ <sub>n</sub> - Diameter of Web Hole; h <sub>w</sub> - Height of Web * L <sub>r</sub> = 450 mm for Φ <sub>n</sub> = 200 mm					

## 7.2.2 Types of GFRP Based Flange-Notch Reinforcer (FNR)

### 7.2.2.1 FNR Type T-1:



a) Option-1



b) Option-2 (with cross GFRP strips)

**Figure 7.1: Type T-1- Flange Notch Reinforcer Reinforcers a) Option-1 and b) Option-2.**

**Figure 7.1** shows the Type T-1 Flange Notch Reinforcer, with a notch cut in the center of the reinforcer, allowing supported passageway for any utility. The reinforcer is 400 mm long ( $L_r$ ). The width of the notch ( $B_n$ ) can be varied from 100 mm to 200 mm depending on the type of the I-

joists. The depth of the notch ( $D_n$ ) can be varied from 100 mm to 150 mm depending on the type and depth of the I-joist. This reinforcer could be in 3 different profiles depending on the size and location of the notch. Profiles are shown in **Figure 7.5**. There are two options for flange notch reinforcers (Option 1 and Option 2) as shown in **Figure 7.1**. Depending on the size and location of the notch, either option can be used to strengthen notched I-joists. The option will be determined based on the design specifications and requirements evaluated by the structural engineers.

#### 7.2.2.2 FNR Type T-2:

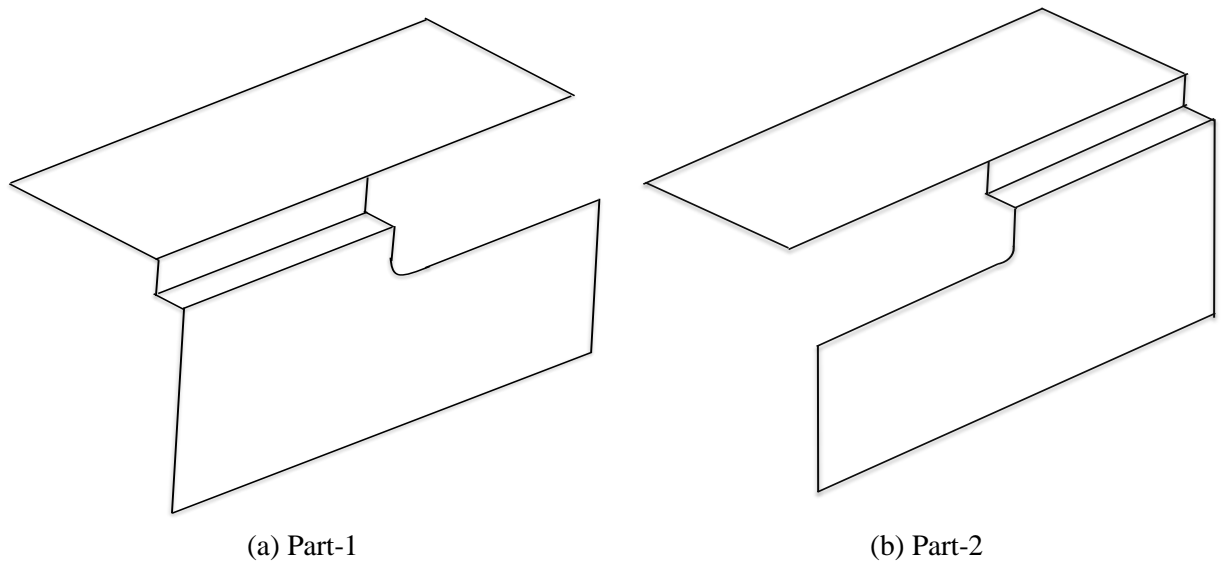


**Figure 7.2: Type T-2- Flange Notch Reinforcer a) Part-1 and b) part- 2.**

Type T-2 Flange Notch Reinforcer consists of two parts as presented in **Figure 7.2**. Each part has a notch cut on opposite ends of the sheet. This is because parts are designed to fit into or connect to each other. Similar to the Type T-1 Flange Notch Reinforcer, the depth of the notch ( $D_n$ ) can be varied from 100 mm to 150mm. The width ( $B_n$ ) of the top part is 150 mm and the length ( $L_n$ ) of the sheet is 400 mm, with the notch commencing halfway, at the center (at 200mm). After attaching both parts, final length of the reinforcer would be 500 mm ( $L_r + B_n + L_r = 200 + 100 + 200$ ).

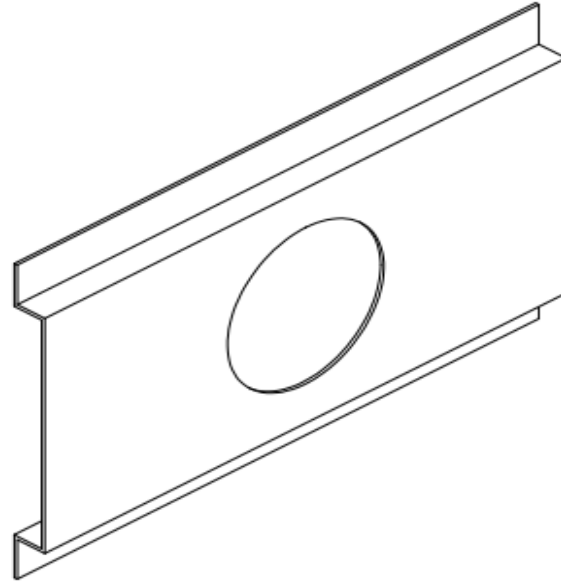
### **7.2.2.3 FNR Type T-3:**

Type T-3 flange notch reinforcer is similar to Type T-1 flange notch reinforcer. Type T-3 has only two cross strips (Option-2) as shown in *Figure 7.1 (b)* and it was directly laid-up on the beam.

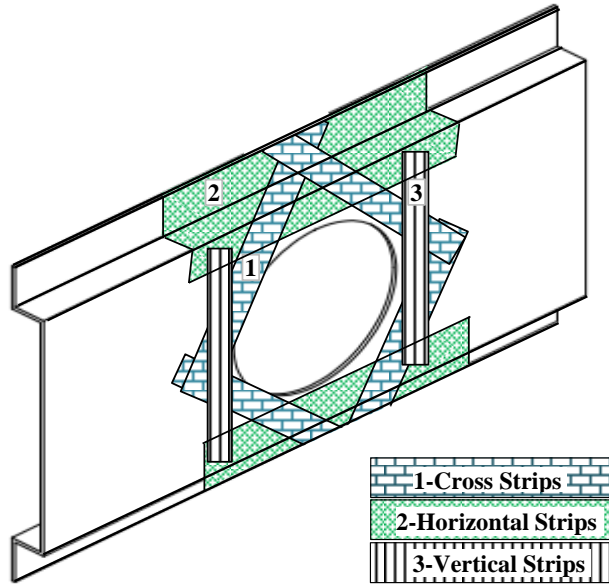
**Direct Hand Layup Procedure:** Direct hand-layup procedure starts with thorough cleaning of web and flange of I-joists (area adjacent to the notch location, where GFRP will be attached) with sand papers (grades #80 and #120). Sanding of the surfaces also helps create micro scratches, which can ensure a better bonding between the GFRP Layup and OSB/Timber. Then, all dusts are removed with clean clothes and air blower, and a coat of resin mixture is thoroughly applied on the OSB and Timber surfaces.

## 7.2.3 Web Hole Reinforcer

### 7.2.3.1 Type T-1:



a) Option-1



b) Option-2 (with cross GFRP strips)

**Figure 7.3: Type T-1- Web Hole Reinforcers a) Option-1 and b) Option-2.**

Type T-1 Web Hole Reinforcer, shown in **Figure 7.3 (a)**, has a hole cut in the center of the sheet. Each side of sheet contains 2 bends. The size of the web-holes can be varied from 100 mm to 200 mm. The depth of the reinforcer shall be the same as that of the I-joist, whereas the length



( $L_n$ ) is about 400 and 500 mm for the hole diameters of 150 and 200 mm, respectively. Profile and cross sectional dimensions of the reinforcers are provided in accordance with the cross sectional dimensions of the I-Joist to which it will be attached. There are two options for web hole reinforcers (Option 1 and Option 2) as shown in **Figure 7.3**. Depending on the size and location of the hole, either option can be used to strengthen the holed I-joists. The option will be determined based on the design specifications and requirements evaluated by the structural engineers.

#### 7.2.3.2 Type T-2:

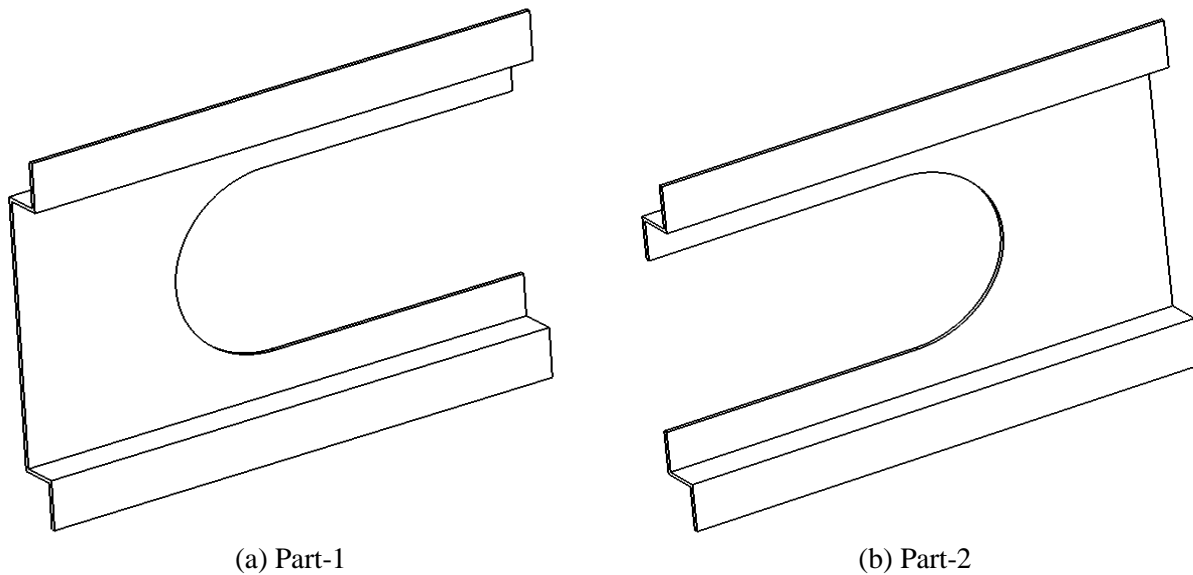


**Figure 7.4: Type T-2 Web Hole Reinforcer a) Part-1 and b) Part-2**

Type T-2 Web Hole Reinforcer has two parts with a slot cut on opposite sides of each part with a dimension of the web hole to be retrofitted as shown in **Figure 7.4**. Similar to the Type T-2 Flange notch reinforcer, each part is designed to fit into or connect to each other. Here, two web hole diameters (150 mm, and 200 mm) are considered. The length ( $L_n$ ) is 400 or 450 mm depending on the hole diameter ( $\Phi_n$ ) to maintain the same bond length (or area) on both sides of the web hole. For example, for a diameter of 150 mm, the length ( $L_n$ ) of the GFRP plate is 400 mm, whereas for

a diameter of 200 mm, it is 450 mm. The two end bends are 38 mm wide, which is used to match the depth ( $h_f$ ) of the I-Joist flange to be reinforced as shown in **Figure 7.9 (b)**.

### 7.2.3.3 Type T-3:

Type T-3 web hole reinforcer is similar to Type T-1 flange notch reinforcer. Type T-3 has only two cross strips (Option-2) as shown in **Figure 7.3 (b)** and was laid up on the beam directly by following the same procedure discussed in earlier section. However, the elevated heat curing and post fabrication steps were not followed for this type of reinforcer.

### 7.2.4 Variations in Cross Sectional Profile:

Variations in cross sectional profile are designed to provide better stiffness and bonding between the reinforcer and I-joist.

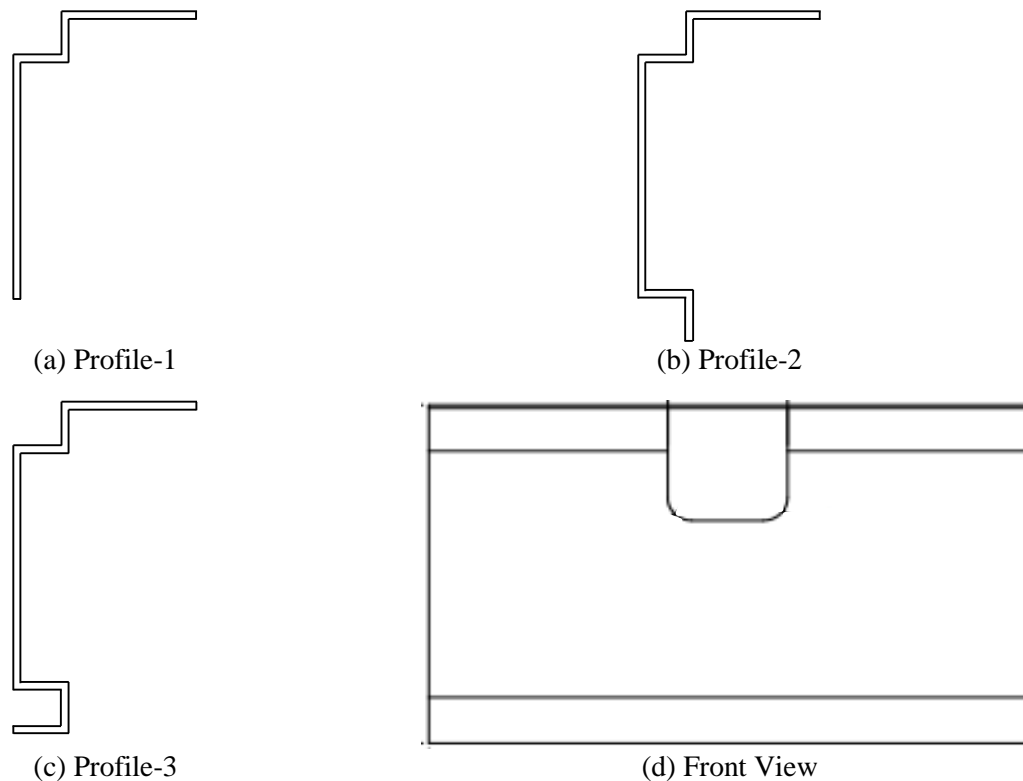


**Figure 7.5: Different Cross Sectional Profiles for Flange Notch Reinforcer**

The Flange Notch Reinforcer can have 3 profiles represented in **Figure 7.5 (a–c)**. The size and location of the notch or hole are determining factors in selecting a particular profile. All profiles consist of a top wing with a length of 150 to 200 mm, which will be attached to the bottom of the floor sheathing, and a bottom part, which must match with the cross sectional dimension of the I-joist to be retrofitted or strengthened. Profile 1 is the primary profile, which can be altered to profile 2 if the size or location of the notch changes. Profile 2 can then be altered to Profile 3 in order to provide additional stiffness and bonding between FRP reinforcer and I-Joist. It can be seen from **Figure 7.5** that the difference between Profile 1 and 2 is the addition of a bend at the bottom end of the reinforcer, and likely, the difference between profile 2 and profile 3 is the addition of a bend to fit to the flange profile. **Figure 7.5 (d)** represents the typical front view for Flange Notch Reinforcers.

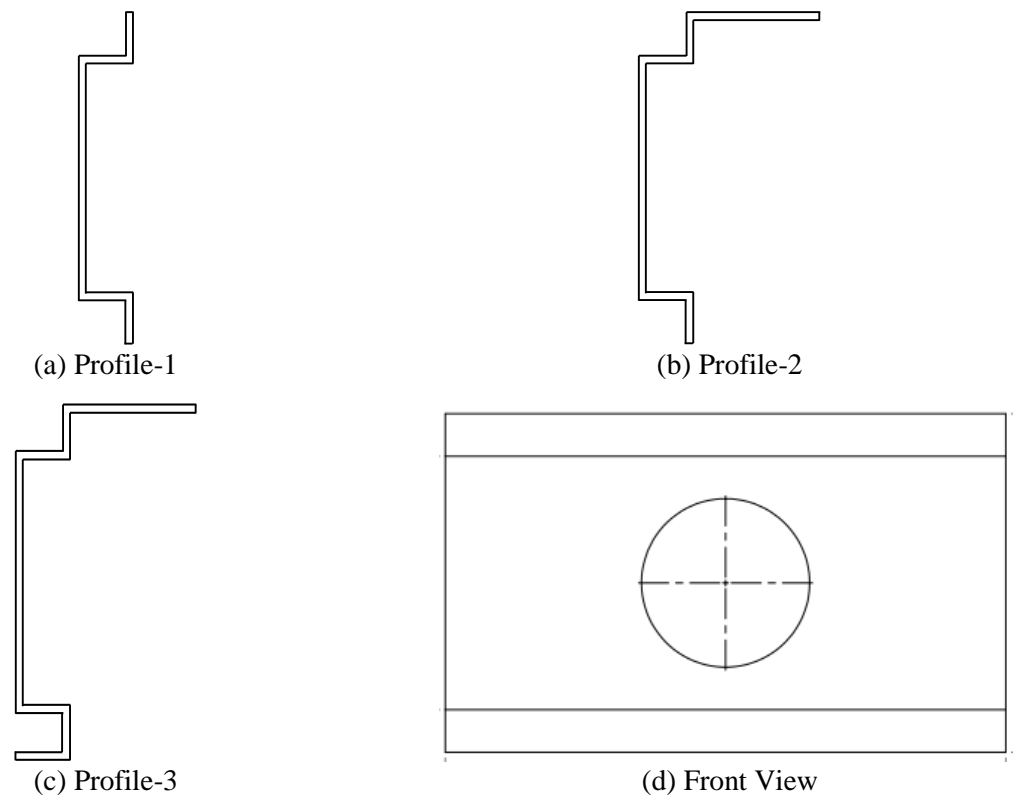


**Figure 7.6: Different Cross Sectional Profiles for Web Hole Reinforcer**

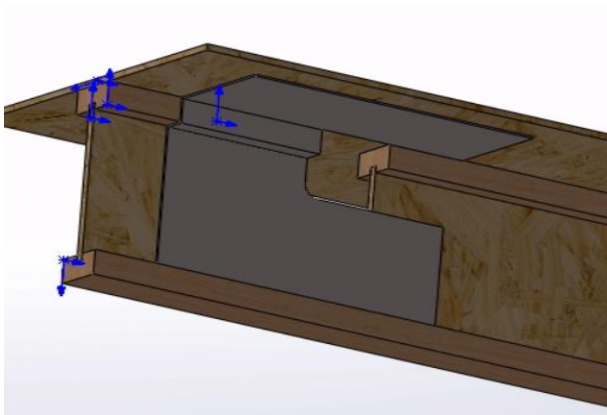
The Web Hole Reinforcer can be either of the three cross sectional profiles presented in **Figure 7.6 (a–c)**. Similar to the Flange Notch Reinforcers, the size and location of the notch or hole are determining factors in selecting a particular profile. Profile 1 is the primary profile, but depending on a change in the size or location of the web holes, it can be altered to Profile 2 or Profile 3 by adding a top wing having a length of 150 to 200 mm or a bend at the bottom end of the reinforcer. The length of the wings remain the same for each profile at 150 mm and 225.5mm, along with the width of the bend at 38 mm. **Figure 7.6 (d)** represents the typical front view for Web Hole Reinforcers..

#### **7.2.5 Installation Procedure:**

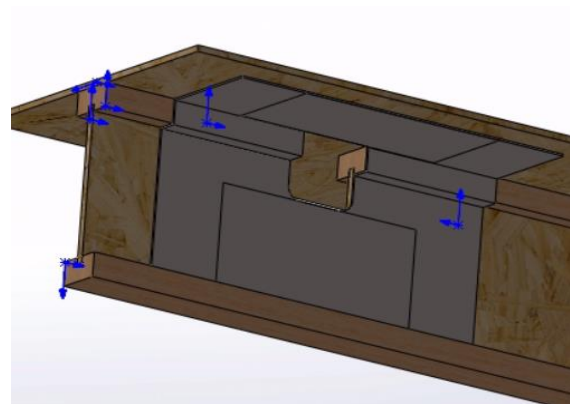
The reinforcers described in this study are all glued to the timber I-Joist in a similar manner. In this section of experimental study Sikadur-30 adhesive was used to attach the GFRP reinforcer to the notched or holed I-joists. Sikadur-30 is a two components based high strength epoxy adhesive (*Sika Canada Inc. 2015*). In addition to the Sikadur-30 adhesive, a set of screws was used for additional support and to maintain the bonding pressure over the GFRP reinforcer. The reinforcers may be glued and screwed either on one side or both side based on the design specifications and requirements evaluated by a structural engineer. In this section of the experimental study, only one sided reinforcers were used to evaluate the performance of GFRP reinforced I-joist having a notch/hole. Top wing of the flange notch reinforcer will be glued to the OSB board of sheathing. Different thicknesses of reinforcer will be between 2 mm to 6 mm, depending on the strength and required capacity improvement. However, Type T-2 reinforcers (flange notch and web hole) will be installed in two steps as shown in **Figure 7.7**. Part 1 as shown in **Figure 7.7 (b)** was installed and then, part 2 was glued on top of the part 1, as shown in **Figure 7.7 (c)**.



a. I joist with a Flange Notch



b. Step-1: Install the Part-1 of Type T-2 Flange Notch Reinforcer



c. Step-2: Install the Part-2 of Type T-2 Flange Notch Reinforcer

***Figure 7.7: Installation Steps of Flange Notch Reinforcer (Type 2).***

**On Site Application:** The flange notched and web holed reinforcers (Type T-1) can be also installed by using hand lay-up method at the construction or project sites by following specific guidelines, which is identified as Type T-3. Hand layup should be done with the specific resin suggested by the manufacturer/engineers.

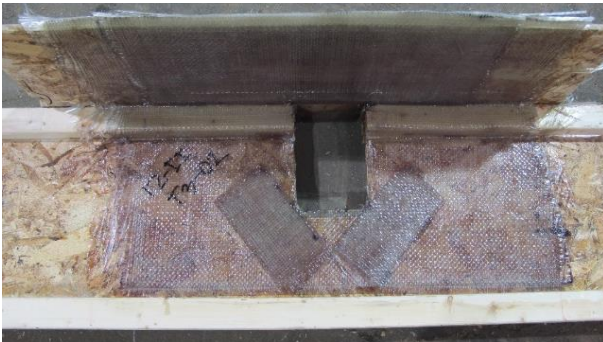
### Flange Notch Reinforcer



a) Type T-1



c) Type T-2

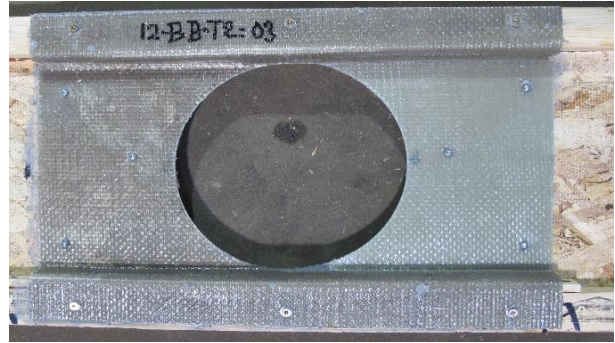


e) Type T-3

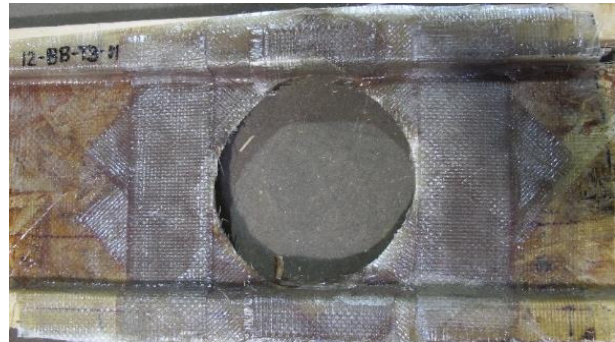
### Web Hole Reinforcer



b) Type T-1



d) Type T-2



f) Type T-3

**Figure 7.8: Different types of GFRP based Reinforcers a) Flange Notch Type T-1; b) Web Hole Type T-1; c) Flange Notch Type T-2; d) Web Hole Type T-2; e) Flange Notch Type T-3; and f) Web Hole Type T-3**

## 7.2.6 Experimental Procedure and Specimen Details

To evaluate the performance of flange notched I-joists retrofitted with GFRP based reinforcers as mentioned in earlier sections, a four point bending test was performed in accordance with the ASTM standard (*ASTM-D5055 2013*). Three HD cameras were used to measure the continuous deflection, monitor the crack growth and failure types at three different locations, as shown in *Figure 7.9*. In addition, an extensometer was used to measure the mid-point deflection of the I-joists and validate the deflection points measured through image processing technique. However, the extensometer was removed after a certain time (either reaching at 1500 N or the maximum allowable limit of the extensometer, which is 50 mm) to avoid it from any damage. MATLAB image processing toolbox (*The MathWorks Inc. 2012*) was used to calculate the deflection of the I-joists. To prevent the lateral buckling of the I-joists, a series of lateral support was used with an average spacing of 450 mm.

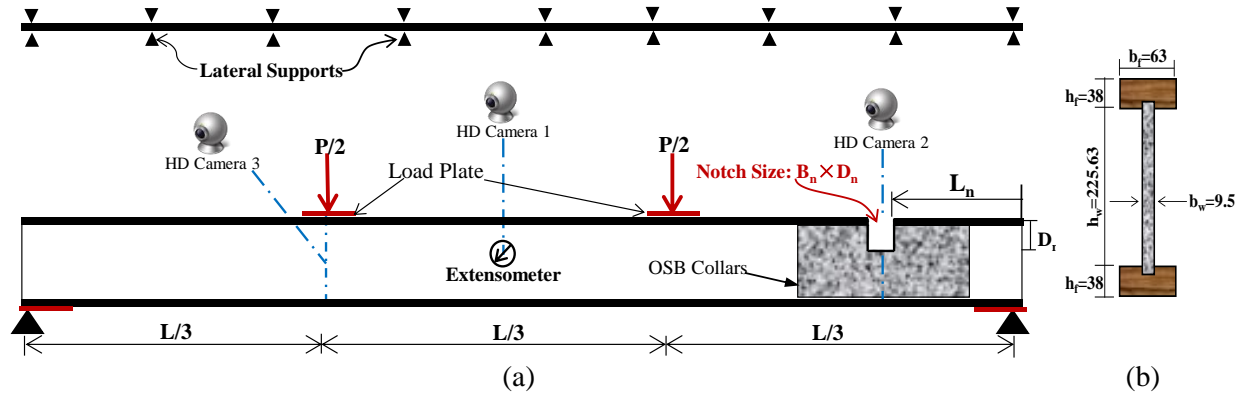


**Figure 7.9: Experimental setup of GFRP retrofitted I-Joists with flange notch and cross sectional dimensions of the tested I-joists (dimensions are in mm).**

In this section of the experimental study a total of 36 series of I-joists were tested as presented in *Table 7.4* and *Table 7.5*. In these 36 series of tested I-joists, two types of flange notch (100 mm x 100 mm at 610 mm and 100 mm x 150mm at 455 mm) and two types of web hole ( $\Phi_n = 200$  mm at 610 mm and  $\Phi_n = 150$  mm at 455 mm) were investigated along with two control series for two

span lengths (12 ft and 20 ft). 12-A and 20-A series were the control I-joists series and each series contains 10 I-joists having no flange notch or web hole. Flange notched (series 12-H, 12-I, 20-M and 20-N) and web holed I-joists (series 12-B, 12-D, 20-B and 20-D) also contain 10 specimens in each series. Retrofitted I-joists with GFRP reinforcers contain 3 specimens in each series whereas the I-joists retrofitted with OSB collar series contain 10 specimens in each series. For GFRP retrofitted I-joists, only three specimens were tested due to the long and complex fabrication process as stated in the earlier section (*Section 7.2.1*). All the tested specimens were prepared from the materials, which were sampled directly from the I-joist manufacturing product line of AcuTruss Industries Limited in Kelowna, BC, Canada.



**Table 7.4 Specimen details of Flange Notched I-Joists reinforced with FRP Reinforcer.**

Series	Span L <sub>o</sub> (mm)	Notch size (B <sub>n</sub> x D <sub>n</sub> ) (mm)	Location (L <sub>n</sub> ) (mm)	Reinforcement Type	No. of Specimen
12-A (Control)	3650	-	-	-	10
12-H				-	10
R-12-Q	3650	100x100	610	OSB-T1	10
R-12-HH-T1				FRP-T1	3
R-12-HH-T2				FRP-T2	3
12-I				-	10
R-12-SF				OSB-T2	10
R-12-II-T1	3650	100x150	455	FRP-T1	3
R-12-II-T2				FRP-T2	3
R-12-II-T3				FRP-T3	3
20-A (Control)	6100	-	-	-	10
20-M				-	10
R-20-QF	6100	100x100	610	OSB-T2	10
R-20-MM-T1				FRP-T1	3
R-20-MM-T2				FRP-T2	3
20-N				-	10
R-20-SF	6100	100x150	455	OSB-T2	10
R-20-NN-T1				FRP-T1	3
R-20-NN-T2 *				FRP-T2	3
Total					127
* To attach the reinforcers Polyester Resin Mix was used instead of the Sikadur-30					

**Table 7.5 Specimen details of Web holed I-Joists reinforced with FRP Reinforcer.**

Series	Span L <sub>o</sub> (mm)	Hole size (Φ <sub>n</sub> ) (mm)	Location (L <sub>n</sub> ) (mm)	Reinforcement Type	No. of Specimen
12-A (Control)	3650	-	-	-	10
12-B				-	10
12-F (J)				OSB	10
R-12-BB-T1	3650	200	305	FRP-T1	3
R-12-BB-T2				FRP-T2	3
R-12-BB-T3				FRP-T3	3
12-D				-	10
12-H (L)	3650	150	305	OSB	10
R-12-DD-T1				FRP-T1	3
R-12-DD-T2				FRP-T2	3
20-A (Control)	6100	-	-	-	10
20-B				-	10
20-F	6100	200	305	OSB	10
R-20-BB-T1				FRP-T1	3
R-20-BB-T2 *				FRP-T2	3
20-D				-	10
20-H	6100	150	305	OSB	10
R-20-DD-T1				FRP-T1	3
R-20-DD-T2 *				FRP-T2	3
<b>Total</b>					<b>127</b>
* To attach the reinforcers Polyester Resin Mix was used instead of the Sikadur-30					

## 7.3 Results

### 7.3.1 Flange Notched I-Joists and its Retrofitting

#### 7.3.1.1 Short Span (12 feet) I-Joist

##### **Structural Capacity ( $P_u$ ):**

The average structural capacity ( $P_u$ ) obtained from the four point bending test of short span (12 ft) control, flange notched I-joists and the retrofitted ones with different GFRP reinforcers and OSB collars are presented and compared in **Figure 7.10**. It can be observed that the presence of flange-notch can significantly reduce (70 to 82%) the structural capacity of I-joist. While using GFRP reinforcers, it could improve (374 to 441% for Type T-1; 434 to 519% for Type T-2; and 605% for Type T-3) the structural capacity significantly in comparison to that of the flange-notched I-joists (Series 12-H and 12-I). In comparison to the flange-notched I joist (series 12-I), the capacity of the retrofitted I-joist increased up to 605% for Type T-3 reinforcer, which was retrofitted directly on the beam surface using the hand lay-up technique (Series R-12-II-T3). Moreover it is also found that the structural capacity ( $P_u$ ) of I-Joists retrofitted with GFRP reinforcers improves (51 to 150% for Type T-1; 70 to 182% for Type T-2; and 96% for Type T-3) significantly, in comparison to that of the retrofitted flange-notched with OSB collar (Series R-12-Q and R-12-SF).

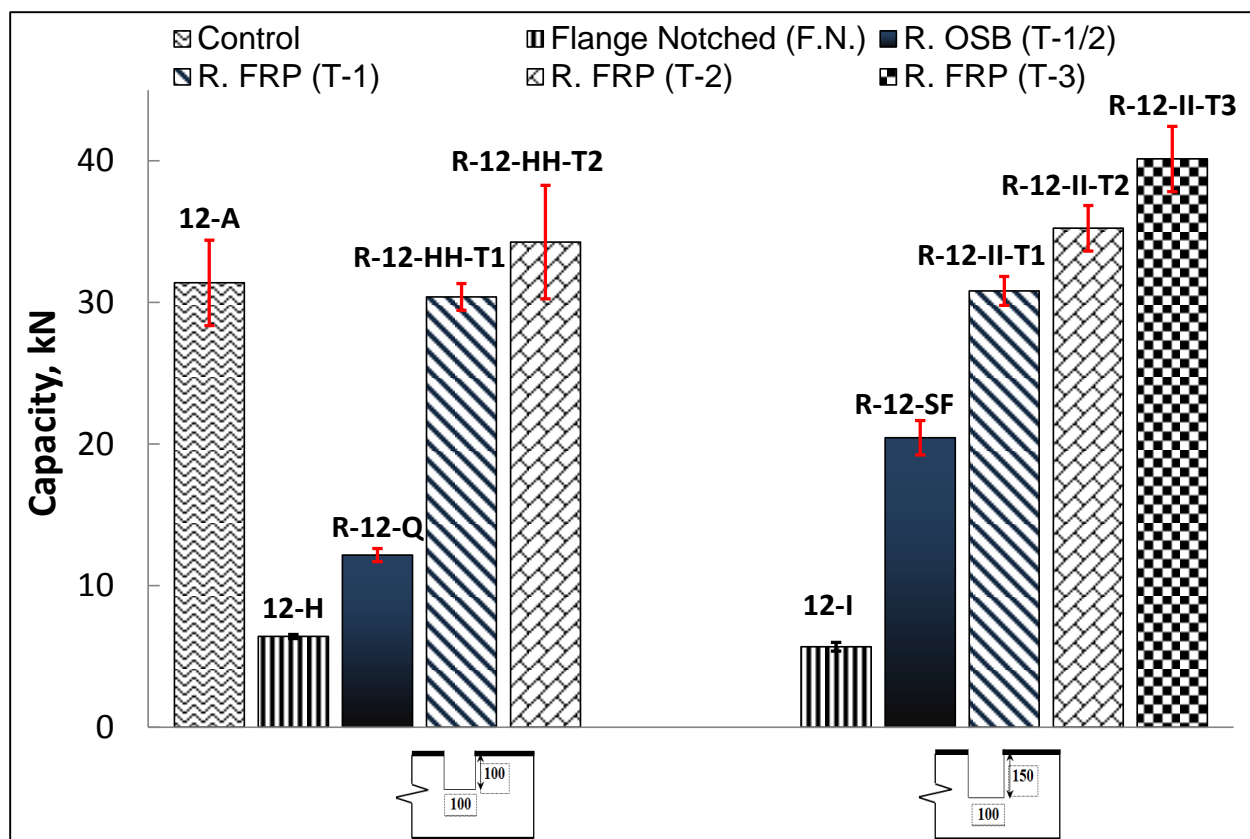


**Figure 7.10: Comparison of Structural Capacity ( $P_u$ ) of 12 ft flange notched I-Joists**

#### Stiffness:

The best fitted Load-Deflection ( $P-\Delta$ ) responses of 12 ft flange notched I-joist series have been presented in **Figure 7.11**. Load-Deflection ( $P-\Delta$ ) responses of each individual I-Joists have been presented in **Appendix D**. It is found that coefficient of determination ( $R^2$ ) values of best fitted curves are very close to one. Based on the Load-Deflection ( $P-\Delta$ ) responses, the average stiffness of each series of I-joist was calculated and presented in **Figure 7.12**. As can be seen in **Figure 7.12**, the stiffness ( $K$ ) of short span flange-notched I-joists retrofitted with GFRP reinforcers improved up to 62% - 89%, whereas the improvement for the I-joists retrofitted with OSB collar was 18%-45% with respect to the stiffness of the flange-notched I-Joist. Interestingly, it was found that the increase in stiffness of the I-joists having a flange notch of 100 mm x 100 mm located at

455 mm from the support and retrofitted with Type T3 (Series R-12-II-T3) was not significant compared to the increase in strength. Although its strength far exceeded (by 28%) the capacity of control I-joist, its stiffness was 11% lower compared to that of the control one. This is due to the strength and stiffness of the adhesive (polyester resin mixture) used for this series (R-12-II-T3) are lower compared to those of the Sikadur 30 used in other series to attach GFRP reinforcers.

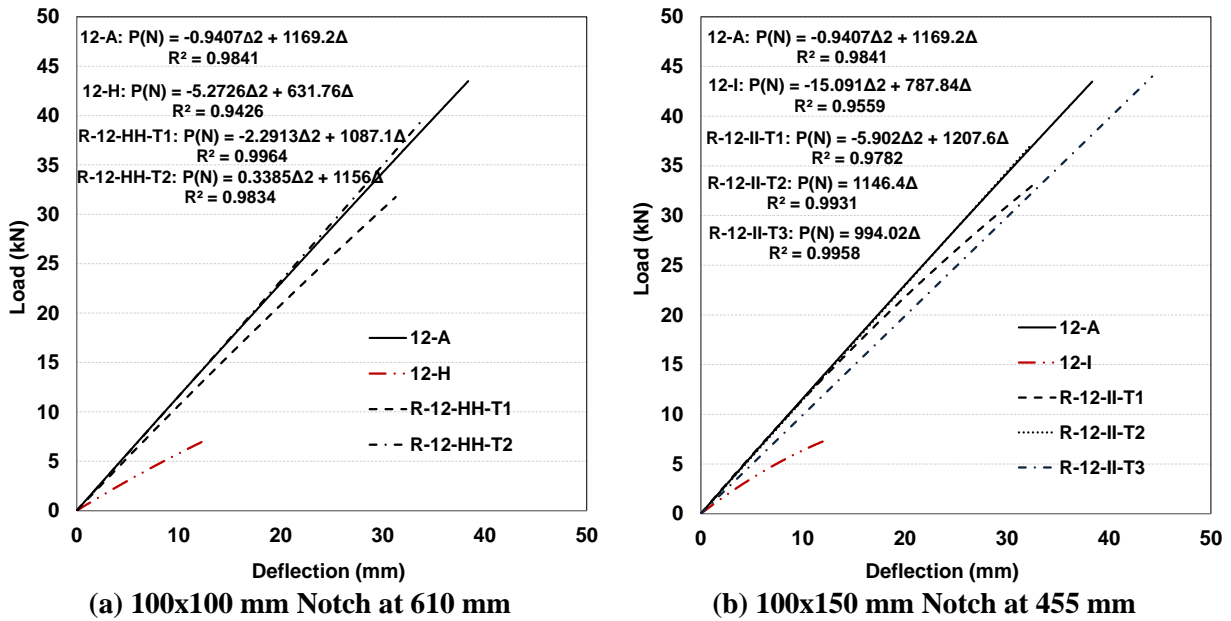


**Figure 7.11: Average Load-Deflection response of 12 ft flange notched I-Joists a) 100x100 mm Notch at 610 mm and b) 100x150 mm Notch at 455 mm**

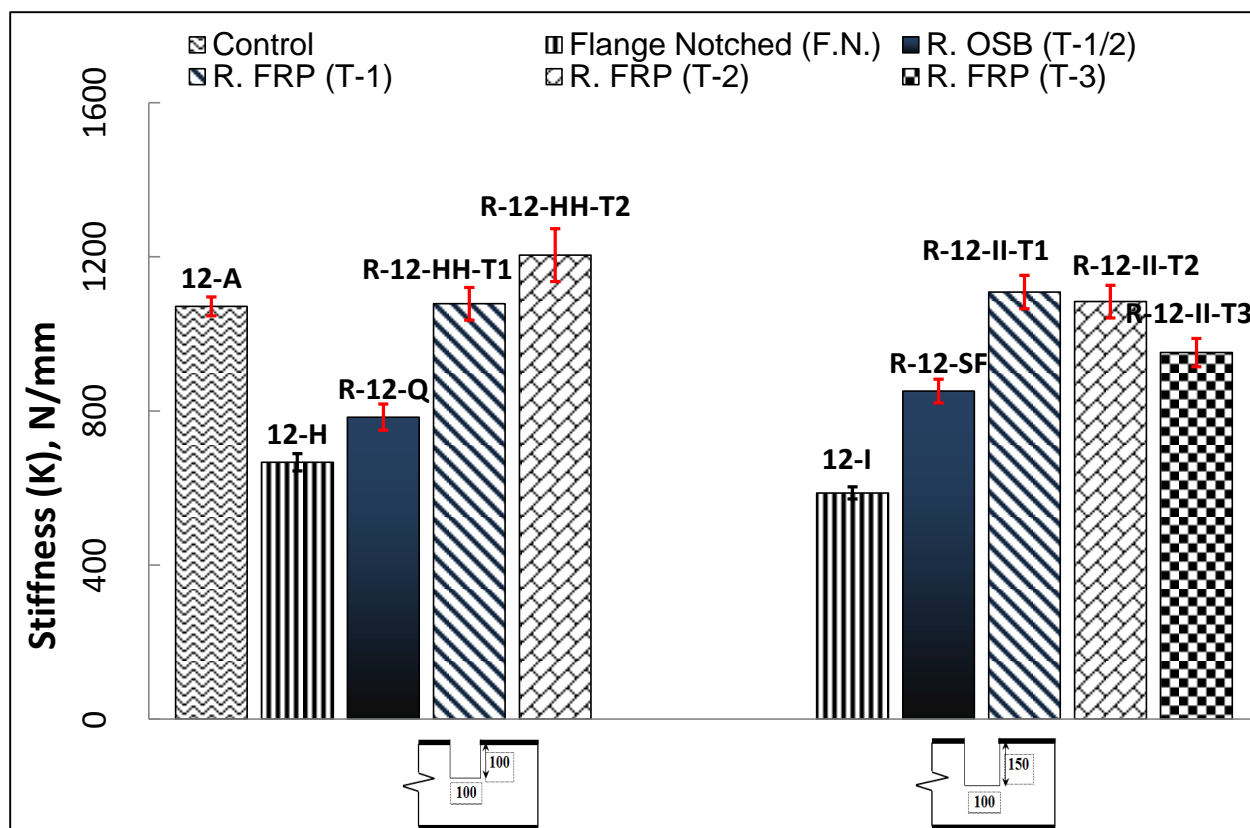


**Figure 7.12: Comparison of Stiffness (K) of 12 ft flange notched I-Joists**

### 7.3.1.2 Long Span (20 feet) I-Joist

#### Structural Capacity (Pu):

**Figure 7.13** 11 presents the average structural capacity of the long span (20 ft) control, flange notched, and retrofitted I-joists with different GFRP reinforcers and OSB collars. It can be observed that the average structural capacity of GFRP retrofitted flange-notched I-joists exceeded the average structural capacity of the control I-joists (20-A) by 245% to 307%. Hence, both of the GFRP reinforcers (Type T-1 and T-2) can effectively reinforce these flange notched I-joists, and can fully restore the structural capacity (0.3% to 8% higher in comparison with the control I-joist's capacity) as shown in **Figure 7.13**. The tested I-Joist specimen R-20-MM-T2-03 was an outlier as it was suddenly failed in a brittle mode due to the presence of a significantly large knot at the

bottom flange. Hence, it was not considered in calculating the average structural capacity of this series. To retrofit longer span flange notched I-joists, type T-3 GFRP reinforcer was not used as GFRP reinforcer type T-1 and type T-2 were capable to fully restore the capacity of the control I-joists as well as its better performance observed for shorter span I-joists.

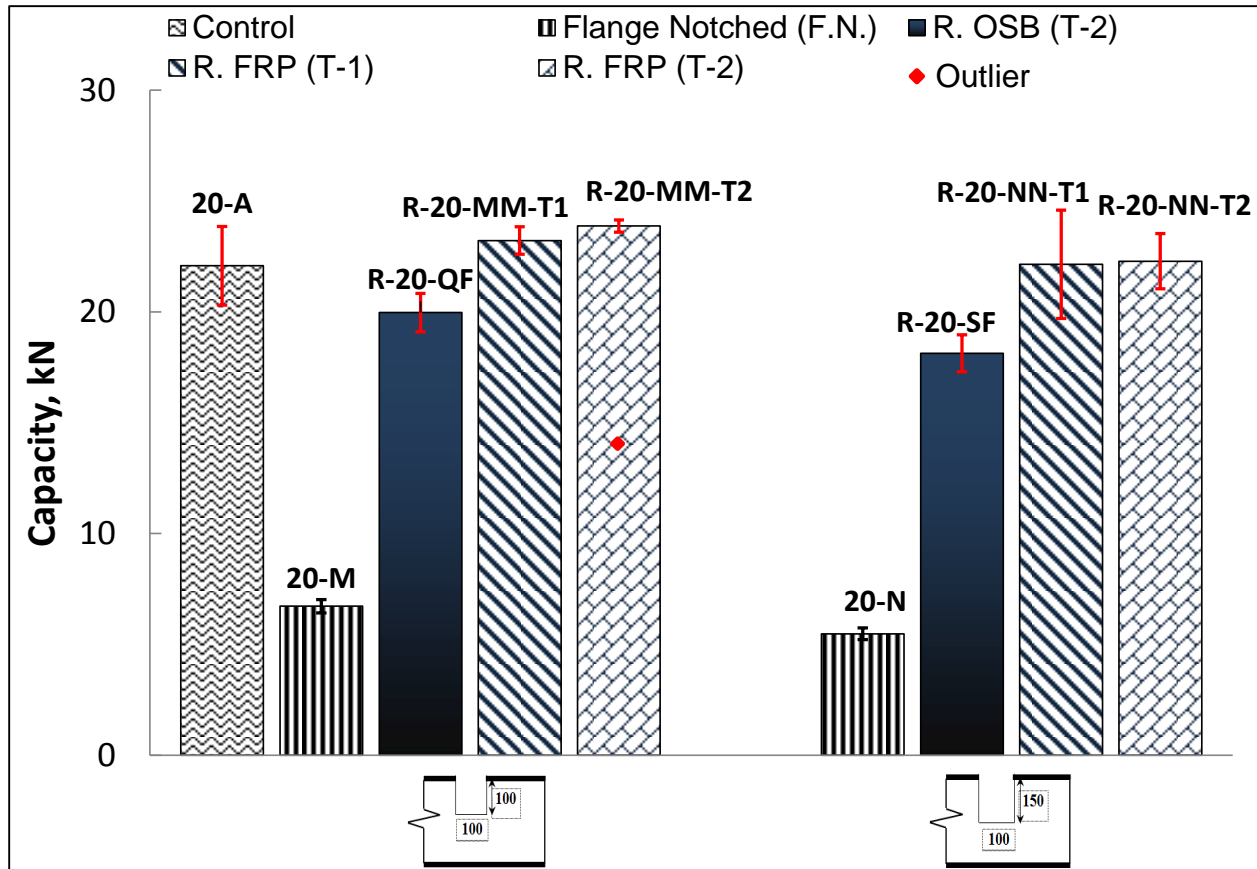


**Figure 7.13: Comparison of Capacity ( $P_u$ ) of 20 ft flange notched I-Joists**

#### Stiffness:

The best fitted Load-Deflection ( $P-\Delta$ ) responses for long span flange notched I-joist series have been presented in **Figure 7.14**. Based on the Load-Deflection ( $P-\Delta$ ) responses, the average stiffness of each series of long span I-joist was calculated and compared in **Figure 7.15**. As observed in **Figure 7.15**, the stiffness ( $K$ ) of long span flange notched I-joists retrofitted with GFRP reinforcers

improved up to 10% to 25% whereas a superior improvement (29% to 40%) was observed for I-joists retrofitted with OSB collar with respect to the flange notched I-Joist. It can be concluded that the GFRP retrofitted I-joists are less stiff compared to those of the I-joists retrofitted with OSB collar. It is due to a lower in-plane/planar bending stiffness of the GFRP plates. As reported by several researchers (*Deogonda and Chalwa 2013; Rathnakar and Shivanand 2012*), the in-plane/planar bending stiffness of GFRP plates is lower than that of OSB/timber.

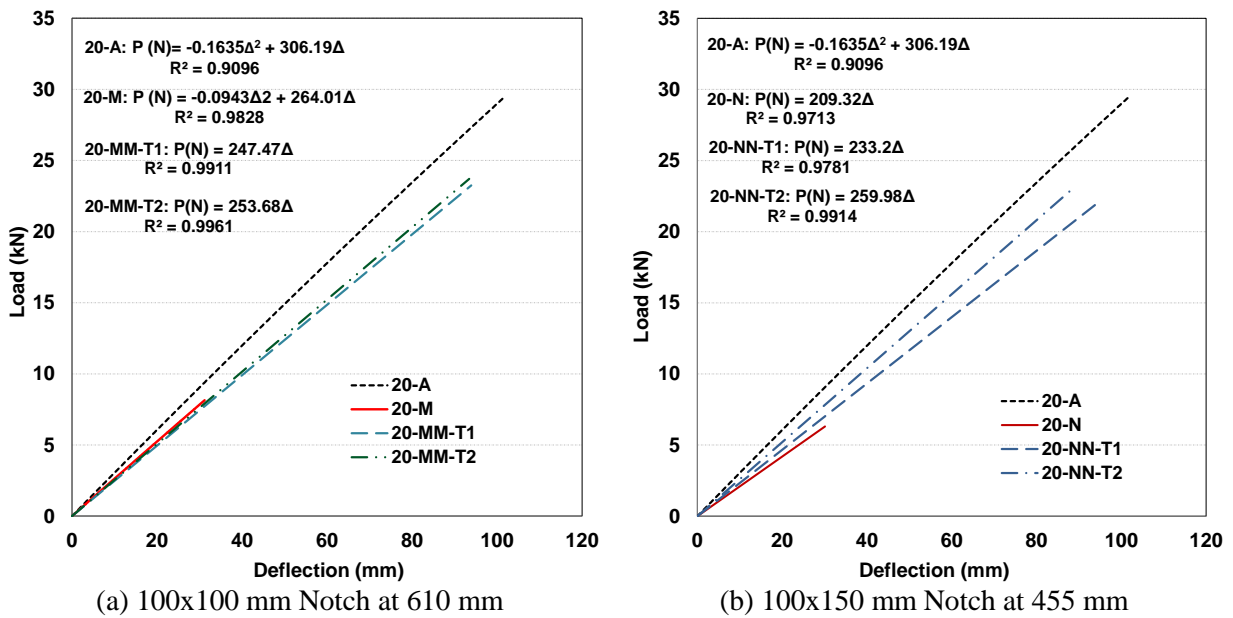


**Figure 7.14: Average Load-Deflection response of 20 ft flange notched I-Joists a) 100x100 mm Notch at 610 mm and b) 100x150 mm Notch at 455 mm**



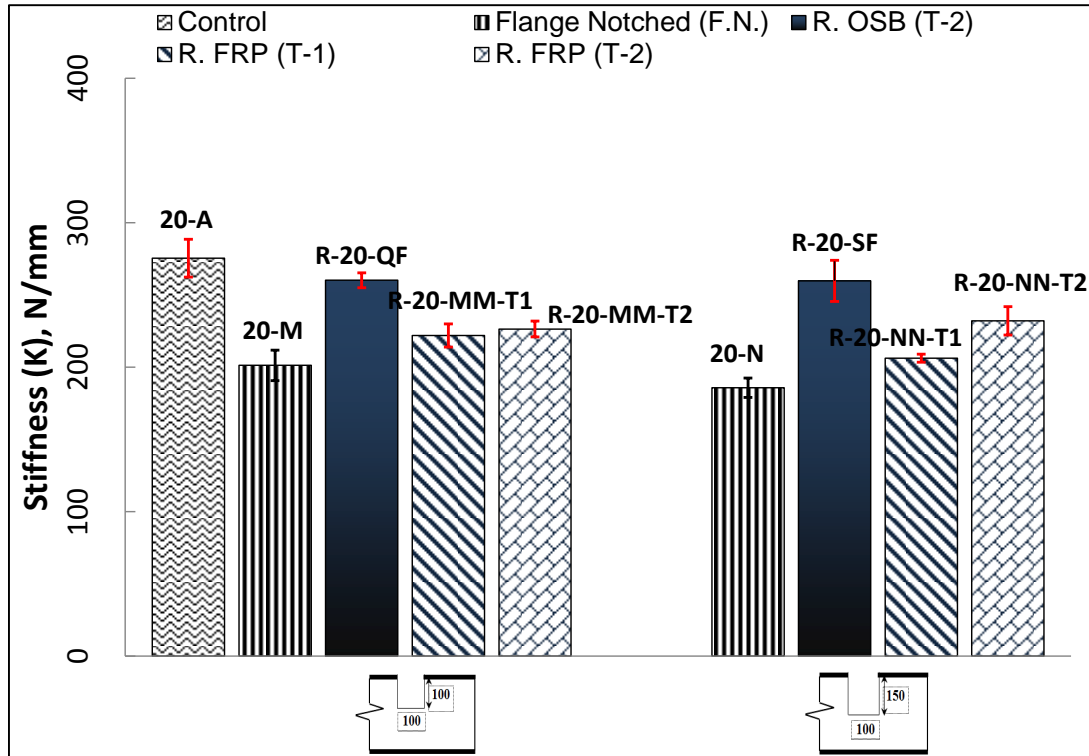


Figure 7.15: Comparison of Stiffness (K) of 20 ft flange notched I-Joists

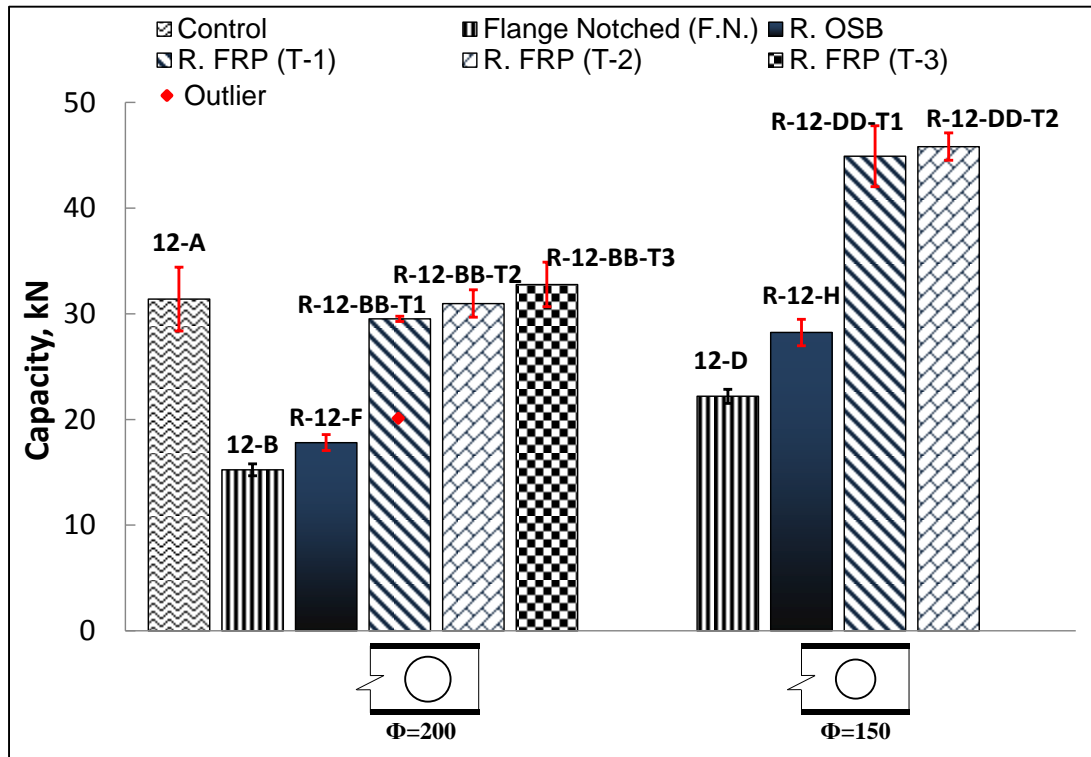
### 7.3.2 Web Hole I-Joists Retrofitted with FRP Reinforcer

#### 7.3.2.1 Short Span (12 feet) I-Joist

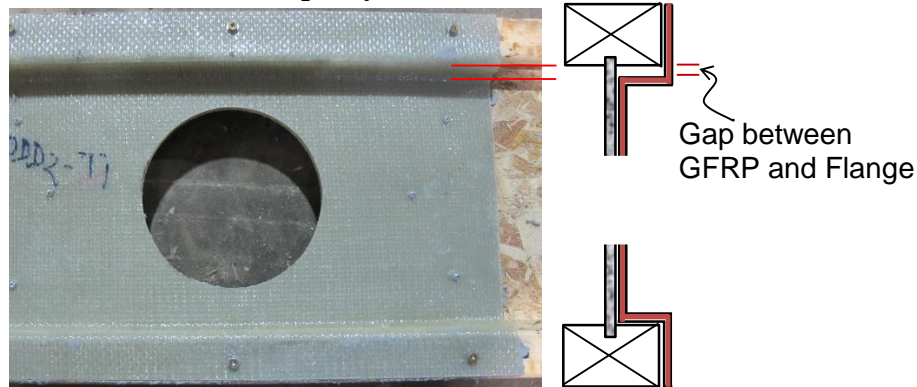
##### Structural Capacity ( $P_u$ ):

Structural capacity ( $P_u$ ) of tested short span (12 ft) I-joists with a web hole retrofitted with GFRP reinforcers have been compared with the control I-joists (series: 12-A), web holed I-joists (series: 12-B & 12-D), and web holed I-joists retrofitted with OSB collar (series: R-12-F & R-12-H) in **Figure 7.16 (a)**. From this figure, it can be observed that most of the web holed I-joists retrofitted with GFRP reinforcers can regain the structural capacity of control I-joists except the I-joist series R-12-BB-T1 having a larger web hole ( $\varnothing = 200\text{mm}$ ) and retrofitted with Type T-1 GFRP reinforcer. After testing this series of I-joists, all three I-joists were carefully investigated and it was found that a 3-7 mm gap existed between the bottom of top flange and the reinforcer as

shown in **Figure 7.16 (b)**. This might be the main reason of having lower capacity ( $P_u$ ) for this series as it reduces the load transferring contact area between the reinforcer and the I-joists. To avoid this capacity reduction for other I-joists, a timber strip was added using glue and four screws in order to increase the load transferring contact area by filling the gap. It was also found that the structural capacity of GFRP retrofitted I-joists having a smaller web hole ( $\varnothing = 150$  mm) exceeded the capacity of the control I-joists by 43% and 46% for series R-12-DD-T1 and R-12-DD-T2, respectively. In the case of series R-12-BB-T1, the specimen number 02 was an outlier due to the presence of a large knot at the bottom cord of the mid-span where failure took place. Hence, it was discarded in calculating the average capacity of this series.



a) Capacity ( $P_u$ ) of 12 ft web holed I-Joists



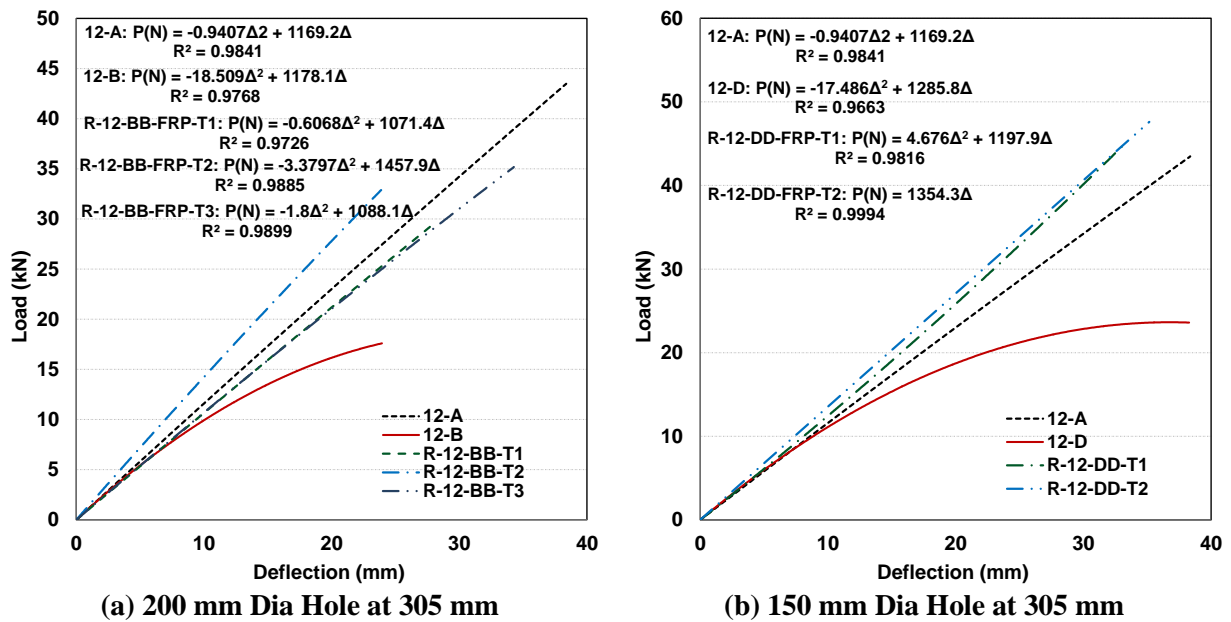
b) Contact less gap between flange and GFRP plate

Figure 7.16: Comparison of Capacity ( $P_u$ ) of 12 ft web holed I-Joists

### Stiffness:

Similar to the flange notched I-joists, the best fitted load-deflection ( $P-\Delta$ ) responses for short span web holed I-joists are shown in **Figure 7.17**. It can be observed that the GFRP retrofitted I-joists exhibit similar response as that of the control series. From these load-deflection ( $P-\Delta$ ) responses, the stiffness values were measured for the web-holed I-joists retrofitted with GFRP

reinforcer and OSB collar and compared in **Figure 7.18**. The stiffness (K) of short span I-joists retrofitted with GFRP reinforcers improved up to 30% and 47% compared to that of the web holed I-joists having a small and large hole diameter, respectively. The stiffness of GFRP retrofitted web holed I-Joists are higher by 3%-43% compared to that of the OSB collar retrofitted I-joist as the shear rigidity (through thickness) of GFRP plate is higher in comparison to the through thickness rigidity of the OSB collar (*CSA-O86 2014*) & (*Ashland Inc. 2007*).



**Figure 7.17: Average Load-Deflection response of 12 ft web holed I-Joists a) 200 mm Dia Hole at 305 mm and b) 150 mm Dia Hole at 305 mm.**

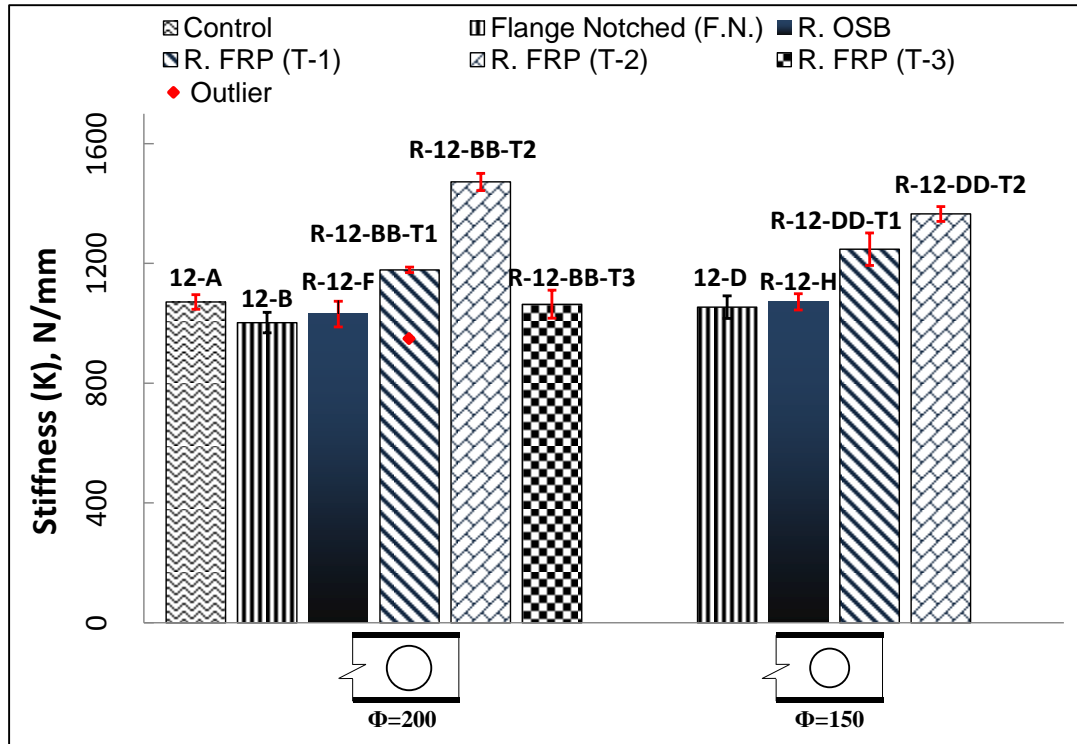
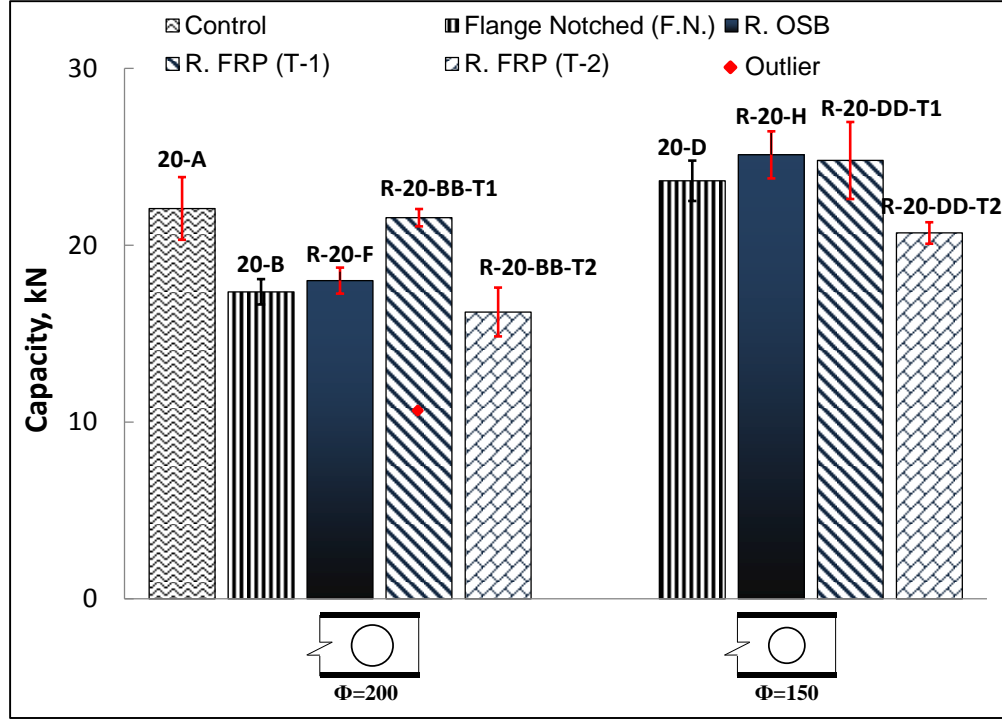


Figure 7.18: Comparison of Stiffness (K) of 12 ft web holed I-Joists

### 7.3.2.2 Long Span (20 feet) I-Joist

#### Structural Capacity ( $P_u$ ):

The average structural capacities ( $P_u$ ) based on the four point bending tests of long span (20 ft) retrofitted I-joists were compared with those of control and web-holed I-joist in **Figure 7.19**. It was found that Type T-1 GFRP reinforcers (both series of I-Joists R-20-BB-T1 and R-20-DD-T1) were able to restore the capacity ( $P_u$ ) to that of the control I-joist for. However, neither of the Type T-2 reinforcers (R-20-BB-T2 & R-20-DD-T2) could restore the capacity ( $P_u$ ) to that of the control series. The average capacity ( $P_u$ ) of these two series of I-joist R-20-BB-T2 and R-20-DD-T2 was reduced by 27% and 6%, respectively compared to that of the control series. This is because of the adhesive (polyester resin mixture) used to attach the reinforcers to the I-joist for retrofitting the web hole, while for other series Sikadur 30 was used to attach GFRP reinforcers.



**Figure 7.19: Comparison of Capacity ( $P_u$ ) of 20 ft web holed I-Joists**

#### Stiffness:

Similar to the short span (12 ft) retrofitted I-joists, best fitted Load-Deflection ( $P-\Delta$ ) responses for long span (20 ft) web holed I-joists are shown in **Figure 7.20**. From the best fitted Load-Deflection ( $P-\Delta$ ) responses, the stiffness of each retrofitted web holed I-joist series was calculated and compared to the stiffness of control I-joist, web holed I-joist and retrofitted with OSB collar I-joist series, in **Figure 7.21**. It can be observed from **Figure 7.21** that the stiffness of series R-20-BB-T2 and R-20-DD-T2 was 19% and 23% lower, respectively, compared to that of the control I-joist. This is because of the lower stiffness of the adhesive (polyester resin) used to attach the Type T-2 reinforcer compared to the stiffness of another adhesive (*Sikadur 30*) used for Type T-1 reinforcer (*Ashland Inc. 2007; Sika Canada Inc. 2015*). Flange-notched I-joist retrofitted with Type T-2 reinforcer would provide greater stiffness ( $K$ ) than that of the Type T-1 retrofitting as the thickness of the reinforcer for T-2 is twice at the critical section (at the notch location) for same

bonding agent or glue (Sikadur 30). Due to the increased thickness of Type T-2 reinforcer at the critical section the shear stress at the web is lower and the bending stiffness (EI) value is higher compared to that of the Type T-1 reinforcer.

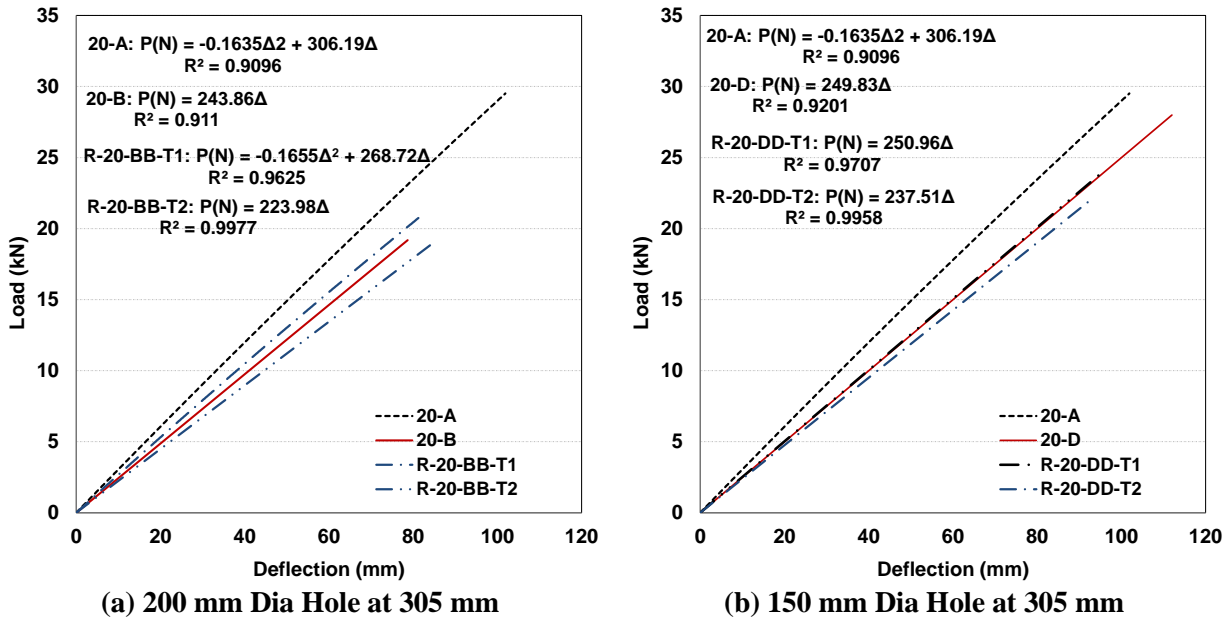


**Figure 7.20: Average Load-Deflection response of 20 ft web holed I-Joists a) 200 mm Dia Hole at 305 mm and b) 150 mm Dia Hole at 305 mm.**

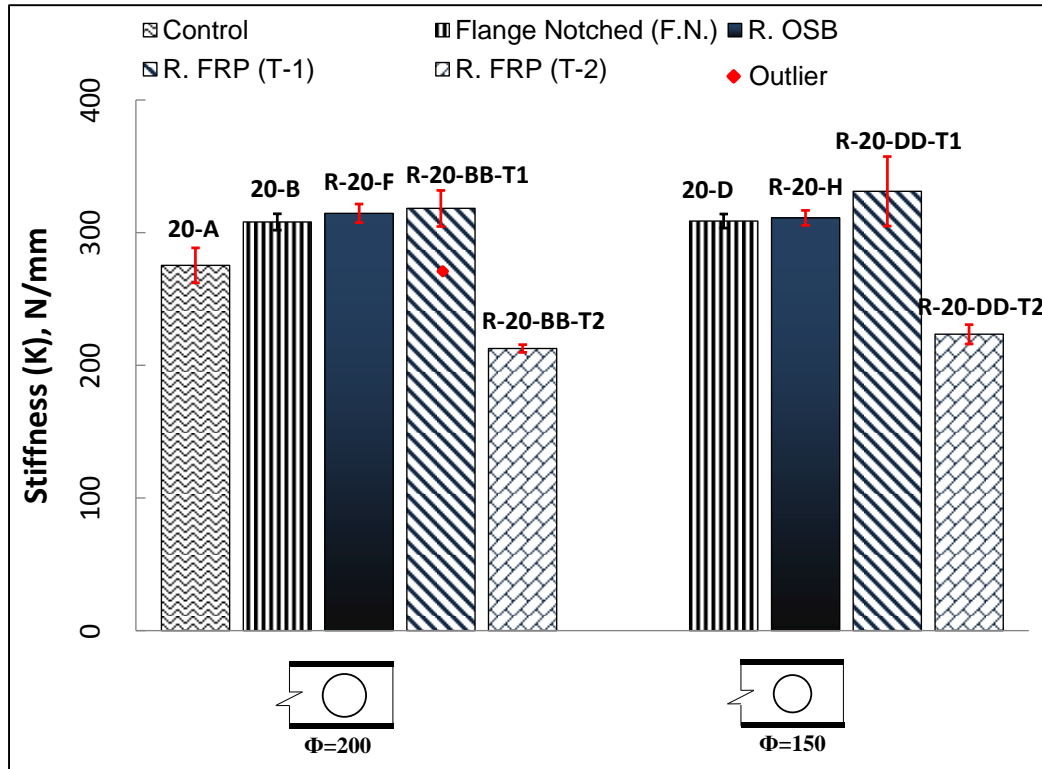


Figure 7.21: Comparison of Stiffness (K) of 20 ft web holed I-Joists

### 7.3.3 Comparison with Allowable Capacity and Stiffness

The test capacity of the 12 ft and 20 ft GFRP retrofitted flange-notched I-joists respectively was at least 2.53 and 3.09 times to that of the design capacity specified by the manufacturer. Whereas the test capacity of the 12 ft and 20 ft web holed I-joists retrofitted with GFRP reinforcers was at least 2.46 and 2.25 times higher, respectively than that of the design capacity. According to *ASTM-D5055 (2013)*, the allowable capacity of wood I-joists should be “the lower 5% tolerance limit with 75% confidence divided by 2.104”. The factor of safety from the test results was found to conform with this requirement. Similarly, the average stiffness of retrofitted flange notched and web holed I-joists were at least 1.86 and 1.93 times the specified design stiffness, respectively.



#### 7.3.4 Failure Types and Location

Failure types and location of failure observed in each GFRP reinforcer based retrofitted I-joists have been summarized in **Table 7.6** and **Table 7.7** for retrofitted flange notched and web holed I-joist, respectively. For the short span flange notched I-joists retrofitted with GFRP reinforcer, 53% of the specimens failed at the notch location, whereas for long span I-joist only one I-joist (R-20-MM-T2-03) was failed at the notch location. However, *Islam et al. (2015)* reported that flange notch I-joists and the retrofitted I-joists with OSB collar failed mainly at notch location. Similar to their findings, it was also observed that 80% of the tested short span flange notched I-joists retrofitted with GFRP reinforcers failed due to bending either at mid span or notch location. Most of the bending failure at notch location occurred due to compression bending at the top wings of the reinforcer at the notch location. However, for long span flange notched I-joists retrofitted with GFRP reinforcers, 92% of the tested I-joists failed due to bending but not at notch location. Mostly, they failed at the web to web joints due to the excessive deflection occurred at the mid span for the longer span. Different types of failure occurred at notch location of the I-joists retrofitted with the GFRP reinforcers as presented in **Figure 7.22**.

**Table 7.6 Summary of Failure Location and Types occurred in Tested Flange Notched I-Joists reinforced with FRP Reinforcer.**

Series	Specimen 1		Specimen 2		Specimen 3		Legend:
	L.F.	T.F.	L.F.	T.F.	L.F.	T.F.	
R-12-HH-T1	1	BF	2	BF	2	BF	<b><u>Location of Failure (L.F.)</u></b>  1 At End Span containing Notch/Hole 2 At Mid Span 3 At other End Span
R-12-HH-T2	1	BF	1	BF	1	JF	
R-12-II-T1	1	BF	1	BF	3	JF	
R-12-II-T2	1	BF	2	KF	1	RSF	<b><u>Types of Failure (T.F.)</u></b>  BF Bending Failure SF Shear Failure SBF Combined Failure KF Failure due to Knot JF Joint Failure RSF Rolling Shear Failure
R-12-II-T3	2	BF	2	BF	2	BF	
R-20-MM-T1	2	KF	2	JF	2	JF	
R-20-MM-T2	2	JF	3	JF	1	KF	
R-20-NN-T1	2	KF	2	SBF	2	BF	
R-20-NN-T2	2	BF	2	BF	2	BF	

For the short span (12 ft) web holed I-joists retrofitted with GFRP plates, 40% of the tested I-joists failed at hole location whereas only one beam failed at the hole location for the long span I-joists (20 ft). Hence, it can be concluded that the short span web holed I-joists are more susceptible to the load capacity than the long span web holed I-joists retrofitted with GFRP reinforcers. The same finding was found by a group of researchers for the web holed I-joists reinforced with OSB collars (*Shahnewaz et al. 2016*). It was also observed that the most critical zone is the web-flange joints at the top and bottom of the hole as shown in *Figure 7.22 (b)*.



(a) Flange Notch Failure:Type-T1



(b) Web Hole Failure:Type-T1



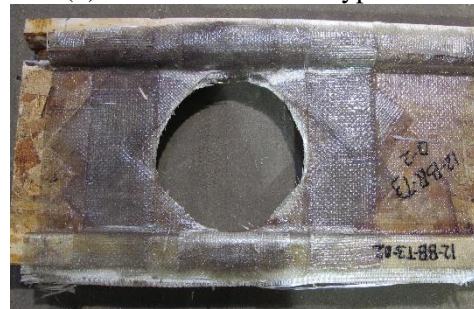
(c) Flange Notch Failure:Type-T2



(d) Web Hole Failure:Type-T2



(e) Flange Notch Failure:Type-T3



(f) Web Hole Failure:Type-T3

**Figure 7.22: Types of Failure occurred in I-joists Retrofitted with GFRP reinforcers a) Flange Notch Failure: Type T-1; b) Web Hole Failure: Type T-1; c) Flange Notch Failure: Type T-2; d) Web Hole Failure: Type T-2; e) Flange Notch Failure: Type T-3; and f) Web Hole Failure: Type T-3.**

**Table 7.7 Summary of Failure Location and Types occurred in Tested Web Holed I-Joists reinforced with FRP Reinforcer.**

Series	Specimen 1		Specimen 2		Specimen 3		Legend:
	L.F.	T.F.	L.F.	T.F.	L.F.	T.F.	
R-12-BB-T1	1	BF	2	KF	1	RSF	<b><u>Location of Failure (L.F.)</u></b>
R-12-BB-T2	2	BF	2	BF	3	KF	1 At End Span containing Notch/Hole
R-12-BB-T3	1	SF	1	RSF	1	RSF	2 At Mid Span
R-12-DD-T1	2	BF	2	BF	1	RSF	3 At other End Span
R-12-DD-T2	2	JF	2	BF	2	BF	<b><u>Types of Failure (T.F.)</u></b>
R-20-BB-T1	2	BF	3	JF	2	BF	BF Bending Failure
R-20-BB-T2	2	BF	2	KF	1	KF	SF Shear Failure
R-20-DD-T1	2	KF	2	BF	2	BF	SBF Combined Failure
R-20-DD-T2	2	JF	2	BF	2	BF	KF Failure due to Knot
							JF Joint Failure
							RSF Rolling Shear Failure

#### 7.4 Proposed Analytical Model to Predict Retrofitted I-joist capacity

Based on the four point bending test results, a regression analysis was performed to develop models for predicting the capacity of I-joists retrofitted with GFRP reinforcers (Type-T1, T2, and T3) having flange notch or web hole. I-joist span length ( $L$ ), height ( $D$ ), opening size ( $D_n$  or  $\Phi_n$ ), and location ( $L_n$ ) affect the capacity of I-joist and as a result were considered important parameters in the regression model. Initially, an effect analysis was performed to determine the significant parameters. Based on the effect analysis, non-significant parameters such as higher orders of ( $D_n/D$ ) and ( $\Phi_n/D$ ) as well as their interactions with ( $L_n/L$ ) were discarded in the model. The proposed equations for retrofitted flange notch and web hole I-joists are presented in **Eq. 7-1 and Eq. 7-2**. The adjusted coefficient of determination (Adjusted  $R^2$ ) values of the proposed models are 0.87 and 0.84, but after considering those discarded parameters the adjusted  $R^2$  values are reduced to 0.68 and 0.44 for retrofitted flange-notched and web-holed I-Joists, respectively

$$P_{u(GFRP-FNR)} = -30.13 + 3.33(T) + 32.9 \left( \frac{D_n}{D} \right) + 524.4 \left( \frac{L_n}{L} \right) - 1471.7 \left( \frac{L_n}{L} \right)^2 \quad \text{Eq. 7-1}$$

$$P_{u(GFRP-WHR)} = 28.9 - 1.060(T) - 55.7 \left( \frac{\phi_h}{D} \right) + 516.4 \left( \frac{L_n}{L} \right) \quad \text{Eq. 7-2}$$

where,  $L$  is the I-joist span length (mm),  $D$  is the height of I-joists,  $D_n$  is the depth of notch,  $\phi_h$  diameter of the web hole,  $L_n$  is the location of the notch or hole, and  $T$  is the type of GFRP reinforcer (1, 2 or 3).

The predicted capacities of retrofitted flange notch and web hole I-joists with GFRP reinforcer were calculated using the proposed regression models, as shown in **Eq. 7-1 and Eq. 7-2**. The predicted capacities of retrofitted flange notched and web holed I-joist were presented in **Table 7.8** and **Table 7.9**, respectively. The maximum error observed in retrofitted flange notched and web holed I-joist models were 6% and 23%, respectively. The accuracies of the proposed models were evaluated using five descriptive statistical parameters: a) average performance factor (PF): the average ratio of predicted capacity to experimental capacity ( $P_{Pred.}/P_{Exp.}$ ); b)  $\chi$  factor: inverse of the slope of a linear least square regression of the predicted capacity ( $P_{Pred}$ ) versus the experimental capacity ( $P_{exp}$ ); c) standard deviation ( $SD$ ); d) co-efficient of variation ( $COV$ ); and e) average absolute error (AAE). The analysis showed that the proposed models are highly accurate for predicting the capacity of retrofitted flange notched and web holed I-joists with different GFRP reinforcers, knowing that all statistical measures were found very low, as shown in **Table 7.10** and **Figure 7.23**. The proposed models show good accuracy with average PF and  $\chi$  value being close to 1.0. Moreover, the maximum COV values of the proposed models (retrofitted flange notched and web holed I-joists) were only 5.5% and 16.2%, respectively.

**Table 7.8 Comparison between experimental and predicted Capacity ( $P_u$ ) for Retrofitted Flange Notched I-joist with GFRP reinforcers**

Type	Series	$D_n$ (mm)	$L_n$ (mm)	$L$ (mm)	$D_n/D$	$L_n/L$	$(L_n/L)^2$	$P_{u (Exp.)}$ kN	$P_{u (Pred.)}$ kN	A.Error %	PF
1	R-12-HH-T1	100	610	3658	0.33	0.17	0.03	30.39	30.65	1	1.01
	R-12-II-T1	150	455	3658	0.50	0.12	0.02	30.81	32.06	4	1.04
	R-20-MM-T1	100	610	6096	0.33	0.10	0.01	23.22	21.87	6	0.94
	R-20-NN-T1	150	455	6096	0.50	0.07	0.01	22.14	20.54	7	0.93
2	R-12-HH-T2	100	610	3658	0.33	0.17	0.03	34.26	33.98	1	0.99
	R-12-II-T2	150	455	3658	0.50	0.12	0.02	35.24	35.39	0	1.00
	R-20-MM-T2	100	610	6096	0.33	0.10	0.01	23.87	25.20	6	1.06
	R-20-NN-T2	150	455	6096	0.50	0.07	0.01	22.28	23.87	7	1.07
3	R-12-II-T3	150	455	3658	0.50	0.12	0.02	40.14	38.72	4	0.96

**Table 7.9 Comparison between experimental and predicted Capacity ( $P_u$ ) for Retrofitted Web Holed I-joist with GFRP reinforcers**

Type	Series	$\Phi_h$ (mm)	$L_n$ (mm)	$L$ (mm)	$\Phi_h/D$	$L_n/L$	$P_{u (Exp.)}$ kN	$P_{u (Pred.)}$ kN	A.Error %	PF
1	R-12-DD-T1	150	305	3658	0.50	0.08	45	43	4	0.96
	R-12-BB-T1	200	305	3658	0.66	0.08	30	34	15	1.15
	R-20-DD-T1	150	305	6096	0.50	0.05	25	26	5	1.05
	R-20-BB-T1	200	305	6096	0.66	0.05	22	17	23	0.77
2	R-12-DD-T2	150	305	3658	0.50	0.08	46	42	8	0.92
	R-12-BB-T2	200	305	3658	0.66	0.08	31	33	6	1.06
	R-20-DD-T2	150	305	6096	0.50	0.05	21	25	20	1.20
	R-20-BB-T2	200	305	6096	0.66	0.05	16	16	4	0.96
3	R-12-BB-T3	200	305	3658	0.66	0.08	33	32	3	0.97

**Table 7.10 Performance evaluation of proposed models**

Parameters			Avg. PF	$\chi$	SD	COV (%)	AAE (%)
Retrofitted I-Joists	Flange Notch	Type-T1	0.98	0.99	0.05	5.48	4.48
		Type-T2	1.03	1.02	0.04	3.75	3.48
		Type-T3	0.96	0.96	-	-	3.54
	Web Hole	Type-T1	0.98	1.00	0.16	16.19	11.50
		Type-T2	1.04	0.99	0.13	12.10	9.51
		Type-T3	0.97	0.97	-	-	3.05

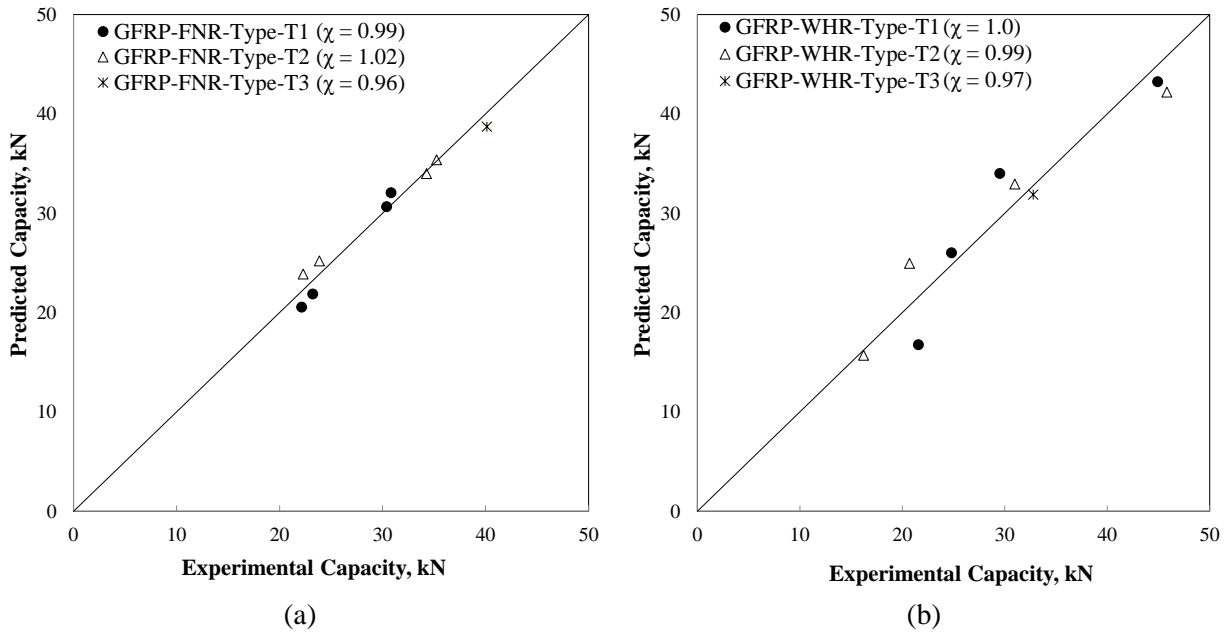


**Figure 7.23: Predicted vs experimental capacity of I-joists retrofitted with GFRP reinforcers with a) flange notch and b) web hole.**

## 7.5 Summary

The experimental investigation on the performance of 12ft and 20ft composite flange notched and web holed wood I-joists retrofitted with GFRP reinforcers allows the following conclusions to be drawn:

- Stiffness of retrofitted web holed I-Joists are higher compared to that of the OSB collar retrofitted I-joist as the in-plane/planar stiffness of GFRP plate is higher in comparison to the through thickness stiffness of the GFRP plate.
- Retrofitted I-joists with GFRP based reinforcers are comparable to the control I-joists in terms of structural capacity and stiffness.
- Structural capacity of the flange notched and web holed I-joists can be improved significantly by retrofitting with GFRP reinforcers for both short and long span I-joists.
- Stiffness of the flange notched and web holed I-joists retrofitted with GFRP reinforcers for both short and long span I-joists were lower compared to that of the control I-joists.
- Regression models to predict the capacity of flange notched and web holed I-joists retrofitted with the GFRP plates are accurate with a performance factors (PFs) close to one.
- Further investigation can be conducted by varying the length and thickness of the FRP reinforcer to determine the effective length and thickness for both options as presented in **Figure 7.1** and **Figure 7.3**. A reliability analysis can be performed to determine the performance improvement factor by optimizing the performance function of the I-joist reinforced with the GFRP reinforcer having a web hole and flange notch. Moreover, a comprehensive study should be conducted on the bond behavior between GFRP plates and Timber/OSB by using the adhesives (Sikadur 30 & Polyester Resin) used in the experimental study.



## CHAPTER 8: PERFORMANCE EVALUATION OF DEFICIENT AND RETROFITTED I-JOISTS HAVING A FLANGE NOTCH OR WEB HOLES: AN ANALYTICAL APPROACH

### 8.1 General

Composite I-joists are engineered wood products with a cross section of “I” shaped containing a web and two flanges referred to as top and bottom flange. Top and bottom flanges are connected with a relatively thin web. Typically flanges are made of solid lumber or structural composite lumber (SCL) such as laminated veneer lumber (LVL) or parallel strand lumber (PSL). Oriented Strand Board (OSB) is the most common web material where occasionally ply wood is also used as web materials.

For light framing structures, use of long and deep lumbers are common but are becoming more expensive and harder to find. Some researchers reported that approximately 50% of the wood fiber can be saved by using different prefabricated engineered wood composite products instead of the solid sawn lumber (*Leichti et al. 1989, Jiao 2012*). Uses of prefabricated wood I-joist became popular since 1960s all around the world because of its light weight, dimensional stability, low uncertainty in performance or quality of products, and ease of construction compared to the solid sawn lumber to carry the same load. Besides, it allows head room to pass the mechanical and plumbing systems of the building easily (*Leichti et al. 1990* and *Forest Products Laboratory 1999*). Moreover, the I-shaped section of the prefabricated composite I-joist provides an efficient structural performance as the flanges and web can be made of different materials, where the flange and web material can provide the bending stiffness and shear rigidity of the joist, respectively.

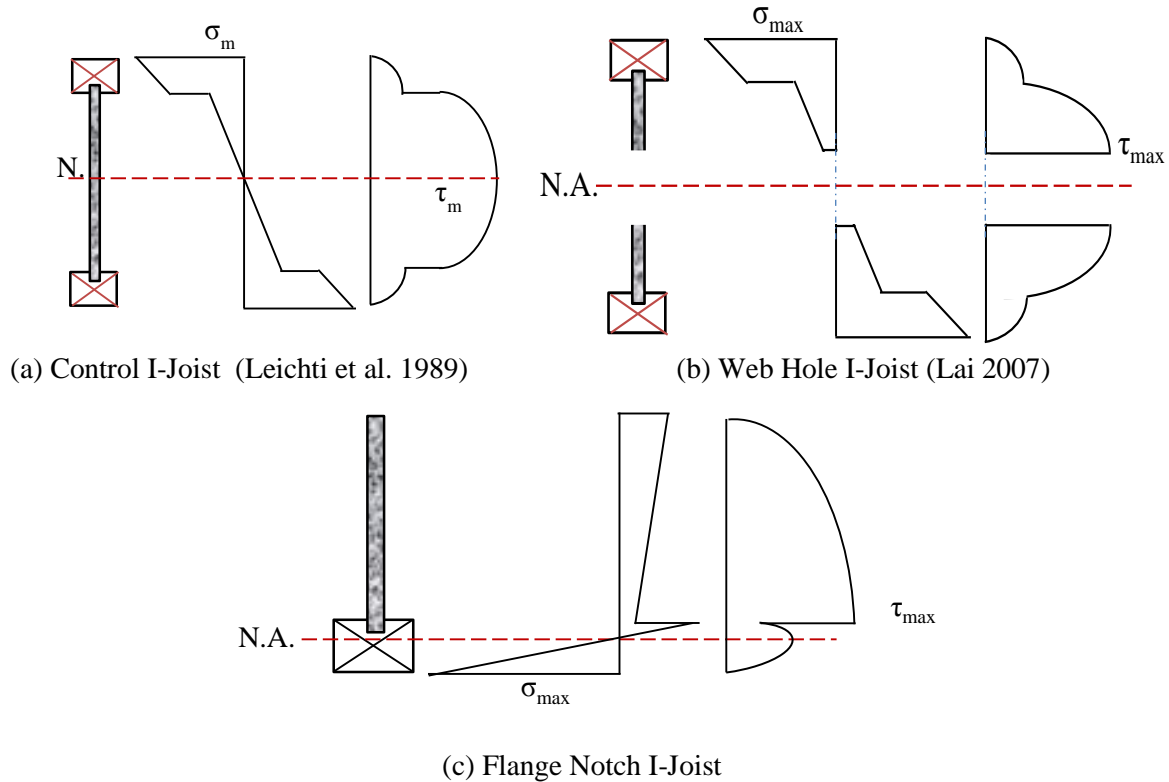


**Figure 8.1 Flexural and Shear Stress Distribution of I-Joist sections a) Control, b) Web Hole & c) Flange Notch.**

The flanges of an I-joist possesses comparatively higher modulus of elasticity ( $E$ ) than the web, which implies that the flexural tension and compression stresses are amplified in the flanges (*Samson 1983; Samson 1981*). Flexural and shear stress distributions of control, Flange Notched and Web Holed I-joists have been presented in **Figure 8.1**. I-joist web resists shear forces while the flanges resist the tension and compression stresses due to bending. The flange material properties and grades can vary significantly while not using engineered wood products. These flange properties are critical in evaluating the contributions of the flange in the performance of I-joists (*Jiao 2012*). To identify the effect of flange stiffness on the performance of I-joists, *Samson (1983)* carried out an investigation on double-webbed I-joists and found that the variation in the average modulus of elasticity (MOE) of tension flange has a significant effect on the performance of I-joists by more than 50% variations. It was also found that flanges were most effective when

the MOE of the tension flange was 1.25 times higher than that of the compression flange. **Hilson and Rodd (1979)** carried out another study on hardboard webbed I-joists and found that the flanges with a higher MOE resist shape changes and greater shear forces after web buckling, and leads to an increased capacity.

As shown in **Figure 8.1**, the web of I-joist mainly resists the shear forces of the I-Joist induced by the gravity loads. Hence, I-joist webs are usually made with the material which has a greater shear modulus and shear strength (through the thickness), such as Oriented Strand Board (OSB), Plywood, Wafer Board, Particle Board etc. (**Leichti et al. 1989**). **Leichti and Tang (1983)** investigated the influence of the modulus of rigidity ( $G$ ) of the web materials on the total beam deflections by using strain energy approach and reported that a greater shear deflection was observed with a lower modulus of rigidity ( $G$ ). An earlier investigation by **Booth (1974)**, also showed that the deflection due to shear is a major component to the total deflection which cannot be ignored in the design procedure of the I-joists based flooring systems. The performance of OSB webbed I-joists is better than those with plywood or wafer board webs, although both have similar strengths (**Leichti et al. 1989**).

**Foliente and Mclain (1993)** proposed a new technique to design notched beams based on the critical fillet hoop stress (CFHS) theory. Design of a notched beam based on CFHS method was compared with the available notch factor or linear-elastic fracture mechanics (LEFM) approaches. However, they didn't consider I-shaped composite I-joists in their investigation. Several researchers (**Morris et al. 1996 ; Zhu 2003**) reported that the Modulus of Elasticity ( $E$ ), Poisson's ratio and Modulus of Rigidity ( $G$ ) in Y and Z directions (i.e.  $E_y$ ,  $E_z$ ,  $\nu_{xz}$ ,  $\nu_{yz}$ ,  $G_{xz}$ , and  $G_{yz}$ ) of OSB web have no significant effects on the total deflection of I-joist. They also found that Poisson's

ratio has no effect on deflection of I-joist due to shear. However, the use of **Eq. 3-1** for determining the  $G_{xy}$  requires  $\nu_{xy}$ . If the modulus of rigidity has to be determined by using **Eq. 3-1**, the model can be considered to be sensitive to  $G_{xy}$ ,  $E_x$ ,  $E_y$ ,  $E_{D45}$  and  $\nu_{xy}$ . Hence, these properties of OSB or web materials must be determined experimentally for I-joist modeling (Grandmont et al. 2010a).

As specified in chapter 1, the aim of this chapter is to formulate the analytical models for I-joists having a flange notch or a web hole and their retrofitted I-joists. The objectives of this chapter are summarized as follows:

- i) To develop analytical models for I-joists having a flange notch or web hole subjected to a four-point load.
- ii) To compare the analytical models with experimental results of four-point bending tests of I-joist with a flange notch or web hole.
- iii) To compare the analytical models with experimental results of four-point bending tests of I-joist having a flange notch or web hole retrofitted with OSB collars and GFRP plates.

## 8.2 Methodology

### 8.2.1 Energy Method

Energy methods for determining the deflection of beams are very popular in the engineering mechanics field. In 1879, Alberto Castigliano proposed a method for determining the deflection and slope of a body at a point based on the conservation of energy, i.e.  $U_i = U_e$ . This method is known as the **Castigliano's Second theorem**. Most of the Mechanics of Materials books (*Hibbeler 2011; Beer et al. 2015; Gere 2004*) covered the derivation of the **Castigliano's Second theorem** for beam deflection due to bending, shear, torsion, axial and other forces acting in the body. The

application of *Castigliano's Second theorem* in determining the maximum deflection and the deflection profile of a beam have been demonstrated in the flow chart presented in **Figure 8.2**.

**Assumptions:**

Assumptions in the *Castigliano's theorem* are-

- i) *Castigliano's theorem* is applicable to the bodies that have materials with linear elastic behavior at constant temperature.
- ii) For determining deflection or displacement, the body has to meet the compatibility requirements.

In the first step, the location of the virtual load ( $P_c$ ) is considered at the Mid Span to determine the Maximum deflection of the I-joist. By following all these steps as described in **Figure 8.2**, the location of the maximum deflection ( $X_{\Delta max}$ ) is determined and compared with the initial location of the virtual load ( $P_c$ ).

Trials have been continued until the location of maximum deflection ( $X_{\Delta max}$ ) and location of the virtual Load  $P_c$  ( $X_c$ ) converge (i.e.  $X_{\Delta max} = X_c$ ).

Finally, the analytical models based on the *Castigliano's theorem* for the control, flange notched & web holed I-joists and their retrofitted I-joists have been validated by comparing with the experimental results obtained from the four point bending test performed as per (**ASTM-D5055 2013**). To do that, the performance factors (**PFs**) of the analytical models were calculated as follows

$$PF = K_A/K_E \quad \text{Eq. 8-1}$$

Where,

$K_A$ = Stiffness of Analytical Model

$K_E$ = Stiffness of the Best Fitted Model based on the Experimental Results

### **Limitations:**

To calculate the deflection due to shear, only the area and the shear modulus of web (OSB) were considered. As the shear stresses at flanges are very low, it does not have any significant effects on the deflection compared to the deflection due to bending.

## **8.1 Formulation of Models**

To formulate the model for I-joists, strain energy based *Castigliano's theorem* was employed as described in the previous section. Deflection due to bending and shear for the applied loads were incorporated in the model formulation. Deflection of the beam can be calculated by using *Eq. 8-2 and Eq. 8-3*. A Matlab (*The MathWorks Inc.; Natick 2012*) script was written to perform this symbolic integration for model formulations.

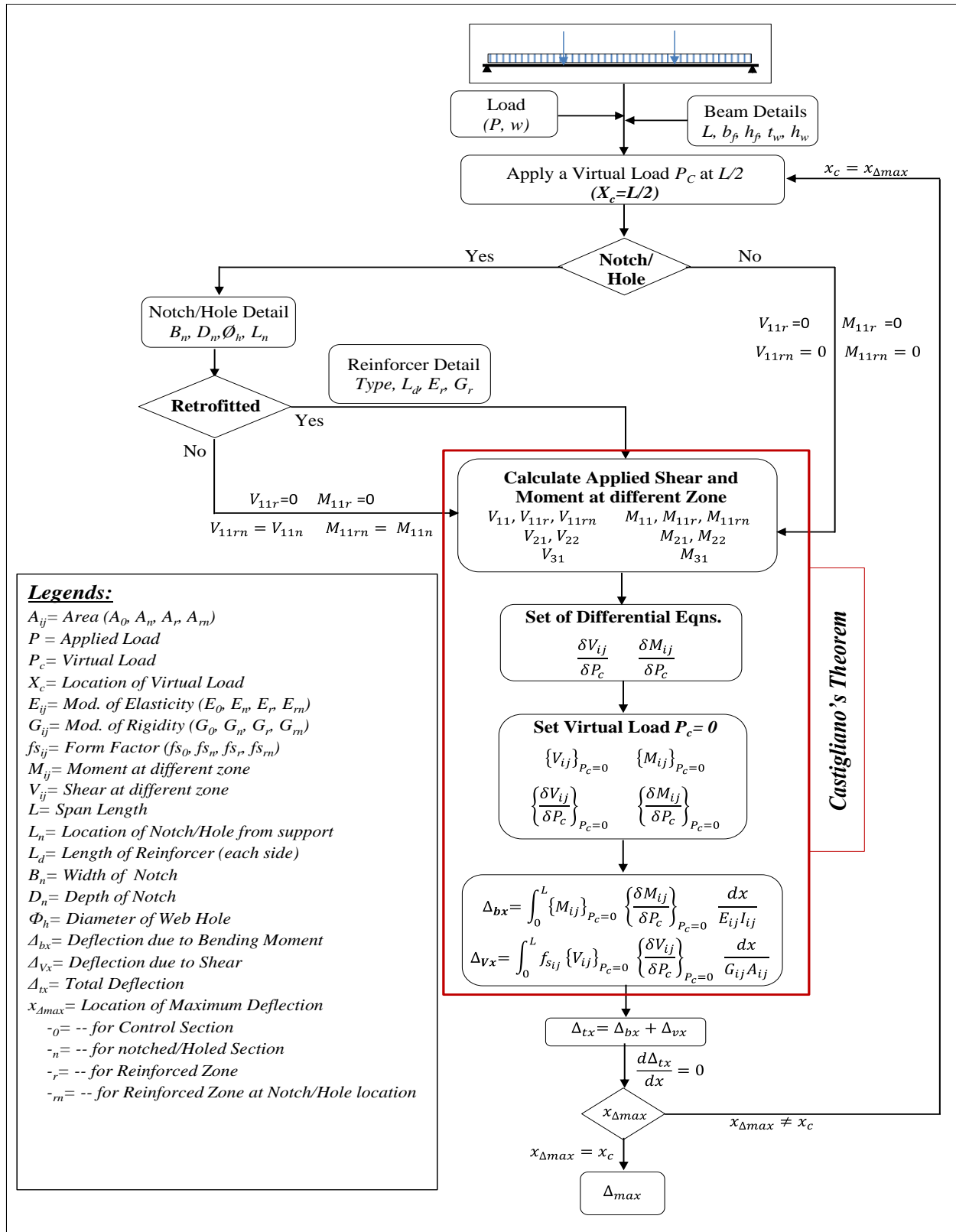


**Figure 8.2** Flow chart for calculating the maximum deflection of a flange notched or web holed I-joists.

$$\text{Total deflection, } \Delta_{tx} = \Delta_{bx} + \Delta_{vx} \quad \text{Eq. 8-2}$$

Where,

$$\text{Deflection due to Bending,} \quad \Delta_{bx} = \int_0^L \{M_{ij}\}_{P_c=0} \left\{ \frac{\delta M_{ij}}{\delta P_c} \right\}_{P_c=0} \frac{dx}{E_{ij} I_{ij}} \quad \text{Eq. 8-2 a}$$

$$\text{Deflection due to Shear,} \quad \Delta_{vx} = \int_0^L f_{s_{ij}} \{V_{ij}\}_{P_c=0} \left\{ \frac{\delta V_{ij}}{\delta P_c} \right\}_{P_c=0} \frac{dx}{G_{ij} A_{ij}} \quad \text{Eq. 8-2 b}$$

By combining **Eq. 8-2**, **Eq. 8-2a**, & **Eq. 8-2b**, we can get,

$$\Delta_{tx} = \int_0^L \{M_{ij}\}_{P_c=0} \left\{ \frac{\delta M_{ij}}{\delta P_c} \right\}_{P_c=0} \frac{dx}{E_{ij} I_{ij}} + \int_0^L f_{s_{ij}} \{V_{ij}\}_{P_c=0} \left\{ \frac{\delta V_{ij}}{\delta P_c} \right\}_{P_c=0} \frac{dx}{G_{ij} A_{ij}} \quad \text{Eq. 8-3}$$

### 8.1.1 Deflection for Mid-Span:

#### 8.1.1.1 Control I-Joists

To derive the analytical model of control I-joist, the entire span length was divided into three zones: Zone 1- Left Span, Zone 2- Mid-Span, and Zone 3- Right Span as shown in **Figure 8.3**. To determine the deflection profile of a zone ( $y_1$ ,  $y_2$  ( $\Delta_{tx}$ ) or  $y_3$ ), a virtual load  $P_c$  is applied to that zone at  $X_c$  distance from the left support. The virtual load  $P_c$  further divides the corresponding zone into two subzones, for which **Eq. 8-2** and **Eq. 8-3** can be reformed to integrate along the span length.

$$\text{Deflection due to Bending,} \quad \Delta_{bx} = \int_0^{L/3} f_b(x) + \int_{L/3}^{X_c} f_b(x) + \int_{X_c}^{2L/3} f_b(x) + \int_{2L/3}^L f_b(x) \quad \text{Eq. 8-4}$$

$$\text{Deflection due to Shear,} \quad \Delta_{vx} = \int_0^{L/3} f_v(x) + \int_{L/3}^{X_c} f_v(x) + \int_{X_c}^{2L/3} f_v(x) + \int_{2L/3}^L f_v(x) \quad \text{Eq. 8-5}$$



Where,

$$f_b(x) = \{M_{ij}\}_{P_c=0} \left\{ \frac{\delta M_{ij}}{\delta P_c} \right\}_{P_c=0} \frac{dx}{E_{ij} I_{ij}}$$

$$f_v(x) = f_{s_{ij}} \{V_{ij}\}_{P_c=0} \left\{ \frac{\delta V_{ij}}{\delta P_c} \right\}_{P_c=0} \frac{dx}{G_{ij} A_{ij}}$$

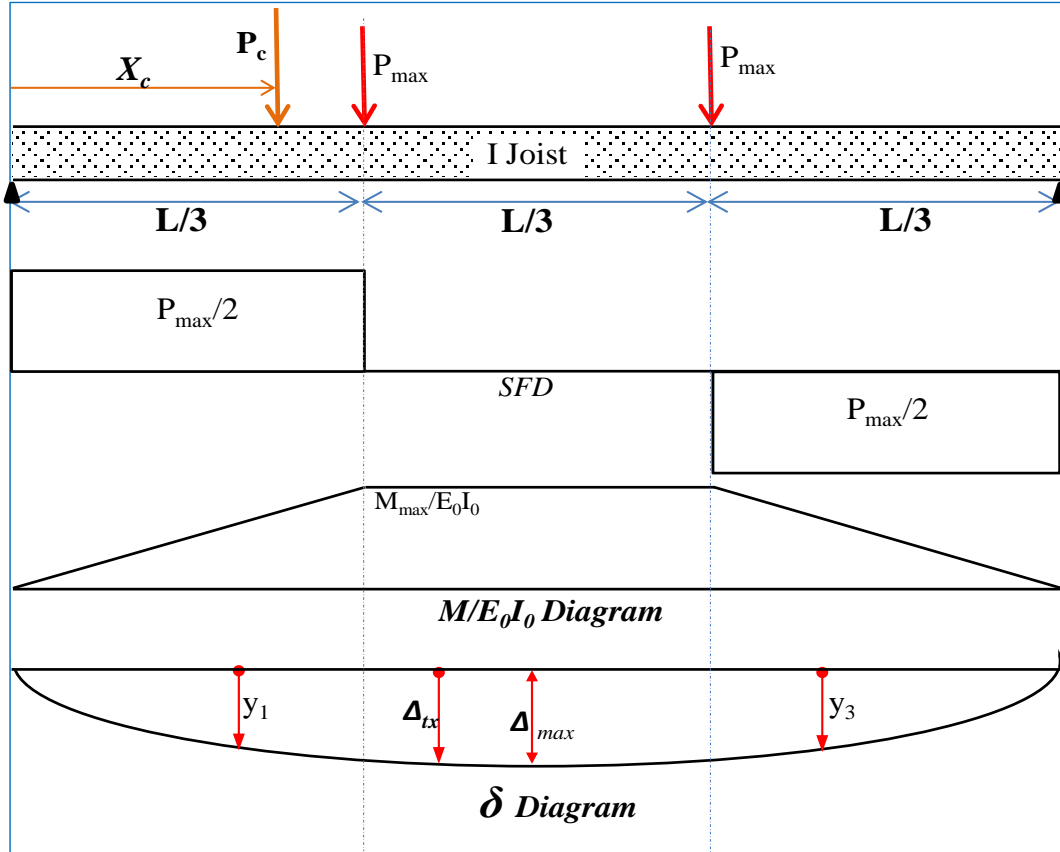


Figure 8.3 Application of Castigliano's theorem to develop the analytical models for control I-joists.

For the mid span deflection profile of a control I-joist, integrating and combining *Eq. 8-4 and Eq. 8-5* yields to *Eq. 8-6 and Eq. 8-7* respectively.

$$\Delta_{vx} = \frac{P \cdot f_s \cdot x}{3 \cdot A \cdot G} + \frac{P \cdot f_s \cdot (L - x)}{3 \cdot A \cdot G} \quad \text{Eq. 8-6}$$

$$\Delta_{bx} = \frac{L^2 \cdot P \cdot x}{81 \cdot E \cdot I} + \frac{L^2 \cdot P \cdot (L - x)}{81 \cdot E \cdot I} + \frac{P \cdot x \cdot (8 \cdot L^2 - 18 \cdot L \cdot x + 9 \cdot x^2)}{54 \cdot E \cdot I} - \frac{P \cdot (L - x) \cdot (L^2 - 9 \cdot x^2)}{54 \cdot E \cdot I} \quad \text{Eq. 8-7}$$

By combining equations *Eq. 8-6 & Eq. 8-7*, the location of maximum deflection ( $X_{\Delta_{max}}$ ) can be determined by differentiating that at zero (i.e.  $\frac{d\Delta_{tx}}{dx} = 0$ ), which yields to

$$X_{\Delta_{max}} = L/2 \quad \text{Eq. 8-8}$$

Maximum Deflection at  $X_{\Delta_{max}}$  i.e.  $L/2$  can be found as follows:

$$\Delta_{max} = \frac{23 \cdot P \cdot L^3}{648 \cdot E \cdot I} + \frac{P \cdot L \cdot f_s}{3 \cdot A \cdot G} \quad \text{Eq. 8-9}$$

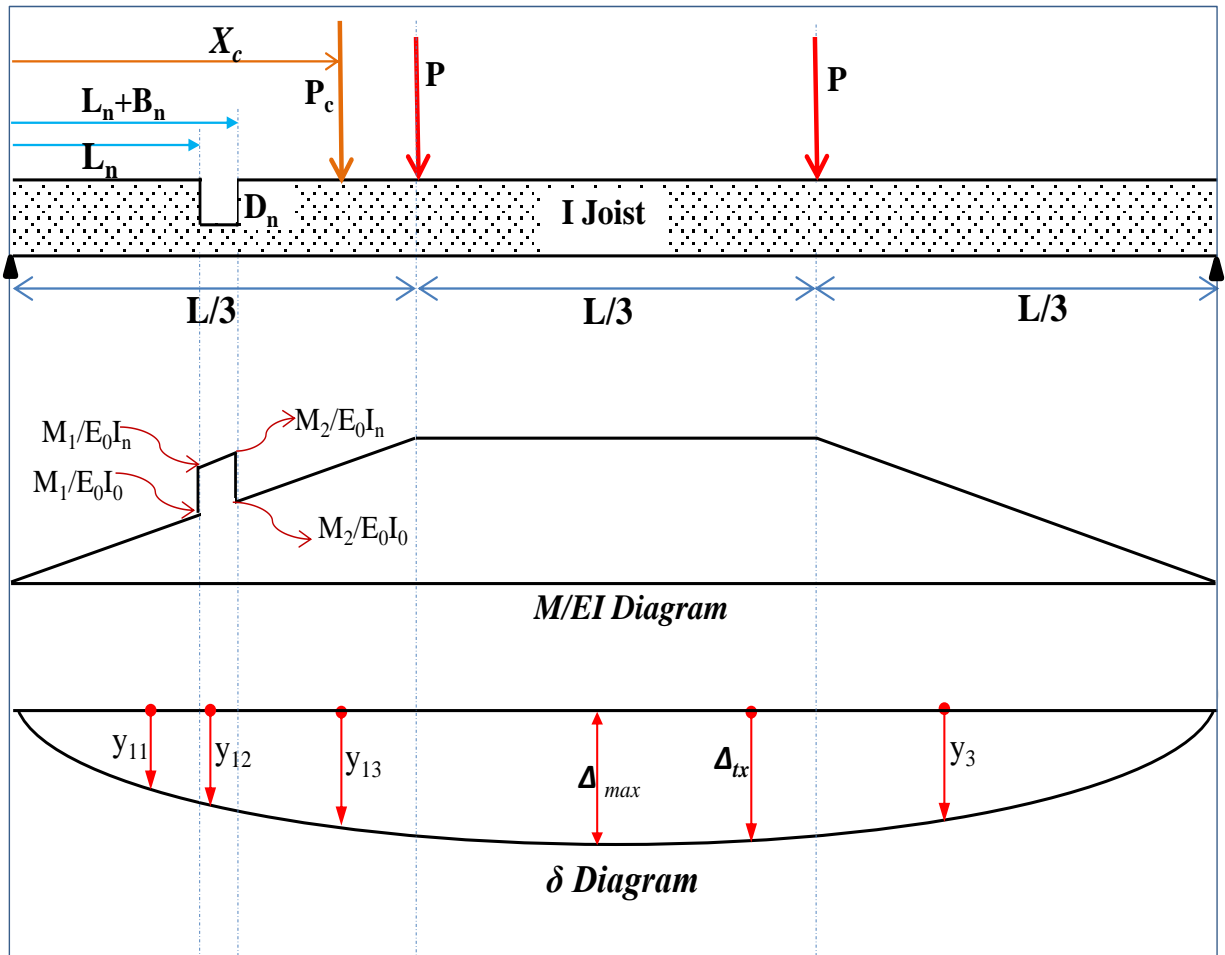


**Figure 8.4** Application of Castigliano's theorem to develop the analytical models for flange notched I-joists.

### 8.1.1.2 Flange Notched I-Joists

To derive the analytical model of flange notched I-joist, the entire span length was divided into three zones similar to the control I-joist. However, Zone 1 is subdivided into another three zones to incorporate the flange notch as shown in

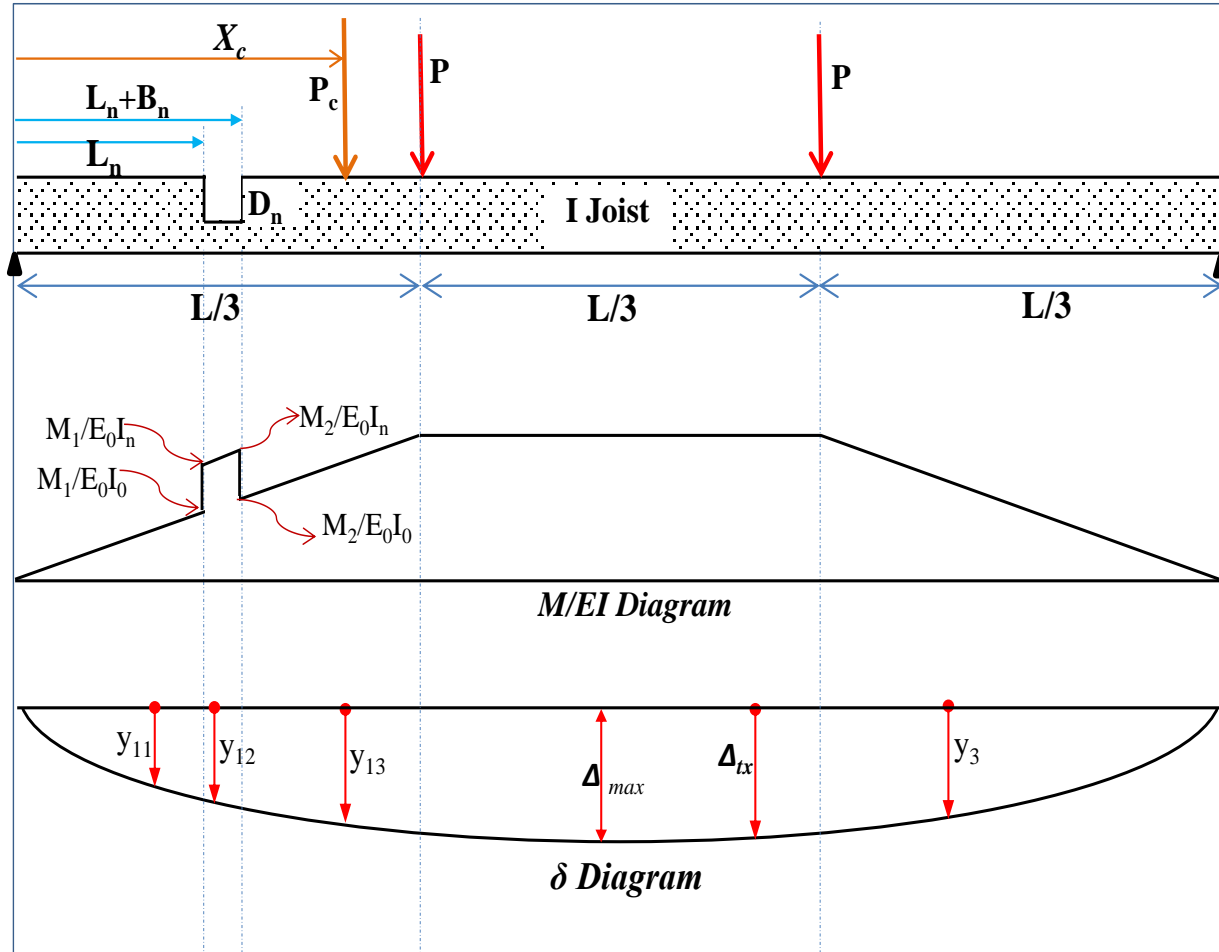


**Figure 8.4.** To determine the deflection profile of a zone ( $y_{1j}$  ( $j=1-3$ ),  $y_2$  ( $\Delta_{tx}$ ) or  $y_3$ ), a virtual load  $P_c$  is applied to that zone at  $X_c$  distance from the left support. The virtual load  $P_c$  further divides the corresponding zone into two sub-zones, for which *Eq. 8-2* and *Eq. 8-3* can be reformed to integrate along the span length.

*Deflection due to Bending,*

$$\Delta_{bx} = \int_0^{Ln} f_b(x) + \int_{Ln}^{Ln+Bn} f_b(x) + \int_{Ln+Bn}^{L/3} f_b(x) + \int_{L/3}^{Xc} f_b(x) + \int_{Xc}^{2L/3} f_b(x) + \int_{2L/3}^L f_b(x) \quad \text{Eq. 8-10}$$

*Deflection due to Shear,*

$$\Delta_{vx} = \int_0^{Ln} f_v(x) + \int_{Ln}^{Ln+Bn} f_v(x) + \int_{Ln+Bn}^{L/3} f_v(x) + \int_{L/3}^{Xc} f_v(x) + \int_{Xc}^{2L/3} f_v(x) + \int_{2L/3}^L f_v(x) \quad \text{Eq. 8-11}$$

*Where,*

$$f_b(x) = \{M_{ij}\}_{P_c=0} \left\{ \frac{\delta M_{ij}}{\delta P_c} \right\}_{P_c=0} \frac{dx}{E_{ij} I_{ij}}$$

$$f_v(x) = f_{s_{ij}} \{V_{ij}\}_{P_c=0} \left\{ \frac{\delta V_{ij}}{\delta P_c} \right\}_{P_c=0} \frac{dx}{G_{ij} A_{ij}}$$

The mid span deflection profile of a flange notch I-joist can be determined by integrating and combining *Eq. 8-10* and *Eq. 8-11* yielding to *Eq. 8-12*.

$$\Delta_{tx} = \frac{P \cdot L^2 \cdot x}{81 \cdot E \cdot I} + \frac{P \cdot L^2 \cdot (L - x)}{81 \cdot E \cdot I} + \frac{P \cdot x \cdot (8 \cdot L^2 - 18 \cdot L \cdot x + 9 \cdot x^2)}{54 \cdot E \cdot I} + \frac{P \cdot f_s \cdot x}{3 \cdot A \cdot G} - \frac{P \cdot (L - x) \cdot (B_n + L_n)^3}{3 \cdot E \cdot I \cdot L} - \frac{54 \cdot E \cdot I}{P \cdot (L - x) \cdot (L^2 - 9 \cdot x^2)} + \frac{P \cdot L_n^3 \cdot (L - x)}{3 \cdot E \cdot I \cdot L} + \frac{P \cdot L_n \cdot f_s \cdot (L - x)}{A \cdot G \cdot L} - \frac{P \cdot f_s \cdot (L - x) \cdot (3 \cdot B_n - L + 3 \cdot L_n)}{3 \cdot A \cdot G \cdot L} + \Delta_{bn} + \Delta_{vn} \quad \text{Eq. 8-12}$$

*Where,*

$$\Delta_{bn} = \frac{P \cdot B_n \cdot (L - x) \cdot (B_n^2 + 3 \cdot B_n \cdot L_n + 3 \cdot L_n^2)}{3 \cdot E_n \cdot I_n \cdot L} \quad \text{Eq. 8-12 a}$$

$$\Delta_{vn} = \frac{P \cdot B_n \cdot f_{sn} \cdot (L - x)}{A_n \cdot G_n \cdot L} \quad \text{Eq. 8-12 b}$$

### 8.1.1.3 Retrofitted Flange Notched I-Joists

To derive the analytical model of retrofitted flange notched I-joist, the entire span length was divided into three zones similar to the control I-joist. However, Zone 1 is subdivided into another five zones to incorporate the flange notch and notch reinforcing OSB Collars/ GFRP Plates as shown in **Figure 8.5**. To determine the deflection profile of a zone ( $y_{1j}$  ( $j=1-5$ ),  $y_2$  ( $\Delta_{tx}$ ) or  $y_3$ ), a virtual load  $P_c$  is applied to that zone at  $X_c$  distance from the left support. The virtual load  $P_c$  further divides the corresponding zone into two sub-zones, for which **Eq. 8-2** and **Eq. 8-3** can be reformed to integrate along the span length.

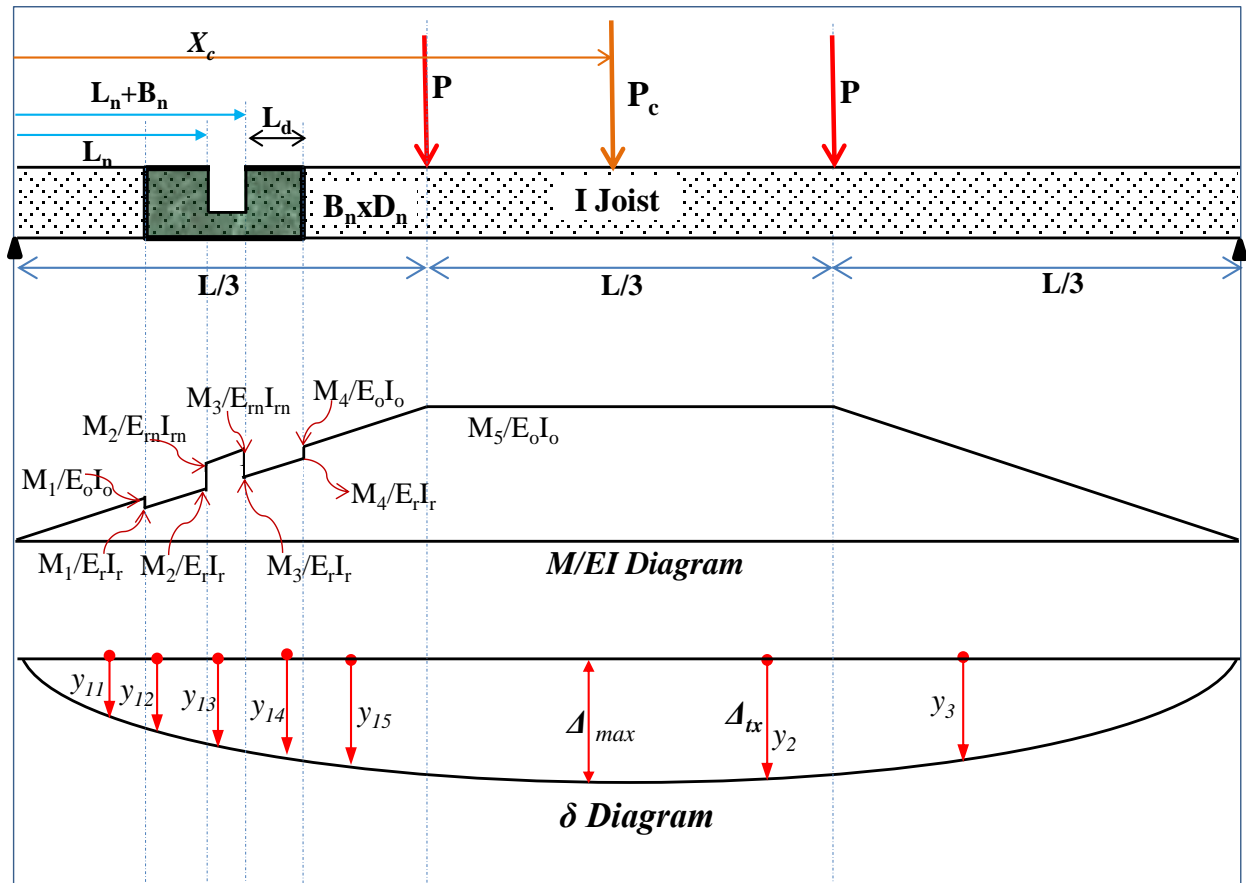


**Figure 8.5** Application of Castigliano's theorem to develop the analytical models for retrofitted flange notched I-joists.

*Deflection due to Bending,*

$$\Delta_{bx} = \int_0^{Lr} f_b(x) + \int_{Lr}^{Ln} f_b(x) + \int_{Ln}^{Ln+Bn} f_b(x) + \int_{Ln+Bn}^{Ln+Bn+Ld} f_b(x) + \int_{Ln+Bn+Ld}^{L/3} f_b(x) + \int_{L/3}^{Xc} f_b(x) + \int_{Xc}^{2L/3} f_b(x) + \int_{2L/3}^L f_b(x) \quad \text{Eq. 8-13}$$

*Deflection due to Shear,*

$$\Delta_{vx} = \int_0^{Lr} f_v(x) + \int_{Lr}^{Ln} f_v(x) + \int_{Ln}^{Ln+Bn} f_v(x) + \int_{Ln+Bn}^{Ln+Bn+Ld} f_v(x) + \int_{Ln+Bn+Ld}^{L/3} f_v(x) + \int_{L/3}^{Xc} f_v(x) + \int_{Xc}^{2L/3} f_v(x) + \int_{2L/3}^L f_v(x) \quad \text{Eq. 8-14}$$

*Where,*

$$f_b(x) = \{M_{ij}\}_{P_c=0} \left\{ \frac{\delta M_{ij}}{\delta P_c} \right\}_{P_c=0} \frac{dx}{E_{ij} I_{ij}}$$

$$f_v(x) = f_{s_{ij}} \{V_{ij}\}_{P_c=0} \left\{ \frac{\delta V_{ij}}{\delta P_c} \right\}_{P_c=0} \frac{dx}{G_{ij} A_{ij}}$$

The mid span deflection profile of a retrofitted flange notch I-joist can be determined by integrating and combining *Eq. 8-13* and *Eq. 8-14* yielding to *Eq. 8-15*.

$$\Delta_{tx} = \frac{L^2 \cdot P \cdot x}{81 \cdot E \cdot I} + \frac{L^2 \cdot P \cdot (L - x)}{81 \cdot E \cdot I} + \frac{P \cdot x \cdot (8 \cdot L^2 - 18 \cdot L \cdot x + 9 \cdot x^2)}{54 \cdot E \cdot I} + \frac{P \cdot f_s \cdot x}{3 \cdot A \cdot G} - \frac{P \cdot (L - x) \cdot \gamma_{rn2}^3}{3 \cdot E_r \cdot I_r \cdot L} - \frac{P \cdot (L - x) \cdot (L^2 - 9 \cdot x^2)}{54 \cdot E \cdot I} - \frac{P \cdot (L - x) \cdot \gamma_{rn1}^3}{3 \cdot E \cdot I \cdot L} + \frac{P \cdot (L - x) \cdot \gamma_{rn1}^3}{3 \cdot E_r \cdot I_r \cdot L} + \frac{P \cdot \gamma_{rn3}^3 \cdot (L - x)}{3 \cdot E \cdot I \cdot L} + \frac{Lr \cdot P \cdot (L - x) \cdot \gamma_{rn4}}{3 \cdot E_r \cdot I_r \cdot L} - \frac{P \cdot f_s \cdot (L - x) \cdot \gamma_{rn5}}{3 \cdot A \cdot G \cdot L} + \frac{2 \cdot Lr \cdot P \cdot f_{sr} \cdot (L - x)}{A_r \cdot G_r \cdot L} + \frac{P \cdot f_s \cdot \gamma_{rn3} \cdot (L - x)}{A \cdot G \cdot L} + \Delta_{vrn} + \Delta_{brn} \quad \text{Eq. 8-15}$$

*Where,*

$$\Delta_{brn} = \frac{B_n \cdot P \cdot (L - x) \cdot (B_n^2 + 3 \cdot B_n \cdot L_n + 3 \cdot L_n^2)}{3 \cdot E_{rn} \cdot I_{rn} \cdot L} \quad \text{Eq. 8-15 a}$$

$$\Delta_{vrn} = \frac{B_n \cdot P \cdot f_{srn} \cdot (L - x)}{A_{rn} \cdot G_{rn} \cdot L} \quad \text{Eq. 8-15 b}$$

$$\begin{aligned}
\gamma_{rn1} &= B_n + L_n + L_d \\
\gamma_{rn2} &= B_n + L_n \\
\gamma_{rn3} &= L_n - L_d \\
\gamma_{rn4} &= 3.L_n^2 - 3.L_n.L_d + L_d^2 \\
\gamma_{rn5} &= 3.B_n - L + 3.L_n + 3.L_d
\end{aligned}
\left. \vphantom{\begin{aligned} \gamma_{rn1} \\ \gamma_{rn2} \\ \gamma_{rn3} \\ \gamma_{rn4} \\ \gamma_{rn5} \end{aligned}} \right\} \text{Eq. 8-15(c-g)}$$

#### 8.1.1.4 Circular Web Holed I-Joists

To develop the analytical models of circular web holed I-joists, a similar approach of the flange notched I-joists was employed as presented in **Figure 8.4**. However, the variations of the cross-sectional area of the I-joists with respect to the longitudinal axis of the beam at the hole location has been considered. The mid span deflection profile of a web hole I-joist can be determined by integrating and combining **Eq. 8-10** and **Eq. 8-11** yielding to **Eq. 8-16**.

$$\begin{aligned}
\Delta_{tx} = & \frac{P.L^2.x}{81.E.I} + \frac{P.L^2.(L-x)}{81.E.I} + \frac{P.x.(8.L^2 - 18.L.x + 9.x^2)}{54.E.I} + \frac{P.f_s.x}{3.A.G} \\
& - \frac{P.(L-x).(\phi_h + L_n)^3}{3.E.I.L} - \frac{P.(L-x).(L^2 - 9.x^2)}{54.E.I} + \frac{P.L_n^3.(L-x)}{3.E.I.L} \\
& + \frac{P.f_s.L_n.(L-x)}{A.G.L} - \frac{P.f_s.(L-x).(3.\phi_h - L + 3.L_n)}{3.A.G.L} + \Delta_{b\phi_h} + \Delta_{v\phi_h}
\end{aligned} \quad \text{Eq. 8-16}$$

Where,

$$\Delta_{b\phi_h} = \int_{L_n}^{L_n+\phi_h} \left( \frac{P.x^2.(L-x_c)}{E_n.L \left( 2.I_{of} + I_{ow} - 2.t_w \left( \frac{\phi_h^2}{4} - \left( \frac{\phi_h}{2} + L_n - x \right)^2 \right)^{\frac{3}{2}} \right)} \right) dx \quad \text{Eq. 8-16 a}$$

$$\Delta_{v\phi_h} = \int_{L_n}^{L_n+\phi_h} \left( \frac{P.f_{sn}.(L-x_c)}{G_n.L \left( A_{ow} - 2.t_w \left( \frac{\phi_h^2}{4} - \left( \frac{\phi_h}{2} + L_n - x \right)^2 \right)^{\frac{1}{2}} \right)} \right) dx \quad \text{Eq. 8-16 b}$$

*Eq. 8-16* can be simplified further and can be written as follows (*Eq. 8-17*). However, *Eq. 8-16a & Eq. 8-16b* can be easily integrated and incorporated in *Eq. 8-16* by providing web hole parameters i.e.  $L_n$ ,  $t_w$  and  $\Phi_h$ .

$$\Delta_{tx} = \frac{P.L^2.x}{81.E.I} + \frac{P.L^2.(L-x)}{81.E.I} + \frac{P.x.(8.L^2 - 18.L.x + 9.x^2)}{54.E.I} + \frac{P.f_s.x}{3.A.G} - \frac{P.(L-x).\gamma_{\phi h2}^3}{3.E.I.L} - \frac{P.(L-x).(L^2 - 9.x^2)}{54.E.I} + \frac{P.L_n^3.(L-x)}{3.E.I.L} + \frac{P.f_s.(L-x)(3.L_n - \gamma_{\phi h1})}{3.A.G.L} + \Delta_{b\phi_h} + \Delta_{v\phi_h} \quad \text{Eq. 8-17}$$

Where,

$$\begin{aligned} \gamma_{\phi h1} &= 3.\phi_h - L + 3.L_n \\ \gamma_{\phi h2} &= \phi_h + L_n \end{aligned}$$

$$\left\{ \begin{array}{l} \text{Eq. 8-17 a} \\ \text{Eq. 8-17 b} \end{array} \right.$$

#### 8.1.1.5 Retrofitted Circular Web Holed I-Joists

To develop the analytical models of retrofitted circular web hole I-joists, a similar approach of the flange notched I-joists was employed as presented in **Figure 8.5**. However, the variations of the cross-sectional area of the I-joists with respect to the longitudinal axis of the beam at the hole location has been considered. For mid span deflection profile of a web hole I-joist, integrating and combining *Eq. 8-13* and *Eq. 8-14* with much simplification yields to *Eq. 8-18*. However, *Eq. 8-16a & Eq. 8-16b* can be easily integrated and incorporated in *Eq. 8-16* by providing web hole parameters i.e.  $L_n$ ,  $t_w$ ,  $t_r$  and  $\Phi_h$ .



$$\begin{aligned}
\Delta_x = & \frac{P \cdot L^2 \cdot x}{81 \cdot E \cdot I} + \frac{P \cdot L^2 \cdot (L - x)}{81 \cdot E \cdot I} + \frac{P \cdot x \cdot (8 \cdot L^2 - 18 \cdot L \cdot x + 9 \cdot x^2)}{54 \cdot E \cdot I} + \frac{P \cdot f_s \cdot x}{3 \cdot A \cdot G} \\
& - \frac{P \cdot (L - x) \cdot \gamma_{r\phi_h 2}^3}{3 \cdot E_r \cdot I_r \cdot L} - \frac{P \cdot (L - x) \cdot (L - 3 \cdot x) \cdot (L + 3 \cdot x)}{54 \cdot E \cdot I} \\
& - \frac{P \cdot (L - x) \cdot \gamma_{r\phi_h 1}^3}{3 \cdot E \cdot I \cdot L} + \frac{P \cdot (L - x) \cdot \gamma_{r\phi_h 1}^3}{3 \cdot E_r \cdot I_r \cdot L} + \frac{P \cdot \gamma_{r\phi_h 3}^3 \cdot (L - x)}{3 \cdot E \cdot I \cdot L} \\
& + \frac{P \cdot L_d \cdot (L - x) \cdot \gamma_{r\phi_h 4}}{3 \cdot E_r \cdot I_r \cdot L} - \frac{P \cdot f_s \cdot (L - x) \cdot \gamma_{r\phi_h 5}}{3 \cdot A \cdot G \cdot L} + \frac{2 \cdot P \cdot L_d \cdot f_{sr} \cdot (L - x)}{A_r \cdot G_r \cdot L} \\
& + \frac{P \cdot f_s \cdot \gamma_{r\phi_h 3} \cdot (L - x)}{A \cdot G \cdot L} + \Delta_{br\phi_h} + \Delta_{vr\phi_h}
\end{aligned} \tag{Eq. 8-18}$$

Where,

$$\begin{aligned}
& \Delta_{br\phi_h} \\
& = \int_{L_n}^{L_n + \phi_h} \left( \frac{P \cdot x^2 \cdot (L - x_c)}{E_{rn} \cdot L \cdot \left( 2 \cdot I_{of} + I_{ow} + I_{ro} - 2 \cdot (t_r + t_w) \cdot \left( \frac{\phi_h^2}{4} - \left( \frac{\phi_h}{2} + L_n - x \right)^2 \right)^{\frac{3}{2}} \right)} \right) dx \tag{Eq. 8-18a}
\end{aligned}$$

$$\begin{aligned}
& \Delta_{vr\phi_h} = \int_{L_n}^{L_n + \phi_h} \left( \frac{P \cdot f_{srn} \cdot (L - x_c)}{G_{rn} \cdot L \cdot \left( A_{ow} + A_{ro} - 2 \cdot (t_r + t_w) \cdot \left( \frac{\phi_h^2}{4} - \left( \frac{\phi_h}{2} + L_n - x \right)^2 \right)^{\frac{1}{2}} \right)} \right) dx \tag{Eq. 8-18 b}
\end{aligned}$$

$$\begin{aligned}
\gamma_{r\phi_h 1} &= \phi_h + L_n + L_d \\
\gamma_{r\phi_h 2} &= \phi_h + L_n \\
\gamma_{r\phi_h 3} &= L_n - L_d \\
\gamma_{r\phi_h 4} &= 3 \cdot L_n^2 - 3 \cdot L_n \cdot L_d + L_d^2 \\
\gamma_{r\phi_h 5} &= 3 \cdot \phi_h - L + 3 \cdot L_n + 3 \cdot L_d
\end{aligned} \tag{Eq. 8-18 (c-g)}$$

## 8.1.2 Maximum Deflection:

### 8.1.2.1 Flange Notched I-Joists

By combining equations *Eq. 8-12*, *Eq. 8-12a* & *Eq. 8-12b*, the location of maximum deflection ( $X_{\Delta max}$ ) can be determined by differentiating that to zero (i.e.  $d\Delta_{tx}/dx = 0$ ;) and after much manipulations, yields to-

$$X_{\Delta max} = \left( \frac{\alpha_{n1} - \alpha_{n2} + \alpha_{n3} - \beta_{n1} + \beta_{n2} - \beta_{n3} - \beta_{n4} + \beta_{n5} + \beta_{n6}}{2 \cdot \alpha_{n3}} \right) \cdot L \quad \text{Eq. 8-19}$$

Where,

$$\alpha_{n1} = 2 \cdot A \cdot An \cdot Bn^3 \cdot En \cdot G \cdot Gn \cdot In$$

$$\alpha_{n2} = 2 \cdot A \cdot An \cdot Bn^3 \cdot E \cdot G \cdot Gn \cdot I$$

$$\alpha_{n3} = A \cdot An \cdot En \cdot G \cdot Gn \cdot In \cdot L^3$$

$$\beta_{n1} = 6 \cdot A \cdot Bn \cdot E \cdot En \cdot G \cdot I \cdot In \cdot f_{sn}$$

$$\beta_{n2} = 6 \cdot An \cdot Bn \cdot E \cdot En \cdot Gn \cdot I \cdot In \cdot f_s$$

$$\beta_{n3} = 6 \cdot A \cdot An \cdot Bn \cdot E \cdot G \cdot Gn \cdot I \cdot Ln^2$$

$$\beta_{n4} = 6 \cdot A \cdot An \cdot Bn^2 \cdot E \cdot G \cdot Gn \cdot I \cdot Ln$$

$$\beta_{n5} = 6 \cdot A \cdot An \cdot Bn \cdot En \cdot G \cdot Gn \cdot In \cdot Ln^2$$

$$\beta_{n6} = 6 \cdot A \cdot An \cdot Bn^2 \cdot En \cdot G \cdot Gn \cdot In \cdot Ln$$

Eq. 8-19 (a-i)

By setting the notch parameters equal to zero (*i.e.*  $B_n=0$ ,  $D_n=0$ , &  $L_n=0$ ) and all section and material properties equal to the control I-joists properties (*i.e.*  $A_n=A$ ,  $I_n=I$ ,  $E_n=E$ ,  $G_n=G$ ,  $f_{sn}=f_s$ ) into **Eq. 8-19**, the location of maximum deflection ( $X_{\Delta max}$ ) becomes the half of the span length **Eq. 8-20**, which is the location of maximum deflection of control I-joists as found in **Eq. 8-8**.

$$X_{\Delta max}^{Check} = \frac{L}{2} \quad \text{Eq. 8-20}$$

When,  $B_n = 0$ ;  $D_n = 0$ ;  $L_n = 0$ ;  $I_n = I$ ;  $E_n = E$ ;  $A_n = A$ ;  $G_n = G$ ;  $f_{sn} = f_s$

The maximum deflection  $\Delta_{max}$  at  $X_{\Delta max}$  through **Eq. 8-12**, **Eq. 8-12a**, **Eq. 8-12b** & **Eq. 8-19**, becomes:

$$\begin{aligned} \Delta_{max} = & \frac{L^2 \cdot P \cdot (L - X_{\Delta max})}{81 \cdot E \cdot I} + \frac{Ln^3 \cdot P \cdot (L - X_{\Delta max})}{\frac{3 \cdot E \cdot I \cdot L}{P \cdot (L - X_{\Delta max}) \cdot (L - 3 \cdot X_{\Delta max}) \cdot (L + 3 \cdot X_{\Delta max})}} \\ & - \frac{54 \cdot E \cdot I}{P \cdot (Bn + Ln)^3 \cdot (L - X_{\Delta max})} + \frac{Bn \cdot P \cdot f_{sn} \cdot (L - X_{\Delta max})}{\frac{3 \cdot E \cdot I \cdot L}{Ln \cdot P \cdot f_s \cdot (L - X_{\Delta max})} - \frac{An \cdot Gn \cdot L}{P \cdot f_s \cdot (L - X_{\Delta max}) \cdot (3 \cdot Bn - L + 3 \cdot Ln)}} \\ & + \frac{A \cdot G \cdot L}{Bn \cdot P \cdot (L - X_{\Delta max}) \cdot (Bn^2 + 3 \cdot Bn \cdot Ln + 3 \cdot Ln^2)} + \frac{P \cdot L^2 \cdot X_{\Delta max}}{\frac{3 \cdot En \cdot In \cdot L}{P \cdot f_s \cdot X_{\Delta max}} + \frac{P \cdot (8 \cdot L^2 - 18 \cdot X_{\Delta max} \cdot L + 9 \cdot (X_{\Delta max})^2) \cdot X_{\Delta max}}{54 \cdot E \cdot I}} \\ & + \frac{81 \cdot E \cdot I}{3 \cdot A \cdot G} \end{aligned} \quad \text{Eq. 8-21}$$

Again by setting the notch parameters equal to zero (*i.e.*  $B_n=0$ ,  $D_n=0$ , &  $L_n=0$ ) and all section and material properties equal to the control I-joists properties (*i.e.*  $A_n=A$ ,  $I_n=I$ ,  $E_n=E$ ,  $G_n=G$ ,  $f_{sn}=f_s$ ) into **Eq. 8-21**, the maximum deflection ( $\Delta_{\max}$ ) becomes **Eq. 8-22**, which is the maximum deflection of control I-joists as found in **Eq. 8-9**.

$$\Delta_{Max}^{Check (x=\frac{L}{2})} = \frac{23 \cdot P \cdot L^3}{648 \cdot E \cdot I} + \frac{P \cdot L \cdot f_s}{3 \cdot A \cdot G} \quad \text{Eq. 8-22}$$

When,  $B_n = 0$ ;  $D_n = 0$ ;  $L_n = 0$ ;  $I_n = I$ ;  $E_n = E$ ;  $A_n = A$ ;  $G_n = G$ ;  $f_{sn} = f_s$

### 8.1.2.2 Retrofitted Flange Notched I-Joists

By combining equations **Eq. 8-15**, **Eq. 8-15a** & **Eq. 8-15b**, the location of maximum deflection ( $X_{\Delta_{\max}}$ ) can be determined by differentiating that at zero (*i.e.*  $d\Delta_{tx}/dx = 0$ ;) and after much manipulations, yields to

$$X_{\Delta_{\max}} = \frac{3 \cdot E \cdot I}{L^2} \left( \frac{2 \cdot \gamma_{rn3}^3 - 2 \cdot \gamma_{rn1}^3 - L^3}{6 \cdot E \cdot I} + \frac{\gamma_{rn1}^3 - \gamma_{rn2}^3 + L_d \cdot \gamma_{rn4}}{3 \cdot E_r \cdot I_r} + \frac{\gamma_{rn6}}{3 \cdot E_{rn} \cdot I_{rn}} \right. \\ \left. + \frac{f_s \cdot (3 \cdot \gamma_{rn3} - L)}{3 \cdot A \cdot G} - \frac{f_s \cdot \gamma_{rn5}}{3 \cdot A \cdot G} + \frac{2 \cdot L_d \cdot f_{sr}}{A_r \cdot G_r} + \frac{B_n \cdot f_{srn}}{A_{rn} \cdot G_{rn}} \right) \quad \text{Eq. 8-23}$$

Where,

$$\left. \begin{aligned} \gamma_{rn1} &= B_n + L_n + L_d \\ \gamma_{rn2} &= B_n + L_n \\ \gamma_{rn3} &= L_n - L_d \\ \gamma_{rn4} &= 3 \cdot L_n^2 - 3 \cdot L_n \cdot L_d + L_d^2 \\ \gamma_{rn5} &= 3 \cdot B_n - L + 3 \cdot L_n + 3 \cdot L_d \\ \gamma_{rn6} &= B_n^3 + 3 \cdot B_n^2 \cdot L_n + 3 \cdot B_n \cdot L_n^2 \end{aligned} \right\} \quad \text{Eq. 8-23 (a-f)}$$

By setting the notch parameters equal to zero (*i.e.*  $B_n=0$ ,  $D_n=0$ ,  $L_n=0$ , &  $L_d=0$ ) and all section and material properties equal to the control I-joists properties (*i.e.*  $A_m=A_n=A$ ,  $I_m=I_n=I$ ,  $E_m=E_n=E$ ,  $G_m=G_n=G$ ,  $I_m=I_n=I$ ) into **Eq. 8-23**, the location of maximum deflection ( $X_{\Delta_{\max}}$ ) becomes the half

of the span length *Eq. 8-24*, which is the location of maximum deflection of control I-joists as found in *Eq. 8-8*.

$$X_{\Delta max}^{Check} = \frac{L}{2} \quad \text{Eq. 8-24}$$

$$\text{When, } B_n = 0; D_n = 0; L_n = 0; L_d = 0; I_{rn} = I_n = I; E_{rn} = E_n = E; A_{rn} = A_n = A; G_{rn} = G_n = G; f_{srn} = f_{sn} = f_s$$

The maximum deflection  $\Delta_{max}$  at  $X_{\Delta max}$  through *Eq. 8-15*, *Eq. 8-15a*, *Eq. 8-15b* & *Eq. 8-23*, becomes

$$\begin{aligned} \Delta_{max} = & \frac{PL^3}{81EI} + \frac{PX_{\Delta max}(8L^2 - 18LX_{\Delta max} + 9X_{\Delta max}^2)}{54EI} \\ & - \frac{P(L - X_{\Delta max})(L^2 - 9X_{\Delta max}^2)}{54EI} \\ & + \frac{P(L - X_{\Delta max})((\gamma_{n3})^3 - (\gamma_{n1})^3)}{3EIL} \\ & + \frac{P(L - X_{\Delta max})((\gamma_{n1})^3 - (\gamma_{n2})^3 + L_r\gamma_{n4})}{3E_rI_rL} + \frac{P(L - X_{\Delta max})\gamma_{n6}}{3E_{rn}I_{rn}L} \\ & - \frac{Pf_s(L - X_{\Delta max})(\gamma_{n5} - 3\gamma_{n3})}{3AGL} + \frac{PX_{\Delta max}f_s}{3AG} \\ & + \frac{B_nPf_{srn}(L - X_{\Delta max})}{A_{rn}G_{rn}L} + \frac{2L_r \cdot P \cdot f_{sr}(L - X_{\Delta max})}{A_rG_rL} \end{aligned} \quad \text{Eq. 8-25}$$

Where,

$$\begin{aligned} \gamma_{rn1} &= B_n + L_n + L_d \\ \gamma_{rn2} &= B_n + L_n \\ \gamma_{rn3} &= L_n - L_d \\ \gamma_{rn4} &= 3 \cdot L_n^2 - 3 \cdot L_n \cdot L_d + L_d^2 \\ \gamma_{rn5} &= 3 \cdot B_n - L + 3 \cdot L_n + 3 \cdot L_d \\ \gamma_{rn6} &= B_n^3 + 3 \cdot B_n^2 \cdot L_n + 3 \cdot B_n \cdot L_n^2 \end{aligned} \quad \left. \vphantom{\begin{aligned} \gamma_{rn1} &= B_n + L_n + L_d \\ \gamma_{rn2} &= B_n + L_n \\ \gamma_{rn3} &= L_n - L_d \\ \gamma_{rn4} &= 3 \cdot L_n^2 - 3 \cdot L_n \cdot L_d + L_d^2 \\ \gamma_{rn5} &= 3 \cdot B_n - L + 3 \cdot L_n + 3 \cdot L_d \\ \gamma_{rn6} &= B_n^3 + 3 \cdot B_n^2 \cdot L_n + 3 \cdot B_n \cdot L_n^2 \end{aligned}} \right\} \quad \text{Eq. 8-25 (a-f)}$$

Again by setting the notch parameters equal to zero (*i.e.*  $B_n=0$ ,  $D_n=0$ ,  $L_n=0$ , &  $L_d=0$ ) and all section and material properties equal to the control I-joists properties (*i.e.*  $A_n=A_m=A$ ,  $I_n=I_m=I$ ,  $E_n=E_m=E$ ,  $G_n=G_m=G$ ,  $I_n=I_m=I$ ) into *Eq. 8-25*, the maximum deflection ( $\Delta_{max}$ ) becomes *Eq. 8-26*, which is the maximum deflection of control I-joists as found in *Eq. 8-9*.

$$\Delta_{Max}^{Check (x=\frac{L}{2})} = \frac{23.P.L^3}{648.E.I} + \frac{P.L.fs}{3.A.G} \quad Eq. 8-26$$

$$\text{When, } B_n = 0; D_n = 0; L_n = 0; L_d = 0; I_{rn} = I_n = I; E_{rn} = E_n = E; A_{rn} = A_n \\ = A; G_{rn} = G_n = G; f_{srn} = f_{sn} = f_s$$

## 8.2 Validation of Analytical Models

In the following sections, developed analytical models have been validated with the experimental results obtained from the four point bending test. Validation has been done for different I-joist series having a flange notch or a web hole at different locations and their retrofitted I-joist with OSB Collars (Type-T2) and GFRP Plates (Type-T1, T2 & T3). Details of flange notch and web hole I-joists and their retrofitted one are presented in previous chapters (*Table 5.1, Table 6.1, Table 7.4 and Table 7.5*). To validate the analytical models, different required parameters are presented in chapter 7 (*Table 7.1*).

### 8.2.1 Control I-joists

To validate the analytical results with the experimental results (as discussed in the earlier chapter; Chapter 4), *Eq. 8-6* and *Eq. 8-7* were used to calculate the bending and shear deflection of the control I-joists respectively. Comparison of the analytical results and experimental results are presented in *Figure 8.6* for 12 feet and 20 feet control I-joists. Analytical models for 12 feet and 20 feet control I-joists can underestimate and overestimate the deflection with a -2% and +3% error compared to the best fitted experimental results. Total deflection of 12 ft and 20 ft control I-joists were 28.05 mm and 72.52 mm. Deflection due to shear was significant, which are 12.29 mm (44% of total deflection) and 15.39 mm (21.22% of total deflection) for 12 ft and 20 ft control I-joist, respectively.

### 8.2.2 Flange Notched I-joists

The deflection of the flange notched I-joists (Series 12-F, 12-G, 12-H, 12-I, 20-K, 20-L, 20-M & 20-N) were calculated based on the proposed analytical models presented in *Eq. 8-12* and compared with the best fitted experimental models as shown in *Figure 8.7*. The performance factors of the analytical models of flange notched I-joists are summarized in *Table 8.1*. It is found that the maximum error (24%) was observed for series 12-H which has a notch of 100 mm x 100 mm at 610 mm from the support.

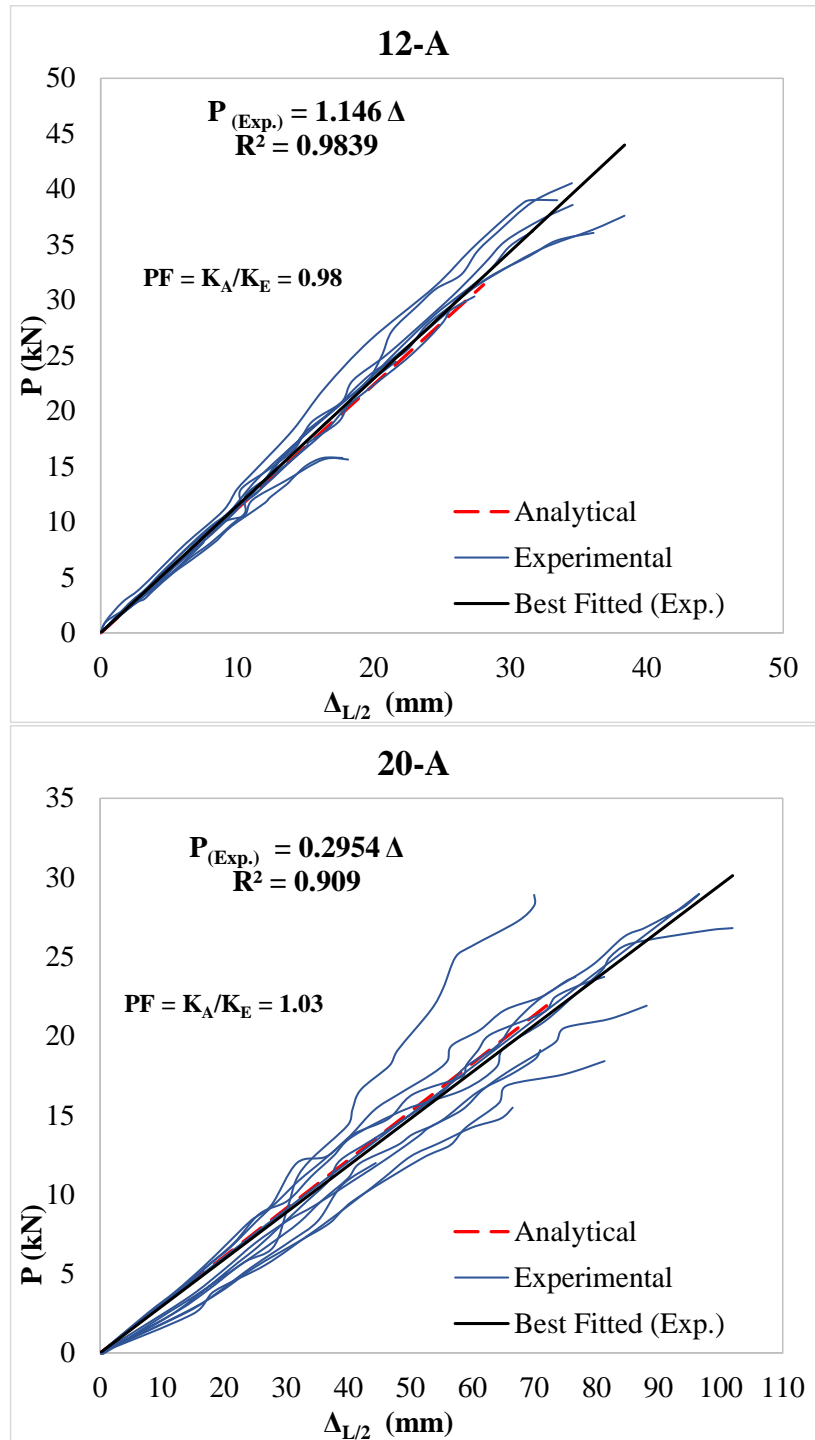


**Figure 8.6 Comparison between Analytical Models and Experimental Results of Control I-joists.**

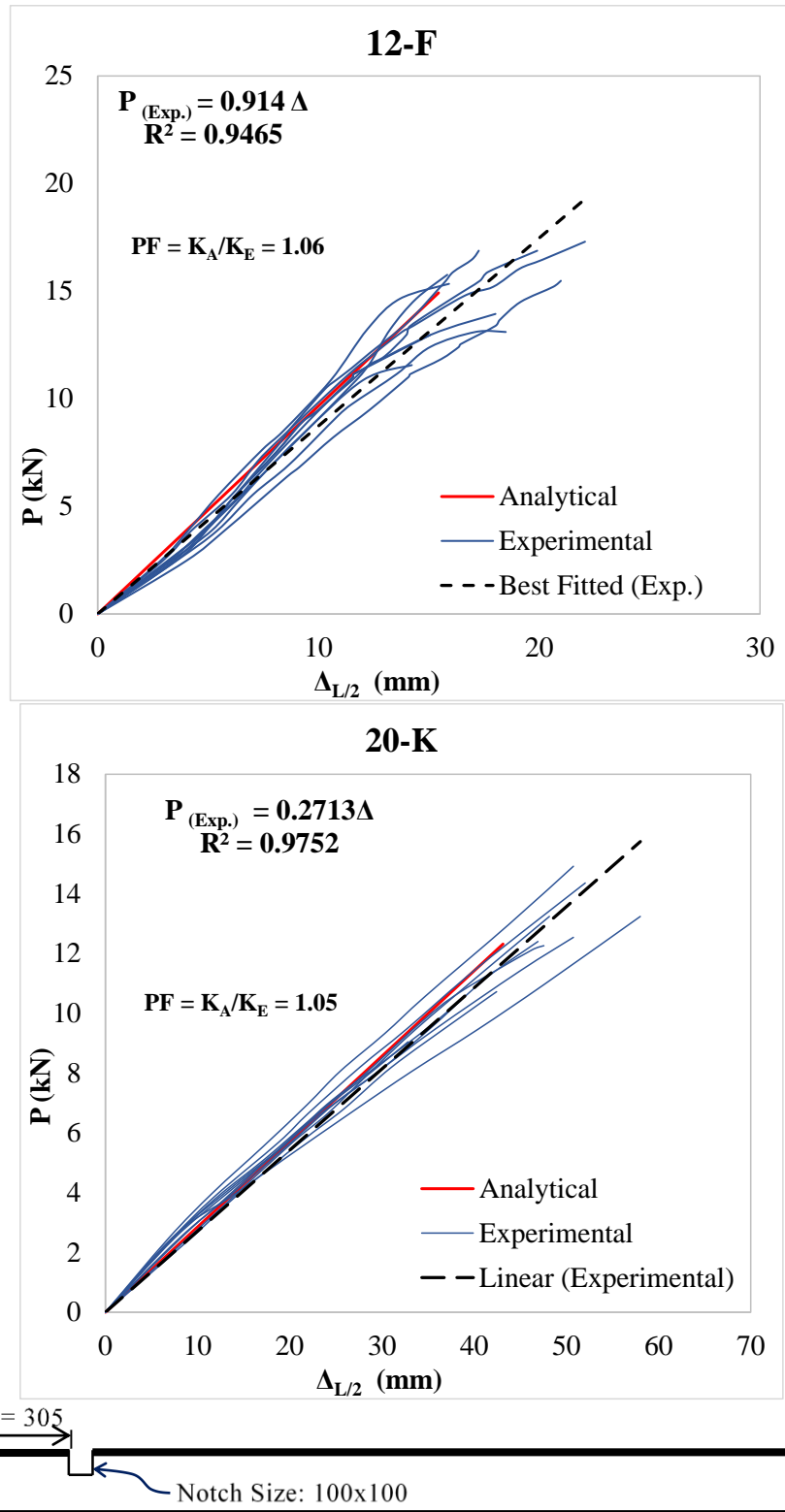


**Figure 8.7 Comparison between Analytical Models and Experimental Results of Flange Notched I-joists.**



**Table 8.1 Performance of Analytical models of Control and Flange Notched I-joists.**

Series	Type	P <sub>u</sub> kN	$\Delta_{(L/2) A}$ (mm)	K <sub>A</sub> (N/mm)	X <sub>max<math>\Delta</math></sub>	$\Delta_{(max).A}$	$\Delta_{(L/2) E}$ (mm)	Avg. K <sub>E</sub> (N/mm)	PF
12-A	Control	31.4	28	1119	1779	28	29.9	1146	0.98
12-F	FN	14.9	16	932	1740	16	17.7	914	1.06
12-G	FN	9.2	11	858	1707	11	13.7	701	1.22
12-H	FN	6.4	8	830	1659	8	10.2	667	1.24
12-I	FN	5.7	7	791	1589	7	10.6	684	1.16
20-A	Control	22.1	73	304	2998	73	79.1	295	1.03
20-K	FN	12.3	43	286	2984	43	52.1	271	1.05
20-L	FN	9.7	36	273	2972	36	42.8	258	1.06
20-M	FN	6.7	25	270	2956	25	28.5	262	1.03
20-N	FN	5.5	22	250	2931	22	25.4	209	1.19

### 8.2.3 Retrofitted Flange Notched I-joists

The deficient flange notched I-joists were retrofitted with OSB collars and their performances were compared with the analytically calculated deflection using **Eq. 8-15**. The performance factors of the analytical models of the retrofitted I-joists with a flange notch (100x100 & 100x150) are summarized in **Table 8.2**. Analytical models of series R-12-SF and R-20-SF joists overestimated the deflection by +12% and +9% for 12 feet and 20 feet joist respectively as shown in **Figure 8.8**. Similar kind of result is observed for 100x100mm and other series of 100x150mm notch size retrofitted with Type-T2 OSB collars (as described in previous chapter). In this case, the analytical models overestimated the deflection by +6% to +12% and +4% to +9% for 12 feet and 20 feet joist, respectively. Deficient flange notched I-joist was retrofitted with a pre-fabricated GFRP Plates (Type-T1, T2 & T3) and similar results were obtained for GFRP retrofitted flange notched I-joists as shown in **Figure 8.9** and **Table 8.3**.

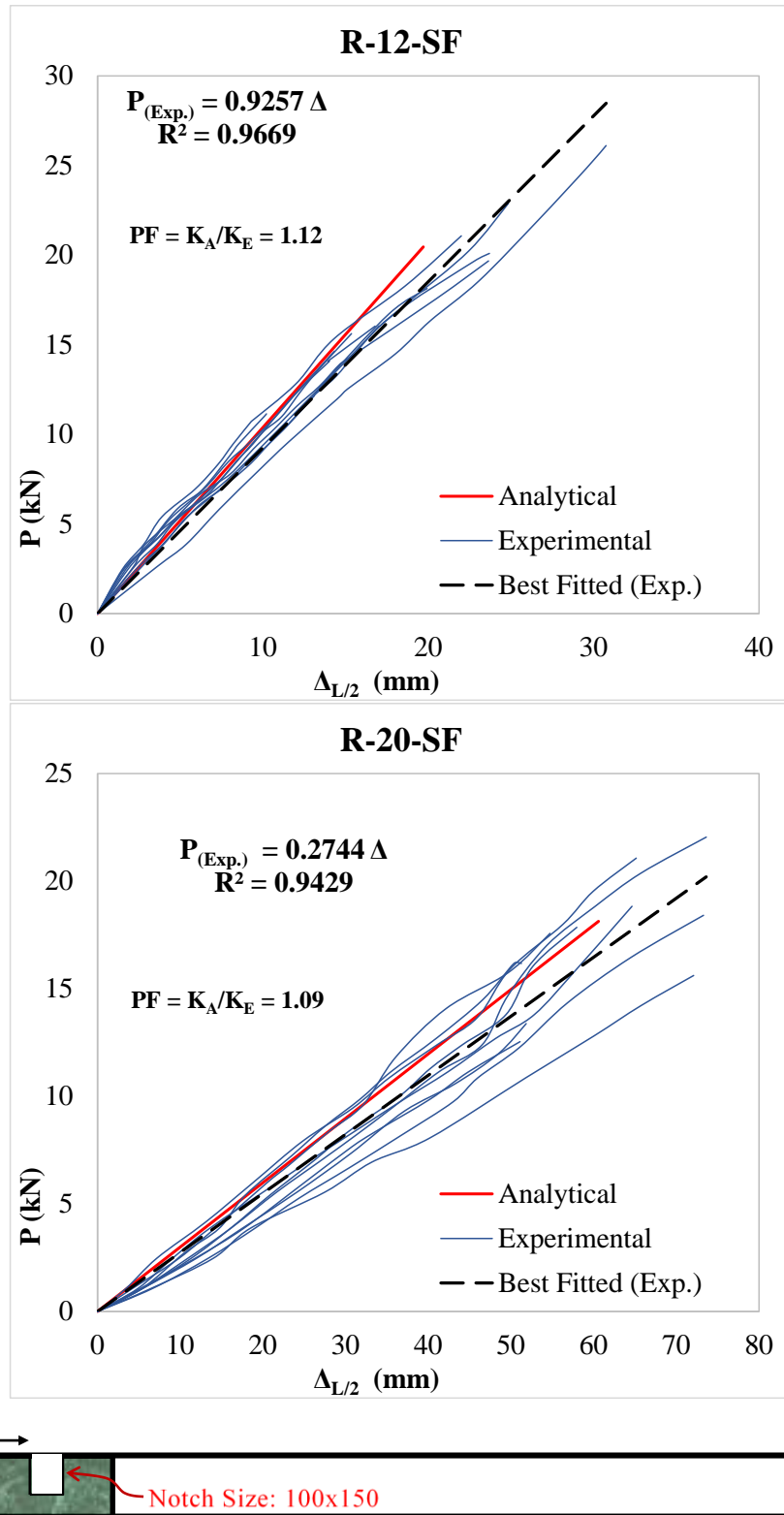


**Figure 8.8 Comparison between Analytical Models and Experimental Results of Flange Notched I-joists Retrofitted with OSB Collars (Type 2).**

**Table 8.2 Performance of Analytical models of Flange Notched I-joists Retrofitted with OSB Collars (Type 2).**

Series	Type	P <sub>u</sub> kN	$\Delta_{(L/2)A}$ (mm)	K <sub>A</sub> (N/mm)	X <sub>max<math>\Delta</math></sub>	$\Delta_{(max).A}$	$\Delta_{(L/2)E}$ (mm)	Avg. K <sub>E</sub> (N/mm)	PF
R-12-OF	FNR	34.2	30.5	1119.5	1926.9	30.7	34.4	1056.2	1.06
R-12-SF	FNR	20.5	19.7	1038.4	1946.6	19.8	25.2	925.7	1.12
R-20-OF	FNR	24.5	82.3	297.6	3050.1	82.3	92.2	287.2	1.04
R-20-PF	FNR	22.6	75.9	297.0	3047.2	76.0	82.5	283.0	1.05
R-20-QF	FNR	20.0	67.4	296.2	3043.1	67.4	71.9	277.2	1.07
R-20-RF	FNR	20.6	67.1	306.4	3095.1	67.2	73.3	283.7	1.08
R-20-SF	FNR	18.1	60.6	299.3	3059.1	60.6	64.1	274.4	1.09

**Table 8.3 Performance of Analytical models of Flange Notched I-joists Retrofitted with GFRP Plates (Type T-1, T-2 & T-3)**

Series	Type	P <sub>u</sub> kN	$\Delta_{(L/2)A}$ (mm)	K <sub>A</sub> (N/mm)	X <sub>max<math>\Delta</math></sub>	$\Delta_{(max).A}$	$\Delta_{(L/2)E}$ (mm)	Avg. K <sub>E</sub> (N/mm)	PF
R-12-HH-T1	FNR	30.4	28	1081	1885	28	25	1042	1.04
R-12-HH-T2	FNR	34.3	31	1093	1899	31	29	1163	0.94
R-12-II-T1	FNR	30.8	29	1077	1880	29	29	1091	0.99
R-12-II-T2	FNR	35.2	30	1182	1891	30	30	1146	1.03
R-12-II-T3	FNR	40.1	37	1082	1886	37	41	994	1.09
R-20-MM-T1	FNR	23.2	87	266.6	3035	87	90	248	1.08
R-20-MM-T2	FNR	20.8	78	267.4	3040	78	80	250	1.07
R-20-NN-T1	FNR	22.1	83	266	3034	83	90	233	1.14
R-20-NN-T2	FNR	22.3	76	295	3037	76	84	260	1.14

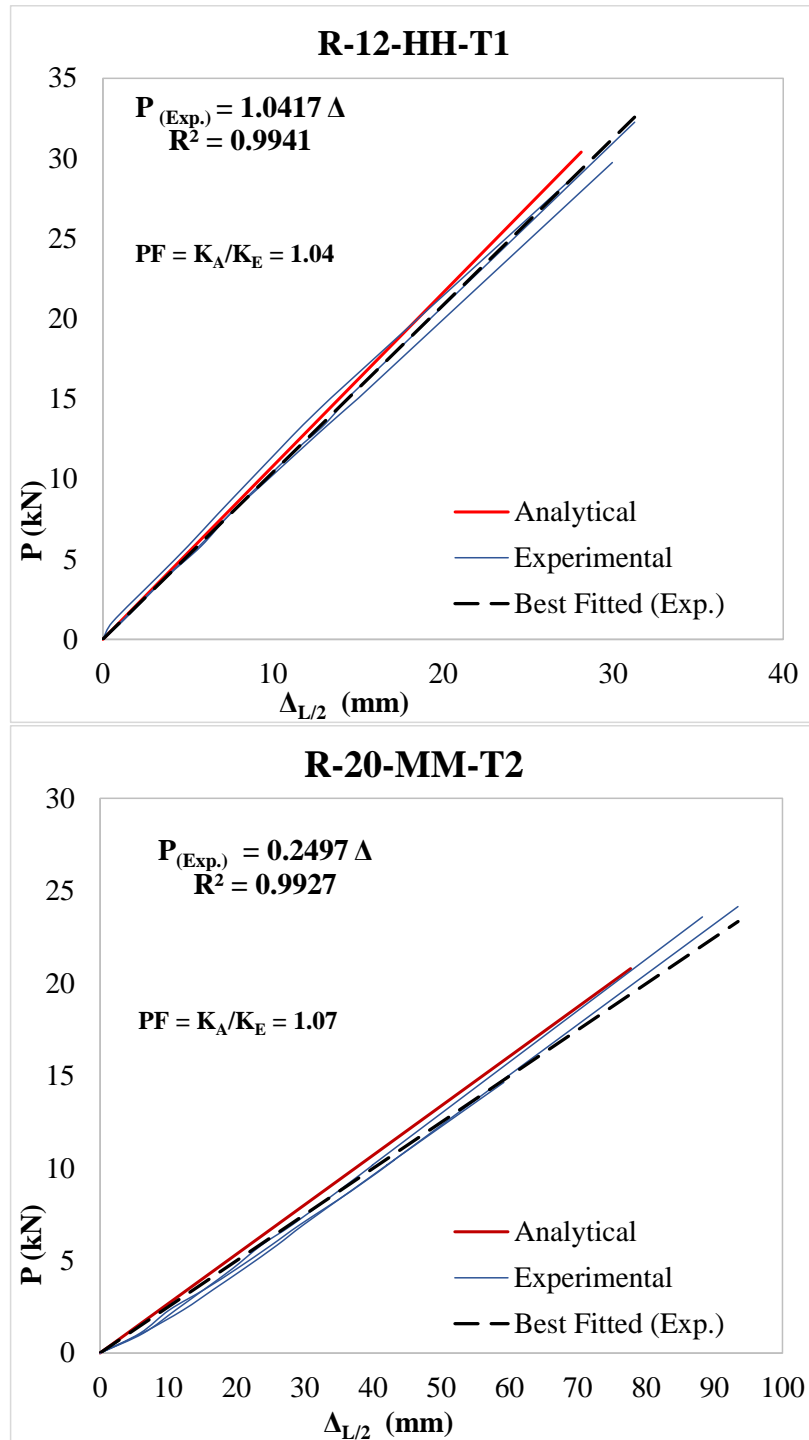


**Figure 8.9 Comparison between Analytical Models and Experimental Results of Flange Notched I-joists Retrofitted with GFRP Plates (Type 1 & Type 2).**

### 8.2.4 Web Holed I-joists

The deflection of the web holed I-joists (Series 12-B, 12-C, 12-D, 12-E, 20-B, 20-C, 20-D & 20-E) were calculated based on the proposed analytical models presented in *Eq. 8-16, Eq. 8-16 a & Eq. 8-16 b* and compared with the best fitted experimental models as shown in *Figure 8.10*. Performance factors of the analytical models of flange notched I-joists are summarized in *Table 8.4*. It is found that the performance factors (PF) are very close to 1 for all web holed I-joist series. The percent error of the analytical models compared to the best fitted experimental results varies only -3% to +5% and  $\pm 5\%$  for 12 feet and 20 feet web holed I-joists, respectively.

**Table 8.4 Performance of Analytical models of Web Holed I-joists.**

Series	Type	Pu kN	$\Delta_{(L/2)A}$ (mm)	$K_A$ (N/mm)	$X_{max\Delta}$	$\Delta_{(max).A}$	$\Delta_{(L/2)E}$ (mm)	Avg. $K_E$ (N/mm)	PF
12-A	Control	31.4	28	1119	1779	28	30	1146	0.98
12-B	WH	15.2	15	1002.7	1789	15	17.9	953.5	1.05
12-C	WH	14.5	15	1002.4	1789	15	17.1	995.3	1.01
12-D	WH	22.2	22	1001.1	1787	22	29.1	978.4	1.02
12-E	WH	30.6	31	997.9	1783	31	33.7	1025.7	0.97
20-A	Control	22.1	73	304	2998	73	79	295	1.03
20-B	WH	17.4	55	316.14	3002	55	56.2	325.5	0.97
20-C	WH	16.9	53	316.07	3001	53	61.3	303.2	1.04
20-D	WH	23.6	75	315.99	3001	75	75.8	327.6	0.96
20-E	WH	20.8	66	315.69	3000	66	80.9	309.0	1.02

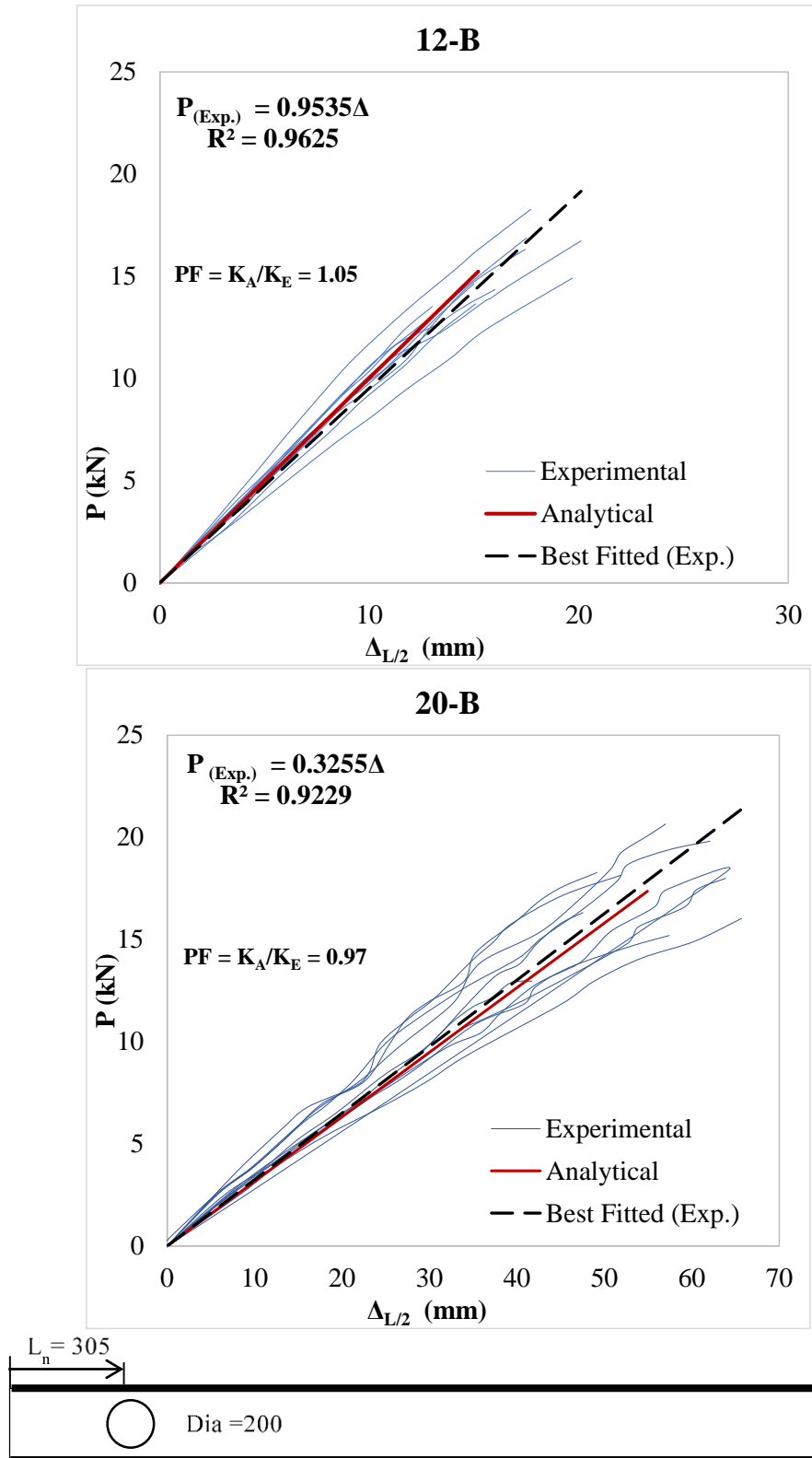


**Figure 8.10 Comparison between Analytical Models and Experimental Results of Web Holed I-joists.**

### 8.2.5 Retrofitted Web Holed I-joists

The deficient web holed I-joists were retrofitted with OSB collars and their performances were compared with the analytically calculated deflection using *Eq. 8-18*. The performance factors of the analytical models of the retrofitted I-joists with a web hole ( $\Phi_h = 200$  & 150 mm) are summarized in *Table 8.5*. Analytical models of the joists with a hole of 200mm retrofitted with OSB collar (Type-T2) overestimated the deflection by +7% for 12 feet and perfectly estimated the deflection for 20 feet joist as shown in *Figure 8.11*. Similar kind of result is observed for 150 mm and other series of 200mm hole size retrofitted with Type -T2 OSB collar (as described in previous chapter). In this case, the analytical models estimated the deflection by -1% to +8% and -4% to +8% for 12 feet and 20 feet joist, respectively. Deficient flange notched I-joists were retrofitted with a pre-fabricated GFRP Plates (Type-T1, T2 & T3) and similar results were obtained for GFRP retrofitted flange notched I-joists as shown in *Figure 8.12* and *Table 8.6*. From *Table 8.6*, it can be seen that the performance factors (PF) for series 20-BB-T4/2 and 20-DD-T4/2 were 1.32 and 1.34, respectively. These higher percentage errors for estimation of deflection were observed as the experimental stiffness were low compared to the other retrofitted I-joist. The experimental stiffness of these two series were low because a different adhesive (Polyester Resin) was used to attach the GFRP Plates, which has a lower stiffness and strength compared to those of the adhesive (Sika dur-30) used for other series.

**Table 8.5 Performance of Analytical models of Web Holed I-joists Retrofitted with OSB Collars.**

Series	Type	Pu kN	$\Delta_{(L/2) A}$ (mm)	$K_A$ (N/mm)	$X_{max\Delta}$	$\Delta_{(max).A}$	$\Delta_{(L/2) E}$ (mm)	Avg. $K_E$ (N/mm)	PF
12-A	Control	31.4	28	1119	1779	28	30	1146	0.98
R-12-F(J)	WHR	17.3	16	1106.6	1913	16	21	1031	1.07
R-12-G(K)	WHR	17.3	16	1108.4	1915	16	24	1094	1.01
R-12-H(L)	WHR	28.2	26	1075.7	1879	26	32	996	1.08
R-12-I(M)	WHR	31.6	30	1046.8	1845	30	32	1054	0.99
R-12-J(N)	WHR	35.9	33	1084.0	1888	33	36	1098	0.99
20-A	Control	22.1	73	304	2998	73	79	295	1.03
R-20-F	WHR	18.0	61	296.6	3045	61	63	297.0	1.00
R-20-G	WHR	18.7	63	296.8	3046	63	73	273.9	1.08
R-20-H	WHR	25.1	85	294.4	3033	85	88	295.4	1.00
R-20-I	WHR	25.1	86	292.2	3021	86	87	296.0	0.99
R-20-J	WHR	22.6	77	295.0	3037	77	75	306.3	0.96



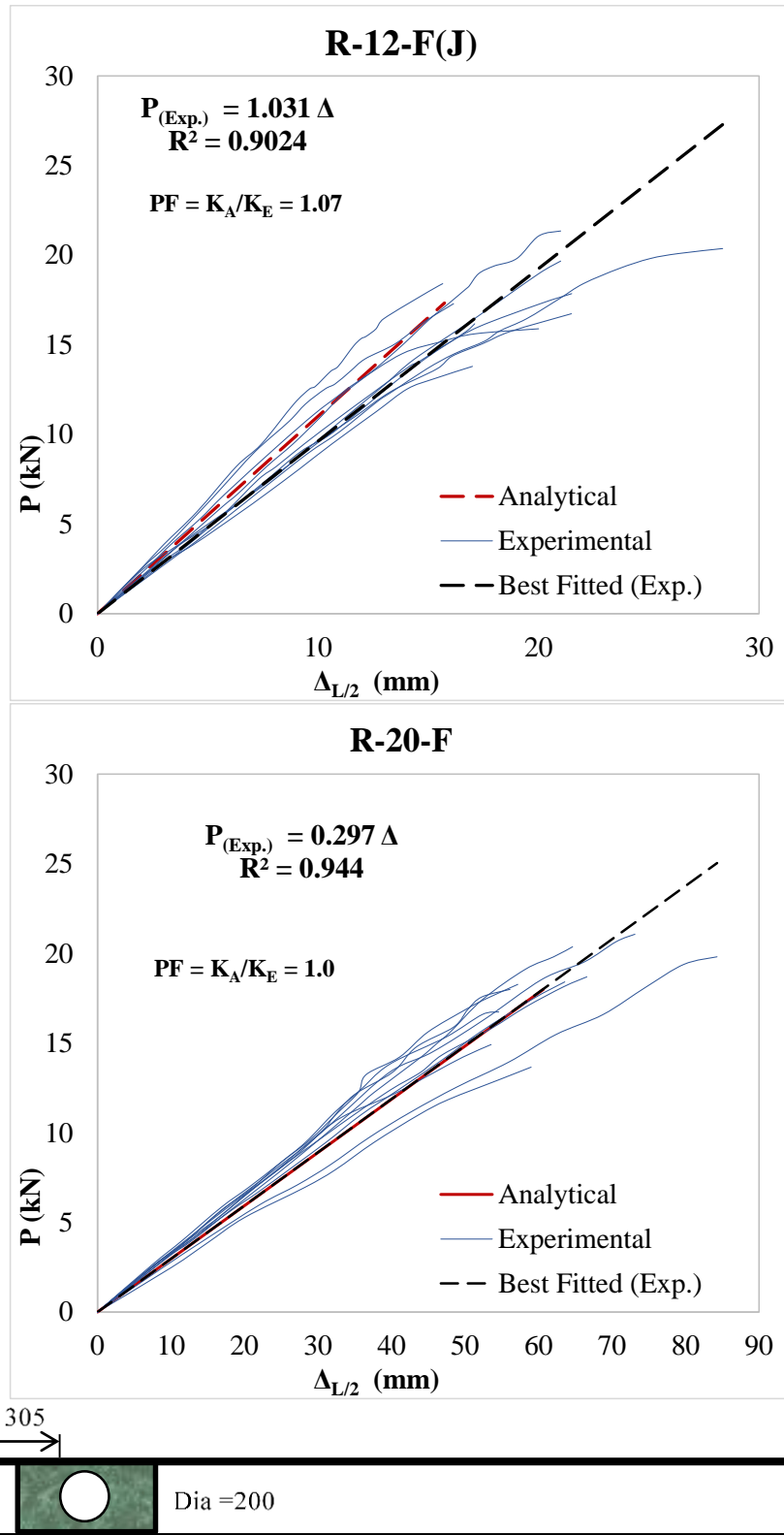


**Figure 8.11 Comparison between Analytical Models and Experimental Results of Web Holed I-joists Retrofitted with OSB Collars.**

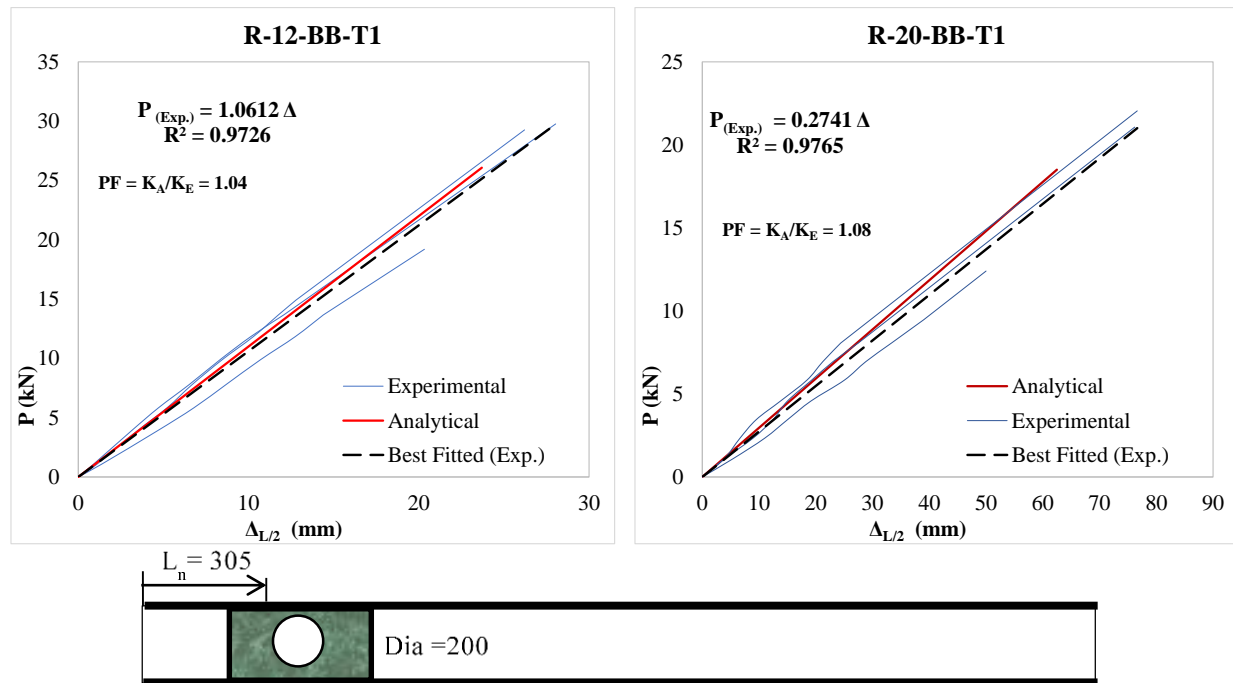


**Figure 8.12 Comparison between Analytical Models and Experimental Results of Flange Notched I-joists Retrofitted with GFRP Plates (Type 1 & Type 2).**

**Table 8.6 Performance of Analytical models of Flange Notched I-joists Retrofitted with GFRP Plates (Type T-1, T-2 & T-3)**

Series	Type	Pu kN	$\Delta_{(L/2) A}$ (mm)	$K_A$ (N/mm)	$X_{max\Delta}$	$\Delta_{(max).A}$	$\Delta_{(L/2) E}$ (mm)	Avg. $K_E$ (N/mm)	PF
R-12-BB-T1	WHR	26.1	24	1100	1906	24	21	1061.2	1.04
R-12-BB-T2	WHR	31.0	23.8	1303.8	1915.7	23.9	21.8	1362.5	0.96
R-12-BB-T3	WHR	32.8	29.8	1101.1	1907.2	29.9	31.6	1047.7	1.05
R-12-DD-T1	WHR	44.9	37.2	1206.2	1895.8	37.4	33.1	1264.4	0.95
R-12-DD-T2	WH	45.8	35.5	1289.7	1902.4	35.7	34.6	1354.3	0.95
R-20-BB-T1	WH	18.5	62.5	296.2	3042.8	62.5	73.2	274.1	1.08
R-20-BB-T4/2	WH	16.2	54.7	296.5	3044.7	54.7	72.9	224.0	1.32
R-20-DD-T1	WH	24.8	78.7	315.1	3038.9	78.7	78.3	269.2	1.17
R-20-DD-T4/2	WH	20.7	65.3	317.2	3040.7	65.3	86.1	237.5	1.34

### 8.3 Summary

In this chapter, analytical models were developed to evaluate the stiffness of OSB webbed composite I-beams with a flange notch or a web hole and their retrofitted one with the conventional

OSB collars and GFRP plates. Experimental tests were carried out to verify the analytical solutions. The analytical solutions were obtained based on the energy method. Good correlations have been obtained between the analytical solutions and experimental results.

- Depth to span length ratio ( $D/L = 0.049$ ) is very low for the 20 ft I-joist hence the stiffness of 20 ft web holed I-joists are based on the stiffness of the two flanges. The change of effective depth to span ratio [ $(D-\Phi)/L = 0.033, 0.025$  &  $0.0166$ ] is negligible for web holes I-joists, hence the stiffness of the 20ft web hole Joists are almost same as per the developed analytical models.
- The maximum deflection and the mid-span deflection are very close for all I-joist series as the location of maximum deflection ( $X_{\Delta_{max}}$ ) found to be very close to the half of the span length ( $L/2$ ).
- The deflection due to shear contributes 30-40% of the total deflection of the maximum deflection as determined by the developed analytical models, hence as suggested by (**Booth 1974**), the deflection due to shear cannot be overlooked.
- Types and mechanical properties of glue was used to retrofit the deficient I-joist has a significant effect on the performance of retrofitted I-joists having a flange notch and web hole. Hence, the types of glue should be incorporated in the analytical model development.
- The performance of analytical model can be further improved by incorporating the effects of Moment-Shear interaction on the I-joists having a flange notch or web hole.

## **CHAPTER 9: CONCLUSIONS**

### **9.1 Summary**

Timber I-joist is a common building construction element in North America and Europe due to its availability and easiness of passing the service conduits and ducts through openings in the Oriented Strand Board (OSB) web of I-joists. However, in order to provide passageway for service conduits and ducts, cuts and notches in the flange of I-joist are frequently made during construction without considering the structural integrity of the system. Flange stiffness is very critical as it provides the flexural strength to the I-joist, hence it is prohibited to cut or notch the I-joist flanges. Making a web hole is allowed to some extent with some limitations as it reduces the load carrying capacity and stiffness for a larger hole.

Retrofitting of deficient I-joists is a promising option instead of replacing those due to its ease of installation, cost effectiveness. This thesis presented a new types of retrofitting options to gain the structural capacity and stiffness of the deficient I-joists due to the presence of the hole at web and notch at top flange.

### **9.2 Conclusion**

The following conclusions can be drawn from this research study:

#### **9.2.1 Material Properties**

- From the tension tests conducted in this chapter, it is observed that under tension OSB and GFRP exhibits the weakest and the strongest mechanical behavior in the transverse and longitudinal directions, respectively, while properties along the diagonal directions are in between the longitudinal and transverse direction.

- Constitutive models developed in this chapter can be utilized to analyze the performance and predict the load carrying capacity of I-joist with a rational accuracy.

### 9.2.2 Deficient I-joists

- The experimental capacity and stiffness of the regular I-Joists without openings were at least three times higher than the specified design values which satisfies the requirements according to *ASCE 7-10.1 (2010)* and *ASTM D5055 (2004)*.
- In terms of failure mode of I-joists with notches, the most common failure mode was the combined flexural and shear failure, where crack initiates at the right bottom corner of the notch and propagates to the bottom flange in an angle ranging from  $63^0$  to  $77^0$  with respect to the I-joist longitudinal axis. However, for combined type failure most of the cases, shear failure was occurred by following flexural failure.
- Due to the presence of flange notches in the I-joists, the load carrying capacity decreased up to 80% in comparison with the uncut I-joist with the increasing distance of the notch from the support, which is due to the increasing flexural stresses.
- With a 100 mm flange notch at a location ( $L_n = 455mm$ ) in the I-joists (series: 12-G and 20-L), the strength of 12ft and 20ft span I-joists reduced to 71% and 56%, respectively compared to that of the uncut/control I-joists. Moreover, further 11% and 19% reductions of strength were observed for 12ft and 20ft span I-joists, respectively for a deeper notch (150 mm) in the I-joists (series: 12-I and 20-N) at the same location ( $L_n = 455mm$ ). It is obvious that this reduction occurred due to the decrease in web materials, which provides the stiffness against shear stress.

- The stiffness of the I-joists with flange notches is reduced up to 46% and 33% from the stiffness of the control I-joists for 12ft and 20ft span length I-joists, respectively.
- Average load for serviceability condition is also reduced up to 50% and 37% from the average load at serviceability condition of the control I-joists for 12ft and 20ft span length I-joists, respectively.
- Notch distance-span ratio has a significant effect on the crack growth direction.
- A stiffness reduction of up to 12% in 12ft series and up to 11% in 20ft series, respectively, was observed compared to the control series. The change in the position of the opening in shear span, however, did not affect the joist stiffness.
- An opening/hole had more impact on smaller span beams. Most of the 12ft test specimens with openings showed premature shear failures at the location of the opening. The capacity of 12ft I-joists was reduced up to 54%, while for 20ft I-joists, the capacity was reduced only up to 21%.
- In the case of 20ft I-joists, presence of web hole about half of the web height did not have any effect on longer span beams.
- The reinforcement of I-Joists using OSB collars was effective to prevent shear failure close to a web opening and increased the stiffness of the I-joists up to 6% and 8% for 12ft and 20ft I-joists, respectively
- The reinforcement of I-Joists with OSB collars significantly increased the capacity (27% and 20% respectively for 12ft and 20ft I-joists). Furthermore, the capacities of the reinforced I-Joists (series I and J) were found almost equal to the control series capacity.
- The newly proposed model to predict I-joist capacity with holes was superior compared to existing models from the literature, while the new model to predict the capacity of an I-

joist with reinforced openings was also sufficiently accurate in predicting capacities from previous tests.

### **9.2.3 Retrofitted I-joists with OSB Collars**

- Type 2 retrofitting technique containing 3 layers of OSB collar improves the load carrying capacity significantly.
- Shear failure was controlled by using reinforcer, which basically reduced the shear stress in the web by increasing the thickness of the web. A different reinforcing technique have to be introduced to increase the flexural stiffness and strength of the notched I-Joists.
- Proposed empirical models are highly accurate to predict the experimental capacity with average PF value being close to 1.0.
- Based on the effect analysis it was found that  $D_n/D$  and  $L_n/L$  had the maximum contribution on unreinforced and reinforced I-joists, respectively.
- Retrofitting of Web Hole I-Joists with OSB collars significantly increased the capacity (27% and 20% respectively for 12ft and 20ft I-joists). Furthermore, the capacities of the reinforced I-Joists (series I and J) were found almost equal to the control series capacity.

### **9.2.4 Retrofitted I-joists with GFRP Plates**

- Retrofitted I-joists with GFRP based reinforcers are comparable to the control I-joists in terms of structural capacity and stiffness.
- Structural capacity of the flange notched and web holed I-joists can be improved significantly by retrofitting with GFRP reinforcers for both short and long span I-joists.
- Stiffness of the flange notched and web holed I-joists retrofitted with GFRP reinforcers for both short and long span I-joists were lower compared to that of the control I-joists.

### 9.2.5 Analytical Models

- Depth to span length ratio ( $D/L = 0.049$ ) is very low for the 20 ft I-joist hence the stiffness of 20 ft web holed I-joists are based on the stiffness of the two flanges. The change of effective depth to span ratio  $[(D-\Phi)/L = 0.033, 0.025 \text{ \& } 0.0166]$  is negligible for web holes I-joists, hence the stiffness of the 20ft web hole Joists are almost same as per the analytical models developed.
- The maximum deflection and the mid-span deflection are very close for all I-joist series as the location of maximum deflection ( $X_{\Delta_{\max}}$ ) found to be very close to the half of the span length ( $L/2$ ).
- The deflection due to shear contributes 30-40% of the total deflection of the maximum deflection as determined by the analytical models developed. Hence, the deflection due to shear cannot be overlooked.

### 9.3 Limitations of the study

Although this research study was conducted based on an extensive experimental investigations, it has some major limitations which includes but not limited to:

- The outcome of this research study can be used as a starting point to implement in the code for allowing a notch or hole in I-joists. Before, introducing the outcome of this research study in the code, further investigation is required with a large number of specimens to achieve confidence or reliability of the performance of OSB collar and GFRP reinforcers.
- Performance of the retrofitted I-joist also depends on the workmanship and types of glue used to attach the reinforcers in the I-joists. To avoid the influence of the workmanship, a specific guideline should be followed to retrofit the deficient I-joists.



- Proposed prediction models are valid only for the specific details of the OSB collars and GFRP reinforcers used in this research study, which may not be applicable for other types of reinforcers.
- Proposed analytical models were validated based on the material properties obtained from a small number of tension tests of OSB, Timber and GFRP. Further validation of this models is required based on reliable material properties of OSB, Timber and GFRP before application of these analytical models.

#### **9.4 Recommendations for future research**

Based on the experimental analytical results obtained in this study on the structural characteristics of OSB webbed I-joists with a web hole or flange notch and their retrofitted I-joists, the following recommendations can be made for future investigations:

- It is recommended that the effects of flange notches in the floor panel system should be investigated for better understanding the performance of the notched I-joists as a structural system.
- It is also recommended that the effects of flange notches in the region of maximum bending stress (at mid span) be investigated separately from the effects of flange notches in the region of maximum shear force to understand the behavior of notched I-joists under bending stress.
- Finite Element Fracture Analysis of flange notched I-joists should be conducted to have better understanding of the stress concentration at the cut zone of the I-joists. Moreover, this analysis will further help investigate the crack growth propagation having different failure criteria.

- Future studies should include wood I-Joists with multiple web openings & flange notch or their combined effects on the performance of I-joists.
- Further investigation can be conducted by varying the length and thickness of the FRP reinforcer to determine the effective length and thickness by optimizing the performance function of the I-joist reinforced with the GFRP reinforcer having a web hole and flange notch.
- For a deficient I-joist retrofitting design procedure can be developed based on the outcomes of this research.
- Though extensive study on stiffness/deflection for composite structures is presented, there is still a need to develop more generic formulations for stability of composite structures. Only some special cases are studied, and their analytical solutions are derived. More generic solutions for various flange notch and web hole shapes and sizes with different loading and boundary conditions should be further developed and validated.

## REFERENCES

- Afzal, M. T., Lai, S., Chui, Y. H., and Pirzada, G. (2006). “Experimental evaluation of wood I-joists with web holes.” *Forest products journal*, 56(10), 26–30.
- American-Wood-Council. (1999). *Guideline Wood I-Joists*.
- Aschheim, M., Gil-martín, L. M., and Hernández-montes, E. (2010). “Engineered Bamboo I-Joists.” 136(December), 1619–1624.
- Ashland Inc. (2007). *Resin Selection Guide*.
- ASTM-D1037. (2014). “Standard Test Methods for Evaluating Properties of Wood-Base Fiber and Particle.” ASTM International, West Conshohocken, PA, 2014.
- ASTM-D143. (2014). “Standard Test Methods for Small Clear Specimens of Timber.” ASTM International, West Conshohocken, PA, 2014.
- ASTM-D4762. (2014). “Standard Guide for Testing Polymer Matrix Composite Materials.” ASTM International, West Conshohocken, PA, 2014.
- ASTM-D5055. (2013). “Standard Specification for Establishing and Monitoring Structural Capacities of Prefabricated Wood I-Joists.” ASTM International, West Conshohocken, PA, 2013.
- ASTM-D638. (2014). “Standard Test Method for Tensile Properties of Plastics.” *Annual Book of ASTM Standards*, ASTM International, West Conshohocken, PA, 2014.
- ASTM-D7205. (2014). “Standard Test Method for Tensile Properties of Fiber Reinforced Polymer Matrix.” ASTM International, West Conshohocken, PA, 2014.
- Ballhause, D., König, M., and Kroplin, B. (2008). “Textile Composites and Inflatable Structures II-Modelling Fabric-Reinforced Membranes with the Discrete Element Method.” E. Onate and B. Kroplin, eds., Springer.

- Beer, F. P., Johnston, E. R., DeWolf, J. T., and Mazurek, D. F. (2015). *Mechanics of Materials*. McGraw-Hill Education, New York, NY 10121.
- Bledzki, A. K., Sperber, V. E., and Faruk, O. (2002). *Natural and Wood Fibre Reinforcement in Polymers*.
- Booth, L. G. (1974). "The effect of flange-web joint design on the design of plywood I-beams." *J. Inst. Wood Sci*, 6(6), 13–24.
- Canadian-Standard-Association. (2013a). "CSA O121- Douglas Fir Plywood." Canadian Standards Association, 2013.
- Canadian-Standard-Association. (2013b). "CSA O153- Poplar plywood." Canadian Standards Association, 2013.
- Canadian-Standard-Association. (2014a). "CSA O86- Engineering Design in Wood." Canadian Standards Association, 2014.
- Canadian-Standard-Association. (2014b). "CSA O151- Canadian softwood plywood." Canadian Standards Association, 2014.
- Canadian-Standard-Association. (2014c). "CSA O112- Evaluation of adhesives for structural wood products."
- Canadian-Standard-Association. (2016). "CSA O325- Construction sheathing." Canadian Standards Association, 2016.
- Chen, G., Li, H., Zhou, T., Li, C., Song, Y., and Xu, R. (2015). "Experimental evaluation on mechanical performance of OSB webbed parallel strand bamboo I-joist with holes in the web." *Construction and Building Materials*, Elsevier Ltd, 101, 91–98.
- Chui, Y. H., Pirzada, G., and Lai, S. (2005). *Enhancing Shear and Bearing Strength of Wood I-joists*.
- Clinch, R. W. (1993). "Effect of holes on static flexural stiffness of a wood composite I-beam."

- Forest Products Journal*, (3), 1–8.
- CSA-O86. (2014). “CSA O86.pdf.” Canadian Standards Association, 2014.
- CWC. (2016). “Canadian Wood Council.” <<http://cwc.ca/wood-products/i-joists/>> (Jun. 12, 2014).
- Damery, B. D. T. (2006). “Engineered Wood Products : Building the Future Recent Developments in Wood Composites.” (August), 14–16.
- Davids, W. G., Rancourt, D. G., and Dagher, H. J. (2011). “Bending Performance of Composite Wood I-Joist / Oriented Strand Board Panel Assemblies.” *Forest products journal*, 61(11), 246–256.
- Deogonda, P., and Chalwa, V. N. (2013). “Mechanical Property of Glass Fiber Reinforcement Epoxy Composites.” *International Journal of Scientific Engineering and Research (IJSER)*, 1(4), 6–9.
- Foliente, B. G. C., and McLain, T. E. (1993). “Design of Notched Beams.” *Journal of Structural Engineering*, 118(9), 2407–2420.
- Forest Products Laboratory. (1999). *Wood Handbook: Wood as an Engineering Material*. FPL-GTR-113.USDA Forest Products Laboratory, Madison, WI.
- Gere, J. M. (2004). *Mechanics of Materials*. Thomson Learning Inc.
- Grandmont, J.-F., Cloutier, A., Gendron, G., and Desjardins, R. (2010a). “Wood I-Joist Model Sensitivity to Oriented Strandboard Web Mechanical Properties.” *Wood and Fiber Science*, 42(3), 352–361.
- Grandmont, J.-F., Cloutier, A., Gendron, G., and Desjardins, R. (2010b). “Effect of Density on the Properties of Oriented Strandboard Web Stock Used in Wood I-Joists.” *Forest products journal*, 60(7/8), 592–598.
- Guan, Z. W., and Zhu, E. C. (2009). “Finite element modelling of anisotropic elasto-plastic timber composite beams with openings.” *Engineering Structures*, Elsevier Ltd, 31(2), 394–403.

- Harte, A. M., and Baylor, G. (2011). "Structural evaluation of castellated timber joists." *Engineering Structures*, Elsevier Ltd, 33(12), 3748–3754.
- Hibbeler, R. C. (2011). *Mechanics of Materials*. Prentice Hall.
- Hilson, B. O., and Rodd, P. D. (1979). "The Ultimate Shearing Strength of Timber I-beams with Hardboard Webs." *The Structural Engineer*, 57(14), 25–36.
- Hindman, D. P., and Loferski, J. R. (2008). "Cold-Formed Steel Reinforcement for Improperly Cut Wood Composite I-Joists." *Practice Periodical on Structural Design and Construction*, ASCE, 13(4), 198–203.
- Islam, M. S., Shahnewaz, M., and Alam, M. S. (2015). "Structural capacity of timber I-joist with flange notch: Experimental evaluation." *Construction and Building Materials*, Elsevier Ltd, 79, 290–300.
- Islam, M. S., Shahnewaz, M., and Alam, M. S. (2016). "Reinforced I-joists with Flange Notch: Experimental and Analytical Investigations." *ASCE Journal of Structural Engineering*.
- Jalla, R. (1999). "Remedial Framing Design for Joists in Residential Construction." *Journal of Architectural Engineering*, ASCE, (June), 57–60.
- Jiao, P. (2012). "Analytical Evaluations of Buckling Behavior of Wood Composite I-Joist with Sinusoidal Web." (May).
- Karacabeyli, E., Lau, P., Henderson, C. R., Meakes, F. V, and Deacon, W. (1996). "Design rated oriented strandboard in CSA standards." 443, 431–443.
- Kaw, A. K. (2006). *Mechanics of Composite Materials*. Taylor & Francis Group, LLC.
- Komeili, M., and Milani, A. S. (2013). "An Elaboration on the Shear Characterization of Dry Woven Fabrics Using Trellising Tests." *Polymer Composites*, 34(3), 359–367.
- Koz, M., and Hulimka, J. (2014). "Load-Bearing Capacity of Hybrid Timber-Glass Beams."

*Architecture Civil Engineering Environment*, 2, 61–71.

Lai, S. (2007). “Failure Behavior and Deflection Performance of Wood I-Joists with Web Holes.”  
THE UNIVERSITY OF NEW BRUNSWICK.

Leichti, R. J., Falk, R. H., and Laufenberg, T. L. (1989). “Prefabricated Wood Composite I-Beams:  
A Literature Review.” *Wood and Fiber Science*, 22(1), 62–79.

Leichti, R. J., Falk, R. H., and Laufenberg, T. L. (1990). “Prefabricated Wood I-Joists - an Industry  
Overview.” *Forest Products Journal*, 40(3), 15–20.

Leichti, R. J., and Tang, R. C. (1983). “Analysis of wood composite I-beams with glued flange-  
web joints.” *Proceedings, Spring Meeting, Society for Experimental Stress Analysis.*,  
Brookfield Center, MA., 45–50.

Maley, J. D. (1987). “Wood I-Beams: A Closer Look.” *Proceedings of Structures Congress/87,*  
*Building Structures, ASCE*, New York, 221–235.

Morris, V., Gustaffson, P., and Serano, E. (1996). “The shear strength of lightweight beams with  
and without a hole-A preliminary study.” *Wood mechanics: Workshop on mechanical*  
*properties of panel products*, 22-23 March 1995, Watford, UK., 199–214.

Morrissey, G. C., Dinehart, D. W., and Dunn, W. G. (2009). “Wood I-Joists with Excessive Web  
Openings: An Experimental and Analytical Investigation.” *Journal of Structural*  
*Engineering*, (June), 655–665.

Nascor. (2010). “Specifier Guide NJ, NJH, NJU Series I-Joists.” <<http://nascor.ca/home>>.

NASCOR. (2010). “I joist Specifier Guide.” <<http://nascor.ca/home>> (Feb. 16, 2013).

NBCC. (2010). “National Building Code of Canada; Part 9 -Specific Provisions.” National  
Research Council of Canada, 2010.

Open Source Physics. (2016). “Tracker 4.94.” <<http://physlets.org/tracker>>.

Pirzada, G. B., Chui, Y. H., and Lai, S. (2008). “Predicting Strength of Wood I-Joist with a Circular

- Web Hole.” *Journal of Structural Engineering, ASCE*, (July), 1229–1234.
- Polocoser, T. (2012). “Evaluation of Remediation Techniques for Circular Holes in the Webs of Wood I- Joists.” MS Thesis, Oregon State University, Corvallis , OR.
- Polocoser, T., Miller, T. H., and Gupta, R. (2012). “Evaluation of Remediation Techniques for Circular Holes in the Webs of Wood I-Joists.” *Journal of Materials in Civil Engineering*.
- Rainforest Information Centre. (2016). “Rainforest Information Centre.” [http://www.rainforestinfo.org.au/good\\_wood/wb\\_compos.htm](http://www.rainforestinfo.org.au/good_wood/wb_compos.htm).
- Rathnakar, G., and Shivanand, H. K. (2012). “Effect of Thickness on Flexural Properties of Epoxy based Glass Fiber Reinforced Laminate.” 2(6), 409–412.
- Samson, M. (1981). “Effect de la qualiti’ des membrures sur la flexion de composites en bois i &me mince. Une etude expkrimentale.” Universiti Laval, Ste-Foy, Quebec.
- Samson, M. (1983). “Influence of flange quality on the loadcarrying capacity of composite webbed I-beams in flexure.” *Forest Products Journal*, 33, 38–42.
- Shahnewaz, M., Islam, M. S., Ahmadipour, M., Tannert, T., and Alam, M. S. (2016). “Reinforced Wood I-Joists with Web Openings.” *ASCE Journal of Structural Engineering*.
- Shrestha, D. (1999). “Shear Properties tests of oriented strandboard panels.pdf.” *Forest products journal*, 49(10), 41–46.
- Sika Canada Inc. (2015). “Sikadur ® 30.” 1–4.
- Skaggs, T. D., and Bender, D. A. (1995). “Shear Deflection of Composite Wood Beams.” *Wood and Fiber Science*, 27(3), 327–338.
- Suchsland, O., and Woodson, G. E. (1986). *Fiberboard manufacturing practices in the United States*. Agric. Handb., Department of Agriculture, Washington, DC: U.S.
- Sultana-Mir, S. (2015). “Toward Better Understanding of Mechanical Response of Fabrics Under Multiple Combined Loading Modes : Experimental and Statistical Analysis.” The University



of British Columbia, Okanagan.

The MathWorks Inc.; Natick, M. (2012). “MATLAB R2012b.”

Vallée, T., Tannert, T., and Fecht, S. (2016). “Adhesively bonded connections in the context of timber engineering.” *Journal of Adhesion*.

Wang, S., and Cheng, J. J. R. (1995). *Shear behaviour of OSB wood composite I-beams with web openings*.

Weyerhaeuser-Trus-Joist. (2014). *TJ-4500-Trus Joist® TJI Joist® Specifier’s Guide (W. Canada)*.

Wisniewski, B., and Manbeck, H. B. (2003). “Residential Floor Systems : Wood I-Joist Creep Behavior.” *Journal of Architectural Engineering, ASCE*, (March), 41–45.

Wood I-Joist Manufacturers Association (WIJMA). (2008). *Establishing Prefabricated Wood I-Joist Composite EI*.

Wu, W., and Asce, M. (2014). “Experimental Analysis of Bending Resistance of Bamboo Composite I-Shaped Beam.” 19(4), 1–13.

Youngquist, J. A. (2010). “FPL Wood Handbook-Wood as an Engineering Material.” Forest Products Laboratory, United States Department of Agriculture Forest Service, Madison, Wisconsin.

Yusof, A., and Saleh, A. L. (2010). “Flexural Strengthening of Timber Beams Using Glass Fibre Reinforced Polymer.” (10).

Zhang, X. J., Hu, Y. C., and Fang, Y. C. (2010). “Study of the Bonding Property between Flanges and Web Plates of Wood I-Joist.” *Advanced Materials Research*, 150–151, 1092–1095.

Zhou, D. (1990). “A study of oriented structural board made from hybrid poplar Physical and mechanical properties of OSB.” 48, 293–296.

Zhu, E. (2003). “Modelling the structural behaviour of OSB webbed timber I-beams.”

- Zhu, E. C., Guan, Z. W., Pope, D. J., and Rodd, P. D. (2007a). "Effect of Openings on Oriented Strand Board Webbed Wood I-Joists." *Journal of Structural Engineering, ASCE*, (January), 145–149.
- Zhu, E. C., Guan, Z. W., Rodd, P. D., and Pope, D. J. (2005a). "A constitutive model for OSB and its application in finite element analysis." *Holz Roh- Werkst*, 63(2), 87–93.
- Zhu, E. C., Guan, Z. W., Rodd, P. D., and Pope, D. J. (2005b). "Finite element modelling of OSB webbed timber I-beams with interactions between openings." *Advances in Engineering Software*, 36(11–12), 797–805.
- Zhu, E. C., Guan, Z. W., Rodd, P. D., and Pope, D. J. (2006). "Buckling of Oriented Strand Board Webbed Wood I-Joists." *Journal of Structural Engineering, ASCE*, 131(10), 1629–1636.
- Zhu, E. C., Guan, Z. W., Rodd, P. D., and Pope, D. J. (2007b). "Finite element modelling of OSB webbed timber I-beams with interactions between openings." *Advances in Engineering Software* 36 797805, 11–12.

## APPENDICES

### Appendix A: Summary of Tested Flange notch I-joists

**Table A.1: Measured Shear ( $V_u$ ), Ultimate Moment ( $M_u$ ), Failure Moment at Notch location ( $M_{Ln}$ ) and Maximum Deflection ( $\Delta$ ) for each type of failure occurred in all tested I-joists**

Specimen Code	Failure Mode	Occurrences	Avg. Capacity (kN)	Avg. Shear $V_u$ (kN)	Avg. $M_u$ (kN-m)	Avg. $M_{Ln}$ (kN-m)	Avg. Max. Deflection $\Delta$ (mm)
12-A	Shear	3	36.41	18.20	65.54	-	29.96
	Flexural	6	28.44	14.22	51.19	-	
	Shear + Flexural	1	38.83	19.42	69.90	-	
12-F	Shear	0	-	0.00	0.00	-	17.29
	Flexural	9	15.12	7.56	27.21	3.06	
	Shear + Flexural	1	15.34	7.67	27.61	3.11	
12-G	Shear	0	-	-	-	-	13.83
	Flexural	5	8.84	4.42	15.91	2.45	
	Shear + Flexural	5	9.47	4.73	17.04	2.63	
12-H	Shear	0	-	-	-	-	9.90
	Flexural	7	6.33	3.16	11.39	2.25	
	Shear + Flexural	3	6.59	3.30	11.87	2.34	
12-I	Shear	0	-	-	-	-	10.67
	Flexural	4	5.11	2.55	9.19	1.42	
	Shear + Flexural	6	6.09	3.05	10.96	1.69	
20-A	Shear	0	-	-	-	-	81.00
	Flexural	10	22.06	11.03	66.75	-	
	Shear + Flexural	0	-	-	-	-	
20-K	Shear	0	-	-	-	-	48.39
	Flexural	9	12.26	6.13	37.09	2.48	
	Shear + Flexural	1	13.24	6.62	40.05	2.68	
20-L	Shear	0	-	-	-	-	38.17
	Flexural	6	10.09	5.05	30.53	2.80	
	Shear + Flexural	4	9.11	4.56	27.57	2.53	
20-M	Shear	0	-	-	-	-	25.85
	Flexural	5	6.78	3.39	20.51	2.41	
	Shear + Flexural	5	6.67	3.33	20.17	2.37	
20-N	Shear	0	-	-	-	-	26.00
	Flexural	6	5.29	2.65	16.01	1.47	
	Shear + Flexural	4	5.76	2.88	17.42	1.60	

## Appendix B: Mat lab Codes for Analytical Model Development based on *Castigliano's Second theorem*

```

%FOR POINT LOAD Retrofitted Notched/Holed Beam
clear all;
close all;
clc;

syms x a b Ac Pc Ld P w L E G A I fs
syms Lo Eo Go Ao Io fso
syms Bn Dn Ln Gn An In En fsn % For Notched Beam
syms Anx Ah Hh tw r I_n I_h Ihf Iof Iow Ihw % For WebHoled Beam
syms Grn Arn Irn Ern fsrn % For Reinforced Beam ; Including
Reinforcer
syms Lr Gr Ar Ir Er fsr % For Reinforced Beam ; Including
Reinforcer
syms Ar Arh

syms yb1(Ac) yb2(Ac) yb3(Ac)

syms M11 M12 M21 M22 M31 M32
syms DM11(Ac,Pc) DM12(Ac,Pc) DM21(Ac,Pc) DM22(Ac,Pc) DM31(Ac,Pc)
DM32(Ac,Pc)
%syms fn1 fn2 fn3
syms fb1 fb2 fb3

syms yv1(Ac) yv2(Ac) yv3(Ac)

syms V11 V12 V21 V22 V31 V32
syms DV11(Ac,Pc) DV12(Ac,Pc) DV21(Ac,Pc) DV22(Ac,Pc) DV31(Ac,Pc)
DV32(Ac,Pc)
syms fv1 fv2 fv3
CONTROLLING PARAMETRS
% ^-----P-----P-----^

n=1/2; % Acs/L
Ld=L*n % Location of Deflection Required
a=L/3; % Load P at a
b=2*L/3; % Load P at b

% Parameters for Sub Cases of Case 1 with Notched/Holed Beam
Lns=455;
Bns=100;
Acs=800; %A-200/B-400/C-500/D-600/E-800

Dns=10; %100; %Dns=0 --> Control; Dns>0 --> Notched Beam
%Dn=200;
Dias=0; %Dias=0 --> Notched/Control Beam; Dias>0 -->
WebHoled Beam
Lrs=100; %Lrs=0 --> Notched Beam; Lrs>0 --> Reinforced Beam

```

```

Ld = L/2

Defining CASE
    if n<=1/3
% CASE 1: Code for Left Span Deflection
        Cs=1;
    elseif n>1/3 && n<2/3
% CASE :2 Code for Mid Span Deflection
        Cs=2;
    else
% CASE :3 Code for Right Span Deflection
        Cs=3;
    end
SUB CASES OF CASE 1
if (Lrs==0)
Sub Cases of Case 1 with Notched/Holed Beam
    if Acs/Lns<1
        SCs=1; % SUB CASE:1nA: ## Pc at the Left side of the Notch
##
    elseif (Acs/(Lns+Bns))>1
        SCs=2; % SUB CASE:1nC ## Pc at the Right side of the Notch
##
    else
        SCs=3; % SUB CASE:1nB ## Pc at the Notch Location ##
    end
else
Sub Cases of Case 1 with Reinforced Beam
    if Acs/(Lns-Lrs)<=1
        SCs=1; % SUB CASE:1nA: ## Pc at the Left side of the
Reinforcer ##
    elseif (Acs/(Lns-Lrs))>1 && Acs/Lns <=1
        SCs=2; % SUB CASE:1nB ## Pc at the Left side of the Notch
at Reinforcer ##
    elseif (Acs/Lns)>1 && Acs/(Lns+Bns) <=1
        SCs=3; % SUB CASE:1nC ## Pc at the location of Notch ##
    elseif Acs/(Lns+Bns)>1 && Acs/(Lns+Bns+Lrs) <=1
        SCs=4; % SUB CASE:1nD ## Pc at the Right side of the Notch
at Reinforcer ##
    else
        SCs=5; % SUB CASE:1nE ## Pc at the right side of the
Reinforcer ##
    end
end
Formulating the Anx & Inx for WebHole
    if Dias>0
Holed Beam
        syms Aow
        r=Dn/2; % i.e Dia=Dn
        Hh=sqrt(r^2-(r-x+Ln)^2);
        %An=2*Hh*tw;

```

```

    Ah=Aow-2*Hh*tw;
    Ihf = 2*Iof;
    Ihw = Iow - tw * (2*Hh) ^ 3 / 12; % Ihw=fnc(x, Dia)
    I_h = Ihf + Ihw
    An=Ah;
    In=I_h;
    Bn=Dn;
    For Reinforced Beam
        syms Aro Iro tr      %Aro & Iro- Area/I of OSB Collars/ Reinforcer
Only
        %Ar=Ao+Aro      %Where, Ao = 2 * Af + Aw
        Arno=Aro-2*Hh*tr; %Area of OSB Collars/ Reinforcer Only at
Notch/Hole
        Arn=An+Arno
        Irn becomes very complicated Function to Integarte as Symbolic
        functions
                                %Ir=Io+Iro
        %Irno=Iro - tr * (2*Hh) ^ 3 / 12; %I of OSB Collars/ Reinforcer
Only at Notch/Hole
        %Irn=In+Irno;
        end
        ##### Castigliano's Theorem (Page 790)
        #####
        %#####
        #####
if (Dns==0) % Control Beam
    Deflection of Control Beam
    Deflction for three Cases
        switch Cs

case 1
    CASE 1: Code for Left Span Deflection
    Zone 1: x>> 0 to L/3
        Z1LL=0;
        Z1ML=Ac;
        Z1UL=a;

        V11=P+Pc*(L-Ac)/L;
        V12=V11-Pc;
        M11=P*x+Pc*(L-Ac)/L*x; % Simply Supported Beam with two Point
Loads P+P at a & b
        M12=M11-Pc*(x-Ac); % Simply Supported Beam with two Point
Loads P+P at a & b

        % Zone 2: x>> L/3 to 2L/3
        Z2LL=Z1UL;
        Z2UL=b;

        V21=V12-P;
        V22=0; %N/A
        M21=M12-P*(x-a); % Simply Supported Beam with two Point Loads

```

```

P+P at a & b
    M22=0; %N/A

    % Zone 3: x>> 2L/3 to L
    Z3LL=Z2UL;
    Z3UL=L;

    V31=V21-P;
    V32=0; %N/A
    M31=M21-P*(x-b); % Simply Supported Beam with two Point Loads
P+P at a & b
    M32=0;

    D11VPc = diff(V11,Pc);
    D12VPc = diff(V12,Pc);
    D21VPc = diff(V21,Pc);
    D22VPc = diff(V22,Pc);
    D31VPc = diff(V31,Pc);
    D32VPc = diff(V32,Pc);

    D11MPc = diff(M11,Pc);
    D12MPc = diff(M12,Pc);
    D21MPc = diff(M21,Pc);
    D22MPc = diff(M22,Pc);
    D31MPc = diff(M31,Pc);
    D32MPc = diff(M32,Pc);

    V11=subs(V11,Pc,0);
        DV11=subs(D11VPc,Pc,0);
    V12=subs(V12,Pc,0);
        DV12=subs(D12VPc,Pc,0);
    V21=subs(V21,Pc,0);
        DV21=subs(D21VPc,Pc,0);
    V22=subs(V22,Pc,0);
        DV22=subs(D22VPc,Pc,0);
    V31=subs(V31,Pc,0);
        DV31=subs(D31VPc,Pc,0);
    V32=subs(V32,Pc,0);
        DV32=subs(D32VPc,Pc,0);

    M11=subs(M11,Pc,0);
        DM11=subs(D11MPc,Pc,0);
    M12=subs(M12,Pc,0);
        DM12=subs(D12MPc,Pc,0);
    M21=subs(M21,Pc,0);
        DM21=subs(D21MPc,Pc,0);
    M22=subs(M22,Pc,0);
        DM22=subs(D22MPc,Pc,0);
    M31=subs(M31,Pc,0);
        DM31=subs(D31MPc,Pc,0);
    M32=subs(M32,Pc,0);

```

```

DM32=subs (D32MPc,Pc,0);

fv11=fs*V11*DV11/ (G*A);
fv12=fs*V12*DV12/ (G*A);
fv21=fs*V21*DV21/ (G*A);
fv22=fs*V22*DV22/ (G*A);
fv31=fs*V31*DV31/ (G*A);
fv32=fs*V32*DV32/ (G*A);

fb11=M11*DM11/ (E*I);
fb12=M12*DM12/ (E*I);
fb21=M21*DM21/ (E*I);
fb22=M22*DM22/ (E*I);
fb31=M31*DM31/ (E*I);
fb32=M32*DM32/ (E*I);

yv1=(int (fv11,x,Z1LL,Z1ML)+int (fv12,x,Z1ML,Z1UL));
yv2=(int (fv21,x,Z2LL,Z2UL));
yv3=(int (fv31,x,Z3LL,Z3UL));

yv1x=subs (yv1,Ac,x);
yv2x=subs (yv2,Ac,x);
yv3x=subs (yv3,Ac,x);
Yv=yv1x+yv2x+yv3x
YvMax=subs (Yv,x,Ld)

yb1=(int (fb11,x,Z1LL,Z1ML)+int (fb12,x,Z1ML,Z1UL));
yb2=(int (fb21,x,Z2LL,Z2UL));
yb3=(int (fb31,x,Z3LL,Z3UL));

yb1x=subs (yb1,Ac,x);
yb2x=subs (yb2,Ac,x);
yb3x=subs (yb3,Ac,x);
Yb=yb1x+yb2x+yb3x
YbMax=subs (Yb,x,Ld)
Case= 'This is Case 1'
    case 2
        CASE :2 Code for Mid Span Deflection
        Zone 1: x>> 0 to L/3
            Z1LL=0;
            Z1UL=a;

            V11=P+Pc*(L-Ac)/L;
            V12=0;
            M11=P*x+Pc*(L-Ac)/L*x; % Simply Supported Beam with two Point
Loads P+P at a & b

            % Zone 2: x>> L/3 to 2L/3
            Z2LL=Z1UL;
            Z2ML=Ac;
            Z2UL=b;

```



```

V21=V11-P;
V22=V21-Pc;
M21=M11-P*(x-a); % Simply Supported Beam with two Point Loads
P+P at a & b
M22=M21-Pc*(x-Ac);

% Zone 3: x>> 2L/3 to L
Z3LL=Z2UL;
Z3UL=L;

V31=V22-P;
V32=0;
M31=M22-P*(x-b); % Simply Supported Beam with two Point Loads
P+P at a & b
M32=0;

D11VPc = diff(V11,Pc);
D12VPc = diff(V12,Pc);
D21VPc = diff(V21,Pc);
D22VPc = diff(V22,Pc);
D31VPc = diff(V31,Pc);
D32VPc = diff(V32,Pc);

D11MPc = diff(M11,Pc);
D12MPc = diff(M12,Pc);
D21MPc = diff(M21,Pc);
D22MPc = diff(M22,Pc);
D31MPc = diff(M31,Pc);
D32MPc = diff(M32,Pc);

V11=subs(V11,Pc,0);
DV11=subs(D11VPc,Pc,0);
V12=subs(V12,Pc,0);
DV12=subs(D12VPc,Pc,0);
V21=subs(V21,Pc,0);
DV21=subs(D21VPc,Pc,0);
V22=subs(V22,Pc,0);
DV22=subs(D22VPc,Pc,0);
V31=subs(V31,Pc,0);
DV31=subs(D31VPc,Pc,0);
V32=subs(V32,Pc,0);
DV32=subs(D32VPc,Pc,0);

M11=subs(M11,Pc,0);
DM11=subs(D11MPc,Pc,0);
M12=subs(M12,Pc,0);
DM12=subs(D12MPc,Pc,0);
M21=subs(M21,Pc,0);
DM21=subs(D21MPc,Pc,0);
M22=subs(M22,Pc,0);

```

```

        DM22=subs (D22MPc,Pc,0);
        M31=subs (M31,Pc,0);
        DM31=subs (D31MPc,Pc,0);
        M32=subs (M32,Pc,0);
        DM32=subs (D32MPc,Pc,0);

fv11=fs*V11*DV11/(G*A);
fv12=fs*V12*DV12/(G*A);
fv21=fs*V21*DV21/(G*A);
fv22=fs*V22*DV22/(G*A);
fv31=fs*V31*DV31/(G*A);
fv32=fs*V32*DV32/(G*A);

fb11=M11*DM11/(E*I);
fb12=M12*DM12/(E*I);
fb21=M21*DM21/(E*I);
fb22=M22*DM22/(E*I);
fb31=M31*DM31/(E*I);
fb32=M32*DM32/(E*I);

yv1=(int (fv11,x,Z1LL,Z1UL));
yv2=(int (fv21,x,Z2LL,Z2ML)+int (fv22,x,Z2ML,Z2UL));
yv3=(int (fv31,x,Z3LL,Z3UL));

yv1x=subs (yv1,Ac,x);
yv2x=subs (yv2,Ac,x);
yv3x=subs (yv3,Ac,x);
Yv=yv1x+yv2x+yv3x
YvMax=subs (Yv,x,Ld)

yb1=(int (fb11,x,Z1LL,Z1UL));
yb2=(int (fb21,x,Z2LL,Z2ML)+int (fb22,x,Z2ML,Z2UL));
yb3=(int (fb31,x,Z3LL,Z3UL));

yb1x=subs (yb1,Ac,x);
yb2x=subs (yb2,Ac,x);
yb3x=subs (yb3,Ac,x);
Yb=yb1x+yb2x+yb3x
YbMax=subs (Yb,x,Ld)
    Finding the Location of Maximum Deflection.
    Yb=Yv+Yb;
DY1 = diff(Yb)
X_Deltamax = solve(DY1,x)

Case= 'This is Case 2'
    case 3
    CASE :3 Code for Right Span Deflection
    Zone 1: x>> 0 to L/3
        Z1LL=0;
        Z1UL=a;

```

```

V11=P+Pc*(L-Ac)/L;
V12=0; %N/A
M11=P*x+Pc*(L-Ac)/L*x; % Simply Supported Beam with two Point
Loads P+P at a & b

% Zone 2: x>> L/3 to 2L/3
Z2LL=Z1UL;
Z2UL=b;

V21=V11-P;
V22=0; %N/A
M21=M11-P*(x-a); % Simply Supported Beam with two Point Loads
P+P at a & b

% Zone 3: x>> 2L/3 to L
Z3LL=Z2UL;
Z3ML=Ac;
Z3UL=L;

V31=V21-P;
V32=V31-Pc; %N/A
M31=M21-P*(x-b); % Simply Supported Beam with two Point Loads
P+P at a & b
M32=M31-Pc*(x-Ac);

D11VPc = diff(V11,Pc);
D12VPc = diff(V12,Pc);
D21VPc = diff(V21,Pc);
D22VPc = diff(V22,Pc);
D31VPc = diff(V31,Pc);
D32VPc = diff(V32,Pc);

D11MPc = diff(M11,Pc);
D12MPc = diff(M12,Pc);
D21MPc = diff(M21,Pc);
D22MPc = diff(M22,Pc);
D31MPc = diff(M31,Pc);
D32MPc = diff(M32,Pc);

V11=subs(V11,Pc,0);
DV11=subs(D11VPc,Pc,0);
V12=subs(V12,Pc,0);
DV12=subs(D12VPc,Pc,0);
V21=subs(V21,Pc,0);
DV21=subs(D21VPc,Pc,0);
V22=subs(V22,Pc,0);
DV22=subs(D22VPc,Pc,0);
V31=subs(V31,Pc,0);
DV31=subs(D31VPc,Pc,0);
V32=subs(V32,Pc,0);
DV32=subs(D32VPc,Pc,0);

```

```

M11=subs (M11,Pc,0);
    DM11=subs (D11MPc,Pc,0);
M12=subs (M12,Pc,0);
    DM12=subs (D12MPc,Pc,0);
M21=subs (M21,Pc,0);
    DM21=subs (D21MPc,Pc,0);
M22=subs (M22,Pc,0);
    DM22=subs (D22MPc,Pc,0);
M31=subs (M31,Pc,0);
    DM31=subs (D31MPc,Pc,0);
M32=subs (M32,Pc,0);
    DM32=subs (D32MPc,Pc,0);

fv11=fs*V11*DV11/(G*A);
fv12=fs*V12*DV12/(G*A);
fv21=fs*V21*DV21/(G*A);
fv22=fs*V22*DV22/(G*A);
fv31=fs*V31*DV31/(G*A);
fv32=fs*V32*DV32/(G*A);

fb11=M11*DM11/(E*I);
fb12=M12*DM12/(E*I);
fb21=M21*DM21/(E*I);
fb22=M22*DM22/(E*I);
fb31=M31*DM31/(E*I);
fb32=M32*DM32/(E*I);

yv1=(int (fv11,x,Z1LL,Z1UL));
yv2=(int (fv21,x,Z2LL,Z2UL));
yv3=(int (fv31,x,Z3LL,Z3ML)+int (fv32,x,Z3ML,Z3UL));

yv1x=subs (yv1,Ac,x);
yv2x=subs (yv2,Ac,x);
yv3x=subs (yv3,Ac,x);
Yv=yv1x+yv2x+yv3x
YvMax=subs (Yv,x,Ld)

yb1=(int (fb11,x,Z1LL,Z1UL));
yb2=(int (fb21,x,Z2LL,Z2UL));
yb3=(int (fb31,x,Z3LL,Z3ML)+int (fb32,x,Z3ML,Z3UL));

yb1x=subs (yb1,Ac,x);
yb2x=subs (yb2,Ac,x);
yb3x=subs (yb3,Ac,x);
Yb=yb1x+yb2x+yb3x
YbMax=subs (Yb,x,Ld)
Case= 'This is Case 3'
    end % End of Switch Cs
    elseif (Dns>0 && Lrs==0)      %    Notched Beam
        Deflction of Notched Beam

```

Three Cases and Three Sub Cases for Case 1  
switch Cs

case 1 % 1N

CASE 1n: Code for Left Span Deflection  
Case 1n consists of three sub cases(SCs).

switch SCs

case 1 % SUBCASE 1nA ## Pc at the Left side of the Notch ##

SUBCASE 1nA

Zone 1a 1b 1c 1d: x>> 0 to a

Z1LL=0;

Z1NLL=Ln;

Z1NUL=Ln+Bn;

Z1ML=Ac;

Z1UL=a;

V11=P+Pc\*(L-Ac)/L;

V12=V11-Pc;

V12n=V12;

M11=P\*x+Pc\*(L-Ac)/L\*x; % Simply Supported Beam with two Point

Loads P+P at a & b

M12=M11-Pc\*(x-Ac); % Simply Supported Beam with two Point

Loads P+P at a & b

M12n=M12;

% Zone 2: x>> a to b

Z2LL=Z1UL;

Z2UL=b;

V21=V12-P;

V22=0; %N/A

M21=M12-P\*(x-a); % Simply Supported Beam with two Point Loads

P+P at a & b

M22=0; %N/A

% Zone 3: x>> b to L

Z3LL=Z2UL;

Z3UL=L;

V31=V21-P;

V32=0; %N/A

M31=M21-P\*(x-b); % Simply Supported Beam with two Point Loads

P+P at a & b

M32=0;

D11VPc = diff(V11,Pc);

D12VPc = diff(V12,Pc);

D12nVPc = diff(V12n,Pc);

D21VPc = diff(V21,Pc);

D22VPc = diff(V22,Pc);

D31VPc = diff(V31,Pc);

```

D32VPc = diff(V32,Pc);

D11MPc = diff(M11,Pc);
D12MPc = diff(M12,Pc);
D12nMPc = diff(M12n,Pc);
D21MPc = diff(M21,Pc);
D22MPc = diff(M22,Pc);
D31MPc = diff(M31,Pc);
D32MPc = diff(M32,Pc);

V11=subs(V11,Pc,0);
    DV11=subs(D11VPc,Pc,0);
V12=subs(V12,Pc,0);
    DV12=subs(D12VPc,Pc,0);
V12n=subs(V12n,Pc,0);
    DV12n=subs(D12nVPc,Pc,0);
V21=subs(V21,Pc,0);
    DV21=subs(D21VPc,Pc,0);
V22=subs(V22,Pc,0);
    DV22=subs(D22VPc,Pc,0);
V31=subs(V31,Pc,0);
    DV31=subs(D31VPc,Pc,0);
V32=subs(V32,Pc,0);
    DV32=subs(D32VPc,Pc,0);

M11=subs(M11,Pc,0);
    DM11=subs(D11MPc,Pc,0);
M12=subs(M12,Pc,0);
    DM12=subs(D12MPc,Pc,0);
M12n=subs(M12n,Pc,0);
    DM12n=subs(D12nMPc,Pc,0);
M21=subs(M21,Pc,0);
    DM21=subs(D21MPc,Pc,0);
M22=subs(M22,Pc,0);
    DM22=subs(D22MPc,Pc,0);
M31=subs(M31,Pc,0);
    DM31=subs(D31MPc,Pc,0);
M32=subs(M32,Pc,0);
    DM32=subs(D32MPc,Pc,0);

fv11=fs*V11*DV11/(G*A);
fv12=fs*V12*DV12/(G*A);
fv12n=fsn*V12n*DV12n/(Gn*An);
fv21=fs*V21*DV21/(G*A);
fv22=fs*V22*DV22/(G*A);
fv31=fs*V31*DV31/(G*A);
fv32=fs*V32*DV32/(G*A);

fb11=M11*DM11/(E*I);
fb12=M12*DM12/(E*I);
fb12n=M12n*DM12n/(En*In);

```

```

fb21=M21*DM21/(E*I);
fb22=M22*DM22/(E*I);
fb31=M31*DM31/(E*I);
fb32=M32*DM32/(E*I);

%yv1=(int(fv11,x,Z1LL,Z1ML)+int(fv12,x,Z1ML,Z1NLL)+int(fv12n,x,Z1NLL,Z
1NUL)+int(fv12,x,Z1NUL,Z1UL));
if Dias>0

yv1=(int(fv11,x,Z1LL,Z1ML)+int(fv12,x,Z1ML,Z1NLL)+int(fv12,x,Z1NUL,Z1U
L));
    yv1n=int(fv12n,x,Z1NLL,Z1NUL)      % Always Display for WebHole Joist
    yv1nx=subs(yv1n,Ac,x)              % Always Display for WebHole Joist
else

yv1=(int(fv11,x,Z1LL,Z1ML)+int(fv12,x,Z1ML,Z1NLL)+int(fv12n,x,Z1NLL,Z1
NUL)+int(fv12,x,Z1NUL,Z1UL));
end
yv2=(int(fv21,x,Z2LL,Z2UL));
yv3=(int(fv31,x,Z3LL,Z3UL));

yv1x=subs(yv1,Ac,x);
yv2x=subs(yv2,Ac,x);
yv3x=subs(yv3,Ac,x);
Yv=yv1x+yv2x+yv3x % Should be added +yv1nx for WebHole Joist
YvMax=subs(Yv,x,Ld)

%yb1=(int(fb11,x,Z1LL,Z1ML)+int(fb12,x,Z1ML,Z1NLL)+int(fb12n,x,Z1NLL,Z
1NUL)+int(fb12,x,Z1NUL,Z1UL));
if Dias>0

yb1=(int(fb11,x,Z1LL,Z1ML)+int(fb12,x,Z1ML,Z1NLL)+int(fb12,x,Z1NUL,Z1U
L));
    yb1n=int(fb12n,x,Z1NLL,Z1NUL)      % Always Display for WebHole Joist
    yb1nx=subs(yb1n,Ac,x) % Always Display for WebHole Joist
else

yb1=(int(fb11,x,Z1LL,Z1ML)+int(fb12,x,Z1ML,Z1NLL)+int(fb12n,x,Z1NLL,Z1
NUL)+int(fb12,x,Z1NUL,Z1UL));
end
yb2=(int(fb21,x,Z2LL,Z2UL));
yb3=(int(fb31,x,Z3LL,Z3UL));

yb1x=subs(yb1,Ac,x);
yb2x=subs(yb2,Ac,x);
yb3x=subs(yb3,Ac,x);
Yb=yb1x+yb2x+yb3x      % Should be added +yb1nx for WebHole Joist
YbMax=subs(Yb,x,Ld)
Case= 'This is Sub Case 1nA'
    case 2 % SUBCASE 1nC ## Pc at the Right side of the Notch ##
        SUBCASE 1nC

```

```

Zone 1a 1b 1c 1d: x>> 0 to a
    Z1LL=0;
    Z1NLL=Ln;
    Z1NUL=Ln+Bn;
    Z1ML=Ac;
    Z1UL=a;

    V11=P+Pc*(L-Ac)/L;
    V11n=V11;
    V12=V11-Pc;
    M11=P*x+Pc*(L-Ac)/L*x; % Simply Supported Beam with two Point
Loads P+P at a & b
    M11n=M11;
    M12=M11-Pc*(x-Ac); % Simply Supported Beam with two Point
Loads P+P at a & b

    % Zone 2: x>> a to b
    Z2LL=Z1UL;
    Z2UL=b;

    V21=V12-P;
    V22=0; %N/A
    M21=M12-P*(x-a); % Simply Supported Beam with two Point Loads
P+P at a & b
    M22=0; %N/A

    % Zone 3: x>> b to L
    Z3LL=Z2UL;
    Z3UL=L;

    V31=V21-P;
    V32=0; %N/A
    M31=M21-P*(x-b); % Simply Supported Beam with two Point Loads
P+P at a & b
    M32=0;

    D11VPc = diff(V11,Pc);
    D11nVPc = diff(V11n,Pc);
    D12VPc = diff(V12,Pc);
    D21VPc = diff(V21,Pc);
    D22VPc = diff(V22,Pc);
    D31VPc = diff(V31,Pc);
    D32VPc = diff(V32,Pc);

    D11MPc = diff(M11,Pc);
    D11nMPc = diff(M11n,Pc);
    D12MPc = diff(M12,Pc);
    D21MPc = diff(M21,Pc);
    D22MPc = diff(M22,Pc);
    D31MPc = diff(M31,Pc);
    D32MPc = diff(M32,Pc);

```



```

V11=subs(V11,Pc,0);
    DV11=subs(D11VPc,Pc,0);
V11n=subs(V11n,Pc,0);
    DV11n=subs(D11nVPc,Pc,0);
V12=subs(V12,Pc,0);
    DV12=subs(D12VPc,Pc,0);
V21=subs(V21,Pc,0);
    DV21=subs(D21VPc,Pc,0);
V22=subs(V22,Pc,0);
    DV22=subs(D22VPc,Pc,0);
V31=subs(V31,Pc,0);
    DV31=subs(D31VPc,Pc,0);
V32=subs(V32,Pc,0);
    DV32=subs(D32VPc,Pc,0);

M11=subs(M11,Pc,0);
    DM11=subs(D11MPc,Pc,0);
M11n=subs(M11n,Pc,0);
    DM11n=subs(D11nMPc,Pc,0);
M12=subs(M12,Pc,0);
    DM12=subs(D12MPc,Pc,0);
M21=subs(M21,Pc,0);
    DM21=subs(D21MPc,Pc,0);
M22=subs(M22,Pc,0);
    DM22=subs(D22MPc,Pc,0);
M31=subs(M31,Pc,0);
    DM31=subs(D31MPc,Pc,0);
M32=subs(M32,Pc,0);
    DM32=subs(D32MPc,Pc,0);

fv11=fs*V11*DV11/(G*A);
fv11n=fsn*V11n*DV11n/(Gn*An);
fv12=fs*V12*DV12/(G*A);
fv21=fs*V21*DV21/(G*A);
fv22=fs*V22*DV22/(G*A);
fv31=fs*V31*DV31/(G*A);
fv32=fs*V32*DV32/(G*A);

fb11=M11*DM11/(E*I);
fb11n=M11n*DM11n/(En*In);
fb12=M12*DM12/(E*I);
fb21=M21*DM21/(E*I);
fb22=M22*DM22/(E*I);
fb31=M31*DM31/(E*I);
fb32=M32*DM32/(E*I);

%yv1=(int(fv11,x,Z1LL,Z1NLL)+int(fv11n,x,Z1NLL,Z1NUL)+int(fv11,x,Z1NUL
,Z1ML)+int(fv12,x,Z1ML,Z1UL));
if Dias>0

```

```

yv1=(int (fv11,x,Z1LL,Z1NLL)+int (fv11,x,Z1NUL,Z1ML)+int (fv12,x,Z1ML,Z1U
L));
    yv1n=int (fv11n,x,Z1NLL,Z1NUL)           % Always Display for WebHole
Joist
    yv1nx=subs (yv1n,Ac,x)                   % Always Display for WebHole
Joist
else

yv1=(int (fv11,x,Z1LL,Z1NLL)+int (fv11n,x,Z1NLL,Z1NUL)+int (fv11,x,Z1NUL,
Z1ML)+int (fv12,x,Z1ML,Z1UL));
end
yv2=(int (fv21,x,Z2LL,Z2UL));
yv3=(int (fv31,x,Z3LL,Z3UL));

yv1x=subs (yv1,Ac,x);
yv2x=subs (yv2,Ac,x);
yv3x=subs (yv3,Ac,x);
Yv=yv1x+yv2x+yv3x    % Should be added +yv1nx for WebHole Joist
YvMax=subs (Yv,x,Ld)

%yb1=(int (fb11,x,Z1LL,Z1NLL)+int (fb11n,x,Z1NLL,Z1NUL)+int (fb11,x,Z1NUL
,Z1ML)+int (fb12,x,Z1ML,Z1UL));
if Dias>0

yb1=(int (fb11,x,Z1LL,Z1NLL)+int (fb11,x,Z1NUL,Z1ML)+int (fb12,x,Z1ML,Z1U
L));
    yb1n=int (fb11n,x,Z1NLL,Z1NUL)           % Always Display for WebHole
Joist
    yb1nx=subs (yb1n,Ac,x)                   % Always Display for WebHole
Joist
else

yb1=(int (fb11,x,Z1LL,Z1NLL)+int (fb11n,x,Z1NLL,Z1NUL)+int (fb11,x,Z1NUL,
Z1ML)+int (fb12,x,Z1ML,Z1UL));
end
yb2=(int (fb21,x,Z2LL,Z2UL));
yb3=(int (fb31,x,Z3LL,Z3UL));

yb1x=subs (yb1,Ac,x);
yb2x=subs (yb2,Ac,x);
yb3x=subs (yb3,Ac,x);
Yb=yb1x+yb2x+yb3x    % Should be added +yb1nx for WebHole Joist
YbMax=subs (Yb,x,Ld)
Case= 'This is Sub Case 1nC'
    case 3 % SUBCASE 1nB    ## Pc at the Notch Location ##
        SUBCASE 1nB
        Zone 1a 1b 1c 1d: x>> 0 to a
            Z1LL=0;
            Z1NLL=Ln;
            Z1NUL=Ln+Bn;
            Z1ML=Ac;

```

```

Z1UL=a;

V11=P+Pc*(L-Ac)/L;
V11n=V11;
V12=V11-Pc;
V12n=V12;
M11=P*x+Pc*(L-Ac)/L*x; % Simply Supported Beam with two Point
Loads P+P at a & b
M11n=M11;
M12=M11-Pc*(x-Ac); % Simply Supported Beam with two Point
Loads P+P at a & b
M12n=M12;

% Zone 2: x>> a to b
Z2LL=Z1UL;
Z2UL=b;

V21=V12-P;
V22=0; %N/A
M21=M12-P*(x-a); % Simply Supported Beam with two Point Loads
P+P at a & b
M22=0; %N/A

% Zone 3: x>> b to L
Z3LL=Z2UL;
Z3UL=L;

V31=V21-P;
V32=0; %N/A
M31=M21-P*(x-b); % Simply Supported Beam with two Point Loads
P+P at a & b
M32=0;

D11VPc = diff(V11,Pc);
D11nVPc = diff(V11n,Pc);
D12VPc = diff(V12,Pc);
D12nVPc = diff(V12n,Pc);
D21VPc = diff(V21,Pc);
D22VPc = diff(V22,Pc);
D31VPc = diff(V31,Pc);
D32VPc = diff(V32,Pc);

D11MPc = diff(M11,Pc);
D11nMPc = diff(M11n,Pc);
D12MPc = diff(M12,Pc);
D12nMPc = diff(M12n,Pc);
D21MPc = diff(M21,Pc);
D22MPc = diff(M22,Pc);
D31MPc = diff(M31,Pc);
D32MPc = diff(M32,Pc);

```

```

V11=subs (V11,Pc,0);
    DV11=subs (D11VPc,Pc,0);
V11n=subs (V11n,Pc,0);
    DV11n=subs (D11nVPc,Pc,0);
V12=subs (V12,Pc,0);
    DV12=subs (D12VPc,Pc,0);
V12n=subs (V12n,Pc,0);
    DV12n=subs (D12nVPc,Pc,0);
V21=subs (V21,Pc,0);
    DV21=subs (D21VPc,Pc,0);
V22=subs (V22,Pc,0);
    DV22=subs (D22VPc,Pc,0);
V31=subs (V31,Pc,0);
    DV31=subs (D31VPc,Pc,0);
V32=subs (V32,Pc,0);
    DV32=subs (D32VPc,Pc,0);

M11=subs (M11,Pc,0);
    DM11=subs (D11MPc,Pc,0);
M11n=subs (M11n,Pc,0);
    DM11n=subs (D11nMPc,Pc,0);
M12=subs (M12,Pc,0);
    DM12=subs (D12MPc,Pc,0);
M12n=subs (M12n,Pc,0);
    DM12n=subs (D12nMPc,Pc,0);
M21=subs (M21,Pc,0);
    DM21=subs (D21MPc,Pc,0);
M22=subs (M22,Pc,0);
    DM22=subs (D22MPc,Pc,0);
M31=subs (M31,Pc,0);
    DM31=subs (D31MPc,Pc,0);
M32=subs (M32,Pc,0);
    DM32=subs (D32MPc,Pc,0);

fv11=fs*V11*DV11/(G*A);
fv11n=fsn*V11n*DV11n/(Gn*An);
fv12=fs*V12*DV12/(G*A);
fv12n=fsn*V12n*DV12n/(Gn*An);
fv21=fs*V21*DV21/(G*A);
fv22=fs*V22*DV22/(G*A);
fv31=fs*V31*DV31/(G*A);
fv32=fs*V32*DV32/(G*A);

fb11=M11*DM11/(E*I);
fb11n=M11n*DM11n/(En*In);
fb12=M12*DM12/(E*I);
fb12n=M12n*DM12n/(En*In);
fb21=M21*DM21/(E*I);
fb22=M22*DM22/(E*I);
fb31=M31*DM31/(E*I);
fb32=M32*DM32/(E*I);

```

```

%yv1=(int (fv11,x,Z1LL,Z1NLL)+int (fv11n,x,Z1NLL,Z1ML)+int (fv12n,x,Z1ML,Z
Z1NUL)+int (fv12,x,Z1NUL,Z1UL));
if Dias>0
    yv1=(int (fv11,x,Z1LL,Z1NLL)+int (fv12,x,Z1NUL,Z1UL));
    yv1n=int (fv11n,x,Z1NLL,Z1ML)+int (fv12n,x,Z1ML,Z1NUL)           %
Always Display for WebHole Joist
    yv1nx=subs (yv1n,Ac,x)                                           % Always Display for WebHole
Joist
else

yv1=(int (fv11,x,Z1LL,Z1NLL)+int (fv11n,x,Z1NLL,Z1ML)+int (fv12n,x,Z1ML,Z
1NUL)+int (fv12,x,Z1NUL,Z1UL));
end
yv2=(int (fv21,x,Z2LL,Z2UL));
yv3=(int (fv31,x,Z3LL,Z3UL));

yv1x=subs (yv1,Ac,x);
yv2x=subs (yv2,Ac,x);
yv3x=subs (yv3,Ac,x);
Yv=yv1x+yv2x+yv3x
YvMax=subs (Yv,x,Ld)

%yb1=(int (fb11,x,Z1LL,Z1NLL)+int (fb11n,x,Z1NLL,Z1ML)+int (fb12n,x,Z1ML,Z
Z1NUL)+int (fb12,x,Z1NUL,Z1UL));
if Dias>0
    yb1=(int (fb11,x,Z1LL,Z1NLL)+int (fb12,x,Z1NUL,Z1UL));
    yb1n=int (fb11n,x,Z1NLL,Z1ML)+int (fb12n,x,Z1ML,Z1NUL)           %
Always Display for WebHole Joist
    yb1nx=subs (yb1n,Ac,x)                                           % Always Display for WebHole
Joist
else

yb1=(int (fb11,x,Z1LL,Z1NLL)+int (fb11n,x,Z1NLL,Z1ML)+int (fb12n,x,Z1ML,Z
1NUL)+int (fb12,x,Z1NUL,Z1UL));
end
yb2=(int (fb21,x,Z2LL,Z2UL));
yb3=(int (fb31,x,Z3LL,Z3UL));

yb1x=subs (yb1,Ac,x);
yb2x=subs (yb2,Ac,x);
yb3x=subs (yb3,Ac,x);
Yb=yb1x+yb2x+yb3x
YbMax=subs (Yb,x,Ld)
Case= 'This is Sub Case 1nB At Notch Location'
    end % End of Switch SCs
    case 2 % 2N
        CASE :2n Code for Mid Span Deflection
        Zone 1: x>> 0 to a
            Z1LL=0;
            Z1NLL=Ln;

```

```

Z1NUL=Ln+Bn;
Z1UL=a;

V11=P+Pc*(L-Ac)/L;
V11n=V11;
V12=0;
M11=P*x+Pc*(L-Ac)/L*x; % Simply Supported Beam with two Point
Loads P+P at a & b
M11n=M11;

% Zone 2: x>> a to b
Z2LL=Z1UL;
Z2ML=Ac;
Z2UL=b;

V21=V11-P;
V22=V21-Pc;
M21=M11-P*(x-a); % Simply Supported Beam with two Point Loads
P+P at a & b
M22=M21-Pc*(x-Ac);

% Zone 3: x>> b to L
Z3LL=Z2UL;
Z3UL=L;

V31=V22-P;
V32=0;
M31=M22-P*(x-b); % Simply Supported Beam with two Point Loads
P+P at a & b
M32=0;

D11VPc = diff(V11,Pc);
D11nVPc = diff(V11n,Pc);
D12VPc = diff(V12,Pc);
D21VPc = diff(V21,Pc);
D22VPc = diff(V22,Pc);
D31VPc = diff(V31,Pc);
D32VPc = diff(V32,Pc);

D11MPc = diff(M11,Pc);
D11nMPc = diff(M11n,Pc);
D12MPc = diff(M12,Pc);
D21MPc = diff(M21,Pc);
D22MPc = diff(M22,Pc);
D31MPc = diff(M31,Pc);
D32MPc = diff(M32,Pc);

V11=subs(V11,Pc,0);
DV11=subs(D11VPc,Pc,0);
V11n=subs(V11n,Pc,0);
DV11n=subs(D11nVPc,Pc,0);

```

```

V12=subs (V12,Pc,0);
DV12=subs (D12VPc,Pc,0);
V21=subs (V21,Pc,0);
DV21=subs (D21VPc,Pc,0);
V22=subs (V22,Pc,0);
DV22=subs (D22VPc,Pc,0);
V31=subs (V31,Pc,0);
DV31=subs (D31VPc,Pc,0);
V32=subs (V32,Pc,0);
DV32=subs (D32VPc,Pc,0);

M11=subs (M11,Pc,0);
DM11=subs (D11MPc,Pc,0);
M11n=subs (M11n,Pc,0);
DM11n=subs (D11nMPc,Pc,0);
M12=subs (M12,Pc,0);
DM12=subs (D12MPc,Pc,0);
M21=subs (M21,Pc,0);
DM21=subs (D21MPc,Pc,0);
M22=subs (M22,Pc,0);
DM22=subs (D22MPc,Pc,0);
M31=subs (M31,Pc,0);
DM31=subs (D31MPc,Pc,0);
M32=subs (M32,Pc,0);
DM32=subs (D32MPc,Pc,0);

fv11=fs*V11*DV11/(G*A);
fv11n=fsn*V11n*DV11n/(Gn*An);
fv12=fs*V12*DV12/(G*A);
fv21=fs*V21*DV21/(G*A);
fv22=fs*V22*DV22/(G*A);
fv31=fs*V31*DV31/(G*A);
fv32=fs*V32*DV32/(G*A);

fb11=M11*DM11/(E*I);
fb11n=M11n*DM11n/(En*In);
fb12=M12*DM12/(E*I);
fb21=M21*DM21/(E*I);
fb22=M22*DM22/(E*I);
fb31=M31*DM31/(E*I);
fb32=M32*DM32/(E*I);

%
yv1=(int (fv11,x,Z1LL,Z1NLL)+int (fv11n,x,Z1NLL,Z1NUL)+int (fv11,x,Z1NUL,
Z1UL));
if Dias>0
    yv1=(int (fv11,x,Z1LL,Z1NLL)+int (fv11,x,Z1NUL,Z1UL));
    yv1n=int (fv11n,x,Z1NLL,Z1NUL) % Always Display for WebHole
Joist
    yv1nx=subs (yv1n,Ac,x) % Always Display for WebHole
Joist

```

```

else

yv1=(int (fv11,x,Z1LL,Z1NLL)+int (fv11n,x,Z1NLL,Z1NUL)+int (fv11,x,Z1NUL,
Z1UL));
end
yv2=(int (fv21,x,Z2LL,Z2ML)+int (fv22,x,Z2ML,Z2UL));
yv3=(int (fv31,x,Z3LL,Z3UL));

yv1x=subs (yv1,Ac,x);
% yv1nx=subs (yv1n,Ac,x)
yv2x=subs (yv2,Ac,x);
yv3x=subs (yv3,Ac,x);
Yv=yv1x+yv2x+yv3x % Should be added +yv1nx for WebHole Joist
YvMax=subs (Yv,x,Ld)

%
yb1=(int (fb11,x,Z1LL,Z1NLL)+int (fb11n,x,Z1NLL,Z1NUL)+int (fb11,x,Z1NUL,
Z1UL));
if Dias>0
    yb1=(int (fb11,x,Z1LL,Z1NLL)+int (fb11,x,Z1NUL,Z1UL));
    yb1n=int (fb11n,x,Z1NLL,Z1NUL) % Always Display for WebHole
Joist
    yb1nx=subs (yb1n,Ac,x) % Always Display for WebHole
Joist
else

yb1=(int (fb11,x,Z1LL,Z1NLL)+int (fb11n,x,Z1NLL,Z1NUL)+int (fb11,x,Z1NUL,
Z1UL));
end
% yb1n =int (fb11n,x,Z1NLL,Z1NUL);
yb2=(int (fb21,x,Z2LL,Z2ML)+int (fb22,x,Z2ML,Z2UL));
yb3=(int (fb31,x,Z3LL,Z3UL));

yb1x=subs (yb1,Ac,x);
% yb1nx=subs (yb1n,Ac,x)
yb2x=subs (yb2,Ac,x);
yb3x=subs (yb3,Ac,x);
Yb=yb1x+yb2x+yb3x % Should be added +yb1nx for WebHole Joist
YbMax=subs (Yb,x,Ld)
    Finding the Location of Maximum Deflection.
    Yt=Yv+Yb;
Yv=subs (Yv,[L,E,I,G,A,fs],[L,Eo,Io,Go,Ao,fso])
Yb=subs (Yb,[L,E,I,G,A,fs],[L,Eo,Io,Go,Ao,fso])
Yt=subs (Yt,[L,E,I,G,A,fs],[L,Eo,Io,Go,Ao,fso])
DYt1 = diff(Yt);
X_Deltamax=solve(DYt1,x)
X_DL_Check=subs (X_Deltamax,[Bn,Dn,Ln,En,In,Gn,
An,fsn],[0,0,0,E,I,G,A,fs])
syms X_max
X_Deltamax=X_max;
YtMax=subs (Yt,x,X_Deltamax)

```



```

YtMax_Check=subs(YtMax,[X_Deltamax,Bn,Dn,Ln,En,In,Gn,An,fsn],[L/2,0,0,
0,E,I,G,A,fs])
Case= 'This is Case 2n'
    case 3 % 3N
    CASE :3n Code for Right Span Deflection
    Zone 1: x>> 0 to L/3
        Z1LL=0;
        Z1NLL=Ln;
        Z1NUL=Ln+Bn;
        Z1UL=a;

        V11=P+Pc*(L-Ac)/L;
        V11n=V11;
        V12=0;
        M11=P*x+Pc*(L-Ac)/L*x; % Simply Supported Beam with two Point
Loads P+P at a & b
        M11n=M11;

        % Zone 2: x>> L/3 to 2L/3
        Z2LL=Z1UL;
        Z2UL=b;

        V21=V11-P;
        V22=0; %N/A
        M21=M11-P*(x-a); % Simply Supported Beam with two Point Loads
P+P at a & b

        % Zone 3: x>> 2L/3 to L
        Z3LL=Z2UL;
        Z3ML=Ac;
        Z3UL=L;

        V31=V21-P;
        V32=V31-Pc; %N/A
        M31=M21-P*(x-b); % Simply Supported Beam with two Point Loads
P+P at a & b
        M32=M31-Pc*(x-Ac);

        D11VPc = diff(V11,Pc);
        D11nVPc = diff(V11n,Pc);
        D12VPc = diff(V12,Pc);
        D21VPc = diff(V21,Pc);
        D22VPc = diff(V22,Pc);
        D31VPc = diff(V31,Pc);
        D32VPc = diff(V32,Pc);

        D11MPc = diff(M11,Pc);
        D11nMPc = diff(M11n,Pc);
        D12MPc = diff(M12,Pc);
        D21MPc = diff(M21,Pc);
        D22MPc = diff(M22,Pc);

```

```

D31MPc = diff(M31,Pc);
D32MPc = diff(M32,Pc);

V11=subs(V11,Pc,0);
    DV11=subs(D11VPc,Pc,0);
V11n=subs(V11n,Pc,0);
    DV11n=subs(D11nVPc,Pc,0);
V12=subs(V12,Pc,0);
    DV12=subs(D12VPc,Pc,0);
V21=subs(V21,Pc,0);
    DV21=subs(D21VPc,Pc,0);
V22=subs(V22,Pc,0);
    DV22=subs(D22VPc,Pc,0);
V31=subs(V31,Pc,0);
    DV31=subs(D31VPc,Pc,0);
V32=subs(V32,Pc,0);
    DV32=subs(D32VPc,Pc,0);

M11=subs(M11,Pc,0);
    DM11=subs(D11MPc,Pc,0);
M11n=subs(M11n,Pc,0);
    DM11n=subs(D11nMPc,Pc,0);
M12=subs(M12,Pc,0);
    DM12=subs(D12MPc,Pc,0);
M21=subs(M21,Pc,0);
    DM21=subs(D21MPc,Pc,0);
M22=subs(M22,Pc,0);
    DM22=subs(D22MPc,Pc,0);
M31=subs(M31,Pc,0);
    DM31=subs(D31MPc,Pc,0);
M32=subs(M32,Pc,0);
    DM32=subs(D32MPc,Pc,0);

fv11=fs*V11*DV11/(G*A);
fv11n=fsn*V11n*DV11n/(Gn*An);
fv12=fs*V12*DV12/(G*A);
fv21=fs*V21*DV21/(G*A);
fv22=fs*V22*DV22/(G*A);
fv31=fs*V31*DV31/(G*A);
fv32=fs*V32*DV32/(G*A);

fb11=M11*DM11/(E*I);
fb11n=M11n*DM11n/(En*In);
fb12=M12*DM12/(E*I);
fb21=M21*DM21/(E*I);
fb22=M22*DM22/(E*I);
fb31=M31*DM31/(E*I);
fb32=M32*DM32/(E*I);

%
yv1=(int(fv11,x,Z1LL,Z1NLL)+int(fv11n,x,Z1NLL,Z1NUL)+int(fv11,x,Z1NUL,

```

```

Z1UL));
if Dias>0
    yv1=(int(fv11,x,Z1LL,Z1NLL)+int(fv11,x,Z1NUL,Z1UL));
    yv1n=int(fv11n,x,Z1NLL,Z1NUL)           % Always Display for WebHole
Joist
    yv1nx=subs(yv1n,Ac,x)                   % Always Display for WebHole
Joist
else

yv1=(int(fv11,x,Z1LL,Z1NLL)+int(fv11n,x,Z1NLL,Z1NUL)+int(fv11,x,Z1NUL,
Z1UL));
end
yv2=(int(fv21,x,Z2LL,Z2UL));
yv3=(int(fv31,x,Z3LL,Z3ML)+int(fv32,x,Z3ML,Z3UL));

yv1x=subs(yv1,Ac,x);
yv2x=subs(yv2,Ac,x);
yv3x=subs(yv3,Ac,x);
Yv=yv1x+yv2x+yv3x % Should be added +yv1nx for WebHole Joist
YvMax=subs(Yv,x,Ld)

%
yb1=(int(fb11,x,Z1LL,Z1NLL)+int(fb11n,x,Z1NLL,Z1NUL)+int(fb11,x,Z1NUL,
Z1UL));
if Dias>0
    yb1=(int(fb11,x,Z1LL,Z1NLL)+int(fb11,x,Z1NUL,Z1UL));
    yb1n=int(fb11n,x,Z1NLL,Z1NUL)           % Always Display for WebHole
Joist
    yb1nx=subs(yb1n,Ac,x)                   % Always Display for WebHole
Joist
else

yb1=(int(fb11,x,Z1LL,Z1NLL)+int(fb11n,x,Z1NLL,Z1NUL)+int(fb11,x,Z1NUL,
Z1UL));
end
yb2=(int(fb21,x,Z2LL,Z2UL));
yb3=(int(fb31,x,Z3LL,Z3ML)+int(fb32,x,Z3ML,Z3UL));

yb1x=subs(yb1,Ac,x);
yb2x=subs(yb2,Ac,x);
yb3x=subs(yb3,Ac,x);
Yb=yb1x+yb2x+yb3x % Should be added +yb1nx for WebHole Joist
YbMax=subs(Yb,x,Ld)
Case= 'This is Case 3n'
    end % End of Switch
    else % Reinforced Beam
    Deflction of Reinforced Beam
    Three Cases and Thre Sub Cases for Case 1
        switch Cs

case 1 % 1R

```

```

CASE 1r: Code for Left Span Deflection
Case 1r consists of three sub cases(SCs).
switch SCs

    case 1 % SUBCASE 1rA  ## Pc at the Left side of the Notch and
Reinforcer ##
SUBCASE 1rA
Zone 1A 1B 1C 1D 1E + 1A' = 6 sub zones: x>> 0 to a
    Z1LL=0;
    Z1RLL=Ln-Lr;
    Z1NLL=Ln;
    Z1NUL=Ln+Bn;
    Z1RUL=Ln+Bn+Lr;
    Z1ML=Ac;
    Z1UL=a;

    V11=P+Pc*(L-Ac)/L;
    V12=V11-Pc;
    V12r=V12;
    V12rn=V12;
    M11=P*x+Pc*(L-Ac)/L*x; % Simply Supported Beam with two Point
Loads P+P at a & b
    M12=M11-Pc*(x-Ac); % Simply Supported Beam with two Point
Loads P+P at a & b
    M12r=M12;
    M12rn=M12;
    % Zone 2: x>> a to b
    Z2LL=Z1UL;
    Z2UL=b;

    V21=V12-P;
    V22=0; %N/A
    M21=M12-P*(x-a); % Simply Supported Beam with two Point Loads
P+P at a & b
    M22=0; %N/A

    % Zone 3: x>> b to L
    Z3LL=Z2UL;
    Z3UL=L;

    V31=V21-P;
    V32=0; %N/A
    M31=M21-P*(x-b); % Simply Supported Beam with two Point Loads
P+P at a & b
    M32=0;

    D11VPc = diff(V11,Pc);
    D12VPc = diff(V12,Pc);
    D12rVPc = diff(V12r,Pc);
    D12rnVPc = diff(V12rn,Pc);
    D21VPc = diff(V21,Pc);

```

```

D22VPc = diff(V22,Pc);
D31VPc = diff(V31,Pc);
D32VPc = diff(V32,Pc);

D11MPc = diff(M11,Pc);
D12MPc = diff(M12,Pc);
D12rMPc = diff(M12r,Pc);
D12rnMPc = diff(M12rn,Pc);
D21MPc = diff(M21,Pc);
D22MPc = diff(M22,Pc);
D31MPc = diff(M31,Pc);
D32MPc = diff(M32,Pc);

V11=subs(V11,Pc,0);
    DV11=subs(D11VPc,Pc,0);
V12=subs(V12,Pc,0);
    DV12=subs(D12VPc,Pc,0);
V12r=subs(V12r,Pc,0);
    DV12r=subs(D12rVPc,Pc,0);
V12rn=subs(V12rn,Pc,0);
    DV12rn=subs(D12rnVPc,Pc,0);
V21=subs(V21,Pc,0);
    DV21=subs(D21VPc,Pc,0);
V22=subs(V22,Pc,0);
    DV22=subs(D22VPc,Pc,0);
V31=subs(V31,Pc,0);
    DV31=subs(D31VPc,Pc,0);
V32=subs(V32,Pc,0);
    DV32=subs(D32VPc,Pc,0);

M11=subs(M11,Pc,0);
    DM11=subs(D11MPc,Pc,0);
M12=subs(M12,Pc,0);
    DM12=subs(D12MPc,Pc,0);
M12r=subs(M12r,Pc,0);
    DM12r=subs(D12rMPc,Pc,0);
M12rn=subs(M12rn,Pc,0);
    DM12rn=subs(D12rnMPc,Pc,0);
M21=subs(M21,Pc,0);
    DM21=subs(D21MPc,Pc,0);
M22=subs(M22,Pc,0);
    DM22=subs(D22MPc,Pc,0);
M31=subs(M31,Pc,0);
    DM31=subs(D31MPc,Pc,0);
M32=subs(M32,Pc,0);
    DM32=subs(D32MPc,Pc,0);

fv11=fs*V11*DV11/(G*A);
fv12=fs*V12*DV12/(G*A);
fv12r=fsr*V12r*DV12r/(Gr*Ar);
fv12rn=fsrn*V12rn*DV12rn/(Grn*Arn);

```

```

fv21=fs*V21*DV21/(G*A);
fv22=fs*V22*DV22/(G*A);
fv31=fs*V31*DV31/(G*A);
fv32=fs*V32*DV32/(G*A);

fb11=M11*DM11/(E*I);
fb12=M12*DM12/(E*I);
fb12r=M12r*DM12r/(Er*Ir);
fb12rn=M12rn*DM12rn/(Ern*Irn);
fb21=M21*DM21/(E*I);
fb22=M22*DM22/(E*I);
fb31=M31*DM31/(E*I);
fb32=M32*DM32/(E*I);

%
yv1=(int(fv11,x,Z1LL,Z1ML)+int(fv12,x,Z1ML,Z1RLL)+int(fv12r,x,Z1RLL,Z1
NLL)+int(fv12rn,x,Z1NLL,Z1NUL)+int(fv12r,x,Z1NUL,Z1RUL)+int(fv12,x,Z1R
UL,Z1UL));
if Dias>0

yv1=(int(fv11,x,Z1LL,Z1ML)+int(fv12,x,Z1ML,Z1RLL)+int(fv12r,x,Z1RLL,Z1
NLL)+int(fv12r,x,Z1NUL,Z1RUL)+int(fv12,x,Z1RUL,Z1UL));
    yv1rn=int(fv12rn,x,Z1NLL,Z1NUL)           % Always Display for WebHole
Joist
    yv1rnx=subs(yv1rn,Ac,x)                   % Always Display for WebHole
Joist
else

yv1=(int(fv11,x,Z1LL,Z1ML)+int(fv12,x,Z1ML,Z1RLL)+int(fv12r,x,Z1RLL,Z1
NLL)+int(fv12rn,x,Z1NLL,Z1NUL)+int(fv12r,x,Z1NUL,Z1RUL)+int(fv12,x,Z1R
UL,Z1UL));
end
yv2=(int(fv21,x,Z2LL,Z2UL));
yv3=(int(fv31,x,Z3LL,Z3UL));

yv1x=subs(yv1,Ac,x);
yv2x=subs(yv2,Ac,x);
yv3x=subs(yv3,Ac,x);
Yv=yv1x+yv2x+yv3x
YvMax=subs(Yv,x,Ld)

% yb1=
(int(fb11,x,Z1LL,Z1ML)+int(fb12,x,Z1ML,Z1RLL)+int(fb12r,x,Z1RLL,Z1NLL)
+int(fb12rn,x,Z1NLL,Z1NUL)+int(fb12r,x,Z1NUL,Z1RUL)+int(fb12,x,Z1RUL,Z
1UL));
if Dias>0
    yb1=
(int(fb11,x,Z1LL,Z1ML)+int(fb12,x,Z1ML,Z1RLL)+int(fb12r,x,Z1RLL,Z1NLL)
+int(fb12r,x,Z1NUL,Z1RUL)+int(fb12,x,Z1RUL,Z1UL));
    yb1rn=int(fb12rn,x,Z1NLL,Z1NUL)           % Always Display for WebHole
Joist

```

```

        yb1rn=subs(yb1rn,Ac,x)                                % Always Display for WebHole
Joist
else
    yb1=
    (int(fb1l,x,Z1LL,Z1ML)+int(fb12,x,Z1ML,Z1RLL)+int(fb12r,x,Z1RLL,Z1NLL)
    +int(fb12rn,x,Z1NLL,Z1NUL)+int(fb12r,x,Z1NUL,Z1RUL)+int(fb12,x,Z1RUL,Z
    1UL));
end
yb2=(int(fb2l,x,Z2LL,Z2UL));
yb3=(int(fb3l,x,Z3LL,Z3UL));

yb1x=subs(yb1,Ac,x);
yb2x=subs(yb2,Ac,x);
yb3x=subs(yb3,Ac,x);
Yb=yb1x+yb2x+yb3x
YbMax=subs(Yb,x,Ld)
Case= 'This is Sub Case 1rA'
    case 2 % SUBCASE 1rB  ## Pc at the Left side of the Notch But over
the Reinforcer ##
        SUBCASE 1rB
            Zone 1A 1B 1C 1D 1E + 1B' = 6 sub zones: x>> 0 to a
                Z1LL=0;
                Z1RLL=Ln-Lr;
                Z1NLL=Ln;
                Z1NUL=Ln+Bn;
                Z1RUL=Ln+Bn+Lr;
                Z1ML=Ac;
                Z1UL=a;

                V1l=P+Pc*(L-Ac)/L;
                V1lr=V1l;
                V12r=V1lr-Pc; % Zone B'
                V12rn=V12r;
                V12=V12rn;
                M1l=P*x+Pc*(L-Ac)/L*x; % Simply Supported Beam with two Point
Loads P+P at a & b
                M1lr=M1l;
                M12r=M1l-Pc*(x-Ac); % Zone B'
                M12rn=M12r; % Simply Supported Beam with two Point Loads P+P
at a & b
                M12=M12rn;

                % Zone 2: x>> a to b
                Z2LL=Z1UL;
                Z2UL=b;

                V21=V12-P;
                V22=0; %N/A
                M21=M12-P*(x-a); % Simply Supported Beam with two Point Loads
P+P at a & b
                M22=0; %N/A

```

```

% Zone 3: x>> b to L
Z3LL=Z2UL;
Z3UL=L;

V31=V21-P;
V32=0; %N/A
M31=M21-P*(x-b); % Simply Supported Beam with two Point Loads
P+P at a & b
M32=0;

D11VPc = diff(V11,Pc);
D11rVPc = diff(V11r,Pc);
D12rVPc = diff(V12r,Pc);
D12rnVPc = diff(V12rn,Pc);
D12VPc = diff(V12,Pc);
D21VPc = diff(V21,Pc);
D22VPc = diff(V22,Pc);
D31VPc = diff(V31,Pc);
D32VPc = diff(V32,Pc);

D11MPc = diff(M11,Pc);
D11rMPc = diff(M11r,Pc);
D12rMPc = diff(M12r,Pc);
D12rnMPc = diff(M12rn,Pc);
D12MPc = diff(M12,Pc);
D21MPc = diff(M21,Pc);
D22MPc = diff(M22,Pc);
D31MPc = diff(M31,Pc);
D32MPc = diff(M32,Pc);

V11=subs(V11,Pc,0);
    DV11=subs(D11VPc,Pc,0);
V11r=subs(V11r,Pc,0);
    DV11r=subs(D11rVPc,Pc,0);
V12r=subs(V12r,Pc,0);
    DV12r=subs(D12rVPc,Pc,0);
V12rn=subs(V12rn,Pc,0);
    DV12rn=subs(D12rnVPc,Pc,0);
V12=subs(V12,Pc,0);
    DV12=subs(D12VPc,Pc,0);
V21=subs(V21,Pc,0);
    DV21=subs(D21VPc,Pc,0);
V22=subs(V22,Pc,0);
    DV22=subs(D22VPc,Pc,0);
V31=subs(V31,Pc,0);
    DV31=subs(D31VPc,Pc,0);
V32=subs(V32,Pc,0);
    DV32=subs(D32VPc,Pc,0);

M11=subs(M11,Pc,0);

```



```

        DM11=subs (D11MPc,Pc,0);
M11r=subs (M11r,Pc,0);
        DM11r=subs (D11rMPc,Pc,0);
M12r=subs (M12r,Pc,0);
        DM12r=subs (D12rMPc,Pc,0);
M12rn=subs (M12rn,Pc,0);
        DM12rn=subs (D12rnMPc,Pc,0);
M12=subs (M12,Pc,0);
        DM12=subs (D12MPc,Pc,0);
M21=subs (M21,Pc,0);
        DM21=subs (D21MPc,Pc,0);
M22=subs (M22,Pc,0);
        DM22=subs (D22MPc,Pc,0);
M31=subs (M31,Pc,0);
        DM31=subs (D31MPc,Pc,0);
M32=subs (M32,Pc,0);
        DM32=subs (D32MPc,Pc,0);

fv11=fs*V11*DV11/(G*A);
fv11r=fsr*V11r*DV11r/(Gr*Ar);
fv12r=fsr*V12r*DV12r/(Gr*Ar);
fv12rn=fsrn*V12rn*DV12rn/(Grn*Arn);
fv12=fs*V12*DV12/(G*A);
fv21=fs*V21*DV21/(G*A);
fv22=fs*V22*DV22/(G*A);
fv31=fs*V31*DV31/(G*A);
fv32=fs*V32*DV32/(G*A);

fb11=M11*DM11/(E*I);
fb11r=M11r*DM11r/(Er*Ir);
fb12r=M12r*DM12r/(Er*Ir);
fb12rn=M12rn*DM12rn/(Ern*Irn);
fb12=M12*DM12/(E*I);
fb21=M21*DM21/(E*I);
fb22=M22*DM22/(E*I);
fb31=M31*DM31/(E*I);
fb32=M32*DM32/(E*I);

%
yv1=(int (fv11,x,Z1LL,Z1RLL)+int (fv11r,x,Z1RLL,Z1ML)+int (fv12r,x,Z1ML,Z
1NLL)+int (fv12rn,x,Z1NLL,Z1NUL)+int (fv12,x,Z1NUL,Z1RUL)+int (fv12,x,Z1R
UL,Z1UL));
if Dias>0

yv1=(int (fv11,x,Z1LL,Z1RLL)+int (fv11r,x,Z1RLL,Z1ML)+int (fv12r,x,Z1ML,Z
1NLL)+int (fv12,x,Z1NUL,Z1RUL)+int (fv12,x,Z1RUL,Z1UL));
        yv1rn=int (fv12rn,x,Z1NLL,Z1NUL)                % Always Display for WebHole
Joist
        yv1rn=subs (yv1rn,Ac,x)                        % Always Display for WebHole
Joist
else

```

```

yv1=(int (fv11,x,Z1LL,Z1RLL)+int (fv11r,x,Z1RLL,Z1ML)+int (fv12r,x,Z1ML,Z
1NLL)+int (fv12rn,x,Z1NLL,Z1NUL)+int (fv12,x,Z1NUL,Z1RUL)+int (fv12,x,Z1R
UL,Z1UL));
end
yv2=(int (fv21,x,Z2LL,Z2UL));
yv3=(int (fv31,x,Z3LL,Z3UL));

yv1x=subs (yv1,Ac,x);
yv2x=subs (yv2,Ac,x);
yv3x=subs (yv3,Ac,x);
Yv=yv1x+yv2x+yv3x
YvMax=subs (Yv,x,Ld)

%
yb1=(int (fb11,x,Z1LL,Z1RLL)+int (fb11r,x,Z1RLL,Z1ML)+int (fb12r,x,Z1ML,Z
1NLL)+int (fb12rn,x,Z1NLL,Z1NUL)+int (fb12,x,Z1NUL,Z1RUL)+int (fb12,x,Z1R
UL,Z1UL)); %???????
if Dias>0

yb1=(int (fb11,x,Z1LL,Z1RLL)+int (fb11r,x,Z1RLL,Z1ML)+int (fb12r,x,Z1ML,Z
1NLL)+int (fb12,x,Z1NUL,Z1RUL)+int (fb12,x,Z1RUL,Z1UL));
    yb1rn=int (fb12rn,x,Z1NLL,Z1NUL) % Always Display for WebHole
Joist
    yb1rnx=subs (yb1rn,Ac,x) % Always Display for WebHole
Joist
else

yb1=(int (fb11,x,Z1LL,Z1RLL)+int (fb11r,x,Z1RLL,Z1ML)+int (fb12r,x,Z1ML,Z
1NLL)+int (fb12rn,x,Z1NLL,Z1NUL)+int (fb12,x,Z1NUL,Z1RUL)+int (fb12,x,Z1R
UL,Z1UL));
end
yb2=(int (fb21,x,Z2LL,Z2UL));
yb3=(int (fb31,x,Z3LL,Z3UL));

yb1x=subs (yb1,Ac,x);
yb2x=subs (yb2,Ac,x);
yb3x=subs (yb3,Ac,x);
Yb=yb1x+yb2x+yb3x
YbMax=subs (Yb,x,Ld)
Case= 'This is Sub Case 1rB'
    case 3 % SUBCASE 1rC ## Pc at the Notch Location ##
    SUBCASE 1rC
    Zone 1A 1B 1C 1D 1E + 1C' = 6 sub zones: x>> 0 to a
        Z1LL=0;
        Z1RLL=Ln-Lr;
        Z1NLL=Ln;
        Z1NUL=Ln+Bn;
        Z1RUL=Ln+Bn+Lr;
        Z1ML=Ac;
        Z1UL=a;

```

```

V11=P+Pc*(L-Ac)/L;
V11r=V11;
V11rn=V11;
V12rn=V11-Pc;
V12r=V12rn;
V12=V12r;
M11=P*x+Pc*(L-Ac)/L*x; % Simply Supported Beam with two Point
Loads P+P at a & b
M11r=M11;
M11rn=M11;
M12rn=M11-Pc*(x-Ac); % Simply Supported Beam with two Point
Loads P+P at a & b
M12r=M12rn;
M12=M12r;
% Zone 2: x>> a to b
Z2LL=Z1UL;
Z2UL=b;

V21=V12-P;
V22=0; %N/A
M21=M12-P*(x-a); % Simply Supported Beam with two Point Loads
P+P at a & b
M22=0; %N/A

% Zone 3: x>> b to L
Z3LL=Z2UL;
Z3UL=L;

V31=V21-P;
V32=0; %N/A
M31=M21-P*(x-b); % Simply Supported Beam with two Point Loads
P+P at a & b
M32=0;

D11VPc = diff(V11,Pc);
D11rVPc = diff(V11r,Pc);
D11rnVPc = diff(V11rn,Pc);
D12rnVPc = diff(V12rn,Pc);
D12rVPc = diff(V12r,Pc);
D12VPc = diff(V12,Pc);
D21VPc = diff(V21,Pc);
D22VPc = diff(V22,Pc);
D31VPc = diff(V31,Pc);
D32VPc = diff(V32,Pc);

D11MPc = diff(M11,Pc);
D11rMPc = diff(M11r,Pc);
D11rnMPc = diff(M11rn,Pc);
D12rnMPc = diff(M12rn,Pc);
D12rMPc = diff(M12r,Pc);

```

```

D12MPc = diff(M12,Pc);
D21MPc = diff(M21,Pc);
D22MPc = diff(M22,Pc);
D31MPc = diff(M31,Pc);
D32MPc = diff(M32,Pc);

V11=subs(V11,Pc,0);
    DV11=subs(D11VPc,Pc,0);
V11r=subs(V11r,Pc,0);
    DV11r=subs(D11rVPc,Pc,0);
V11rn=subs(V11rn,Pc,0);
    DV11rn=subs(D11rnVPc,Pc,0);
V12rn=subs(V12rn,Pc,0);
    DV12rn=subs(D12rnVPc,Pc,0);
V12r=subs(V12r,Pc,0);
    DV12r=subs(D12rVPc,Pc,0);
V12=subs(V12,Pc,0);
    DV12=subs(D12VPc,Pc,0);
V21=subs(V21,Pc,0);
    DV21=subs(D21VPc,Pc,0);
V22=subs(V22,Pc,0);
    DV22=subs(D22VPc,Pc,0);
V31=subs(V31,Pc,0);
    DV31=subs(D31VPc,Pc,0);
V32=subs(V32,Pc,0);
    DV32=subs(D32VPc,Pc,0);

M11=subs(M11,Pc,0);
    DM11=subs(D11MPc,Pc,0);
M11r=subs(M11r,Pc,0);
    DM11r=subs(D11rMPc,Pc,0);
M11rn=subs(M11rn,Pc,0);
    DM11rn=subs(D11rnMPc,Pc,0);
M12rn=subs(M12rn,Pc,0);
    DM12rn=subs(D12rnMPc,Pc,0);
M12r=subs(M12r,Pc,0);
    DM12r=subs(D12rMPc,Pc,0);
M12=subs(M12,Pc,0);
    DM12=subs(D12MPc,Pc,0);
M21=subs(M21,Pc,0);
    DM21=subs(D21MPc,Pc,0);
M22=subs(M22,Pc,0);
    DM22=subs(D22MPc,Pc,0);
M31=subs(M31,Pc,0);
    DM31=subs(D31MPc,Pc,0);
M32=subs(M32,Pc,0);
    DM32=subs(D32MPc,Pc,0);

fv11=fs*V11*DV11/(G*A);
fv11r=fsr*V11r*DV11r/(Gr*Ar);
fv11rn=fsrn*V11rn*DV11rn/(Grn*Arn);

```

```

fv12rn=fsrn*V12rn*DV12rn/(Grn*Arn);
fv12r=fsr*V12r*DV12r/(Gr*Ar);
fv12=fs*V12*DV12/(G*A);
fv21=fs*V21*DV21/(G*A);
fv22=fs*V22*DV22/(G*A);
fv31=fs*V31*DV31/(G*A);
fv32=fs*V32*DV32/(G*A);

fb11=M11*DM11/(E*I);
fb11r=M11r*DM11r/(Er*Ir);
fb11rn=M11rn*DM11rn/(Ern*Irn);
fb12rn=M12rn*DM12rn/(Ern*Irn);
fb12r=M12r*DM12r/(Er*Ir);
fb12=M12*DM12/(E*I);
% fn12n=M12n*DM12n/(En*In);
fb21=M21*DM21/(E*I);
fb22=M22*DM22/(E*I);
fb31=M31*DM31/(E*I);
fb32=M32*DM32/(E*I);
%Deflection due to Shear
%yv1=(int(fv11,x,Z1LL,Z1RLL)+int(fv11r,x,Z1RLL,Z1NLL)+int(fv11rn,x,Z1NLL,Z1ML)+int(fv12rn,x,Z1ML,Z1NUL)+int(fv12r,x,Z1NUL,Z1RUL)+int(fv12,x,Z1RUL,Z1UL));
if Dias>0

yv1=(int(fv11,x,Z1LL,Z1RLL)+int(fv11r,x,Z1RLL,Z1NLL)+int(fv12r,x,Z1NUL,Z1RUL)+int(fv12,x,Z1RUL,Z1UL));
    yv1rn=int(fv11rn,x,Z1NLL,Z1ML)+int(fv12rn,x,Z1ML,Z1NUL) %
Always Display for WebHole Joist
    yv1rn=subs(yv1rn,Ac,x) % Always Display for WebHole Joist
else

yv1=(int(fv11,x,Z1LL,Z1RLL)+int(fv11r,x,Z1RLL,Z1NLL)+int(fv11rn,x,Z1NLL,Z1ML)+int(fv12rn,x,Z1ML,Z1NUL)+int(fv12r,x,Z1NUL,Z1RUL)+int(fv12,x,Z1RUL,Z1UL));
end
yv2=(int(fv21,x,Z2LL,Z2UL));
yv3=(int(fv31,x,Z3LL,Z3UL));

yv1x=subs(yv1,Ac,x);
yv2x=subs(yv2,Ac,x);
yv3x=subs(yv3,Ac,x);
Yv=yv1x+yv2x+yv3x
YvMax=subs(Yv,x,Ld)
%Deflection due to Moment
%
yb1=(int(fb11,x,Z1LL,Z1RLL)+int(fb11r,x,Z1RLL,Z1NLL)+int(fb11rn,x,Z1NLL,Z1ML)+int(fb12rn,x,Z1ML,Z1NUL)+int(fb12r,x,Z1NUL,Z1RUL)+int(fb12,x,Z1RUL,Z1UL));
if Dias>0

```

```

yb1=(int(fb11,x,Z1LL,Z1RLL)+int(fb11r,x,Z1RLL,Z1NLL)+int(fb12r,x,Z1NUL
,Z1RUL)+int(fb12,x,Z1RUL,Z1UL));
    yb1rn=int(fb11rn,x,Z1NLL,Z1ML)+int(fb12rn,x,Z1ML,Z1NUL)           %
Always Display for WebHole Joist
    yb1rn=subs(yb1rn,Ac,x)                                           % Always Display for WebHole
Joist
else

yb1=(int(fb11,x,Z1LL,Z1RLL)+int(fb11r,x,Z1RLL,Z1NLL)+int(fb11rn,x,Z1NL
L,Z1ML)+int(fb12rn,x,Z1ML,Z1NUL)+int(fb12r,x,Z1NUL,Z1RUL)+int(fb12,x,Z
1RUL,Z1UL));
end
yb2=(int(fb21,x,Z2LL,Z2UL));
yb3=(int(fb31,x,Z3LL,Z3UL));

yb1x=subs(yb1,Ac,x);
yb2x=subs(yb2,Ac,x);
yb3x=subs(yb3,Ac,x);
Yb=yb1x+yb2x+yb3x
YbMax=subs(Yb,x,Ld)
Case= 'This is Sub Case 1rC At Notch Location'
    case 4 % SUBCASE 1rD    ## Pc at the Notch Location ##
        SUBCASE 1rD
            Zone 1A 1B 1C 1D 1E + 1D' = 6 sub zones: x>> 0 to a
                Z1LL=0;
                Z1RLL=Ln-Lr;
                Z1NLL=Ln;
                Z1NUL=Ln+Bn;
                Z1RUL=Ln+Bn+Lr;
                Z1ML=Ac;
                Z1UL=a;

                V11=P+Pc*(L-Ac)/L;
                V11r=V11;
                V11rn=V11;
                V12r=V11-Pc;
                V12=V12r;
                M11=P*x+Pc*(L-Ac)/L*x; % Simply Supported Beam with two Point
Loads P+P at a & b
                M11r=M11;
                M11rn=M11;
                M12r=M11-Pc*(x-Ac); % Simply Supported Beam with two Point
Loads P+P at a & b
                M12=M12r;
                % Zone 2: x>> a to b
                Z2LL=Z1UL;
                Z2UL=b;

                V21=V12-P;
                V22=0; %N/A

```

```

M21=M12-P*(x-a); % Simply Supported Beam with two Point Loads
P+P at a & b
M22=0; %N/A

% Zone 3: x>> b to L
Z3LL=Z2UL;
Z3UL=L;

V31=V21-P;
V32=0; %N/A
M31=M21-P*(x-b); % Simply Supported Beam with two Point Loads
P+P at a & b
M32=0;

D11VPc = diff(V11,Pc);
D11rVPc = diff(V11r,Pc);
D11rnVPc = diff(V11rn,Pc);
D12rVPc = diff(V12r,Pc);
D12VPc = diff(V12,Pc);
D21VPc = diff(V21,Pc);
D22VPc = diff(V22,Pc);
D31VPc = diff(V31,Pc);
D32VPc = diff(V32,Pc);

D11MPc = diff(M11,Pc);
D11rMPc = diff(M11r,Pc);
D11rnMPc = diff(M11rn,Pc);
D12rMPc = diff(M12r,Pc);
D12MPc = diff(M12,Pc);
D21MPc = diff(M21,Pc);
D22MPc = diff(M22,Pc);
D31MPc = diff(M31,Pc);
D32MPc = diff(M32,Pc);

V11=subs(V11,Pc,0);
DV11=subs(D11VPc,Pc,0);
V11r=subs(V11r,Pc,0);
DV11r=subs(D11rVPc,Pc,0);
V11rn=subs(V11rn,Pc,0);
DV11rn=subs(D11rnVPc,Pc,0);
%V12rn=subs(V12rn,Pc,0);
%DV12rn=subs(D12rnVPc,Pc,0);
V12r=subs(V12r,Pc,0);
DV12r=subs(D12rVPc,Pc,0);
V12=subs(V12,Pc,0);
DV12=subs(D12VPc,Pc,0);
V21=subs(V21,Pc,0);
DV21=subs(D21VPc,Pc,0);
V22=subs(V22,Pc,0);
DV22=subs(D22VPc,Pc,0);
V31=subs(V31,Pc,0);

```

```

        DV31=subs (D31VPc,Pc,0);
        V32=subs (V32,Pc,0);
        DV32=subs (D32VPc,Pc,0);

        M11=subs (M11,Pc,0);
        DM11=subs (D11MPc,Pc,0);
        M11r=subs (M11r,Pc,0);
        DM11r=subs (D11rMPc,Pc,0);
        M11rn=subs (M11rn,Pc,0);
        DM11rn=subs (D11rnMPc,Pc,0);
        %M12rn=subs (M12rn,Pc,0);
        %DM12rn=subs (D12rnMPc,Pc,0);
        M12r=subs (M12r,Pc,0);
        DM12r=subs (D12rMPc,Pc,0);
        M12=subs (M12,Pc,0);
        DM12=subs (D12MPc,Pc,0);
        M21=subs (M21,Pc,0);
        DM21=subs (D21MPc,Pc,0);
        M22=subs (M22,Pc,0);
        DM22=subs (D22MPc,Pc,0);
        M31=subs (M31,Pc,0);
        DM31=subs (D31MPc,Pc,0);
        M32=subs (M32,Pc,0);
        DM32=subs (D32MPc,Pc,0);

        fv11=fs*V11*DV11/ (G*A);
        fv11r=fsr*V11r*DV11r/ (Gr*Ar);
        fv11rn=fsrn*V11rn*DV11rn/ (Grn*Arn);
        %fv12rn=fsrn*V12rn*DV12rn/ (Grn*Arn);
        fv12r=fsr*V12r*DV12r/ (Gr*Ar);
        fv12=fs*V12*DV12/ (G*A);
        fv21=fs*V21*DV21/ (G*A);
        fv22=fs*V22*DV22/ (G*A);
        fv31=fs*V31*DV31/ (G*A);
        fv32=fs*V32*DV32/ (G*A);

        fb11=M11*DM11/ (E*I);
        fb11r=M11r*DM11r/ (Er*Ir);
        fb11rn=M11rn*DM11rn/ (Ern*Irn);
        fb12r=M12r*DM12r/ (Er*Ir);
        fb12=M12*DM12/ (E*I);
        fb21=M21*DM21/ (E*I);
        fb22=M22*DM22/ (E*I);
        fb31=M31*DM31/ (E*I);
        fb32=M32*DM32/ (E*I);
        %Deflection due to Shear
        %
        yv1=(int (fv11,x,Z1LL,Z1RLL)+int (fv11r,x,Z1RLL,Z1NLL)+int (fv11rn,x,Z1NLL,Z1NUL)+int (fv12r,x,Z1NUL,Z1ML)+int (fv11r,x,Z1ML,Z1RUL)+int (fv12,x,Z1RUL,Z1UL));
        if Dias>0

```



```

yv1=(int (fv11,x,Z1LL,Z1RLL)+int (fv11r,x,Z1RLL,Z1NLL)+int (fv12r,x,Z1NUL
,Z1ML)+int (fv11r,x,Z1ML,Z1RUL)+int (fv12,x,Z1RUL,Z1UL));
    yv1rn=int (fv11rn,x,Z1NLL,Z1NUL)           % Always Display for WebHole
Joist
    yv1rnx=subs (yv1rn,Ac,x)                   % Always Display for WebHole
Joist
else

yv1=(int (fv11,x,Z1LL,Z1RLL)+int (fv11r,x,Z1RLL,Z1NLL)+int (fv11rn,x,Z1NL
L,Z1NUL)+int (fv12r,x,Z1NUL,Z1ML)+int (fv11r,x,Z1ML,Z1RUL)+int (fv12,x,Z1
RUL,Z1UL));
end
yv2=(int (fv21,x,Z2LL,Z2UL));
yv3=(int (fv31,x,Z3LL,Z3UL));

yv1x=subs (yv1,Ac,x);
yv2x=subs (yv2,Ac,x);
yv3x=subs (yv3,Ac,x);
Yv=yv1x+yv2x+yv3x
YvMax=subs (Yv,x,Ld)
%Deflection due to Moment
yb1=(int (fb11,x,Z1LL,Z1RLL)+int (fb11r,x,Z1RLL,Z1NLL)+int (fb11rn,x,Z1NL
L,Z1NUL)+int (fb12r,x,Z1NUL,Z1ML)+int (fb11r,x,Z1ML,Z1RUL)+int (fb12,x,Z1
RUL,Z1UL));
if Dias>0

yb1=(int (fb11,x,Z1LL,Z1RLL)+int (fb11r,x,Z1RLL,Z1NLL)+int (fb12r,x,Z1NUL
,Z1ML)+int (fb11r,x,Z1ML,Z1RUL)+int (fb12,x,Z1RUL,Z1UL));
    yb1rn=int (fb11rn,x,Z1NLL,Z1NUL)           % Always Display for WebHole
Joist
    yb1rnx=subs (yb1rn,Ac,x)                   % Always Display for WebHole
Joist
else

yb1=(int (fb11,x,Z1LL,Z1RLL)+int (fb11r,x,Z1RLL,Z1NLL)+int (fb11rn,x,Z1NL
L,Z1NUL)+int (fb12r,x,Z1NUL,Z1ML)+int (fb11r,x,Z1ML,Z1RUL)+int (fb12,x,Z1
RUL,Z1UL));
end
yb2=(int (fb21,x,Z2LL,Z2UL));
yb3=(int (fb31,x,Z3LL,Z3UL));

yb1x=subs (yb1,Ac,x);
yb2x=subs (yb2,Ac,x);
yb3x=subs (yb3,Ac,x);
Yb=yb1x+yb2x+yb3x
YbMax=subs (Yb,x,Ld)
Case= 'This is Sub Case 1rD At Notch Location'
    case 5 % SUBCASE 1rE    ## Pc at the Notch Location ##
    SUBCASE 1rE
    Zone 1A 1B 1C 1D 1E + 1E' = 6 sub zones: x>> 0 to a

```

```

        Z1LL=0;
        Z1RL=Ln-Lr;
        Z1NL=Ln;
        Z1NUL=Ln+Bn;
        Z1RUL=Ln+Bn+Lr;
        Z1ML=Ac;
        Z1UL=a;

        V11=P+Pc*(L-Ac)/L;
        V11r=V11;
        V11rn=V11;
        V12=V11-Pc;
%         V12r=V12rn;
%         V12=V12r;
        M11=P*x+Pc*(L-Ac)/L*x; % Simply Supported Beam with two Point
Loads P+P at a & b
        M11r=M11;
        M11rn=M11;
        M12=M11-Pc*(x-Ac); % Simply Supported Beam with two Point
Loads P+P at a & b
%         M12r=M12rn;
%         M12=M12r;
        % Zone 2: x>> a to b
        Z2LL=Z1UL;
        Z2UL=b;

        V21=V12-P;
        V22=0; %N/A
        M21=M12-P*(x-a); % Simply Supported Beam with two Point Loads
P+P at a & b
        M22=0; %N/A

        % Zone 3: x>> b to L
        Z3LL=Z2UL;
        Z3UL=L;

        V31=V21-P;
        V32=0; %N/A
        M31=M21-P*(x-b); % Simply Supported Beam with two Point Loads
P+P at a & b
        M32=0;

        D11VPc = diff(V11,Pc);
        D11rVPc = diff(V11r,Pc);
        D11rnVPc = diff(V11rn,Pc);
        D12VPc = diff(V12,Pc);
%         D12rVPc = diff(V12r,Pc);
%         D12VPc = diff(V12,Pc);
        D21VPc = diff(V21,Pc);
        D22VPc = diff(V22,Pc);
        D31VPc = diff(V31,Pc);

```

```

D32VPc = diff(V32,Pc);

D11MPc = diff(M11,Pc);
D11rMPc = diff(M11r,Pc);
D11rnMPc = diff(M11rn,Pc);
D12MPc = diff(M12,Pc);
%      D12rMPc = diff(M12r,Pc);
%      D12MPc = diff(M12,Pc);
D21MPc = diff(M21,Pc);
D22MPc = diff(M22,Pc);
D31MPc = diff(M31,Pc);
D32MPc = diff(M32,Pc);

V11=subs(V11,Pc,0);
    DV11=subs(D11VPc,Pc,0);
V11r=subs(V11r,Pc,0);
    DV11r=subs(D11rVPc,Pc,0);
V11rn=subs(V11rn,Pc,0);
    DV11rn=subs(D11rnVPc,Pc,0);
V12=subs(V12,Pc,0);
    DV12=subs(D12VPc,Pc,0);
V21=subs(V21,Pc,0);
    DV21=subs(D21VPc,Pc,0);
V22=subs(V22,Pc,0);
    DV22=subs(D22VPc,Pc,0);
V31=subs(V31,Pc,0);
    DV31=subs(D31VPc,Pc,0);
V32=subs(V32,Pc,0);
    DV32=subs(D32VPc,Pc,0);

M11=subs(M11,Pc,0);
    DM11=subs(D11MPc,Pc,0);
M11r=subs(M11r,Pc,0);
    DM11r=subs(D11rMPc,Pc,0);
M11rn=subs(M11rn,Pc,0);
    DM11rn=subs(D11rnMPc,Pc,0);
M12=subs(M12,Pc,0);
    DM12=subs(D12MPc,Pc,0);
M21=subs(M21,Pc,0);
    DM21=subs(D21MPc,Pc,0);
M22=subs(M22,Pc,0);
    DM22=subs(D22MPc,Pc,0);
M31=subs(M31,Pc,0);
    DM31=subs(D31MPc,Pc,0);
M32=subs(M32,Pc,0);
    DM32=subs(D32MPc,Pc,0);

fv11=fs*V11*DV11/(G*A);
fv11r=fsr*V11r*DV11r/(Gr*Ar);
fv11rn=fsrn*V11rn*DV11rn/(Grn*Arn);
fv12=fs*V12*DV12/(G*A);

```

```

% fv12r=fsr*V12r*DV12r/(Gr*Ar);
% fv12=fs*V12*DV12/(G*A);
fv21=fs*V21*DV21/(G*A);
fv22=fs*V22*DV22/(G*A);
fv31=fs*V31*DV31/(G*A);
fv32=fs*V32*DV32/(G*A);

fb11=M11*DM11/(E*I);
fb11r=M11r*DM11r/(Er*Ir);
fb11rn=M11rn*DM11rn/(Ern*Irn);
fb12=M12*DM12/(E*I);
fb21=M21*DM21/(E*I);
fb22=M22*DM22/(E*I);
fb31=M31*DM31/(E*I);
fb32=M32*DM32/(E*I);
%Deflection due to Shear
%
yv1=(int(fv11,x,Z1LL,Z1RLL)+int(fv11r,x,Z1RLL,Z1NLL)+int(fv11rn,x,Z1NLL,Z1NUL)+int(fv11r,x,Z1NUL,Z1RUL)+int(fv11,x,Z1RUL,Z1ML)+int(fv12,x,Z1ML,Z1UL));
if Dias>0

yv1=(int(fv11,x,Z1LL,Z1RLL)+int(fv11r,x,Z1RLL,Z1NLL)+int(fv11r,x,Z1NUL,Z1RUL)+int(fv11,x,Z1RUL,Z1ML)+int(fv12,x,Z1ML,Z1UL));
    yv1rn=int(fv11rn,x,Z1NLL,Z1NUL) % Always Display for WebHole
Joist
    yv1rn=subs(yv1rn,Ac,x) % Always Display for WebHole
Joist
else

yv1=(int(fv11,x,Z1LL,Z1RLL)+int(fv11r,x,Z1RLL,Z1NLL)+int(fv11rn,x,Z1NLL,Z1NUL)+int(fv11r,x,Z1NUL,Z1RUL)+int(fv11,x,Z1RUL,Z1ML)+int(fv12,x,Z1ML,Z1UL));
end
yv2=(int(fv21,x,Z2LL,Z2UL));
yv3=(int(fv31,x,Z3LL,Z3UL));

yv1x=subs(yv1,Ac,x);
yv2x=subs(yv2,Ac,x);
yv3x=subs(yv3,Ac,x);
Yv=yv1x+yv2x+yv3x
YvMax=subs(Yv,x,Ld)
%Deflection due to Moment
%
yb1=(int(fb11,x,Z1LL,Z1RLL)+int(fb11r,x,Z1RLL,Z1NLL)+int(fb11rn,x,Z1NLL,Z1NUL)+int(fb11r,x,Z1NUL,Z1RUL)+int(fb11,x,Z1RUL,Z1ML)+int(fb12,x,Z1ML,Z1UL));
if Dias>0

yb1=(int(fb11,x,Z1LL,Z1RLL)+int(fb11r,x,Z1RLL,Z1NLL)+int(fb11r,x,Z1NUL,Z1RUL)+int(fb11,x,Z1RUL,Z1ML)+int(fb12,x,Z1ML,Z1UL));

```

```

        yb1rn=int (fb11rn,x,Z1NLL,Z1NUL)           % Always Display for WebHole
Joist
        yb1rnx=subs (yb1rn,Ac,x)                   % Always Display for WebHole
Joist
else

yb1=(int (fb11,x,Z1LL,Z1RLL)+int (fb11r,x,Z1RLL,Z1NLL)+int (fb11rn,x,Z1NLL,Z1NUL)+int (fb11r,x,Z1NUL,Z1RUL)+int (fb11,x,Z1RUL,Z1ML)+int (fb12,x,Z1ML,Z1UL));
end
yb2=(int (fb21,x,Z2LL,Z2UL));
yb3=(int (fb31,x,Z3LL,Z3UL));

yb1x=subs (yb1,Ac,x);
yb2x=subs (yb2,Ac,x);
yb3x=subs (yb3,Ac,x);
Yb=yb1x+yb2x+yb3x
YbMax=subs (Yb,x,Ld)
Case= 'This is Sub Case 1rE At the Right side of the Reinforcer'
    end % End of Switch SCs
    case 2 % 2R
        CASE :2r Code for Mid Span Deflection
        Zone 1: x>> 0 to a
            Z1LL=0;
            Z1RLL=Ln-Lr;
            Z1NLL=Ln;
            Z1NUL=Ln+Bn;
            Z1RUL=Ln+Bn+Lr;
            Z1ML=Ac;
            Z1UL=a;

            V11=P+Pc*(L-Ac)/L;
            V11r=V11;
            V11rn=V11;
            V12=0;
            M11=P*x+Pc*(L-Ac)/L*x; % Simply Supported Beam with two Point
Loads P+P at a & b
            M11r=M11;
            M11rn=M11;

            % Zone 2: x>> a to b
            Z2LL=Z1UL;
            Z2ML=Ac;
            Z2UL=b;

            V21=V11-P;
            V22=V21-Pc;
            M21=M11-P*(x-a); % Simply Supported Beam with two Point Loads
P+P at a & b
            M22=M21-Pc*(x-Ac);

```

```

% Zone 3: x>> b to L
Z3LL=Z2UL;
Z3UL=L;

V31=V22-P;
V32=0;
M31=M22-P*(x-b); % Simply Supported Beam with two Point Loads
P+P at a & b
M32=0;

D11VPc = diff(V11,Pc);
D11rVPc = diff(V11r,Pc);
D11rnVPc = diff(V11rn,Pc);
D12VPc = diff(V12,Pc);
D21VPc = diff(V21,Pc);
D22VPc = diff(V22,Pc);
D31VPc = diff(V31,Pc);
D32VPc = diff(V32,Pc);

D11MPc = diff(M11,Pc);
D11rMPc = diff(M11r,Pc);
D11rnMPc = diff(M11rn,Pc);
D12MPc = diff(M12,Pc);
D21MPc = diff(M21,Pc);
D22MPc = diff(M22,Pc);
D31MPc = diff(M31,Pc);
D32MPc = diff(M32,Pc);

V11=subs(V11,Pc,0);
DV11=subs(D11VPc,Pc,0);
V11r=subs(V11r,Pc,0);
DV11r=subs(D11rVPc,Pc,0);
V11rn=subs(V11rn,Pc,0);
DV11rn=subs(D11rnVPc,Pc,0);
V12=subs(V12,Pc,0);
DV12=subs(D12VPc,Pc,0);
V21=subs(V21,Pc,0);
DV21=subs(D21VPc,Pc,0);
V22=subs(V22,Pc,0);
DV22=subs(D22VPc,Pc,0);
V31=subs(V31,Pc,0);
DV31=subs(D31VPc,Pc,0);
V32=subs(V32,Pc,0);
DV32=subs(D32VPc,Pc,0);

M11=subs(M11,Pc,0);
DM11=subs(D11MPc,Pc,0);
M11r=subs(M11r,Pc,0);
DM11r=subs(D11rMPc,Pc,0);
M11rn=subs(M11rn,Pc,0);
DM11rn=subs(D11rnMPc,Pc,0);

```

```

M12=subs (M12,Pc,0);
    DM12=subs (D12MPc,Pc,0);
M21=subs (M21,Pc,0);
    DM21=subs (D21MPc,Pc,0);
M22=subs (M22,Pc,0);
    DM22=subs (D22MPc,Pc,0);
M31=subs (M31,Pc,0);
    DM31=subs (D31MPc,Pc,0);
M32=subs (M32,Pc,0);
    DM32=subs (D32MPc,Pc,0);

fv11=fs*V11*DV11/(G*A);
fv11r=fsr*V11r*DV11r/(Gr*Ar);
fv11rn=fsrn*V11rn*DV11rn/(Grn*Arn);
fv12=fs*V12*DV12/(G*A);
fv21=fs*V21*DV21/(G*A);
fv22=fs*V22*DV22/(G*A);
fv31=fs*V31*DV31/(G*A);
fv32=fs*V32*DV32/(G*A);

fb11=M11*DM11/(E*I);
fb11r=M11r*DM11r/(Er*Ir);
fb11rn=M11rn*DM11rn/(Ern*Irn);
fb12=M12*DM12/(E*I);
fb21=M21*DM21/(E*I);
fb22=M22*DM22/(E*I);
fb31=M31*DM31/(E*I);
fb32=M32*DM32/(E*I);

%
yv1=(int (fv11,x,Z1LL,Z1RLL)+int (fv11r,x,Z1RLL,Z1NLL)+int (fv11rn,x,Z1NLL,Z1NUL)+int (fv11r,x,Z1NUL,Z1RUL)+int (fv11,x,Z1RUL,Z1UL));
if Dias>0

yv1=(int (fv11,x,Z1LL,Z1RLL)+int (fv11r,x,Z1RLL,Z1NLL)+int (fv11r,x,Z1NUL,Z1RUL)+int (fv11,x,Z1RUL,Z1UL));
    yv1rn=int (fv11rn,x,Z1NLL,Z1NUL) % Always Display for WebHole
Joist
    yv1rn=subs (yv1rn,Ac,x) % Always Display for WebHole
Joist
else

yv1=(int (fv11,x,Z1LL,Z1RLL)+int (fv11r,x,Z1RLL,Z1NLL)+int (fv11rn,x,Z1NLL,Z1NUL)+int (fv11r,x,Z1NUL,Z1RUL)+int (fv11,x,Z1RUL,Z1UL));
end
yv2=(int (fv21,x,Z2LL,Z2ML)+int (fv22,x,Z2ML,Z2UL));
yv3=(int (fv31,x,Z3LL,Z3UL));

yv1x=subs (yv1,Ac,x);
yv2x=subs (yv2,Ac,x);
yv3x=subs (yv3,Ac,x);

```

```

Yv=yv1x+yv2x+yv3x
YvMax=subs(Yv,x,Ld)

%
yb1=(int(fb11,x,Z1LL,Z1RLL)+int(fb11r,x,Z1RLL,Z1NLL)+int(fb11rn,x,Z1NL
L,Z1NUL)+int(fb11r,x,Z1NUL,Z1RUL)+int(fb11,x,Z1RUL,Z1UL));
if Dias>0

yb1=(int(fb11,x,Z1LL,Z1RLL)+int(fb11r,x,Z1RLL,Z1NLL)+int(fb11r,x,Z1NUL
,Z1RUL)+int(fb11,x,Z1RUL,Z1UL));
    yb1rn=int(fb11rn,x,Z1NLL,Z1NUL)           % Always Display for WebHole
Joist
    yb1rnx=subs(yb1rn,Ac,x)                   % Always Display for WebHole
Joist
else

yb1=(int(fb11,x,Z1LL,Z1RLL)+int(fb11r,x,Z1RLL,Z1NLL)+int(fb11rn,x,Z1NL
L,Z1NUL)+int(fb11r,x,Z1NUL,Z1RUL)+int(fb11,x,Z1RUL,Z1UL));
end
yb2=(int(fb21,x,Z2LL,Z2ML)+int(fb22,x,Z2ML,Z2UL));
yb3=(int(fb31,x,Z3LL,Z3UL));

yb1x=subs(yb1,Ac,x);
yb2x=subs(yb2,Ac,x);
yb3x=subs(yb3,Ac,x);
Yb=yb1x+yb2x+yb3x
YbMax=subs(Yb,x,Ld)

Yv = (P*fs*x)/(3*A*G) - (P*fs*(L - x)*(3*Bn - L + 3*Ln +
3*Lr))/(3*A*G*L) + (Bn*P*fsrn*(L - x))/(Arn*Grn*L) + (2*Lr*P*fsr*(L -
x))/(Ar*Gr*L) + (P*fs*(Ln - Lr)*(L - x))/(A*G*L)

YvMax = (Bn*P*fsrn)/(2*Arn*Grn) - (P*fs*(3*Bn - L + 3*Ln +
3*Lr))/(6*A*G) + (L*P*fs)/(6*A*G) + (Lr*P*fsr)/(Ar*Gr) + (P*fs*(Ln -
Lr))/(2*A*G)

Yb = (L^2*P*x)/(81*E*I) + (L^2*P*(L - x))/(81*E*I) + (P*x*(8*L^2 -
18*L*x + 9*x^2))/(54*E*I) - (P*(L - x)*(Bn + Ln)^3)/(3*Er*Ir*L) -
(P*(L - x)*(L - 3*x)*(L + 3*x))/(54*E*I) - (P*(L - x)*(Bn + Ln +
Lr)^3)/(3*E*I*L) + (P*(L - x)*(Bn + Ln + Lr)^3)/(3*Er*Ir*L) + (P*(Ln -
Lr)^3*(L - x))/(3*E*I*L) + (Bn*P*(L - x)*(Bn^2 + 3*Bn*Ln +
3*Ln^2))/(3*Ern*Irn*L) + (Lr*P*(L - x)*(3*Ln^2 - 3*Ln*Lr +
Lr^2))/(3*Er*Ir*L)

YbMax = (P*(Bn + Ln + Lr)^3)/(6*Er*Ir) - (P*(Bn + Ln + Lr)^3)/(6*E*I)
- (P*(Bn + Ln)^3)/(6*Er*Ir) + (23*L^3*P)/(648*E*I) + (P*(Ln -
Lr)^3)/(6*E*I) + (Bn*P*(Bn^2 + 3*Bn*Ln + 3*Ln^2))/(6*Ern*Irn) +

```



$$(Lr*P*(3*Ln^2 - 3*Ln*Lr + Lr^2))/(6*Er*Ir)$$

Finding the Location of Maximum Deflection.

$$Yt=Yv+Yb$$

$$Yt=subs(Yt,[L,E,I,G,A,fs],[L,Eo,Io,Go,Ao,fso])$$

$$DYt1 = diff(Yt);$$

$$X\_Deltamax=solve(DYt1,x)$$

$$X\_DL\_Check=subs(X\_Deltamax,[Bn,Dn,Ln,Lr,Er,Ir,Gr,Ar,fsr,Ern,Irn,Grn,Arn,fsrn],[0,0,0,0,E,I,G,A,fs,E,I,G,A,fs])$$

$$\text{syms } X\_max$$

$$X\_Deltamax=X\_max;$$

$$YtMax=subs(Yt,x,X\_Deltamax)$$

$$YtMax\_Check=subs(YtMax,[X\_Deltamax,Bn,Dn,Ln,Lr,Er,Ir,Gr,Ar,fsr,Ern,Irn,Grn,Arn,fsrn],[L/2,0,0,0,0,E,I,G,A,fs,E,I,G,A,fs])$$

Case= 'This is Case 2r'

$$Yt = (L^2*P*x)/(81*E*I) + (L^2*P*(L - x))/(81*E*I) + (P*x*(8*L^2 - 18*L*x + 9*x^2))/(54*E*I) + (P*fs*x)/(3*A*G) - (P*(L - x)*(Bn + Ln)^3)/(3*Er*Ir*L) - (P*(L - x)*(L - 3*x)*(L + 3*x))/(54*E*I) - (P*(L - x)*(Bn + Ln + Lr)^3)/(3*E*I*L) + (P*(L - x)*(Bn + Ln + Lr)^3)/(3*Er*Ir*L) + (P*(Ln - Lr)^3*(L - x))/(3*E*I*L) + (Bn*P*(L - x)*(Bn^2 + 3*Bn*Ln + 3*Ln^2))/(3*Ern*Irn*L) + (Lr*P*(L - x)*(3*Ln^2 - 3*Ln*Lr + Lr^2))/(3*Er*Ir*L) - (P*fs*(L - x)*(3*Bn - L + 3*Ln + 3*Lr))/(3*A*G*L) + (Bn*P*fsrn*(L - x))/(Arn*Grn*L) + (2*Lr*P*fsr*(L - x))/(Ar*Gr*L) + (P*fs*(Ln - Lr)*(L - x))/(A*G*L)$$

$$Yt = (L^2*P*x)/(81*Eo*Io) + (L^2*P*(L - x))/(81*Eo*Io) + (P*x*(8*L^2 - 18*L*x + 9*x^2))/(54*Eo*Io) + (P*fso*x)/(3*Ao*Go) - (P*(L - x)*(Bn + Ln)^3)/(3*Er*Ir*L) - (P*(L - x)*(L - 3*x)*(L + 3*x))/(54*Eo*Io) - (P*(L - x)*(Bn + Ln + Lr)^3)/(3*Eo*Io*L) + (P*(L - x)*(Bn + Ln + Lr)^3)/(3*Er*Ir*L) + (P*(Ln - Lr)^3*(L - x))/(3*Eo*Io*L) + (Bn*P*(L - x)*(Bn^2 + 3*Bn*Ln + 3*Ln^2))/(3*Ern*Irn*L) + (Lr*P*(L - x)*(3*Ln^2 - 3*Ln*Lr + Lr^2))/(3*Er*Ir*L) - (P*fso*(L - x)*(3*Bn - L + 3*Ln + 3*Lr))/(3*Ao*Go*L) + (Bn*P*fsrn*(L - x))/(Arn*Grn*L) + (2*Lr*P*fsr*(L - x))/(Ar*Gr*L) + (P*fso*(Ln - Lr)*(L - x))/(Ao*Go*L)$$

$$X\_Deltamax = -(3*Eo*Io*((P*(Bn + Ln + Lr)^3)/(3*Er*Ir*L) - (L^2*P)/(6*Eo*Io) - (P*(Bn + Ln + Lr)^3)/(3*Eo*Io*L) - (P*fso)/(3*Ao*Go) + (P*(Ln - Lr)^3)/(3*Eo*Io*L) - (P*(Bn + Ln)^3)/(3*Er*Ir*L) + (Lr*P*(3*Ln^2 - 3*Ln*Lr + Lr^2))/(3*Er*Ir*L) - (P*fso*(3*Bn - L + 3*Ln + 3*Lr))/(3*Ao*Go*L) + (Bn*P*fsrn)/(Arn*Grn*L) + (2*Lr*P*fsr)/(Ar*Gr*L) + (P*fso*(Ln - Lr))/(Ao*Go*L) + (Bn*P*(Bn^2 + 3*Bn*Ln + 3*Ln^2))/(3*Ern*Irn*L)))/(L*P)$$

$$X\_DL\_Check = L/2$$

$$YtMax = (L^2*P*X\_max)/(81*Eo*Io) + (L^2*P*(L - X\_max))/(81*Eo*Io) +$$

```

(P*X_max*fso)/(3*Ao*Go) + (P*X_max*(8*L^2 - 18*L*X_max +
9*X_max^2))/(54*Eo*Io) - (P*(L - X_max)*(L - 3*X_max)*(L +
3*X_max))/(54*Eo*Io) - (P*(L - X_max)*(Bn + Ln)^3)/(3*Er*Ir*L) - (P*(L
- X_max)*(Bn + Ln + Lr)^3)/(3*Eo*Io*L) + (P*(L - X_max)*(Bn + Ln +
Lr)^3)/(3*Er*Ir*L) + (P*(Ln - Lr)^3*(L - X_max))/(3*Eo*Io*L) +
(Bn*P*(L - X_max)*(Bn^2 + 3*Bn*Ln + 3*Ln^2))/(3*Ern*Irn*L) + (Lr*P*(L
- X_max)*(3*Ln^2 - 3*Ln*Lr + Lr^2))/(3*Er*Ir*L) - (P*fso*(L -
X_max)*(3*Bn - L + 3*Ln + 3*Lr))/(3*Ao*Go*L) + (Bn*P*fsrn*(L -
X_max))/(Arn*Grn*L) + (2*Lr*P*fsr*(L - X_max))/(Ar*Gr*L) + (P*fso*(Ln
- Lr)*(L - X_max))/(Ao*Go*L)

```

```

YtMax_Check = (23*P*L^3)/(648*Eo*Io) + (P*fso*L)/(3*Ao*Go)

```

```

Case = This is Case 2r

```

```

case 3 % 3R
CASE :3r Code for Right Span Deflection
Zone 1: x>> 0 to a
    Z1LL=0;
    Z1RL=Ln-Lr;
    Z1NL=Ln;
    Z1NUL=Ln+Bn;
    Z1RUL=Ln+Bn+Lr;
    Z1ML=Ac;
    Z1UL=a;

    V11=P+Pc*(L-Ac)/L;
    V11r=V11;
    V11rn=V11;
    V12=0; %N/A
    M11=P*x+Pc*(L-Ac)/L*x; % Simply Supported Beam with two Point
Loads P+P at a & b
    M11r=M11;
    M11rn=M11;

    % Zone 2: x>> a to b
    Z2LL=Z1UL;
    Z2UL=b;

    V21=V11-P;
    V22=0; %N/A
    M21=M11-P*(x-a); % Simply Supported Beam with two Point Loads
P+P at a & b

    % Zone 3: x>> b to L
    Z3LL=Z2UL;
    Z3ML=Ac;
    Z3UL=L;

```

```

V31=V21-P;
V32=V31-Pc;
M31=M21-P*(x-b); % Simply Supported Beam with two Point Loads
P+P at a & b
M32=M31-Pc*(x-Ac);

D11VPc = diff(V11,Pc);
D11rVPc = diff(V11r,Pc);
D11rnVPc = diff(V11rn,Pc);
%   D12VPc = diff(V12,Pc);
D21VPc = diff(V21,Pc);
D22VPc = diff(V22,Pc);
D31VPc = diff(V31,Pc);
D32VPc = diff(V32,Pc);

D11MPc = diff(M11,Pc);
D11rMPc = diff(M11r,Pc);
D11rnMPc = diff(M11rn,Pc);
%   D12MPc = diff(M12,Pc);
D21MPc = diff(M21,Pc);
D22MPc = diff(M22,Pc);
D31MPc = diff(M31,Pc);
D32MPc = diff(M32,Pc);

V11=subs(V11,Pc,0);
DV11=subs(D11VPc,Pc,0);
V11r=subs(V11r,Pc,0);
DV11r=subs(D11rVPc,Pc,0);
V11rn=subs(V11rn,Pc,0);
DV11rn=subs(D11rnVPc,Pc,0);
%   V12=subs(V12,Pc,0);
%   DV12=subs(D12VPc,Pc,0);
V21=subs(V21,Pc,0);
DV21=subs(D21VPc,Pc,0);
V22=subs(V22,Pc,0);
DV22=subs(D22VPc,Pc,0);
V31=subs(V31,Pc,0);
DV31=subs(D31VPc,Pc,0);
V32=subs(V32,Pc,0);
DV32=subs(D32VPc,Pc,0);

M11=subs(M11,Pc,0);
DM11=subs(D11MPc,Pc,0);
M11r=subs(M11r,Pc,0);
DM11r=subs(D11rMPc,Pc,0);
M11rn=subs(M11rn,Pc,0);
DM11rn=subs(D11rnMPc,Pc,0);
%   M12=subs(M12,Pc,0);
%   DM12=subs(D12MPc,Pc,0);
M21=subs(M21,Pc,0);
DM21=subs(D21MPc,Pc,0);

```

```

M22=subs (M22,Pc,0);
DM22=subs (D22MPc,Pc,0);
M31=subs (M31,Pc,0);
DM31=subs (D31MPc,Pc,0);
M32=subs (M32,Pc,0);
DM32=subs (D32MPc,Pc,0);

fv11=fs*V11*DV11/(G*A);
fv11r=fsr*V11r*DV11r/(Gr*Ar);
fv11rn=fsrn*V11rn*DV11rn/(Grn*Arn);
% fv12=fs*V12*DV12/(G*A);
fv21=fs*V21*DV21/(G*A);
fv22=fs*V22*DV22/(G*A);
fv31=fs*V31*DV31/(G*A);
fv32=fs*V32*DV32/(G*A);

fb11=M11*DM11/(E*I);
fb11r=M11r*DM11r/(Er*Ir);
fb11rn=M11rn*DM11rn/(Ern*Irn);
fb21=M21*DM21/(E*I);
fb22=M22*DM22/(E*I);
fb31=M31*DM31/(E*I);
fb32=M32*DM32/(E*I);

%
yv1=(int (fv11,x,Z1LL,Z1RLL)+int (fv11r,x,Z1RLL,Z1NLL)+int (fv11rn,x,Z1NLL,Z1NUL)+int (fv11r,x,Z1NUL,Z1RUL)+int (fv11,x,Z1RUL,Z1UL));
if Dias>0

yv1=(int (fv11,x,Z1LL,Z1RLL)+int (fv11r,x,Z1RLL,Z1NLL)+int (fv11r,x,Z1NUL,Z1RUL)+int (fv11,x,Z1RUL,Z1UL));
yv1rn=int (fv11rn,x,Z1NLL,Z1NUL) % Always Display for WebHole
Joist
yv1rn=subs (yv1rn,Ac,x) % Always Display for WebHole
Joist
else

yv1=(int (fv11,x,Z1LL,Z1RLL)+int (fv11r,x,Z1RLL,Z1NLL)+int (fv11rn,x,Z1NLL,Z1NUL)+int (fv11r,x,Z1NUL,Z1RUL)+int (fv11,x,Z1RUL,Z1UL));
end
yv2=(int (fv21,x,Z2LL,Z2UL));
yv3=(int (fv31,x,Z3LL,Z3ML)+int (fv32,x,Z3ML,Z3UL));

yv1x=subs (yv1,Ac,x);
yv2x=subs (yv2,Ac,x);
yv3x=subs (yv3,Ac,x);
Yv=yv1x+yv2x+yv3x
YvMax=subs (Yv,x,Ld)

%
yb1=(int (fb11,x,Z1LL,Z1RLL)+int (fb11r,x,Z1RLL,Z1NLL)+int (fb11rn,x,Z1NLL,Z1NUL)+int (fb11r,x,Z1NUL,Z1RUL)+int (fb11,x,Z1RUL,Z1UL));

```

```

L,Z1NUL)+int(fb11r,x,Z1NUL,Z1RUL)+int(fb11,x,Z1RUL,Z1UL));
if Dias>0

yb1=(int(fb11,x,Z1LL,Z1RLL)+int(fb11r,x,Z1RLL,Z1NLL)+int(fb11r,x,Z1NUL
,Z1RUL)+int(fb11,x,Z1RUL,Z1UL));
    yb1rn=int(fb11rn,x,Z1NLL,Z1NUL)           % Always Display for WebHole
Joist
    yb1rnx=subs(yb1rn,Ac,x)                   % Always Display for WebHole
Joist
else

yb1=(int(fb11,x,Z1LL,Z1RLL)+int(fb11r,x,Z1RLL,Z1NLL)+int(fb11rn,x,Z1NL
L,Z1NUL)+int(fb11r,x,Z1NUL,Z1RUL)+int(fb11,x,Z1RUL,Z1UL));
end
yb2=(int(fb21,x,Z2LL,Z2UL));
yb3=(int(fb31,x,Z3LL,Z3ML)+int(fb32,x,Z3ML,Z3UL));

yb1x=subs(yb1,Ac,x);
yb2x=subs(yb2,Ac,x);
yb3x=subs(yb3,Ac,x);
Yb=yb1x+yb2x+yb3x
YbMax=subs(Yb,x,Ld)
Case= 'This is Case 3r'
    end % End of Switch
    end % End of If
xyz ='Check for Maximum Deflection due to Shear and Moment'
YvMax=subs(YvMax,[Bn,Dn,Ln,Lr,Er,Ir,Gr,Ar,fsr],[0,0,0,0,E,I,G,A,fs])
YbMax=subs(YbMax,[Bn,Dn,Ln,Lr,Er,Ir,Gr,Ar],[0,0,0,0,E,I,G,A])

xyz =

Check for Maximum Deflection due to Shear and Moment

YvMax = (L*P*fs)/(3*A*G)

YbMax = (23*L^3*P)/(648*E*I)

===== END of CODE =====

```

---



---

## Appendix C: Formulated Deflection Equations for Different I-joist (Control, Deficient & Retrofitted)

### C.1 Control (Un-cut) I-Joist

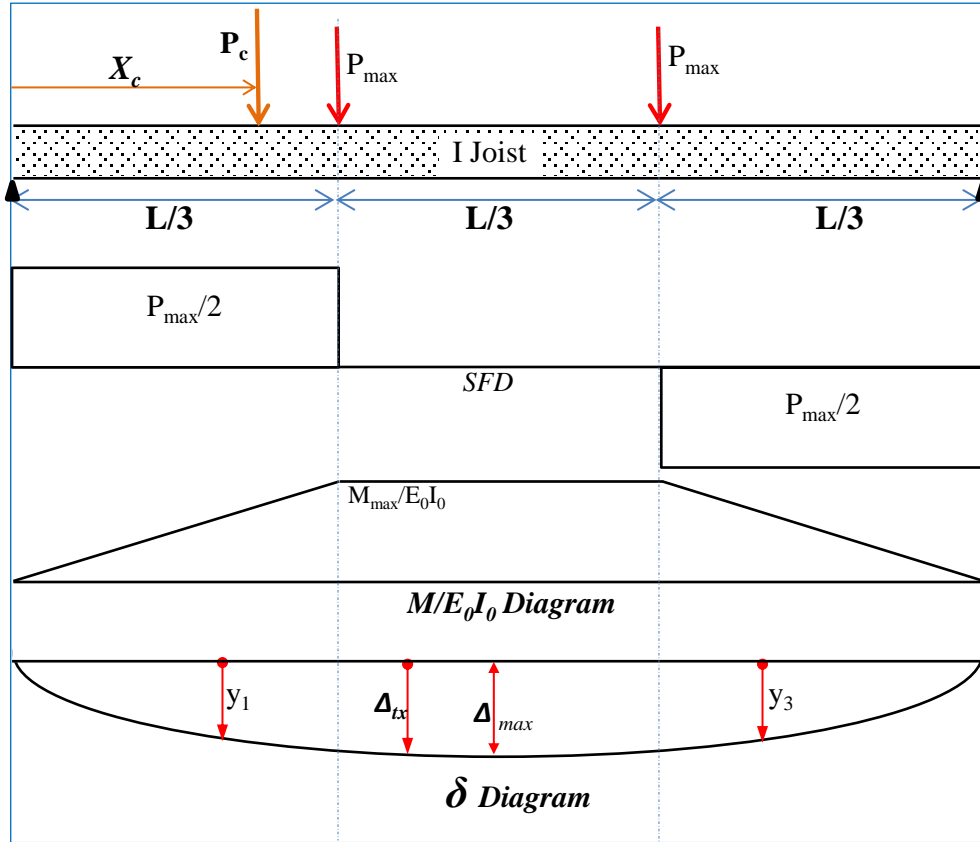


Figure C.1 Loading and Support Condition of Control I-Joists

$$Y_{V1} = \frac{P \cdot f \cdot s x}{3 \cdot A \cdot G} + \frac{P \cdot f s \cdot x \cdot (L - x)}{A \cdot G \cdot L} - \frac{P \cdot f s \cdot x \cdot (L - 3x)}{3 \cdot A \cdot G \cdot L} \quad \text{Eq. C- 1}$$

$$Y_{b1} = \frac{11 \cdot L^2 \cdot P \cdot x}{162 \cdot E \cdot I} + \frac{P \cdot x^3 \cdot (L - x)}{3 \cdot E \cdot I \cdot L} + \frac{P \cdot x \cdot (7 \cdot L^3 - 81 \cdot L \cdot x^2 + 54 \cdot x^3)}{162 \cdot E \cdot I \cdot L} \quad \text{Eq. C- 2}$$

$$Y_{V2} = \frac{P \cdot f s \cdot x}{3 \cdot A \cdot G} + \frac{P \cdot f s \cdot (L - x)}{3 \cdot A \cdot G} \quad \text{Eq. C- 3}$$

$$Y_{b2} = \frac{L^2 \cdot P \cdot x}{81 \cdot E \cdot I} + \frac{L^2 \cdot P \cdot (L - x)}{81 \cdot E \cdot I} + \frac{P \cdot x \cdot (8 \cdot L^2 - 18 \cdot L \cdot x + 9 \cdot x^2)}{54 \cdot E \cdot I} - \frac{P \cdot (L - x) \cdot (L - 3 \cdot x) \cdot (L + 3 \cdot x)}{54 \cdot E \cdot I} \quad \text{Eq. C- 4}$$

$$Y_{v3} = \frac{P \cdot f s \cdot (L - x)}{3 \cdot A \cdot G} + \frac{P \cdot f s \cdot (2 \cdot L^2 - 5 \cdot L \cdot x + 3 \cdot x^2)}{3 \cdot A \cdot G \cdot L} + \frac{P \cdot f s \cdot x \cdot (L - x)}{A \cdot G \cdot L} \quad \text{Eq. C- 5}$$

$$Y_{b3} = \frac{11 \cdot L^2 \cdot P \cdot (L - x)}{162 \cdot E \cdot I} + \frac{P \cdot x \cdot (L - x)^3}{3 \cdot E \cdot I \cdot L} + \frac{P \cdot (-20 \cdot L^4 + 20 \cdot L^3 \cdot x + 81 \cdot L^2 \cdot x^2 - 135 \cdot L \cdot x^3 + 54 \cdot x^4)}{162 \cdot E \cdot I \cdot L} \quad \text{Eq. C- 6}$$

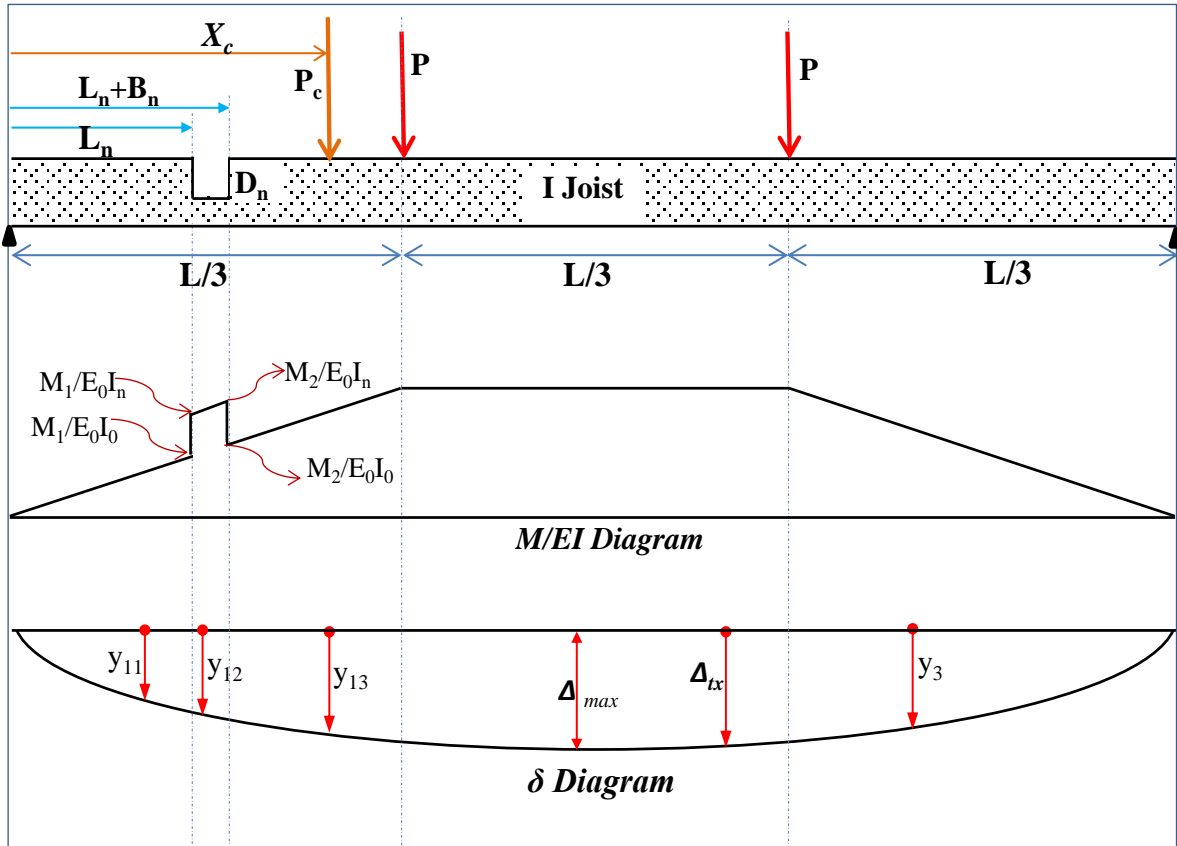


Figure C.2 Loading and Support Condition of Flange Notch I-Joists

$$Y_{v11} = \frac{P \cdot f s \cdot x}{3 \cdot A \cdot G} + \frac{P \cdot f s \cdot x \cdot (L - x)}{A \cdot G \cdot L} - \frac{P \cdot f s \cdot x \cdot (L n - x)}{A \cdot G \cdot L} - \frac{B n \cdot P \cdot f s n \cdot x}{A n \cdot G n \cdot L} + \frac{P \cdot f s \cdot x \cdot (3 \cdot B n - L + 3 \cdot L n)}{3 \cdot A \cdot G \cdot L} \quad \text{Eq. C- 7}$$

$$\begin{aligned}
Y_{b11} = & \frac{11.L^2.P.x}{162.E.I} + \frac{P.x^3.(L-x)}{3.E.I.L} + \frac{Bn^2.Ln - Bn.L.Ln + Bn.Ln^2}{E.I.L} \\
& + \frac{P.x.(54.Bn^3 - 81.Bn^2.L + 7.L^3 - 81.L.Ln^2 + 54.Ln^3)}{162.E.I.L} \\
& - \frac{P.x.(Ln-x).(2.Ln^2 + 2.Ln.x - 3.L.Ln + 2.x^2 - 3.L.x)}{6.E.I.L} \\
& - \frac{Bn.P.x.(2.Bn^2 + 6.Bn.Ln - 3.L.Bn + 6.Ln^2 - 6.L.Ln)}{6.En.In.L}
\end{aligned} \tag{Eq. C- 8}$$

$$\begin{aligned}
Y_{V12} = & \frac{P.fs.x}{3.A.G} - \frac{P.fsn.(L-x).(Ln-x)}{An.Gn.L} - \frac{P.fsn.x.(Bn+Ln-x)}{Ln.P.fs.(L-x)} \\
& + \frac{An.Gn.L}{A.G.L} + \frac{P.fs.x.(3.Bn-L+3.Ln)}{3.A.G.L}
\end{aligned} \tag{Eq. C- 9}$$

$$\begin{aligned}
Y_{b12} = & \frac{11.L^2.P.x}{162.E.I} - \frac{P.(Ln^3 - x^3).(L-x)}{3.En.In.L} + \frac{Ln^3.P.(L-x)}{3.E.I.L} \\
& + \frac{Bn^2.Ln - Bn.L.Ln + Bn.Ln^2}{E.I.L} \\
& + \frac{P.x.(54.Bn^3 - 81.Bn^2.L + 7.L^3 - 81.L.Ln^2 + 54.Ln^3)}{162.E.I.L} \\
& - \frac{P.x.(Bn+Ln-x).(2.Bn^2 + 4.Bn.Ln + 2.Bn.x - 3.L.Bn)}{6.En.In.L} \\
& - \frac{P.x.(Bn+Ln-x).(2.Ln^2 + 2.Ln.x - 3.L.Ln + 2.x^2 - 3.L.x)}{6.En.In.L}
\end{aligned} \tag{Eq. C- 10}$$

$$\begin{aligned}
Y_{V13} = & \frac{P.fs.x}{3.A.G} - \frac{P.fs.x.(L-3.x)}{3.A.G.L} - \frac{P.fs.(L-x).(Bn+Ln-x)}{Bn.P.fsn.(L-x)} \\
& + \frac{An.Gn.L}{A.G.L} + \frac{Ln.P.fs.(L-x)}{A.G.L}
\end{aligned} \tag{Eq. C- 11}$$

$$\begin{aligned}
Y_{b13} = & \frac{11.L^2.P.x}{162.E.I} + \frac{P.x.(7.L^3 - 81.L.x^2 + 54.x^3)}{162.E.I.L} \\
& - \frac{P.(L-x).(Bn^3 + 3.Bn^2.Ln + 3.Bn.Ln^2 + Ln^3 - x^3)}{3.E.I.L} \\
& + \frac{Ln^3.P.(L-x)}{3.E.I.L}
\end{aligned} \tag{Eq. C- 12}$$

$$\begin{aligned}
Y_{V2} = & \frac{P.fs.x}{3.A.G} + \frac{Bn.P.fsn.(L-x)}{An.Gn.L} + \frac{Ln.P.fs.(L-x)}{P.fs.(L-x).(3.Bn-L+3.Ln)} \\
& - \frac{A.G.L}{3.A.G.L}
\end{aligned} \tag{Eq. C- 13}$$



$$Y_{b2} = \frac{L^2 \cdot P \cdot x}{81 \cdot E \cdot I} + \frac{L^2 \cdot P \cdot (L - x)}{81 \cdot E \cdot I} + \frac{P \cdot x \cdot (8 \cdot L^2 - 18 \cdot L \cdot x + 9 \cdot x^2)}{54 \cdot E \cdot I} - \frac{P \cdot (L - x) \cdot (L - 3 \cdot x) \cdot (L + 3 \cdot x)}{P \cdot (L - x) \cdot (Bn + Ln)^3} - \frac{P \cdot (L - x) \cdot (Bn + Ln)^3}{54 \cdot E \cdot I} + \frac{Bn \cdot P \cdot (L - x) \cdot (Bn^2 + 3 \cdot Bn \cdot Ln + 3 \cdot Ln^2)}{3 \cdot En \cdot In \cdot L} + \frac{3 \cdot E \cdot I \cdot L}{Ln^3 \cdot P \cdot (L - x)} + \frac{Ln^3 \cdot P \cdot (L - x)}{3 \cdot E \cdot I \cdot L} \quad \text{Eq. C- 14}$$

$$Y_{V3} = \frac{P \cdot fs \cdot (2 \cdot L^2 - 5 \cdot L \cdot x + 3 \cdot x^2)}{3 \cdot A \cdot G \cdot L} + \frac{P \cdot fs \cdot x \cdot (L - x)}{A \cdot G \cdot L} + \frac{Bn \cdot P \cdot fsn \cdot (L - x)}{An \cdot Gn \cdot L} + \frac{Ln \cdot P \cdot fs \cdot (L - x)}{A \cdot G \cdot L} - \frac{P \cdot fs \cdot (L - x) \cdot (3 \cdot Bn - L + 3 \cdot Ln)}{3 \cdot A \cdot G \cdot L} \quad \text{Eq. C- 15}$$

$$Y_{b3} = \frac{11 \cdot L^2 \cdot P \cdot (L - x)}{162 \cdot E \cdot I} + \frac{P \cdot (-20 \cdot L^4 + 20 \cdot L^3 \cdot x + 81 \cdot L^2 \cdot x^2 - 135 \cdot L \cdot x^3 + 54 \cdot x^4)}{162 \cdot E \cdot I \cdot L} + \frac{P \cdot x \cdot (L - x)^3}{3 \cdot E \cdot I \cdot L} - \frac{P \cdot (L - x) \cdot (Bn + Ln)^3}{3 \cdot E \cdot I \cdot L} + \frac{Ln^3 \cdot P \cdot (L - x)}{3 \cdot E \cdot I \cdot L} + \frac{Bn \cdot P \cdot (L - x) \cdot (Bn^2 + 3 \cdot Bn \cdot Ln + 3 \cdot Ln^2)}{3 \cdot En \cdot In \cdot L} \quad \text{Eq. C- 16}$$

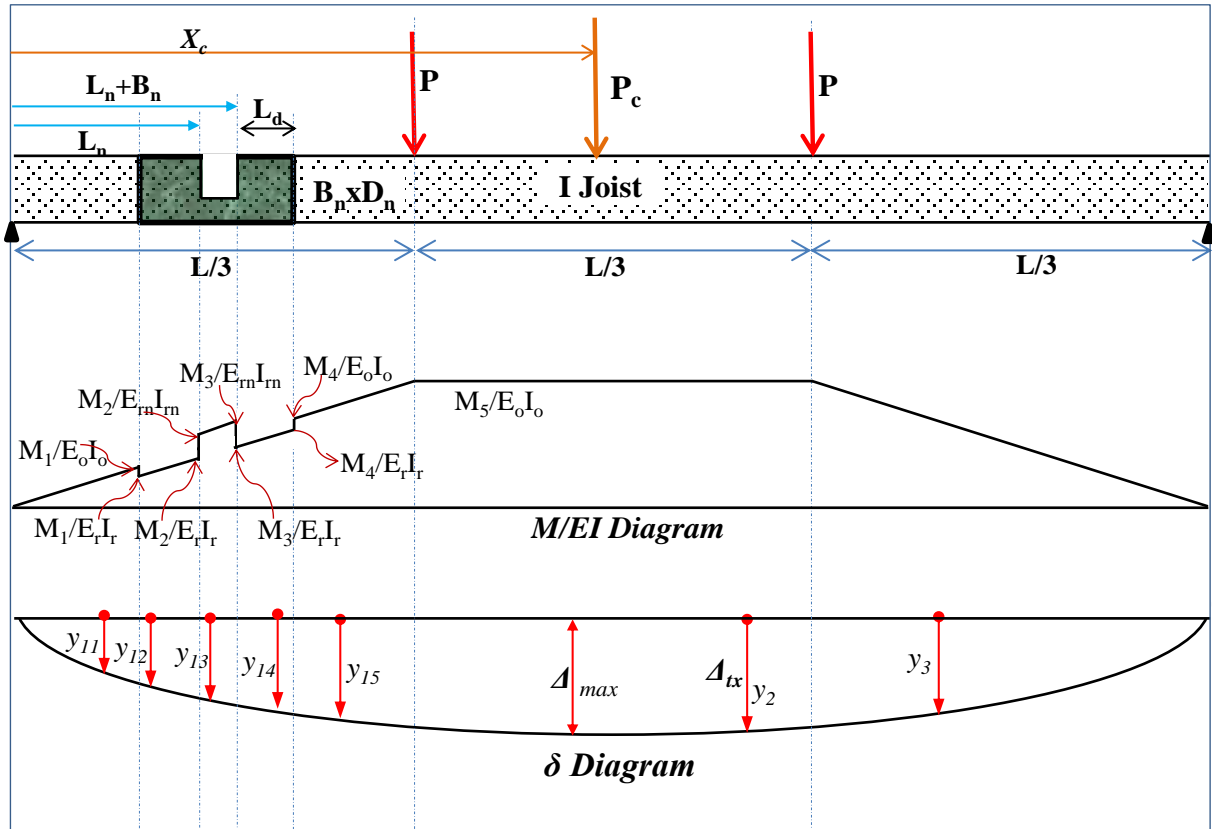


Figure C.3 Loading and Support Condition of Retrofitted Flange Notch I-Joists

$$\begin{aligned}
& Y_{b11} \\
& L^2 \cdot \left( \frac{P \cdot x}{2 \cdot E \cdot I} + \frac{L \cdot P \cdot \left( \frac{L-x}{L} - 1 \right)}{9 \cdot E \cdot I} \right) \\
& = \frac{9}{\left( \frac{P \cdot x}{2 \cdot E \cdot I} + \frac{P \cdot \left( \frac{L-x}{L} - 1 \right) \cdot (B_n + L_n + L_d)}{3 \cdot E \cdot I} \right) \cdot (B_n + L_n + L_d)^2} \\
& + \frac{11 \cdot L^2 \cdot P \cdot x}{162 \cdot E \cdot I} + \frac{P \cdot x^3 \cdot (L-x)}{3 \cdot E \cdot I \cdot L} + \frac{L_d \cdot P \cdot x \cdot (6 \cdot B_n + 6 \cdot L_n + 3 \cdot L_d)}{6 \cdot E_r \cdot I_r} \\
& - \frac{B_n \cdot P \cdot x \cdot (2 \cdot B_n^2 + 6 \cdot B_n \cdot L_n - 3 \cdot L \cdot B_n + 6 \cdot L_n^2 - 6 \cdot L \cdot L_n)}{6 \cdot E_{rn} \cdot I_{rn} \cdot L} \\
& - \frac{L_d \cdot P \cdot x \cdot (6 \cdot B_n^2 + 12 \cdot B_n \cdot L_n + 6 \cdot B_n \cdot L_d + 6 \cdot L_n^2 + 6 \cdot L_n \cdot L_d + 2 \cdot L_d^2)}{6 \cdot E_r \cdot I_r \cdot L} \\
& - \frac{L_d \cdot P \cdot x \cdot (6 \cdot L_n^2 - 6 \cdot L_n \cdot L_d - 6 \cdot L \cdot L_n + 2 \cdot L_d^2 + 3 \cdot L \cdot L_d)}{6 \cdot E_r \cdot I_r \cdot L} \\
& + \frac{P \cdot x \cdot (L_d - L_n + x) \cdot (2 \cdot L_n^2 - 4 \cdot L_n \cdot L_d + 2 \cdot L_n \cdot x - 3 \cdot L \cdot L_n)}{6 \cdot E \cdot I \cdot L} \\
& + \frac{P \cdot x \cdot (L_d - L_n + x) \cdot (2 \cdot L_d^2 - 2 \cdot L_d \cdot x + 3 \cdot L \cdot L_d + 2 \cdot x^2 - 3 \cdot L \cdot x)}{6 \cdot E \cdot I \cdot L}
\end{aligned} \tag{Eq. C- 17}$$

$$\begin{aligned}
Y_{v11} &= \frac{P \cdot f_s \cdot x}{3 \cdot A \cdot G} + \frac{P \cdot f_s \cdot x \cdot (L-x)}{A \cdot G \cdot L} + \frac{P \cdot f_s \cdot x \cdot (L_d - L_n + x)}{A \cdot G \cdot L} \\
&+ \frac{P \cdot f_s \cdot x \cdot (3 \cdot B_n - L + 3 \cdot L_n + 3 \cdot L_d)}{3 \cdot A \cdot G \cdot L} - \frac{B_n \cdot P \cdot f_{srn} \cdot x}{A_{rn} \cdot G_{rn} \cdot L} \\
&- \frac{2 \cdot L_d \cdot P \cdot f_{sr} \cdot x}{A_r \cdot G_r \cdot L}
\end{aligned} \tag{Eq. C- 18}$$

$$\begin{aligned}
& Y_{b12} \\
& L^2 \cdot \left( \frac{P \cdot x}{2 \cdot E \cdot I} + \frac{L \cdot P \cdot \left( \frac{L-x}{L} - 1 \right)}{9 \cdot E \cdot I} \right) \\
& = \frac{9}{\left( \frac{P \cdot x}{2 \cdot E \cdot I} + \frac{P \cdot \left( \frac{L-x}{L} - 1 \right) \cdot (B_n + L_n + L_d)}{3 \cdot E \cdot I} \right) \cdot (B_n + L_n + L_d)^2 + \frac{11 \cdot L^2 \cdot P \cdot x}{162 \cdot E \cdot I}} \\
& + \frac{L_d \cdot P \cdot x \cdot (6 \cdot B_n + 6 \cdot L_n + 3 \cdot L_d)}{6 \cdot E \cdot I} \\
& + \frac{P \cdot (L-x) \cdot (-L_n^3 + 3 \cdot L_n^2 \cdot L_d - 3 \cdot L_n \cdot L_d^2 + L_d^3 + x^3)}{3 \cdot E_r \cdot I_r \cdot L} + \frac{P \cdot (L_n - L_d)^3 \cdot (L-x)}{3 \cdot E \cdot I \cdot L} \\
& - \frac{P \cdot x \cdot (L_n - x) \cdot (2 \cdot L_n^2 + 2 \cdot L_n \cdot x - 3 \cdot L \cdot L_n + 2 \cdot x^2 - 3 \cdot L \cdot x)}{6 \cdot E_r \cdot I_r \cdot L} \\
& - \frac{B_n \cdot P \cdot x \cdot (2 \cdot B_n^2 + 6 \cdot B_n \cdot L_n - 3 \cdot L \cdot B_n + 6 \cdot L_n^2 - 6 \cdot L \cdot L_n)}{6 \cdot E_{rn} \cdot I_{rn} \cdot L} \\
& - \frac{L_d \cdot P \cdot x \cdot (6 \cdot B_n^2 + 12 \cdot B_n \cdot L_n + 6 \cdot B_n \cdot L_d + 6 \cdot L_n^2 + 6 \cdot L_n \cdot L_d + 2 \cdot L_d^2)}{6 \cdot E \cdot I \cdot L}
\end{aligned} \tag{Eq. C- 19}$$

$$\begin{aligned}
Y_{v12} &= \frac{P \cdot f_s \cdot x}{3 \cdot A \cdot G} - \frac{P \cdot f_{sr} \cdot x \cdot (L_n - x)}{A_r \cdot G_r \cdot L} + \frac{P \cdot f_{sr} \cdot (L-x) \cdot (L_d - L_n + x)}{A_r \cdot G_r \cdot L} \\
&+ \frac{P \cdot f_s \cdot x \cdot (3 \cdot B_n - L + 3 \cdot L_n + 3 \cdot L_d)}{3 \cdot A \cdot G \cdot L} - \frac{B_n \cdot P \cdot f_{srn} \cdot x}{A_{rn} \cdot G_{rn} \cdot L} - \frac{L_d \cdot P \cdot f_s \cdot x}{A \cdot G \cdot L} \\
&+ \frac{P \cdot f_s \cdot (L_n - L_d) \cdot (L-x)}{A \cdot G \cdot L}
\end{aligned} \tag{Eq. C- 20}$$

$$\begin{aligned}
Y_{v13} &= \frac{P \cdot f_s \cdot x}{3 \cdot A \cdot G} - \frac{P \cdot f_{srn} \cdot (L-x) \cdot (L_n - x)}{A_{rn} \cdot G_{rn} \cdot L} - \frac{P \cdot f_{srn} \cdot x \cdot (B_n + L_n - x)}{A_{rn} \cdot G_{rn} \cdot L} \\
&+ \frac{P \cdot f_s \cdot x \cdot (3 \cdot B_n - L + 3 \cdot L_n + 3 \cdot L_d)}{3 \cdot A \cdot G \cdot L} - \frac{L_d \cdot P \cdot f_{sr} \cdot x}{A_r \cdot G_r \cdot L} \\
&+ \frac{L_d \cdot P \cdot f_{sr} \cdot (L-x)}{A_r \cdot G_r \cdot L} + \frac{P \cdot f_s \cdot (L_n - L_d) \cdot (L-x)}{A \cdot G \cdot L}
\end{aligned} \tag{Eq. C- 21}$$

$$\begin{aligned}
& Y_{b13} \\
& L^2 \cdot \left( \frac{P \cdot x}{2 \cdot E \cdot I} + \frac{L \cdot P \cdot \left( \frac{L-x}{L} - 1 \right)}{9 \cdot E \cdot I} \right) \\
& = \frac{9}{\left( \frac{P \cdot x}{2 \cdot E \cdot I} + \frac{P \cdot \left( \frac{L-x}{L} - 1 \right) \cdot (B_n + L_n + L_d)}{3 \cdot E \cdot I} \right) \cdot (B_n + L_n + L_d)^2 + \frac{11 \cdot L^2 \cdot P \cdot x}{162 \cdot E \cdot I}} \\
& + \frac{L_d \cdot P \cdot x \cdot (6 \cdot B_n + 6 \cdot L_n + 3 \cdot L_d)}{6 \cdot E_r \cdot I_r} - \frac{P \cdot (L_n^3 - x^3) \cdot (L - x)}{3 \cdot E_{rn} \cdot I_{rn} \cdot L} \\
& + \frac{P \cdot (L_n - L_d)^3 \cdot (L - x)}{3 \cdot E \cdot I \cdot L} + \frac{L_d \cdot P \cdot (L - x) \cdot (3 \cdot L_n^2 - 3 \cdot L_n \cdot L_d + L_d^2)}{3 \cdot E_r \cdot I_r \cdot L} \\
& - \frac{L_d \cdot P \cdot x \cdot (6 \cdot B_n^2 + 12 \cdot B_n \cdot L_n + 6 \cdot B_n \cdot L_d + 6 \cdot L_n^2 + 6 \cdot L_n \cdot L_d + 2 \cdot L_d^2)}{6 \cdot E_r \cdot I_r \cdot L} \\
& - \frac{P \cdot x \cdot (B_n + L_n - x) \cdot (2 \cdot B_n^2 + 4 \cdot B_n \cdot L_n + 2 \cdot B_n \cdot x - 3 \cdot L \cdot B_n)}{6 \cdot E_{rn} \cdot I_{rn} \cdot L} \\
& - \frac{P \cdot x \cdot (B_n + L_n - x) \cdot (2 \cdot L_n^2 + 2 \cdot L_n \cdot x - 3 \cdot L \cdot L_n + 2 \cdot x^2 - 3 \cdot L \cdot x)}{6 \cdot E_{rn} \cdot I_{rn} \cdot L}
\end{aligned} \tag{Eq. C- 22}$$

$$\begin{aligned}
& Y_{b14} \\
& L^2 \cdot \left( \frac{P \cdot x}{2 \cdot E \cdot I} + \frac{L \cdot P \cdot \left( \frac{L-x}{L} - 1 \right)}{9 \cdot E \cdot I} \right) \\
& = \frac{9}{\left( \frac{P \cdot x}{2 \cdot E \cdot I} + \frac{P \cdot \left( \frac{L-x}{L} - 1 \right) \cdot (B_n + L_n + L_d)}{3 \cdot E \cdot I} \right) \cdot (B_n + L_n + L_d)^2 + \frac{11 \cdot L^2 \cdot P \cdot x}{162 \cdot E \cdot I}} \\
& - \frac{P \cdot x^3 \cdot (L - x)}{3 \cdot E_r \cdot I_r \cdot L} + \frac{P \cdot (L - x) \cdot (B_n + L_n + L_d)^3}{3 \cdot E_r \cdot I_r \cdot L} + \frac{P \cdot (L_n - L_d)^3 \cdot (L - x)}{3 \cdot E \cdot I \cdot L} \\
& + \frac{B_n \cdot P \cdot (L - x) \cdot (B_n^2 + 3 \cdot B_n \cdot L_n + 3 \cdot L_n^2)}{3 \cdot E_{rn} \cdot I_{rn} \cdot L} \\
& + \frac{L_d \cdot P \cdot (L - x) \cdot (3 \cdot L_n^2 - 3 \cdot L_n \cdot L_d + L_d^2)}{3 \cdot E_r \cdot I_r \cdot L} \\
& + \frac{P \cdot x \cdot (B_n + L_n - x) \cdot (2 \cdot B_n^2 + 4 \cdot B_n \cdot L_n + 2 \cdot B_n \cdot x - 3 \cdot L \cdot B_n)}{6 \cdot E_r \cdot I_r \cdot L} \\
& + \frac{P \cdot x \cdot (B_n + L_n - x) \cdot (2 \cdot L_n^2 + 2 \cdot L_n \cdot x - 3 \cdot L \cdot L_n + 2 \cdot x^2 - 3 \cdot L \cdot x)}{6 \cdot E_r \cdot I_r \cdot L}
\end{aligned} \tag{Eq. C- 23}$$

$$\begin{aligned}
Y_{v14} = & \frac{P \cdot f_s \cdot x}{3 \cdot A \cdot G} + \frac{P \cdot f_{sr} \cdot x \cdot (B_n + L_n - x)}{A_r \cdot G_r \cdot L} \\
& + \frac{P \cdot f_s \cdot x \cdot (3 \cdot B_n - L + 3 \cdot L_n + 3 \cdot L_d)}{3 \cdot A \cdot G \cdot L} \\
& + \frac{P \cdot f_{sr} \cdot (L - x) \cdot (B_n + L_n + L_d - x)}{A_r \cdot G_r \cdot L} + \frac{B_n \cdot P \cdot f_{srn} \cdot (L - x)}{A_{rn} \cdot G_{rn} \cdot L} \\
& + \frac{L_d \cdot P \cdot f_{sr} \cdot (L - x)}{A_r \cdot G_r \cdot L} + \frac{P \cdot f_s \cdot (L_n - L_d) \cdot (L - x)}{A \cdot G \cdot L}
\end{aligned} \tag{Eq. C- 24}$$

$$\begin{aligned}
Y_{b15} = & \frac{11 \cdot L^2 \cdot P \cdot x}{162 \cdot E \cdot I} + \frac{P \cdot x^3 \cdot (L - x)}{3 \cdot E \cdot I \cdot L} + \frac{P \cdot x \cdot (7 \cdot L^3 - 81 \cdot L \cdot x^2 + 54 \cdot x^3)}{162 \cdot E \cdot I \cdot L} \\
& - \frac{P \cdot (L - x) \cdot (B_n + L_n)^3}{3 \cdot E_r \cdot I_r \cdot L} - \frac{P \cdot (L - x) \cdot (B_n + L_n + L_d)^3}{3 \cdot E \cdot I \cdot L} \\
& + \frac{P \cdot (L - x) \cdot (B_n + L_n + L_d)^3}{3 \cdot E_r \cdot I_r \cdot L} + \frac{P \cdot (L_n - L_d)^3 \cdot (L - x)}{3 \cdot E \cdot I \cdot L} \\
& + \frac{B_n \cdot P \cdot (L - x) \cdot (B_n^2 + 3 \cdot B_n \cdot L_n + 3 \cdot L_n^2)}{3 \cdot E_{rn} \cdot I_{rn} \cdot L} \\
& + \frac{L_d \cdot P \cdot (L - x) \cdot (3 \cdot L_n^2 - 3 \cdot L_n \cdot L_d + L_d^2)}{3 \cdot E_r \cdot I_r \cdot L}
\end{aligned} \tag{Eq. C- 25}$$

$$\begin{aligned}
Y_{v15} = & \frac{P \cdot f_s \cdot x}{3 \cdot A \cdot G} - \frac{P \cdot f_s \cdot x \cdot (L - 3 \cdot x)}{3 \cdot A \cdot G \cdot L} - \frac{P \cdot f_s \cdot (L - x) \cdot (B_n + L_n + L_d - x)}{A \cdot G \cdot L} \\
& + \frac{B_n \cdot P \cdot f_{srn} \cdot (L - x)}{A_{rn} \cdot G_{rn} \cdot L} + \frac{2 \cdot L_d \cdot P \cdot f_{sr} \cdot (L - x)}{A_r \cdot G_r \cdot L} \\
& + \frac{P \cdot f_s \cdot (L_n - L_d) \cdot (L - x)}{A \cdot G \cdot L}
\end{aligned} \tag{Eq. C- 26}$$

$$\begin{aligned}
Y_{b2} = & \frac{L^2 \cdot P \cdot x}{81 \cdot E \cdot I} + \frac{L^2 \cdot P \cdot (L - x)}{81 \cdot E \cdot I} + \frac{P \cdot x \cdot (8 \cdot L^2 - 18 \cdot L \cdot x + 9 \cdot x^2)}{54 \cdot E \cdot I} \\
& - \frac{P \cdot (L - x) \cdot (B_n + L_n)^3}{3 \cdot E_r \cdot I_r \cdot L} - \frac{P \cdot (L - x) \cdot (L - 3 \cdot x) \cdot (L + 3 \cdot x)}{54 \cdot E \cdot I} \\
& - \frac{P \cdot (L - x) \cdot (B_n + L_n + L_d)^3}{3 \cdot E \cdot I \cdot L} + \frac{P \cdot (L - x) \cdot (B_n + L_n + L_d)^3}{3 \cdot E_r \cdot I_r \cdot L} \\
& + \frac{P \cdot (L_n - L_d)^3 \cdot (L - x)}{3 \cdot E \cdot I \cdot L} \\
& + \frac{B_n \cdot P \cdot (L - x) \cdot (B_n^2 + 3 \cdot B_n \cdot L_n + 3 \cdot L_n^2)}{3 \cdot E_{rn} \cdot I_{rn} \cdot L} \\
& + \frac{L_d \cdot P \cdot (L - x) \cdot (3 \cdot L_n^2 - 3 \cdot L_n \cdot L_d + L_d^2)}{3 \cdot E_r \cdot I_r \cdot L}
\end{aligned} \tag{Eq. C- 27}$$

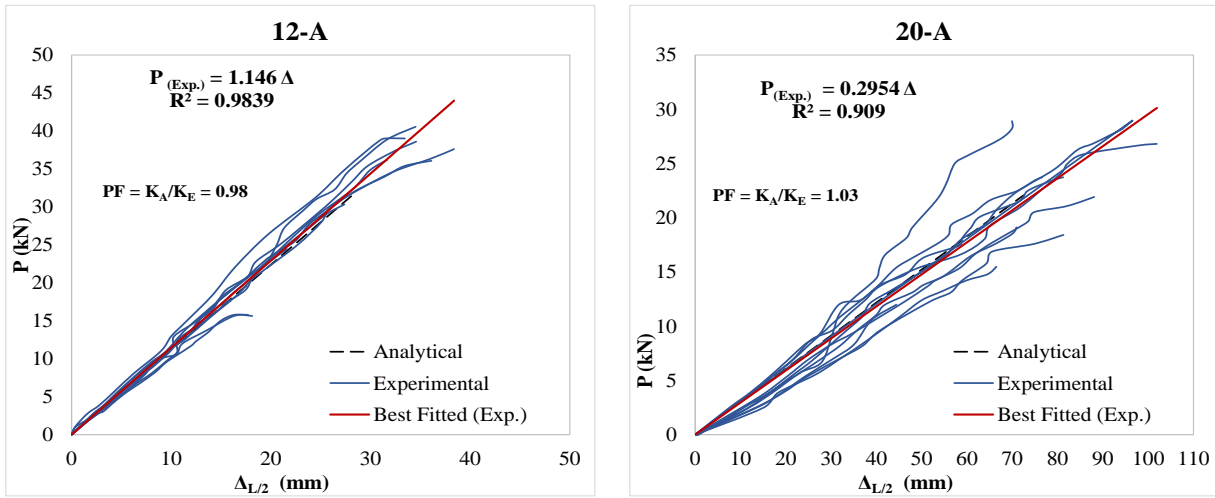
$$\begin{aligned}
Y_{v2} = & \frac{P \cdot f_s \cdot x}{3 \cdot A \cdot G} - \frac{P \cdot f_s \cdot (L - x) \cdot (3 \cdot B_n - L + 3 \cdot L_n + 3 \cdot L_d)}{3 \cdot A \cdot G \cdot L} \\
& + \frac{B_n \cdot P \cdot f_{srn} \cdot (L - x)}{A_{rn} \cdot G_{rn} \cdot L} + \frac{2 \cdot L_d \cdot P \cdot f_{sr} \cdot (L - x)}{A_r \cdot G_r \cdot L} \\
& + \frac{P \cdot f_s \cdot (L_n - L_d) \cdot (L - x)}{A \cdot G \cdot L}
\end{aligned} \tag{Eq. C- 28}$$

$$\begin{aligned}
Y_{b3} = & \frac{11 \cdot L^2 \cdot P \cdot (L - x)}{162 \cdot E \cdot I} + \frac{P \cdot (-20 \cdot L^4 + 20 \cdot L^3 \cdot x + 81 \cdot L^2 \cdot x^2 - 135 \cdot L \cdot x^3 + 54 \cdot x^4)}{162 \cdot E \cdot I \cdot L} \\
& + \frac{P \cdot x \cdot (L - x)^3}{3 \cdot E \cdot I \cdot L} - \frac{P \cdot (L - x) \cdot (B_n + L_n)^3}{3 \cdot E_r \cdot I_r \cdot L} \\
& - \frac{P \cdot (L - x) \cdot (B_n + L_n + L_d)^3}{3 \cdot E \cdot I \cdot L} + \frac{P \cdot (L - x) \cdot (B_n + L_n + L_d)^3}{3 \cdot E_r \cdot I_r \cdot L} \\
& + \frac{P \cdot (L_n - L_d)^3 \cdot (L - x)}{3 \cdot E \cdot I \cdot L} + \frac{B_n \cdot P \cdot (L - x) \cdot (B_n^2 + 3 \cdot B_n \cdot L_n + 3 \cdot L_n^2)}{3 \cdot E_{rn} \cdot I_{rn} \cdot L} \\
& + \frac{L_d \cdot P \cdot (L - x) \cdot (3 \cdot L_n^2 - 3 \cdot L_n \cdot L_d + L_d^2)}{3 \cdot E_r \cdot I_r \cdot L}
\end{aligned} \tag{Eq. C- 29}$$

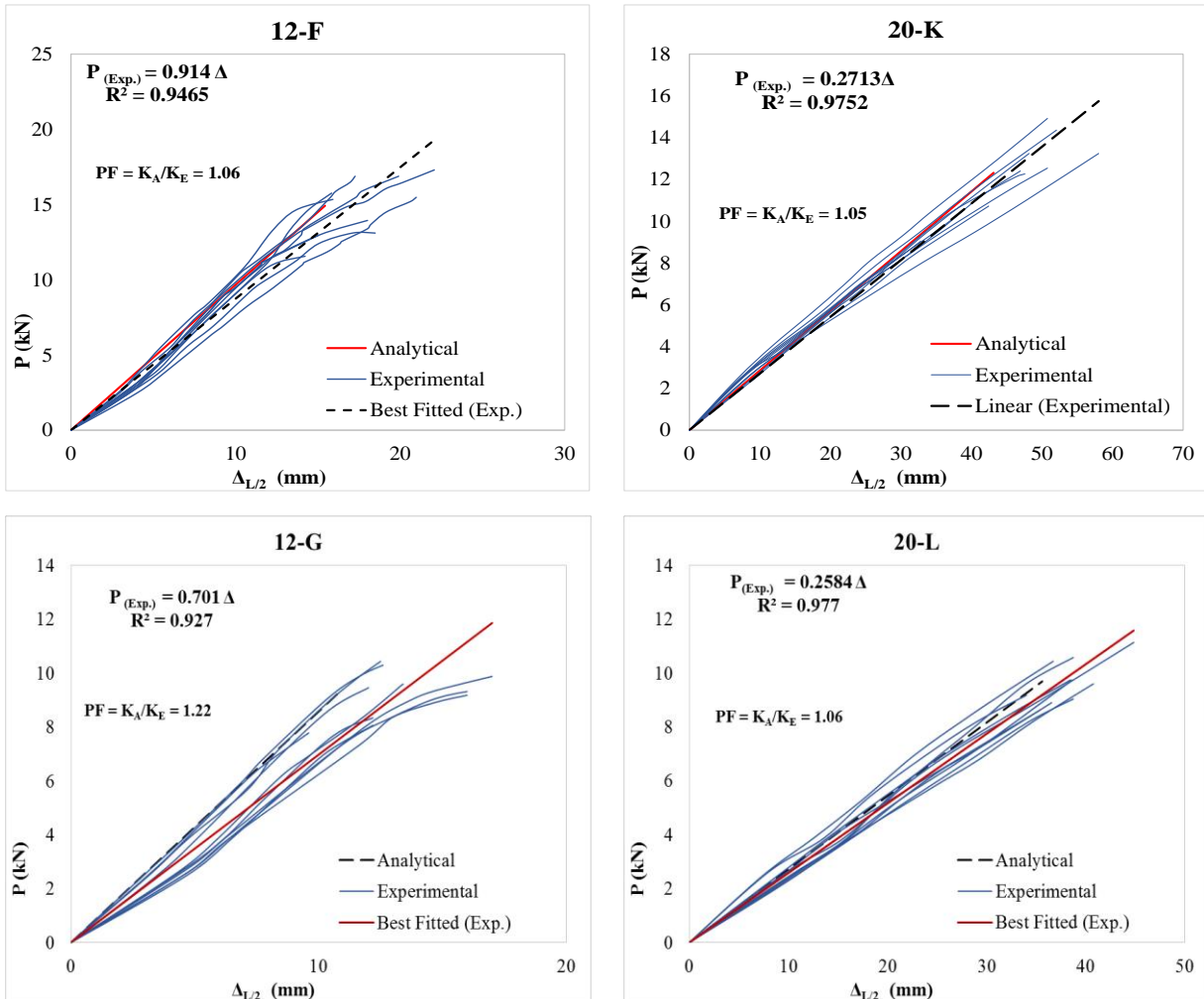
$$\begin{aligned}
Y_{v3} = & \frac{P \cdot f_s \cdot (2 \cdot L^2 - 5 \cdot L \cdot x + 3 \cdot x^2)}{3 \cdot A \cdot G \cdot L} + \frac{P \cdot f_s \cdot x \cdot (L - x)}{A \cdot G \cdot L} \\
& - \frac{P \cdot f_s \cdot (L - x) \cdot (3 \cdot B_n - L + 3 \cdot L_n + 3 \cdot L_d)}{3 \cdot A \cdot G \cdot L} \\
& + \frac{B_n \cdot P \cdot f_{srn} \cdot (L - x)}{A_{rn} \cdot G_{rn} \cdot L} + \frac{2 \cdot L_d \cdot P \cdot f_{sr} \cdot (L - x)}{A_r \cdot G_r \cdot L} \\
& + \frac{P \cdot f \cdot (L_n - L_d) \cdot (L - x)}{A \cdot G \cdot L}
\end{aligned} \tag{Eq. C- 30}$$

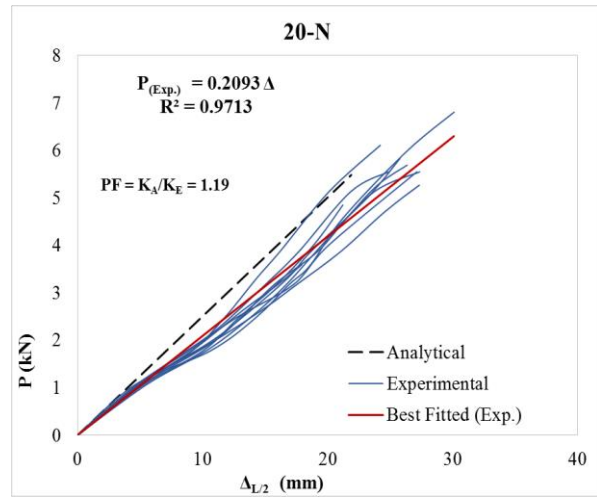
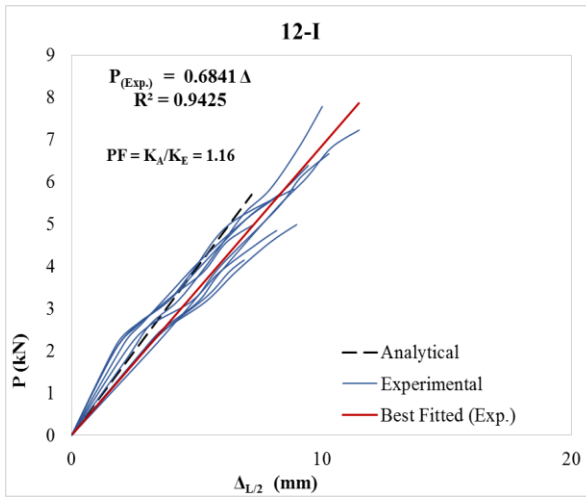
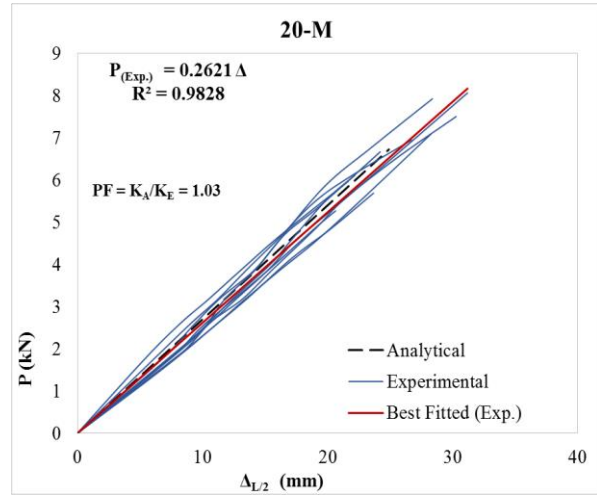
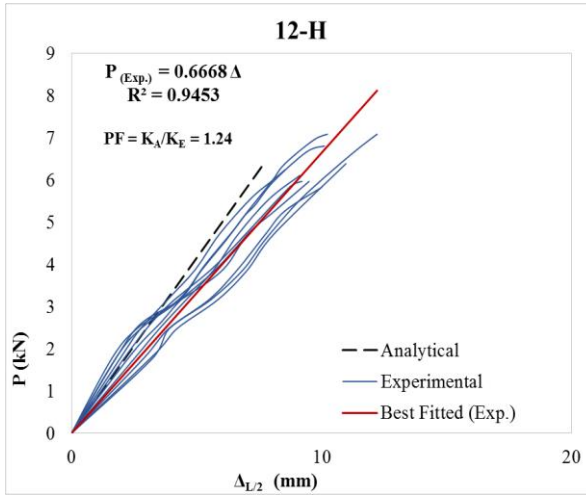
## Appendix D: Validation of the Analytical Models

### CONTROL I-JOISTS

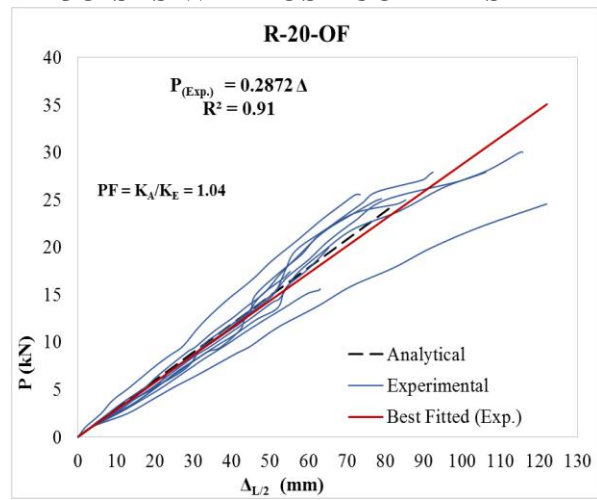
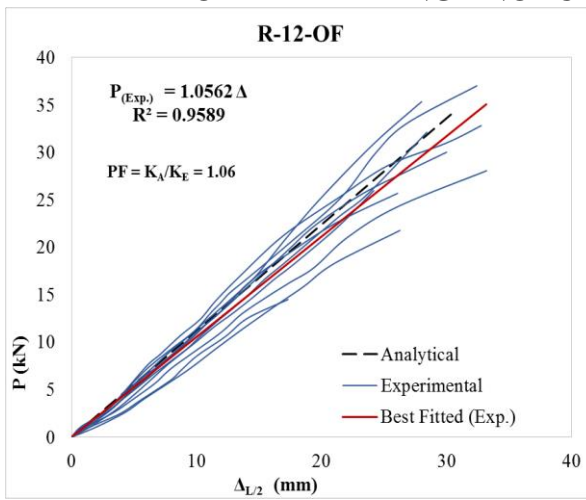


### FLANGE NOTCHED I-JOISTS

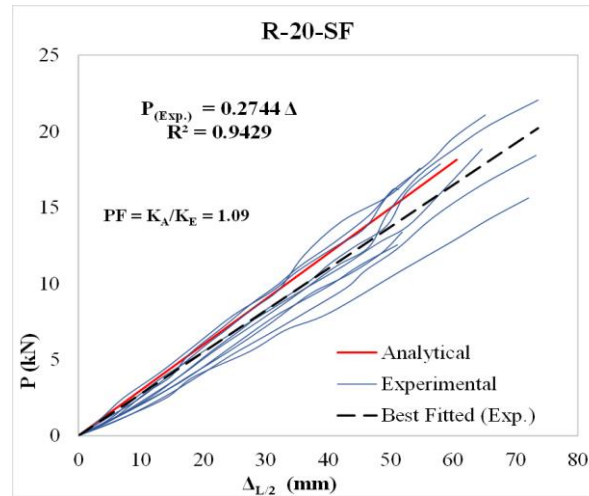
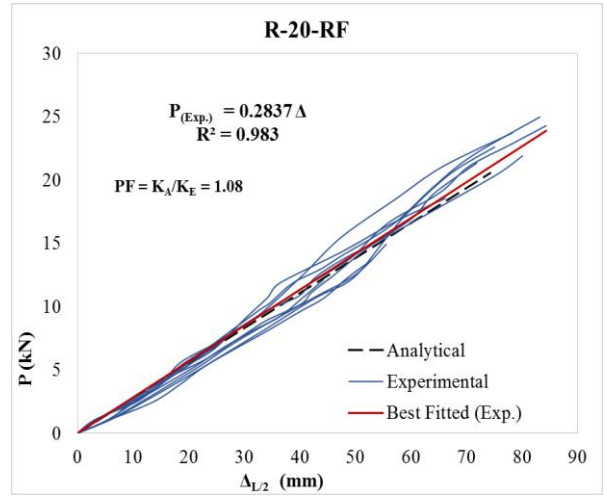
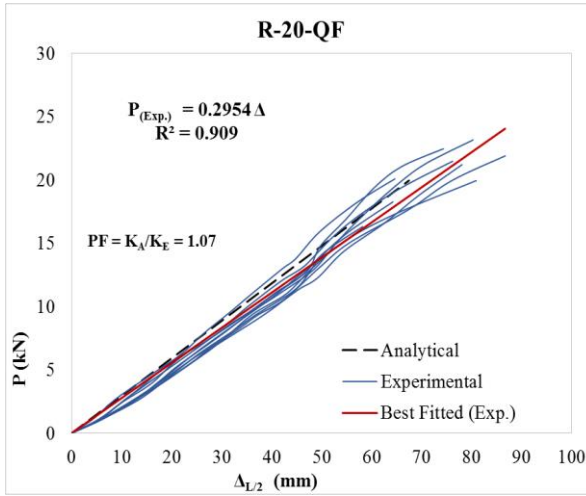
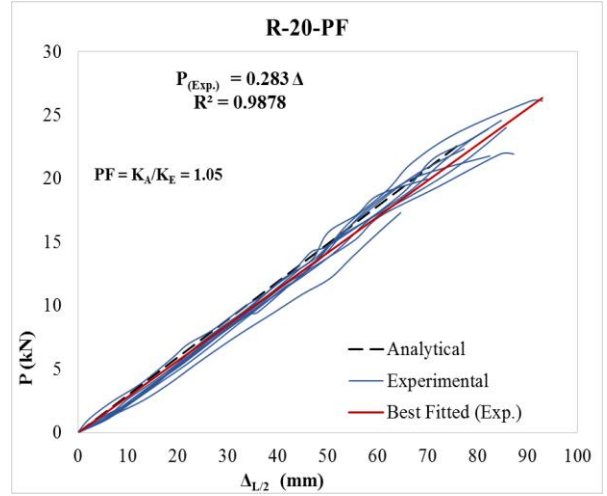
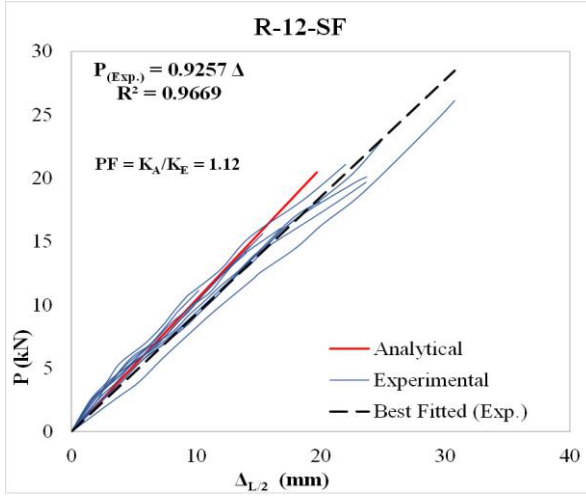




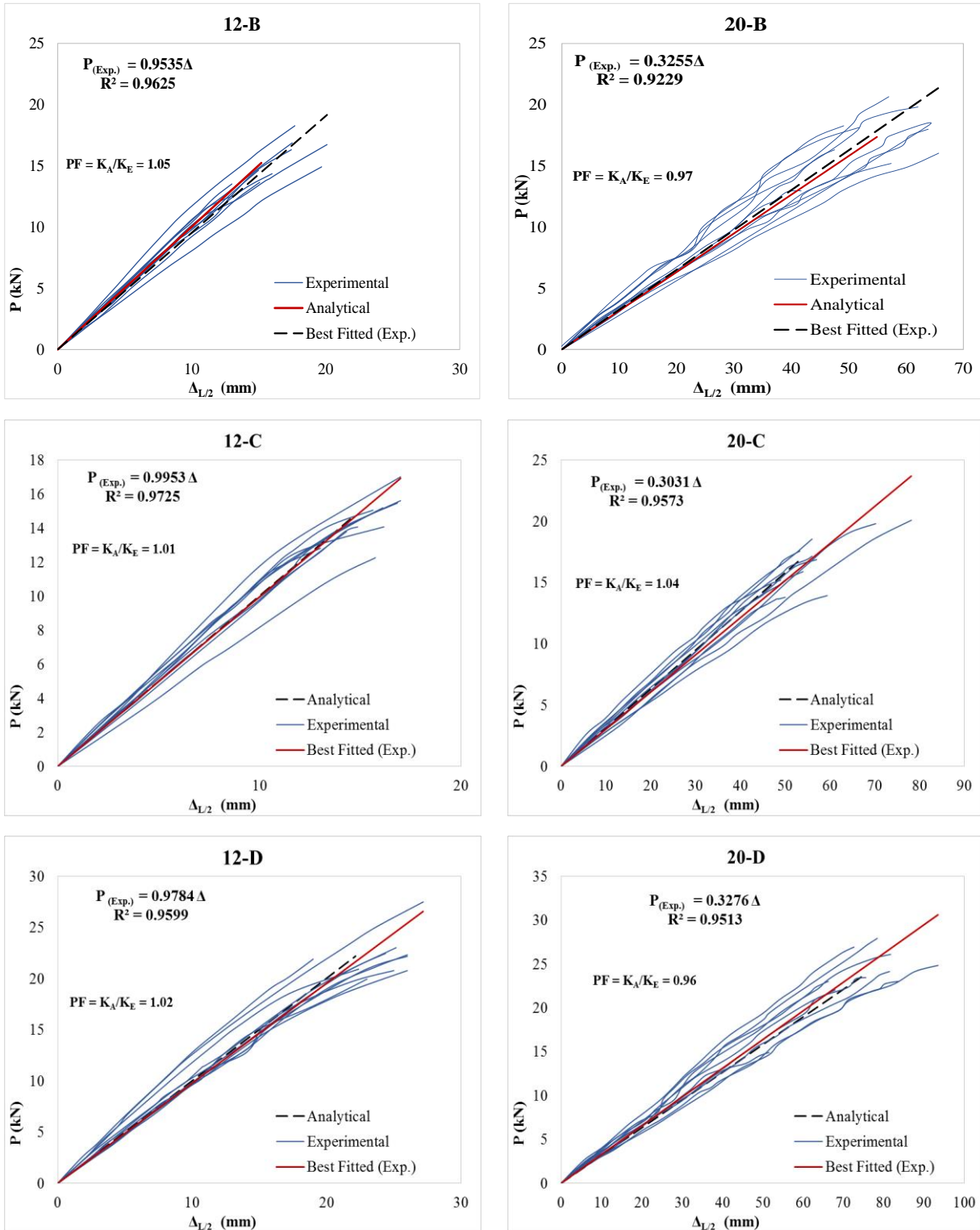
## RETROFITTED FLANGE NOTCHED I-JOISTS WITH OSB COLLARS

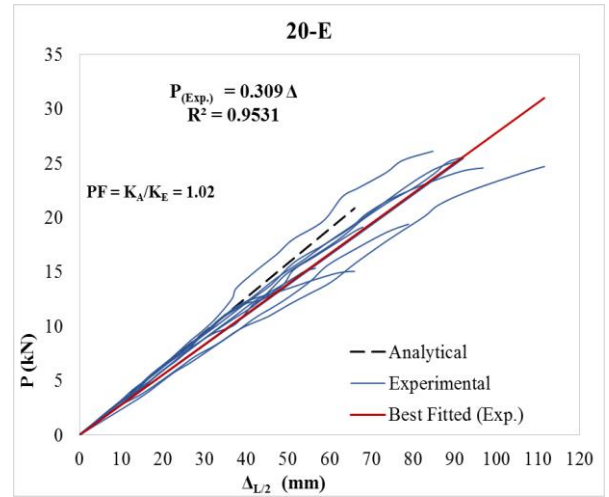
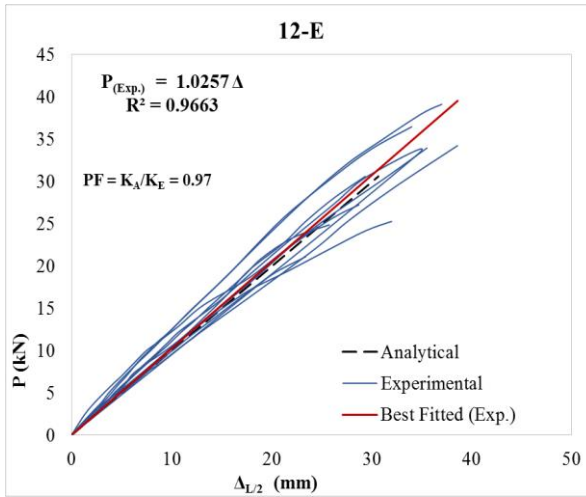




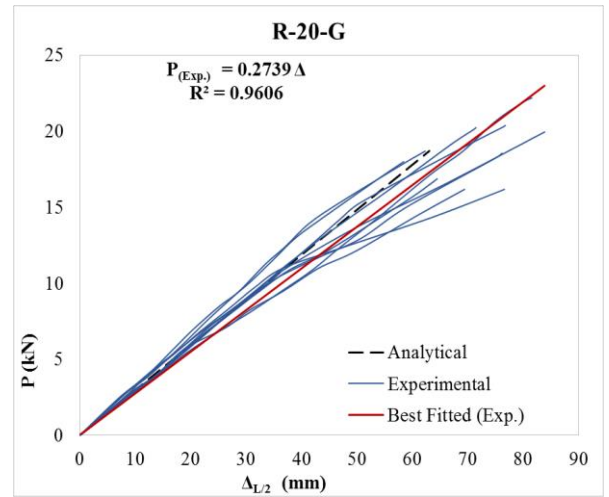
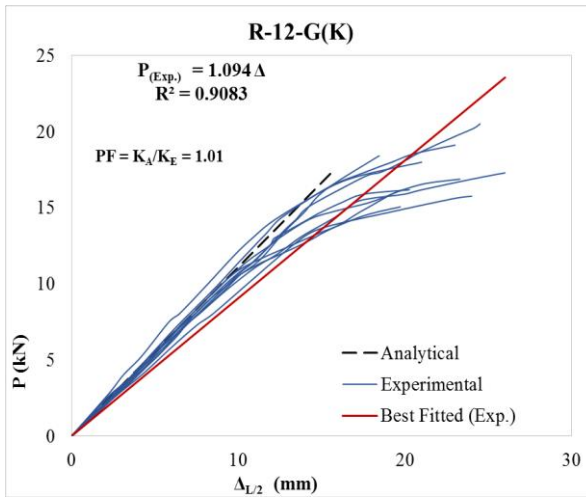
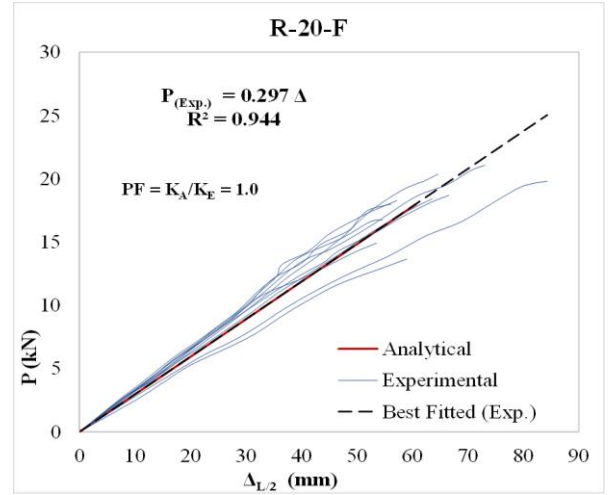
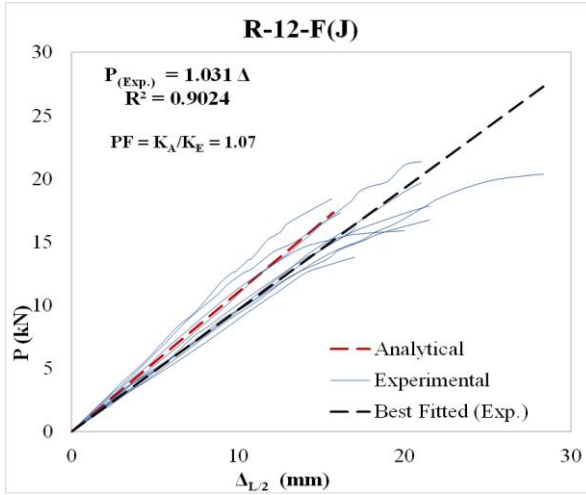


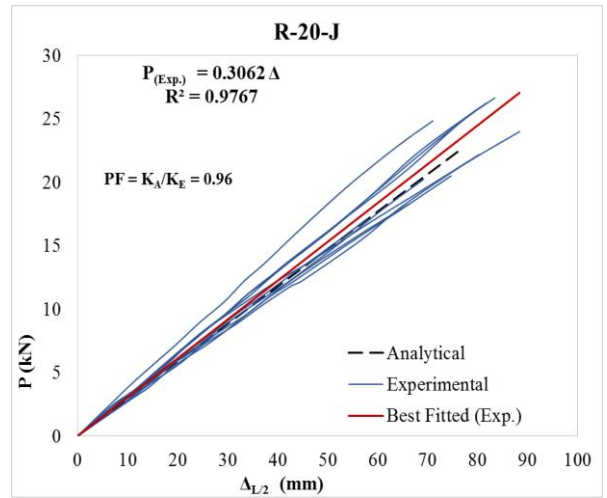
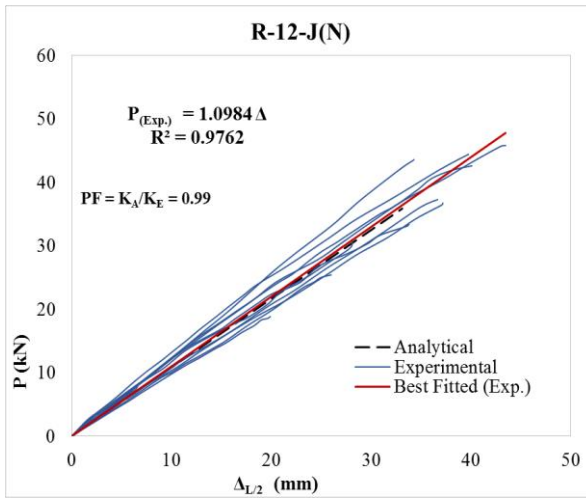
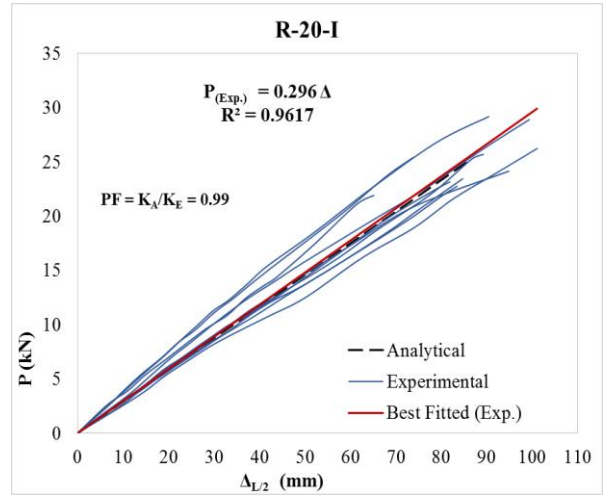
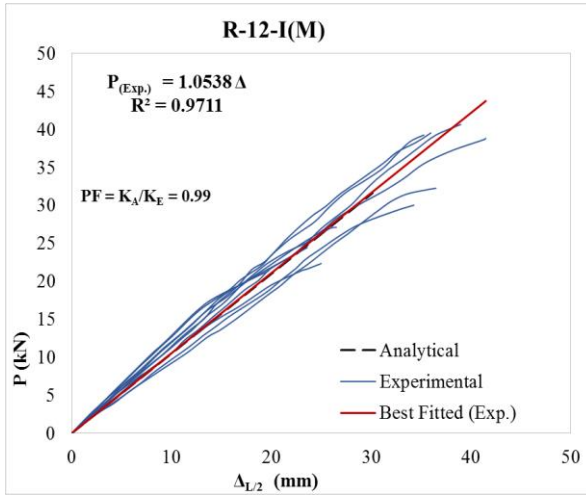
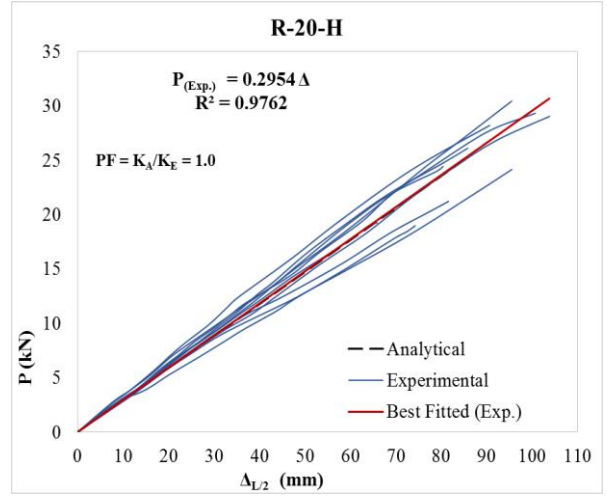
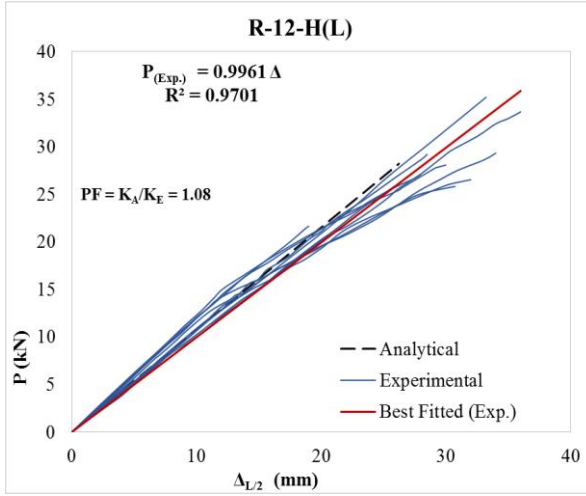
## WEB HOLE I-JOISTS



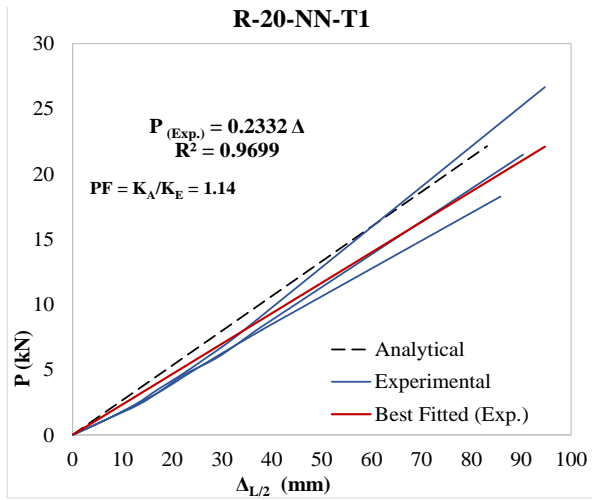
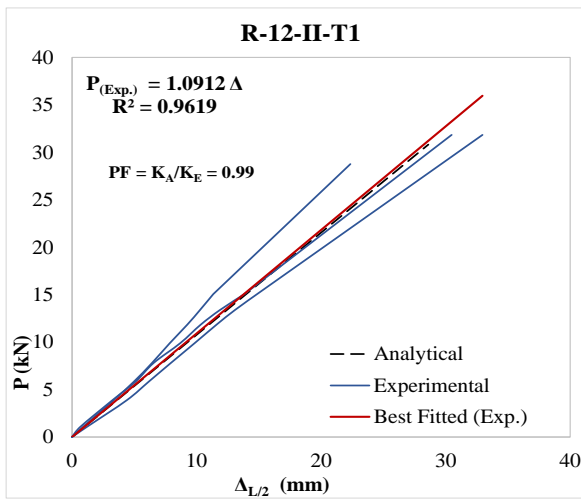
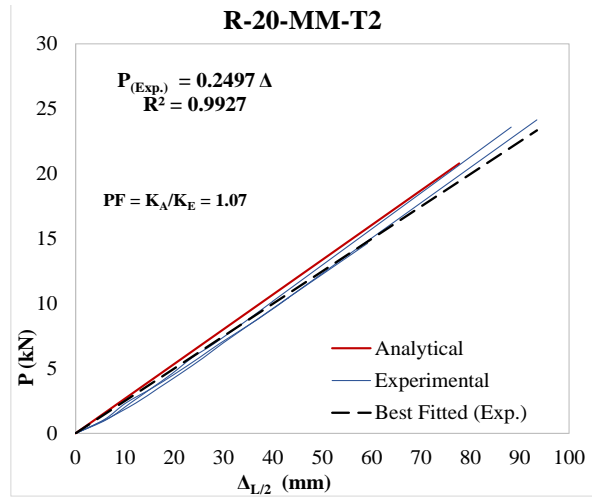
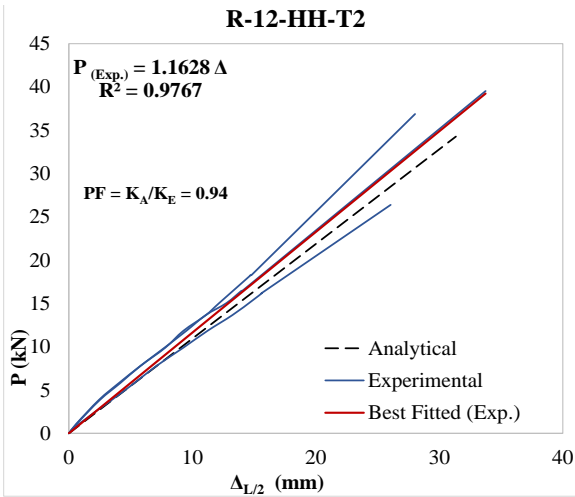
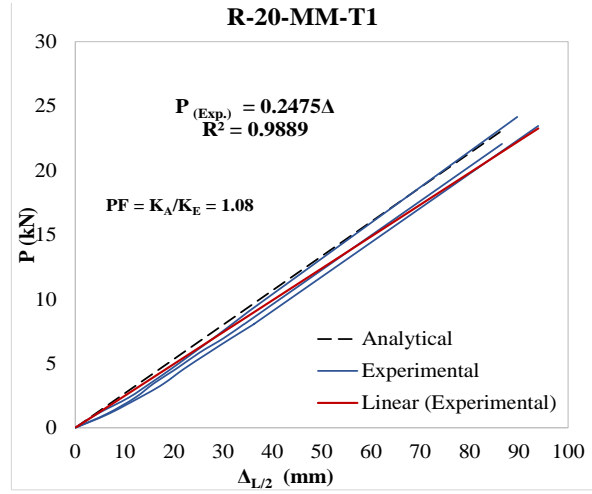
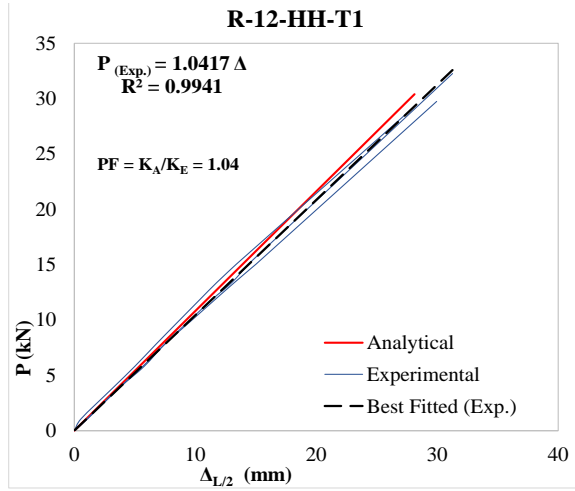


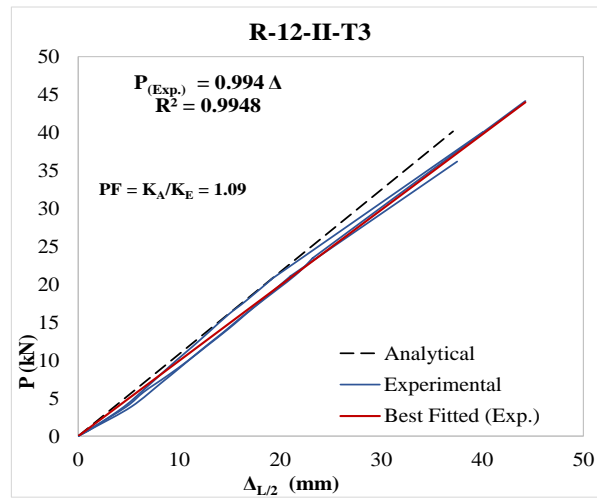
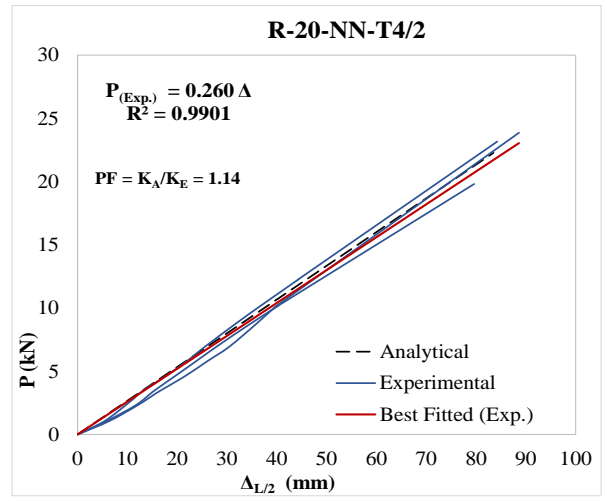
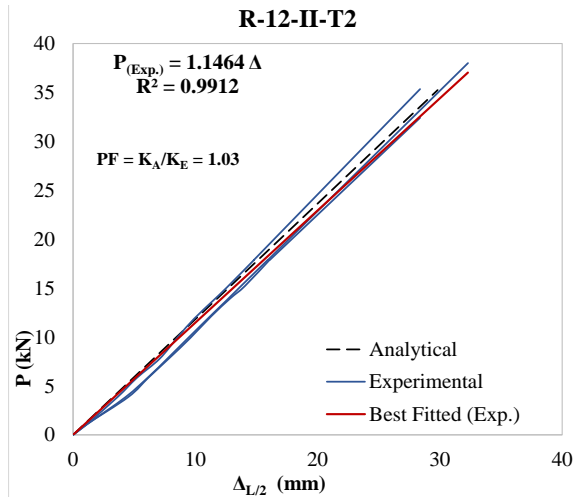
## RETROFITTED WEB HOLE I-JOISTS WITH OSB COLLARS





## RETROFITTED FLANGE NOTCHED I-JOISTS WITH GFRP PLATES





## RETROFITTED WEB HOLED I-JOISTS WITH GFRP PLATES

